DC MicroGrids Control for renewable energy integration

Sabah Benamane Siad

université PARIS-SACLAY

BNNT: 2019SACLE006

Thèse de doctorat

DC MicroGrids Control for renewable energy integration

Thèse de doctorat de l'Université Paris-Saclay
préparée à l'Université d'Évry-Val-d'Essonne (UEVE)

École doctorale n° 580 Sciences et technologies
de l'information et de la communication (STIC)

Discipline : Automatique

Thèse présentée et soutenue a L'université d'Évry, le 05 Avril 2019, par

Sabah Benamane Siad

Composition du jury:

Jean-Pierre Barbot Professeur, Université de Cergy Pontoise	Rapporteur
Seddik Bacha Professeur, Université de Grenoble	Rapporteur
Jean-Luc Thomas Professeur, Le Cnam de Paris	President
Françoise Lamnabhi-Lagarrigue Directrice de Recherche, CNRS.	Examinateur
Luiz Lopes Professeur, Université de Concordia (Canada)	Examinateur
Abdelkrim Benchaib Chercheur, HDR, Supergrid institute	Examinateur
Lilia Galai-Dol Chargée de recherche Efficacity Institute	Encadreur
Gilney Damm Maıtre de conférences,HDR,Université d'Évry	Directeur de thése

Acknowledges

I would like to express my gratitude to Gilney Damm for agreeing to be my thesis director, to Lilia Galai Dol for being my advisor and for all the reviews that she has done in this work.
I would like to thank professor Luiz Lopes for their invaluable help and wise advices.I would like to highlight the work done by Ahmad Malkawi in the test bench development.
My deepest gratitude to Abdelkrim Benchaib for being the person which trusted in me and encouraged me to carry out this thesis.
I would like to thank the members of the jury, Prof: Jean Luc Thomas, Prof : Seddik Bacha, Prof : Jean-Pierre Barbot and Prof: Françoise Lamnabhi-Lagarrigue for their comments, questions and suggestions.
Last, my deepest gratitude is undoubtedly to my families who are always beside me and support me. I want to thank my husband, who always supported and encouraged me. I want to thank my son and my daughter for their patience and understanding. I'm so thankful that I have such wonderful families.

A la mémoire de mon père

Contents

1 General Introduction 15
1.1 Introduction . . . 15
1.1.1 Context . . . 15
1.1.2 Renewable Sources Production Management Via Storage . . . 16
1.1.3 DC MicroGrid . . . 17
1.2 Motivations and objectives . . . 19
1.3 Thesis Contribution . . . 20
1.4 Thesis outcomes . . . 21

2 MicroGrids Overview 23
2.1 Introduction . . . 23
2.2 What is the MicroGrid ? (MicroGrid definition) . . . 23
2.3 MicroGrid concept . . . 24
2.4 Impact of MicroGrid on distribution system . . . 25
2.5 Type of MicroGrid . . . 25
2.5.1 AC MicroGrid . . . 25
2.5.2 DC MicroGrid . . . 26
2.5.3 Hybrid AC/DC MicroGrid System . . . 27
2.6 MicroGrid Architecture . . . 27
2.6.1 Radial Grid Configuration . . . 27
2.6.2 Ring Grid Configuration . . . 28
2.6.3 Mesh Type MicroGrid Configuration . . . 29
2.6.4 Network configuration summary in low and medium voltages . . . 30
2.7 Operation and control of MicroGrids . . . 30
2.7.1 MicroGrid control classification . . . 31
2.7.2 Hierarchical Control . . . 32
2.7.3 Timescale Analysis . . . 33
2.7.4 Overview of local control in MicroGrids . . . 34
2.8 Components of a MicroGrid . . . 35
2.9 DC MicroGrid used in our study . . . 36
2.10 DC MicroGrid Components . . . 37

2.10.1 Photovoltaic System . . . 37
2.10.2 Architectures of photovoltaic arrays . . . 37
2.10.3 Maximum power point tracking . . . 39
2.10.4 Braking Energy Recovery System . . . 44
2.10.5 Energy Storage System . . . 46
2.10.6 Energy storage technologies . . . 46
2.10.7 Power electronic converters . . . 53
2.11 Conclusion . . . 55

3 Modeling of MicroGrid 57
3.1 Introduction . . . 57
3.2 Photovoltaic System . . . 57
3.2.1 Solar cell modeling . . . 57
3.2.2 Constitution of a photovoltaic generator (PVG) . . . 61
3.2.3 Maximum power point tracking . . . 62
3.3 Braking Energy Recovery System . . . 63
3.3.1 Standard voltages . . . 63
3.3.2 Contact System . . . 63
3.3.3 energy-saving techniques . . . 64
3.4 Energy Storage System . . . 66
3.4.1 Hybrid Energy Storage System . . . 66
3.4.2 Batteries model . . . 66
3.4.3 Supercapacitor Model . . . 71
3.5 Power electronic converters . . . 75
3.5.1 DC/DC Converter Modeling . . . 75
3.6 MicroGrid Model . . . 84
3.7 Conclusion . . . 85

4 Microgrids Control 87
4.1 Introduction . . . 87
4.2 Context and Problem Position . . . 87
4.3 DC MicroGrid Configuration . . . 88
4.4 High Level Controller . . . 88
4.4.1 PV Power source . . . 89
4.4.2 Storage system . . . 89
4.4.3 Time scales Concept . . . 90
4.4.4 Stabilization strategy . . . 91
4.5 Local Control . . . 95
4.5.1 PV System Component Modeling and Control . . . 95
4.5.2 Storage System Local Control . . . 103
4.6 Stability study of interconnected System . . . 114
4.7 Simulations Result . . . 117
4.8 Comparison with PI control . . . 123
4.9 Conclusion . . . 124

5 Braking Energy Recovery power 125
5.1 Introduction . . . 125
5.2 Braking energy recovery system scheme . . . 126
5.3 High Level Controller for storage system . . . 126
5.3.1 High level control for Power source . . . 127
5.4 Control for the source . . . 128
5.5 Storage System Control . . . 134
5.5.1 Calculation of High Level Controller . . . 134
5.5.2 Current Control Law for the battery . . . 136
5.5.3 Current Control Law for the Supercapacitor . . . 137
5.5.4 stability of storage system . . . 138
5.6 Stability study of interconnected System . . . 140
5.7 Simulations result . . . 145
5.8 Conclusion . . . 149

6 Control Application 151
6.1 Introduction . . . 151
6.2 System Configuration . . . 151
6.2.1 Model of Three-Input DC–DC Boost Converter . . . 152
6.3 Grid Control Strategy . . . 153
6.3.1 High level controller . . . 153
6.4 Non linear Control . . . 155
6.4.1 Control law of PV . . . 155
6.4.2 Storage System Control . . . 159
6.4.3 Stability Study for the Interconnected System . . . 162
6.5 Simulation Result . . . 167
6.5.1 Reference split with a $f_c = 20Hz$ Low-pass Filter (LPF) . . . 168
6.5.2 Reference split with a $f_c = 2Hz$ Low-pass Filter (LPF) . . . 169
6.5.3 Reference split with a $f_c = 100Hz$ Low pass Filter (LPF) . . . 169
6.6 Experimental investigation and demonstration . . . 172
6.6.1 Reference decomposition with a $f_c = 2Hz$ LPF . . . 177
6.6.2 Reference decomposition by a $f_c = 100Hz$ LPF . . . 180
6.7 Comparison with PI control . . . 183
6.7.1 Base results with Nonlinear control . . . 183
6.7.2 Linear control . . . 184
6.7.3 Simulation Results and Comparison . . . 185
6.8 Conclusion . . . 188

7 General Conclusion 189
7.1 Conclusion . . . 189
7.2 Main results . . . 190
7.3 Perspectives for future work . . . 191

Abstract 192

Bibliography 192

List of Figures

1.1 Weekly Loading of transformer station in the rural area of LEW-Verteilnetz GmbH Germany, in 2003 and 2011 . . . 16
1.2 Power Profile to be provided for the grid . . . 16
1.3 Clipping consumption peaks . . . 17
1.4 DC MicroGrid as Fire wall . . . 18

2.1 MicroGrid structure . . . 24
2.2 AC MicroGrid . . . 26
2.3 DCMicroGrid . . . 26
2.4 Hybrid AC/DC MicroGrid System . . . 27
2.5 Radial, grid configurations . . . 27
2.6 Ring configurations of Microgrid . . . 28
2.7 MESH grid configurations . . . 29
2.8 Classification of MicroGrid control techniques and functional layer structure 31
2.9 Hierarchical control levels . . . 32
2.10 Timing Classification of power control function of MicroGrid . . . 34
2.11 MicroGrid System . . . 36
2.12 Stand alone system . . . 38
2.13 Grid connected system . . . 39
2.14 Solar cell operating point . . . 39
2.15 Divergence of P and O from MPP . . . 40
2.16 Flow chart of P and O algorithm . . . 41
2.17 Flow chart of IncCond algorithm . . . 42
2.18 braking energy recovery system . . . 44
2.19 braking energy recovery system with storage . . . 45
2.20 Power Profile of braking energy recovery system . . . 45
2.21 Topology of Flywheel Energy Storage System . . . 47
2.22 NAS Diagram . . . 49
2.23 Typical storage capacity versus discharge . . . 51
2.24 Functional circuit of a buck converter . . . 53
2.25 Functional circuit of a boost converter . . . 54

2.26 Functional circuit of inverter 55

3.1 Equivalent circuit model of solar cell 58
3.2 Solar cell characteristics 60
3.3 Series and parallel connection of solar cells 61
3.4 PV Array 62
3.5 Third rail System 63
3.6 Overhead line 64
3.7 Energy-saving techniques in DC-electrified railway systems 64
3.8 Substation Architecture 65
3.9 Metro line residual braking energy measurement 65
3.10 Basic structure of a HESS [1]. 66
3.11 Schematic diagram of the Rint model. 67
3.12 Resistive Thevenin battery model scheme 68
3.13 Dynamic Thevenin equivalent battery model scheme 68
3.14 Model scheme 69
3.15 Equivalent circuit model of an supercapacitor 72
3.16 Equivalent circuit of an supercapacitor, realistic model 73
3.17 Equivalent circuit of a practical supercapacitor, three-branch model 73
3.18 DC/DC Boost Converter Circuit 76
3.19 The equivalent circuit in interval $[0, u_1T]$ 76
3.20 The equivalent circuit in interval $[u_1T, T]$ 77
3.21 The BOOST converter and corresponding state space nonlinear average model 79
3.22 Current characteristics for $u_1 = 0.8$ 79
3.23 DC Bidirectional Converter Circuit 80
3.24 The equivalent circuit in interval $[0, u_2T]$ 81
3.25 Structure convertisseur DC/DC dans l'intervalle $[u_2T, T]$ 82
3.26 The Bidirectional converter and correspond state space nonlinear average model 83
3.27 The comparison results between the real circuit and average model ($u_2 = 0.8$) 84
3.28 Comparison results between the real circuit and the average model ($u_2 = 0.2$) 85
3.29 DC Microgrid studied topology 85

4.1 DC Microgrid global structure 88
4.2 DCMicrogrid Configuration 89
4.3 Power Flow 90
4.4 Signal decomposition 91
4.5 Control Strategy 92
4.6 DC/Control of PV system 96
4.7 PV power with Varying Irradiance 119
4.8 Reference power components 120

4.9 Control inputs u_2 and u_3 . . . 120
4.10 Output power of battery and supercapacitor . . . 121
4.11 Output Power . . . 121
4.12 DC MicroGrid voltage . . . 122
4.13 Dynamic response of the system . . . 122
4.14 Comparison of the V_{DC} dynamics by applying nonlinear control in red and classical PI control in blue . . . 124

5.1 System Configuration . . . 126
5.2 Power Flow of DC MicroGrid . . . 127
5.3 Voltage metro profiles measurements [2] . . . 128
5.4 DC/DC buck Converter . . . 128
5.5 DC/DC Buck Converter Control . . . 129
5.6 Output current and Output Power . . . 146
5.7 Control inputs u_1, u_2 and u_3 . . . 147
5.8 Current references . . . 147
5.9 DC MicroGrid voltage . . . 148
5.10 Output power and state of the charge of the battery and supercapacitor . . . 148

6.1 Three-Input DC–DC Boost Converter Circuit . . . 152
6.2 Signal Decompostion . . . 155
6.3 Time scale presentation . . . 166
6.4 Dynamic response of the system . . . 168
6.5 Dynamic response of the system . . . 169
6.6 Dynamic response of the system . . . 170
6.7 Example of the Current reference for the storage . . . 171
6.8 Example of reference for the Battery . . . 171
6.9 Example of the reference for the Battery . . . 172
6.10 Experimental setup . . . 173
6.11 Dynamic Response during increasing load with battery discharging . . . 174
6.12 Dynamic Response during step increase load with battery discharging . . . 174
6.13 Dynamic Response during deacreasing load with battery discharging . . . 175
6.14 Dynamic response during decreasing load with battery charging . . . 176
6.15 Dynamic Response during increasing load with battery charging . . . 176
6.16 Dynamic response during increasing load with battery discharging with $f_c = 2hz$ . . . 177
6.17 Dynamic Response during decreasing load with battery discharging . . . 178
6.18 Dynamic Response during decreasing load with battery charging . . . 178
6.19 Dynamic Response during increasing load with battery charging . . . 179
6.20 Dynamic Response during increasing load with battery discharging with $f_c = 100hz$ . . . 180
6.21 Dynamic Response during decreasing load with battery discharging . . . 181
6.22 Dynamic Response during decreasing load with battery charging . . . 181
6.23 Dynamic Response during increasing load with battery charging . . . 182

6.24 Dynamic response of the system for Nonlinear Control 183
6.25 Storage Structure Control of Linear Control 184
6.26 Comparison of the V_{DC} dynamics by applying nonlinear control in red and classical PI control in blue 186
6.27 Comparison of the Current dynamics by applying nonlinear control and classical PI control 187
6.28 Comparison of the V_{DC} dynamics by applying nonlinear control in red and classical PI control in blue 187

Chapter 1

General Introduction

1.1 Introduction

1.1.1 Context

To meet the growing energy demand, reduce $CO2$ emissions and cope with environmental concerns, renewable energy is expected to play a key role in the future.
This clean energy can be integrated at transmission level as well as at distribution level. At transmission level, wind energy is the main driver, particularly in Europe. For example in northern Europe, one can witness many offshore wind farms connected to the main transmission grid via AC or DC links. Due to their intermittent nature and the fact that these wind farms are connected to the grid via power electronics converters, the power grid becomes more vulnerable and subject to instability. With more power electronics converters in the power grid, the power network will have reduced inertia and consequently will be more prone to frequency and angle instability as transient stability phenomena (see Migrate European project for example). Though these issues are not within the scope of the thesis, they are a driver for addressing renewable energy sources (renewables) in a more efficient way, avoiding to bring instability for the main grid.

In the medium and low voltage distribution level, until recently substations were loads axe connected and always represented positive loads, implying in a static sizing and implementation of this distribution grid. From now on, these distribution substations will often represent negative loads, manly due to the integration of Photo-Voltaic (PV) energy as shown in the following figure.

The integration of Distributed Generation (DG) in the grid changes the behaviour of consumers who may also become producers. Figure (1.1) [3] shows the load profile for a substation in countryside Germany where it can be seen that much solar power was included to the grid. While during the night the load is roughly the same, during the day (when sun shines) the load becomes negative (power flux inversion flowing to the high voltage), and may represent several times the consuming load.
Two power management philosophies can be used in order to deal with this new phenomena. The first way is to send this excess of power along the distribution network in order to

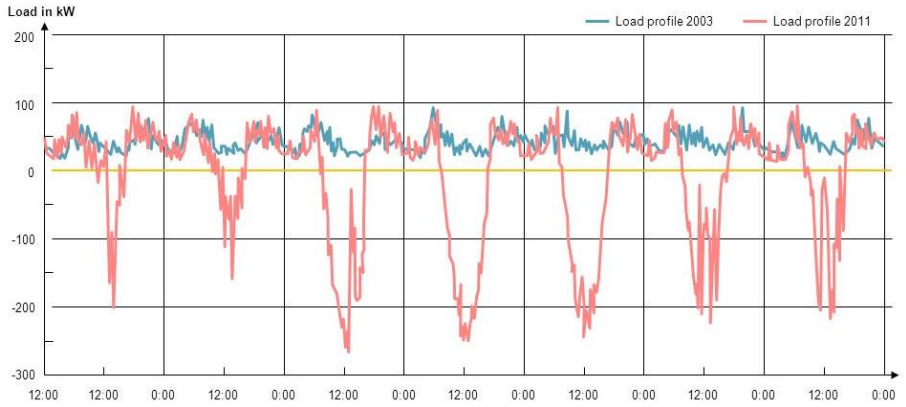

Figure 1.1: Weekly Loading of transformer station in the rural area of LEW-Verteilnetz GmbH Germany, in 2003 and 2011

be used where needed. This way of managing local production will generate constraints as power congestion, voltage instability and additional losses, what would need in many cases to re-size the distribution network, what is not a cost-effective way of managing the integration of this DG.
The other way for managing DG is to either consume in nearby, or store the excess of power in order to be consumed later. This can be done via the so called MicroGrid.

In the future, in order to preserve network reliability and integrity, the electrical distribution system operator will impose additional constraints (Grid Codes) on decentralised renewable energy producers. Then, a desired daily production curve must be respected, as is already the case of solar energy producers in Reunion island (see [4]).

Figure 1.2: Power Profile to be provided for the grid

1.1.2 Renewable Sources Production Management Via Storage

In this work we considered two power sources of renewable production: classic renewables as photovoltaic arrays and Braking Energy Recovery in Railway Stations. These power sources have an uncertain and intermittent production which requires the use of a storage system. Storage gives us the opportunity to clip consumption peaks at end-of-day (see Figure (1.3)). The storage system in this thesis will consist of a battery and a supercapacitor, the battery for energy flow management and supercapacitor for power flow

management. The storage system composed by batteries makes it possible to deliver high energy densities over long periods, while the supercapacitor based storage system delivers a high power density over short time. Using a battery to stabilise the flow of energy is similar to an energy buffer between the rate requested by the load or network and the flow supplied by power sources, but most batteries cannot respond to rapid load variations, then supercapacitor is used to respond to high power demands in the very short time. Indeed, supercapacitors have a very high power density and a fast discharging.

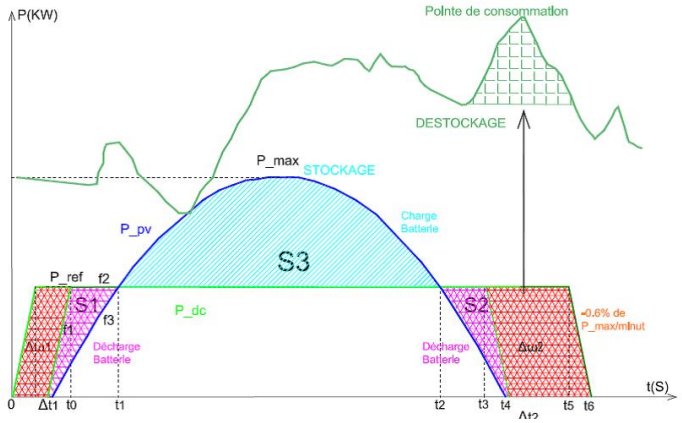

Figure 1.3: Clipping consumption peaks

Among the many existing storage technologies we use stationary batteries, namely lead acid and Lithium ion batteries. The lead acid battery is the most used in stationary storage for its price and its well-known technology, but in recent years the price per cycle of the lithium ion battery becomes lower than that of the lead battery [5], which encourages the use of the Lithium ion battery in certain applications such as the braking energy recovery system.

The choice of battery technologies depends on intermittency of the solar energy; the electric energy is stored during the production period in the day and returned at night fall. Energy storage must also be adapted to network operation and availability in the case of connected systems.

1.1.3 DC MicroGrid

For large scale development and integration of renewables, it is necessary to solve the intermittency problem of DG. To attain this goal, we consider a storage system to increase the penetration of this type of energy. But a power flow management in this new type of system then becomes necessary, bringing us to the concept of MicroGrids. MicroGrids appear as a solution to integrate renewable energy sources, to meet the requirements of network operators, and ensure the reactivity of the electrical system to unpredictable energy sources .

Two different types of MicroGrids can be considered:

- AC MicroGrid
- DC MicroGrid

AC MicroGrids are not the focus of this thesis, we will indeed focus on DC MicroGrids in the following.
Since PVs' output is in the form of Direct Current, as well as several storage systems as batteries and supercapacitors, DC grids can be used as an efficient system for integrating renewables, for assuring energy security and protecting power systems. For this reason, it has seem natural in this work to consider a DC grid to integrate sources as PV arrays and storage. The produced energy is then integrated to an AC grid through a power converter. In the same way, several loads (in particular electric vehicles) are naturally DC, and the use of a DC MicroGrid allows to reduce power losses and to guarantee a better power quality.

The DC MicroGrid developed in this study is able to correctly feed a load of desired power while ensuring voltage stability, to assure reliability against strong changes in the grid like faults, and to eliminate disturbances and to assure high power quality.

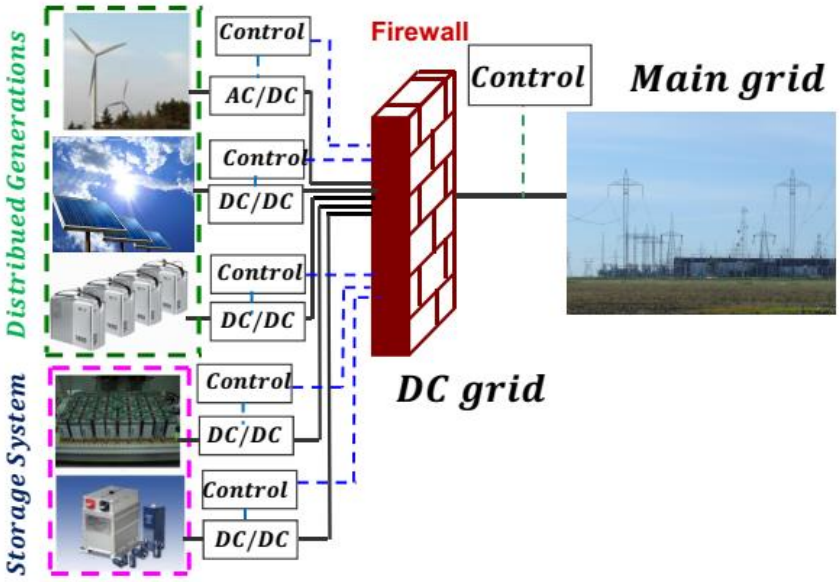

Figure 1.4: DC MicroGrid as Fire wall

The DC MicroGrid guarantees the power exchange with the main grid and can also supply loads such as charging stations for electric cars. The objective of this study is the stabilisation of the DC MicroGrid's voltage in spite of variations on production and consumption, to create a reliable and independent system. For that we will exploit the physical characteristics of each element of system. In the framework of this thesis, we have a decentralised source interconnected through a power converter to a DC MicroGrid and a storage system composed by a battery for long energy needs and a supercapacitor for rapid variations of production or the load. Because of the objective of assuring stable and performing operation in a wide range of situations, and because the nature of the considered systems is nonlinear, it was mainly used nonlinear control theory to develop the algorithms. In the same way, an important characteristic of the MicroGrid studied is its ability to disconnect from the main grid and to operate in island mode.

In this work it was followed the methodology of:

- Establish the control philosophy to cope with each case.
- Model each system elements.
- Design local and global control algorithms for the system according to the objectives.
- Study the dynamic stability of the overall interconnected system.

1.2 Motivations and objectives

This thesis is motivated by the challenges in the control design of DC MicroGrid systems and analysis of DC MicroGrid system's dynamic behaviour.

- Contribute to the study of decentralised energy sources in the current energy context and reduce emissions of greenhouse gases.
- Design a system that integrates the electrical network without compromising its stability.
- Facilitate large-scale penetration of renewable energy sources into the power production system.
- Design of a flexible DC MicroGrid capable of integrating decentralised generation power sources without impacting network stability.

Here it is used a "System of systems approach": the control is designed globally and accomplished locally (see [6] and [7]), also used in [8]. In the present case, the control structure of DC MicroGrid is designed with two levels, the low level controller based on nonlinear control theory (Lyapunov, backstepping and input/output feedback linearization) assures (exponential) stability of each element to its own reference. On top of that, a high level controller gives references based on different control objectives, and in particular accomplish power flow [9], [10]. The system's stability is formally analysed by constructive Lyapunov functions, and assures exponential stability of the whole system under mild conditions, that in their turn define the operation region of the grid. The obtained system can then present good dynamic performance and flexibility.

We propose an hierarchical control scheme, based on nonlinear control theory to stabilise the system.

- For the PV power source system: extract the maximum power and optimise the performance of PV panels. For this we will design a local controller capable of monitoring the variations of atmospheric conditions and the current and voltage references given by the Maximum Power Point Tracking (MPPT).
- For the storage system: the battery responds to the slow power variations between production and consumption. The supercapacitor responds to the rapid power variation between production and consumption. According to the power reserve on the DC MicroGrid, we will decompose the voltage variation ($\frac{dV}{dt}$) in two components. A slow component is provided as a reference to the battery, and a fast component is provided to the supercapacitor.

The challenge is to design a controller in such way that the interconnection of the DG to the network does not disturb the main grid, and to assure stability of the whole system under variation of production and consumption. The usual approach for controlling MicroGrids is linear control due its simplicity and robustness. In addition such techniques are widely known in both industry and academia, either based on frequency domain approaches via transfer functions, or in space state. In practice, nested PIDs and sometimes robust techniques as LQR are the most used strategies. For example, the minor loop gain is a linear controller presented in [11] that relates source and load impedance to determine stability in the grid. This controller has the advantage of maintaining system dynamics even when connecting more devices like filters. This impedance-based approach is also well fit when using state space modelling [12, 13].

Nevertheless, linear control in general is based on a linearized model, designed for only one operating point. This may represent an important inconvenient for the integration of varying sources like renewables, applied to also varying loads [14, 15, 16]. In addition to overcome limitations of linear theory, the real system is split in several sub-systems with dedicated controllers for each. The final structure includes nested controllers, where the effects of one controller and its tuning on the others is never formally established. The system may then become very complex, and their tuning a real challenge. For all these reasons, nonlinear theory may provide a much broader approach that can cover all aspects, and provide rigorous analysis of the overall system. In addition, the final controllers are not much more complex than linear ones, and end up much simpler to tune.

The thesis motivation is that an energy management system can not be designed specifically for each installation. It must be configurable, adaptable, in a "Plug and Play Systems" philosophy. This requires new algorithms that can adapt to different configurations. In operation, it is necessary to design energy management systems adaptable to the variety of contexts and particularly robust to the uncertainties of the equipment behaviours and also on the demands of services.

1.3 Thesis Contribution

This thesis constitutes a step forward for DC MicroGrid control and introduces a rigorous dynamics' analysis, taking into account intermittency effects. The stabilisation of the system is based on storage devices: batteries for energy balance and long term response of power flow, while supercapacitors deal with power balance and fast response. The thesis main contributions are:

- Design of a flexible MicroGrid capable of integrating different intermittent sources without perturbing the power distribution network.
- Modelling of this DC MicroGrid.
- Analysis of the stabilisation problem of DC MicroGrids and proposing adapted solutions according to the physical characteristics of their components.
- Design a control structure that can assure power flow completion and voltage stability.

- Analyse the dynamic behaviour of DC MicroGrids and establish formal stability studies.
- The MicroGrid is designed to integrate different intermittent energy sources ensuring the stability of the overall system in both cases of connected or islanded MicroGrid.
- Stabilisation of DC MicroGrid using the different time-scale behaviour of storage devices.

1.4 Thesis outcomes

- Management of the interconnection of intermittent photovoltaic systems through a DC link and storage,
  A. Iovine, S. B. Siad, A. Benchaib, G. Damm, ERCIM News 97, 2014.
- Nonlinear Control of a DC MicroGrid for the Integration of Photovoltaic Panels,
  A. Iovine, S. B. Siad, G. Damm, E, G. Damm, E. De Santis, M. D. Di Benedetto,
  IEEE Transactions on Automation Science and Engineering 2017
- Design and Control of a DC Grid for Railway Stations
  S. B. Siad, G. Damm, L. Galai Dol, De Bernardinis.A,
  2017 International Exhibition and Conference for Power Electronics and Energy Management (PCIM 2017) Nuremberg, Germany.
- Nonlinear control of a DC MicroGrid for the integration of distributed generation based on different time scale.
  Sabah Siad, Ahmad Malkawi,Gilney Damm, Luiz Lopes and Lilia Galai Dol.
  International Journal of Electrical Power and Energy Systems,2019.

Chapter 2

MicroGrids Overview

2.1 Introduction

Power systems in general are centralized, constituted by big power generation plants which electricity is transferred to consumption over long distance transmission lines. It is aimed to replace the current fossil fuel and nuclear plants by sustainable energy generation to achieve goals of energy transition.

The integration of renewable energy sources (renewables) is a delicate matter for the electric grid. It is possible to produce large quantities of electricity from those sources, but in an intermittent and rather unpredictable way. In addition, most renewables are integrated in medium or low voltage levels. The grid was not planned like this, and very difficult problems have risen from this new reality. To cope with these new problems, it is necessary to bring together the classical power grid, with new devices from power electronics and new information technologies like advanced control systems. These new grids are called SmartGrids, which include several more specific concepts like MicroGrids.

Indeed the question is how shares of renewable energy sources can increase without affecting security, stability and reliability of the grid. The emergence of the MicroGrid in the last years is one possible answer for this issue.

2.2 What is the MicroGrid ? (MicroGrid definition)

MicroGrids are small power systems containing energy sources (distributed generation), storage and loads they can operate, while connected to the main AC grid or not (islanded mode). They maintain in real time the power balance between consumption and generation, mainly by managing the storage, and assure all states (relevant variables) are kept stable and inside operating margins. The concept of MicroGrid provides an appropriate solution to integrate more and more renewables in the existing distribution network. At the same time MicroGrids can supply the local and sensitive loads, and then this feature together with the capability of operation in both islanded and connected modes increases the reliability of the power grid from the view point of loads /costumers [17]. The defini-

tion of MicroGrids may be followed by wordings from the United State.
U.S. Department of Energy MicroGrid Exchange Group (DOE MEG) and the Conseil International des Grandes Réseaux Électriques Working Group C6.22 (CIGRE C6.22 WG).

U.S. Department of Energy MicroGrid Exchange Group:
A MicroGrid is a group of interconnected loads and distributed energy resources within clearly defined electrical boundaries that acts as a single controllable entity with respect to the grid. A MicroGrid can connect and disconnect from the grid to enable it to operate in both grid-connected or island-mode.[18]

CIGRÉ C6.22 Working Group, MicroGrid Evolution Roadmap:
MicroGrids are electricity distribution systems containing loads and distributed energy resources, (such as distributed generators, storage devices, or controllable loads) that can be operated in a controlled, coordinated way either while connected to the main power network or while islanded[19].

2.3 MicroGrid concept

The Consortium for Electric Reliability Technology Solution (CERTS) states [18] :
"The MicroGrid structure assumes an aggregation of loads and microsources operating as a single system providing both power and heat. The majority of the microsources must be power electronic based to provide the required flexibility to insure controlled operation as a single aggregated system. This control flexibility allows the MicroGrid to present itself to the bulk power system as a single controlled unit, have plug-and-play simplicity for each microsource, and meet the customers' local needs. These needs include increased local reliability and security. [Consortium for Electric Reliability Technology Solutions White Paper on Integration of Distributed Energy Resources]" The MicroGrid includes control for each power source as management of power flow and MicroGrid voltage.

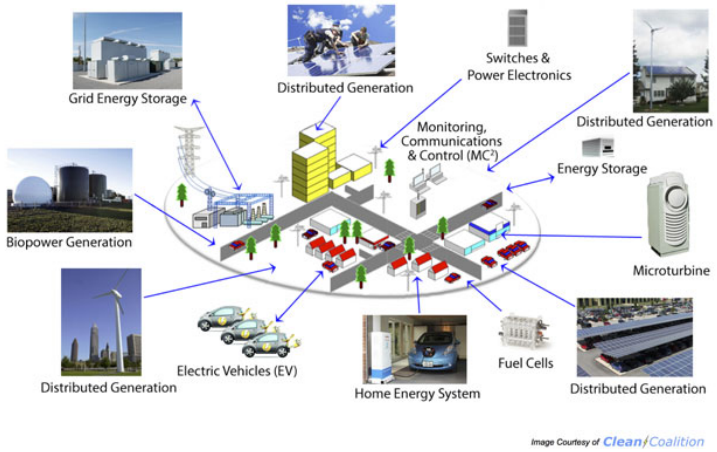

Figure 2.1: MicroGrid structure

As shown in figure (2.1) a MicroGrid, is composed of one or more power generation and

multiple users in a limited area. The connection of a different power source to the Micro-Grid offer energy independence for local power generation and costumers. The MicroGrid can operate in low voltage or high voltage.

2.4 Impact of MicroGrid on distribution system

Energy storage devices improve the reliability of the overall system, supporting the Distributed Generation (DG) power capability in cases when they can't supply the full power required by consumers. A MicroGrid reduces the power losses in the electric distribution network, improves the power capacity of the grid, provides local voltage and frequency regulation support, improves the reliability and reduces the CO_2 emissions. Moreover, MicroGrids reduce the high investment costs required for network upgrades [20].

MicroGrids represent a new approach to integrate DG into utility grid. The opportunities and benefits of integrating DERs into a MicroGrid exist for both end-users and electricity utilities, transmitters, and distributors to supply a variety of loads including residences, offices, industrial parks, commercial, and institutional campus [21].

MicroGrid implementation can also benefit local utilities by allowing system's maintenance without disconnecting customers, allowing dispatchable load during peak power conditions, and lowering stress on the transmission and distribution system. [21]. MicroGrids improve reliability for customers, having a great impact on the security of the distribution system, maintaining desired performance of the system through generation redundancy. The operation of the MicroGrids in island mode can mitigate the effects of faults in upstream networks. This requires control, communication infrastructures and sophisticated protection in order to be able to isolate faults and provide stable autonomous operation.

2.5 Type of MicroGrid

MicroGrids can be designed using Direct Current (DC) or Alternating Current (AC). AC power network is the traditional choice for energy systems; the very easy transformation of AC voltage into different levels, such as to have transmission power over a long distance, facilitates the AC current deployment over the word since late 19^{th} century.

The penetration of renewable energies in the production system has changed this status quo in the last years.

2.5.1 AC MicroGrid

Power generation is connected to the common AC bus via power converters. AC power output line can operate in connected mode or islanded mode. Block diagram of AC MicroGrid is shown in figure (2.2).

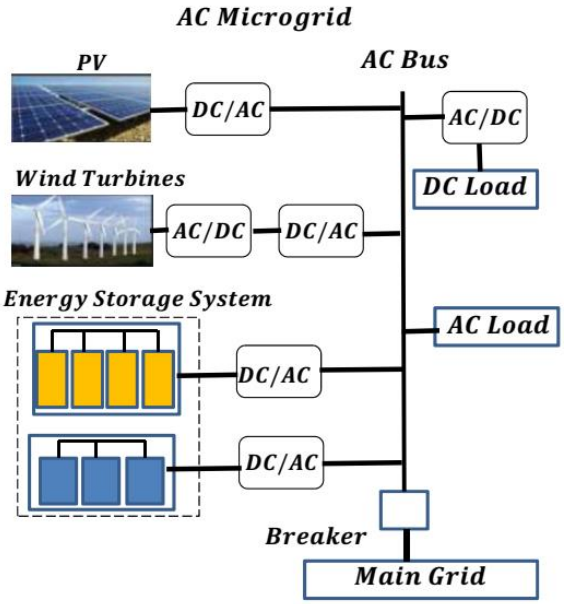

Figure 2.2: AC MicroGrid

2.5.2 DC MicroGrid

Energy storage devices and DG as PV and fuel cells produces the DC power which is connected to the DC bus; many loads are also in DC current (leds), or can use either (heating).

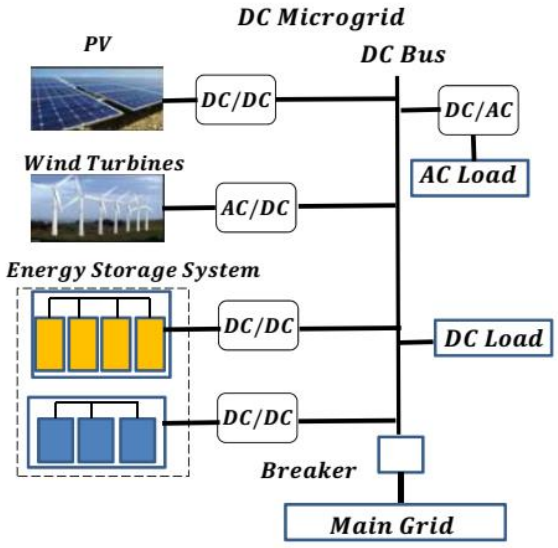

Figure 2.3: DCMicroGrid

DC MicroGrid system is shown in figure (2.3). Utilising a DC bus in MicroGrid may avoid power losses caused by power conversion.

2.5.3 Hybrid AC/DC MicroGrid System

The configuration of the hybrid system is shown in figure (2.4).The different AC and DC sources and loads are connected to the corresponding AC bus and DC bus. The AC bus and DC bus are linked through power inverters and transformers

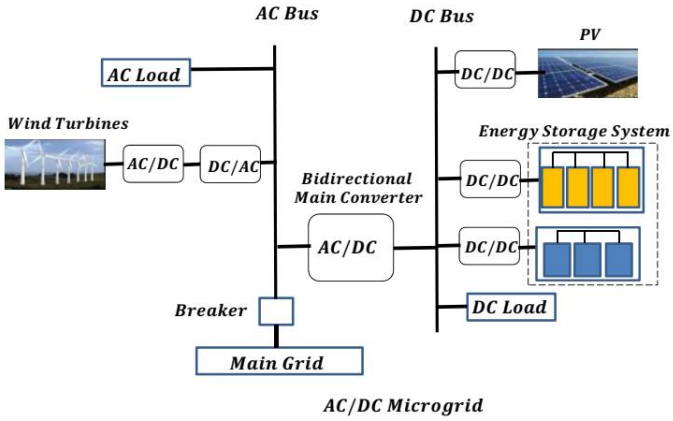

Figure 2.4: Hybrid AC/DC MicroGrid System

2.6 MicroGrid Architecture

Different architectures are possible for MicroGrids, we will review some common connection schemes which have been shown in the literature in last years.

2.6.1 Radial Grid Configuration

The radial configuration is the most used structure [21],[22] ,[23] and can be seen in Figure 2.5.

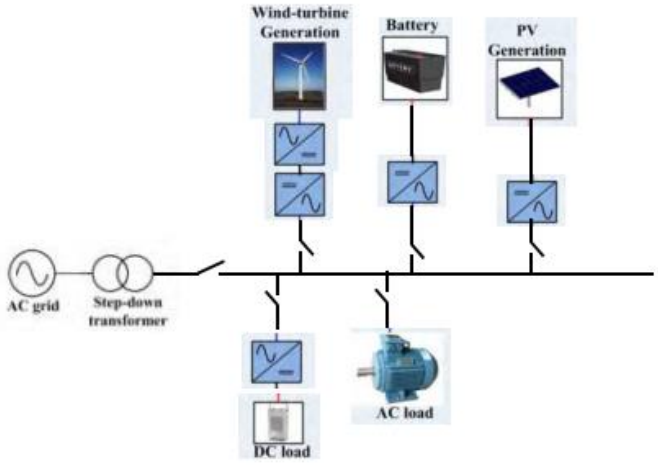

Figure 2.5: Radial, grid configurations

A radial grid configuration is based on one main line (or multiple parallel lines in real life) to which power consumers and generation are connected. This configuration is the simplest and has the advantage of being the easiest to technically implement, particularly in rural areas [23].

- Advantages of Radial Network Architecture [24]:
  - Radial network system has a relatively simple circuit protection scheme to coordinate and design. With radial network it is quite simple to settle the system component's rating requirements.
  - Another benefit while working with radial networks is that voltage compensation techniques such as reactive power compensators can be easily implemented.
  - The initial cost of this network is low, and it can be very useful in cases of generation at low voltage.
- Disadvantages of Radial Network Architecture:
  - Radial networks have limited growing flexibility.
  - This because the integration of new load or generation would need to install new cables or other components except if the initially installed cables and components were oversized. Hence, this will add on to extra costs.
  - In radial networks, consumers are dependent on a single feeder and distributor. Any fault in the system will cause interruption in power supply to all the consumers connected to the distributor.

2.6.2 Ring Grid Configuration

Ring configuration, Figure 2.6, consists of lines creating a geometrical loop or ring shape, thus enabling two alternative routes for power flow to any given point of the network [21], [22], [23].

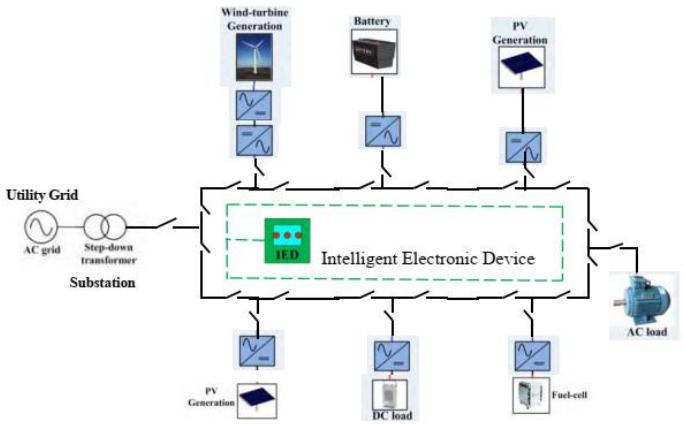

Figure 2.6: Ring configurations of Microgrid

This offers better voltage stability and lower power losses, but also requires a more sophisticated protection system.

- Advantages of Ring Network Architecture [24]:
  - Ring network is known to be the most structured one since it forms a closed loop by joining nodes to each other. Due to this, several zones of protection within the ring network can be implemented.
  - This network structure has a better performance compared to radial ones with higher reliability. In case one feeder is under fault or maintenance, the ring distributor is still energised by other feeders connected to it whilst saving in cabling/copper compared to parallel feeders [25]. Furthermore, according to previous research, a protection scheme for distributed networks was proposed with ring network structure [26].

- Disadvantages of Ring Network Architecture:
  - A major disadvantage of this structure is that the network is highly dependent on the cables that connect other components to the network. In terms of complexity, a loop feeder system is only slightly more complicated than a radial system and has a major drawback of catering the capacity and cost of the loop system [27].

2.6.3 Mesh Type MicroGrid Configuration

Figure 2.7 presents the Mesh configuration for a MicroGrid.

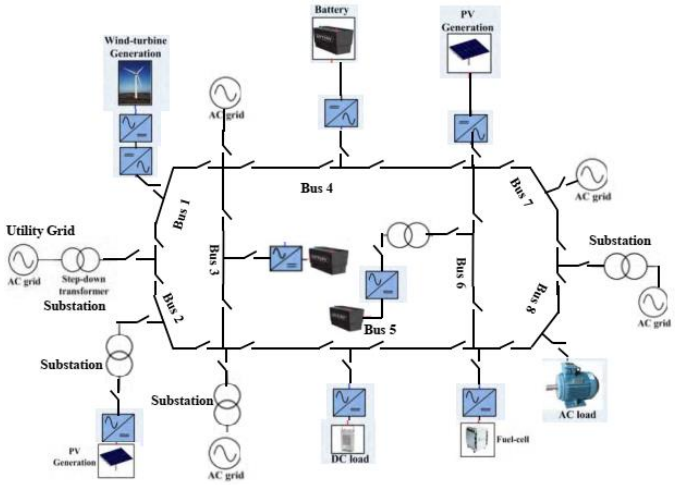

Figure 2.7: MESH grid configurations

Mesh configuration further increases redundancy by offering multiple alternative connections to all network nodes. It provides the greatest flexibility, but also makes operation and protection of the MicroGrid challenging [21], [22], [23].

- Advantages of Mesh Network Architecture:
  - Mesh MicroGrid structure is efficient for short-distance transmissions and very well incorporates an existing network structure. That is, it can effectively be upgraded from a radial to a mesh network structure. The power transmission

in mesh architecture can be carried to an aggregation point, often a sub-station that allows for reliability and a control over the fluctuating power generation [28].

  - The simplest network structures to protect are radial systems while meshed distribution networks have a higher short circuit power. The advantage of meshed networks is relatively balanced voltage profile and high reliability through redundancy [29].

- Disadvantages of Mesh Network Architecture:
  - In comparison to ring and radial configurations, mesh grid has the most complicated configuration since it includes many alternative connections between nodes. This significantly makes the operation and protection of the distributed network challenging [28].

2.6.4 Network configuration summary in low and medium voltages

In order to help differentiate between the several MicroGrids, they can be regrouped into four categories [21]:

- Islanded MicroGrid: an island MicroGrid, a combination of DG units and DS units provides enough electricity for one customer or small community separate from the utility grid, because its remoteness often makes it difficult to connect to the grid .
- Low voltage customer MicroGrid: a low voltage (LV) customer MicroGrid services the power demands of one customer, like a farm or detached house by connecting and operates parallel to the grid. Then when there is a fault in the utility grid, the customer's power needs are met by one or two of their own DG and DS units in islanding mode.
- Low voltage MicroGrid: in this case, an LV MicroGrid, is characterized by a group of LV customers, where power production is based on many small scale DGs, like solar panels on the roof of a house and a microturbine, for example. The LV MicroGrid can range from just a few consumption points to an entire low voltage network fed by an MV/LV transformer.
- Medium voltage feeder MicroGrid: LV MicroGrids can be grouped into a MV MicroGrid where bigger production units, like wind power parks can be applied. These are then centrally connected at one HV/MV substation, and can consist of partial or the entire output of the HV/MV substation.

2.7 Operation and control of MicroGrids

The balance of power in an electric grid is maintained if output power including losses is equal to the input power.

The integration of renewables through power converters in MicroGrids requires control to assure the voltage stability and to maintain the power balance between the power

sources, storage and the loads.

Since micro-source based DGs are normally controlled and connected to the grid through power converters, by coordinating and controlling these power electronics interface, the MicroGrid has significant flexibility to fulfill system requirements in terms of efficiency, security, reliability, power quality, etc. In addition, a MicroGrid with collective actions of DGs can provide several ancillary services to the main power system through proper control and communication [30].

MicroGrids can operate in two modes: grid-connected mode and islanded mode. The proper control of MicroGrid is a prerequisite for stable and economically efficient operation. The principal roles of the microgrid control structure are as follows: [31]

- Voltage and frequency regulation for both operating modes,
- Proper load sharing and DG coordination.
- MicroGrid resynchronization with the main grid.
- Power flow control between the microgrid and the main grid.
- Optimizing the microgrid operating cost.
- Proper handling of transients and restoration of desired conditions when switching between connected mode and islanded mode.

2.7.1 MicroGrid control classification

According with [32] MicroGrid control systems can be broadly divided into four types: centralized, decentralized, distributed and hierarchical framework [32], [17], [33], [31], [34].

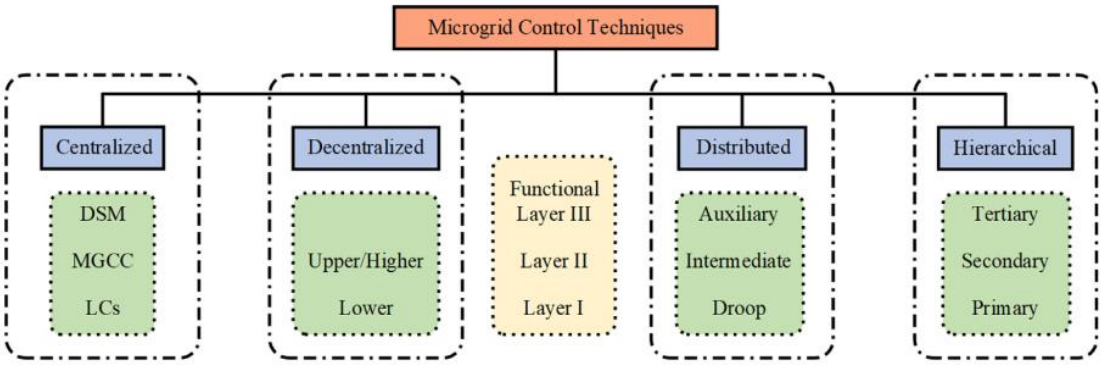

Figure 2.8: Classification of MicroGrid control techniques and functional layer structure

Centralized control

The centralized approach suggests that the central processing unit collect all the measurement and decide next action for coordinated operation inside MicroGrid. The goal is to coordinate and to schedule generators and controllable load in order to maximize the revenue from energy market participation [17], [32], [33].

Decentralized control

In the decentralized approach, it is suggested to use the controllers in distributed nodes forming a distributed control system [17].
The decentralized control method uses local measurements and is based upon pre-defined algorithms embedded in each node, deciding actions at the component level [32].

Distributed control

The distributed control architecture is a version of decentralized technique, where each Local Controller communicate with its neighbouring ones to attain some advantages of centralized architecture meant for the whole MG. It means, each device is controlled based upon local measurements by taking account of neighbours' response [32], [33].

Hierarchical control

Hierarchical control structure is based upon the difference in time scales of various control requirements. MicroGrids are operating by using several control loops [17], [32], [33], [35], [34].

2.7.2 Hierarchical Control

Power systems require control strategies to assure its proper operation. The control strategies must take into account all time scales of the system. This is usually done by an hierarchical control structure of MGs that may present three control levels in order to keep the same structure of AC grids: primary control, secondary control and tertiary control. Figure (2.9) describes the hierarchical pyramid.

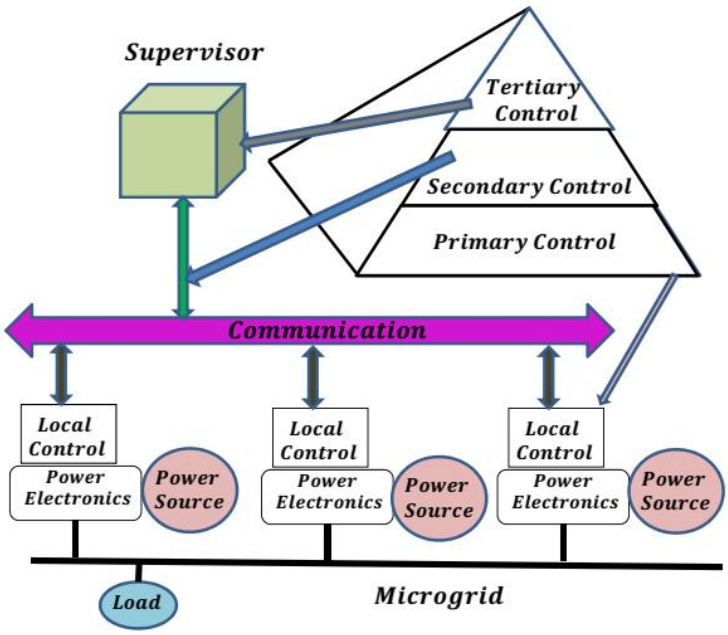

Figure 2.9: Hierarchical control levels

The primary controller is responsible for the local voltage control and for ensuring a proper power sharing between multiple DG units and a stable MicroGrid operation. The secondary and tertiary controllers support the MicroGrid operation and often include the concepts of optimally, communication and prediction, addressing multiple objectives. The primary control is an independent local control strategy that allows each DG unit to operate autonomously. Primary controllers are responsible for the reliability and stability of the system. Because of the fast dynamics in the MicroGrid, which mostly lacks a significant amount of rotating inertia, the primary controller should be fast, i.e., in time scales of milliseconds. This local primary control includes fundamental control of the hardware, and must assure stability of DGs' internal voltage and current (traditionally by independent control loops), by measuring and controlling the local signals [17].
In the literature [32],[17],primary control are usually classified as follow : droop control, Voltage and frequency control, active and reactive Power sharing and Energy management system (EMS).
Secondary control provides power sharing as a communication-based method for parallel configuration of DGs and compensates the voltage and frequency deviations caused by the load variations and local control operation [17]. The tertiary control level and correlated tertiary reserve allocation is designed to optimize the dispatch of distributed energy resources and to provide load balancing in a local power distribution network. Dispatch optimization can include economical, technical, and environmental optimization [36].

This tertiary control is responsible for coordinating the operation of multiple MicroGrids interacting with one another, and exchanges with the main grid (buying or selling power, providing ancillary services as voltage support and frequency regulation, etc). This control level typically operates with a time step in the order of several minutes to hours, providing signals to secondary level at MicroGrids and other subsystems that form the full grid. Secondary control on the other hand, coordinates internal primary controls within the MicroGrids and subsystems in the span of a few minutes. Finally, primary controls are designed to operate independently and react in predefined ways instantaneously to local events[33].

2.7.3 Timescale Analysis

MicroGrid supervision and power management can be analyzed through various function which are classified in different time scales as shown in Figure 2.10.
The short time energy management corresponds to the local controller and includes the real time balancing and power dispatching among Distributed Generations and Energy storage systems according to the storage level capacity and specific requirement/limitation of each unit. It includes information on available power from renewable sources and Primary regulation of voltage and frequency.
In the medium term, energy management includes the adjustment of renewable energy production, the available Energy Storage, load prediction and the available Energy Storage estimation. In the long term, energy management includes the hourly renewables production forecast including the time dependency of the power source environmental impact.

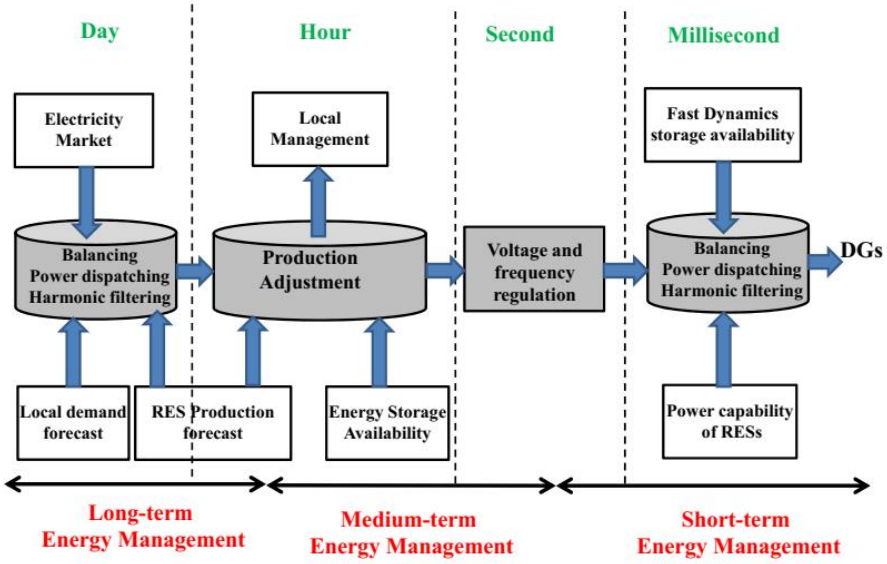

Figure 2.10: Timing Classification of power control function of MicroGrid

2.7.4 Overview of local control in MicroGrids

Classically, different control techniques have been employed in the control of MicroGrids such as PI/PID linear control, sliding mode and linear quadratic.

PI/PID linear control

Because of their simple structure, the PI/PID controller is employed extensively in the industrial field for power systems. PID/PI is a robust, reliable, and provides near-optimal performance of the control system with appropriate tuning of gains [37]. Nevertheless, the PI/PID tuning methods have limited capability of optimally tuning the PID gains for nonlinear and complex systems. Within this framework, the PID performance significantly depends on the suitable values of the PID parameters [37], [34]. Furthermore, as a linear approach, its performance may highly change if the system is used in a wide operation range.

Linear quadratic regulator

The concept of linear quadratic regulation LQR is to minimize or maximize an utility cost function and to calculate the optimal control policy. The challenging with linear quadratic regulator is the selection of the weighted matrices Q and R to attain the proper response [37].

PI/PID Nonlinear control, Feedback linearization and backstopping

Since MicroGrids are nonlinear system, nonlinear approaches as feedback linearization , PI/PID Nonlinear control ,and backstepping are used in order to design the controller for these systems .

These methodologies have been widely explored for the stabilization of the Micrigrids [10], [38]..

Sliding mode control

Sliding mode control has been intensively investigated for nonlinear robust control to ensure stability subject to parameter constraints [37], [34].

Model predictive control

Predictive control techniques are improved to forecast the reference signals. An interesting characteristic of these schemes is that they may reduce the tracking error [37].

Artificial-intelligence-based control

In the literature, a variety of heuristic algorithms have been applied to improve the control and optimization for MGs and DG units, among which one can cite use of particle swarm optimization, fuzzy logic, neural network, and genetic algorithm. Thus, intelligent and evaluation techniques are effectively applied in both the grid-connected and islanded modes of MicroGrid operation [37], [34].

Adaptive control

Adaptive control strategies are mainly employed to deal with parametric uncertainties and disturbances. Beyond any doubt, adaptive control strategies can effectively ensure sustained stability, robustness convergence, and tracking of the system dynamics under mild conditions. It should be noted that the operating point of the system may change much. Consequently, the controller performance in the plant might not be optimal. In order to overcome such challenges, adaptive solutions are exhaustively used to search for quasi-optimal operation conditions [37], [34].

2.8 Components of a MicroGrid

As presented above, the MicroGrid is a combination of distributed generation units, storage, loads and connection to other grids (AC or DC), connected through a physical network, and managed by advanced control methods to operate the distribution of energy flows and provide energy usage information.

MicroGrids are generally composed by:

- Distributed energy Generation as small wind turbines, photovoltaic arrays, fuel cells, braking energy recovery system, internal combustion engines with generators and micro turbines. These DG units are small sources of energy located near costumers.
- Distributed storage are devices as batteries, Supercapacitors, flywheels and superconductors.Storage units can balance reserves ranging from short terms to long terms application.

- Power electronics interface: the components are connected to medium or low voltage networks through power electronic interfaces. Power electronics interface could contribute to the power balance in the system.
- The load(s) of a MicroGrid are the components that consume electricity.
- Control and communication: is an essential MicroGrid component, they operate and control DG units together with DS units and controllable loads. Advanced power electronic conversion and control capabilities are necessary to integrate communication between all components into a coordinated MicroGrid management system.

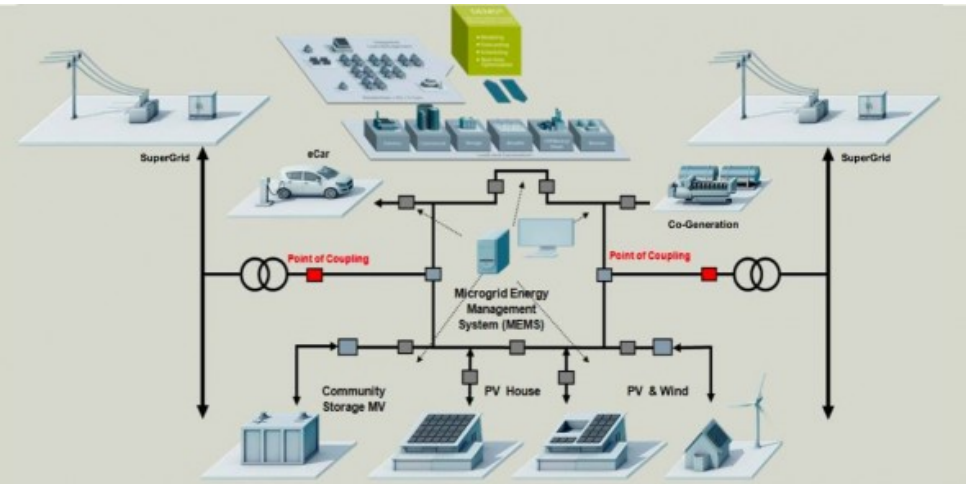

Figure 2.11: MicroGrid System

Figure (2.11) shows different components of MicroGrids.

2.9 DC MicroGrid used in our study

DC MicroGrids have recently earned significant attention. The technical challenges associated with AC MicroGrids (e.g., synchronization of DERs, reactive power control, harmonic currents, and voltage unbalance at critical buses) do no exist in DC MicroGrids. Moreover, DC MicroGrids facilitate seamless interfacing of DC sources such as photovoltaic panels, fuel cells, and battery storage devices without the requirement of DC-AC converters, an as a consequence reduce energy dissipation and power loss.
Therefore, DC MicroGrids are a suitable solution for sensitive applications that require high power quality. Similar to AC MicroGrids, a hierarchical control structure can be adopted to control DC MicroGrids, [39],[40]. For all this reasons We will study DC MicroGrids in this thesis.

The considered DC MicroGrid topology is composed by photovoltaic panels connected through $DC-DC$ boost converters for the source, a battery and supercapacitor as elements of the storage system connected to $DC-DC$ bidirectional boost converters with radial configuration.

2.10 DC MicroGrid Components

2.10.1 Photovoltaic System

The photovoltaic energy is based on the photoelectric effect. This one creates an electrical current from an electromagnetic radiation. Sun emits radiation of this type, and has the advantage of being inexhaustible and to be used at any point of a territory.
This is also a clean energy since the energy production from PV modules does not emit greenhouse gases. This resource however has two drawbacks, the production is intrinsically linked to climatic conditions; and a large surface is necessary to produce large amounts of energy since the performance of PV is relatively low [41].

Photovoltaic cell

The photovoltaic cell is based on the physical phenomenon of a PV establishing an electromotive force when the surface of the cell is exposed to light. The voltage generated can vary between 0.3 V and 0.7 V Depending on the material used, its interconnection, the cell's temperature and aging [41].
A PV cell is made from two layers of silicon, a P-doped (doped boron) and a n-doped (phosphorous doped) creating a PN junction with a barrier potential. When photons are absorbed by the semiconductor, they transfer their energy to the atoms of the PN junction so that the electrons of these atoms are released and create electrons (N) and holes (P charges). This creates a difference potential between the two layers. This potential difference is measured between the connections of the positive and negative terminals of the cell. Through a continuous load, it can reap more of the carriers [42].

2.10.2 Architectures of photovoltaic arrays

Photovoltaic systems are used in many different areas. They are generally classified according to their functional and operational requirements, their component configurations and how the equipment is connected to the other power sources and electric loads. According to the different requirement of the application areas, different architectures of the photovoltaic system are adopted. Generally speaking, the two principal classifications are stand-alone systems and grid-connected systems.

Stand-alone PV system

The stand-alone photovoltaic system is not connected to the grid but works independently to supply a DC or AC load with required electric power. There are three types of structures in the stand-alone photovoltaic system:

- Direct-coupled system Direct-coupled system connects directly the PV panels to the load without controller or converter. This kind of system requires an optimal load operating within a certain range of voltage that is around the voltage at the maximum power point of the installed PV panel in order to maximize the output power of the PV panel. The consumer served should not have a strict requirement of operating power because the

output of the PV panel varies a lot during the daytime and is equal to zero during the night. Since there is no storage neither MPPT tracker coupled in the system, high degree of freedom is necessary in this configuration such as to satisfy simultaneously the respective operation of PV panels and the consumer.

-MPPT coupled system

MPPT (Maximum Power Point Tracking) coupled system provides a much more flexible coupling between the PV panel and the consumer than the direct-coupled system. The MPPT tracker can guarantee that the PV panel operates at MPP (Maximum Power Point) while the converter satisfies the operation requirement of the load. However, without storage, the consumer must operate at variable power and consume all the power supplied by the panel instantaneously.

-MPPT and storage coupled system

Stand-alone PV system coupled with MPPT and storage is able to provide a constant and high efficient electric power to the load.

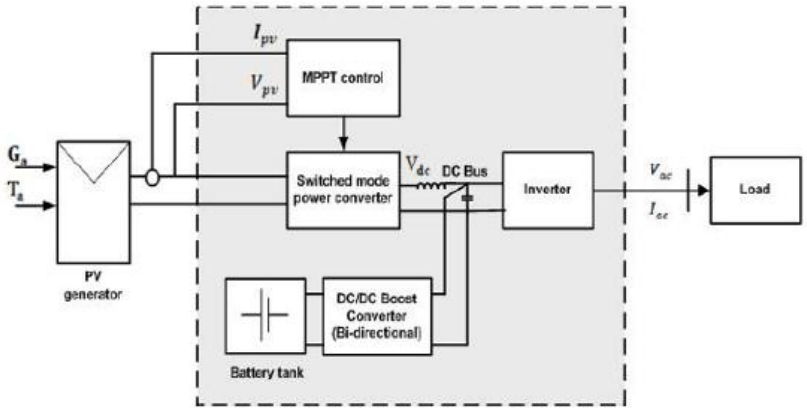

Figure 2.12: Stand alone system

Grid-connected system

- Simple grid-connected system

Simple grid-connected system allows economizing the storage component and injecting the electric power provided by PV panel directly into the grid. There are two types of structures classified as simple grid-connected system: system with DC/DC converter and system without DC/DC converter.

- Grid-connected system with storage

Grid-connected system with storage provides a secure electric production to the grid both in the daytime and in the night. Moreover, this kind of system allows the stand-alone operation disconnected to the grid for a limited time as well, thanks to its storage. However,

this system is relatively costly as a result of its storage devices demanding an adapted local technology.

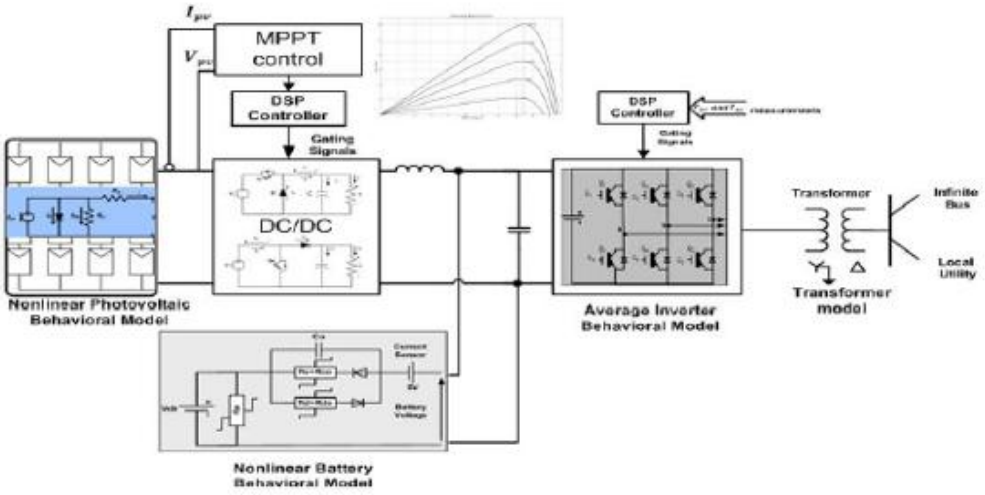

Figure 2.13: Grid connected system

2.10.3 Maximum power point tracking

Introduction

The performance of a PV cell is measured in terms of its efficiency at transforming sunlight into electricity. Only sunlight of at least a minimum amount of energy will work efficiently to create electricity, and much of it is reflected or absorbed by the material that makes up the cell.

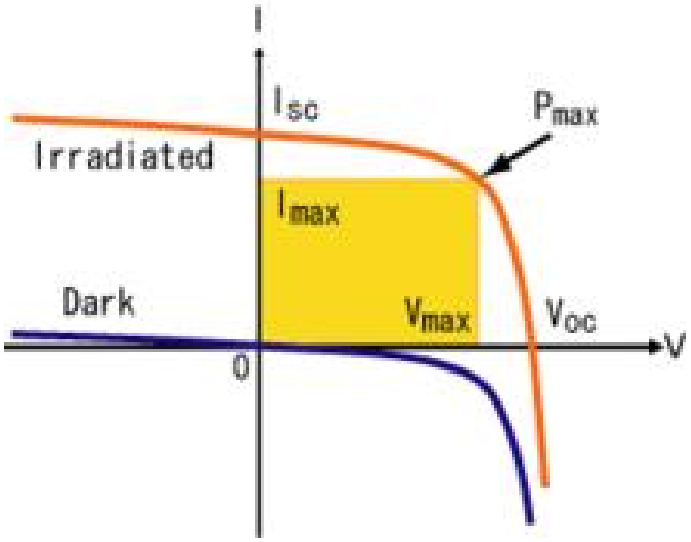

Figure 2.14: Solar cell operating point

Every photovoltaic cell has an optimal operating point, called the maximum power point (MPP), which varies depending on cell temperature and irradiance level. Figure (2.14) shows a typical current-voltage curve to represent PV cell's output characteristics under a certain cell temperature and solar irradiance level.

Maximum power point tracking, frequently refereed as MPPT, is an optimization algorithm that frequently adjusts the electrical operating point of the modules so that the photovoltaic modules are able to deliver maximum available power [43], [44].

MPPT algorithms

- Perturb and observe (P and O)

P and O algorithms operate by periodically perturbing (i.e. incrementing or decrementing) the array terminal voltage or current and comparing the PV output power with that of the previous perturbation cycle. If the PV array operating voltage changes and power increases ($\frac{dP}{dV}PV > 0$) the control system moves the PV array operating point in that direction; otherwise the operating point is moved in the opposite direction. In the next perturbation cycle the algorithm continues in the same way [45].

A common problem in P and O algorithms is that the array terminal voltage is perturbed every MPPT cycle; therefore when the MPP is reached, the output power oscillates around the maximum, resulting in power loss in the PV system. This is especially true in constant or slowly-varying atmospheric conditions [46].

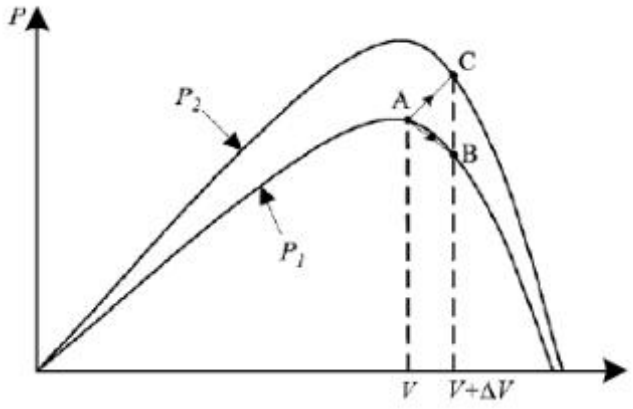

Figure 2.15: Divergence of P and O from MPP

Furthermore, P and O methods can fail under rapidly changing atmospheric conditions (see Figure (2.15)). Starting from an operating point A, if atmospheric conditions stay approximately constant, in the next step there will be applied a perturbation ΔV and the voltage V will bring the operating point to B and the perturbation will be reversed due to a decrease in power. However, if the irradiance increases and shifts the power curve from $P1$ to $P2$ within one sampling period, the operating point will move from A to C. This represents an increase in power and the perturbation is kept the same. Consequently, the operating point diverges from the MPP and will keep diverging if the irradiance steadily increases.

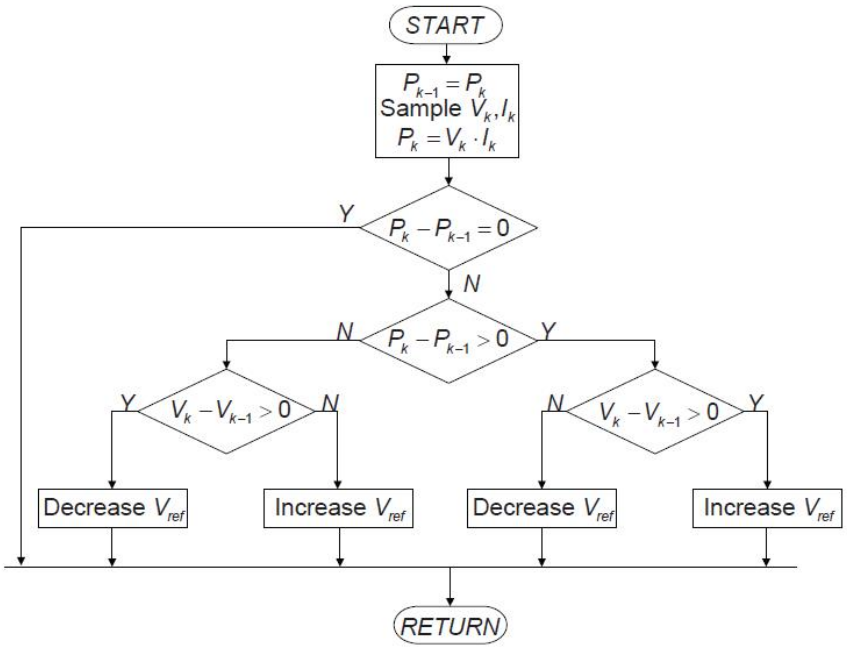

Figure 2.16: Flow chart of P and O algorithm

Despite the remarkable advantage of the ease of implementation, P and O algorithm has two major drawbacks.

1. It oscillates around the MPP in steady state operation.
2. Under rapidly varying atmospheric conditions, it can also go in the wrong direction

-Incremental conductance (IncCond) [47], [48]
Incremental Conductance algorithm is based on differentiation of the PV power in respect to its voltage, and when reaching condition of zero slope of $P-V$, it is considered that the curve is on the maximum power point (MPP). Indeed, differencing PV power and replacing in equation(2.1)

$$\frac{dP}{dV} = \frac{dIV}{dV} = I + V\frac{dI}{dV} \tag{2.1}$$

From equation (2.1) and taking into account the basic condition of zero slope of $P-V$ curve, equation (2.2) is deduced:

$$\frac{dP}{dV} = 0$$

$$I + V\frac{dI}{dV} = 0$$

$$-I/V = \frac{dI}{dV} \tag{2.2}$$

$-I/V$represents the opposite of instantaneous conductance of PV cells and $\frac{dI}{dV}$ the incremental conductance.

According to equation (2.2) these two quantities must be equal in MPP. Moreover if one considers the PV curve, in the right of the MPP it is true that $\frac{dI}{dV} < -\frac{I}{V}$, thus a reduction in PV's voltage is essential to achieve MPP. Similarly, in the left of MPP it is true that $\frac{dI}{dV} > -\frac{I}{V}$, thus an increase in PV's voltage is essential to achieve MPP. These changes in PV's voltage may be done by coupling a DC/DC converter to PV and controlling properly its duty cycle u. Most common used DC/DC converters in MPPT are the buck and boost, due to easy usage of duty cycle control.

Compared to P and O algorithm, IncCond algorithm can determine where the operating point of PV array is precisely on the $P-V$curve by measuring I and V. Thus, IncCond algorithm can determine if the MPPT has reached the MPP and when to stop perturbing the operating point for keeping the operating point on MPP at steady atmospheric conditions.
Also, incremental conductance can track rapidly increasing and decreasing irradiance and temperature conditions with higher accuracy than perturb and observe. The disadvantage of this algorithm is the increased complexity when compared to perturb and observe. This increases computational time and slows down the sampling frequency of the array voltage and current. Moreover, in practice the equality $\frac{dI}{dV} = -\frac{I}{V}$ is seldom obtained and therefore either a small marginal error has to be allowed, which will limit the sensitivity of the tracker, or it will also show oscillations around the MPP.

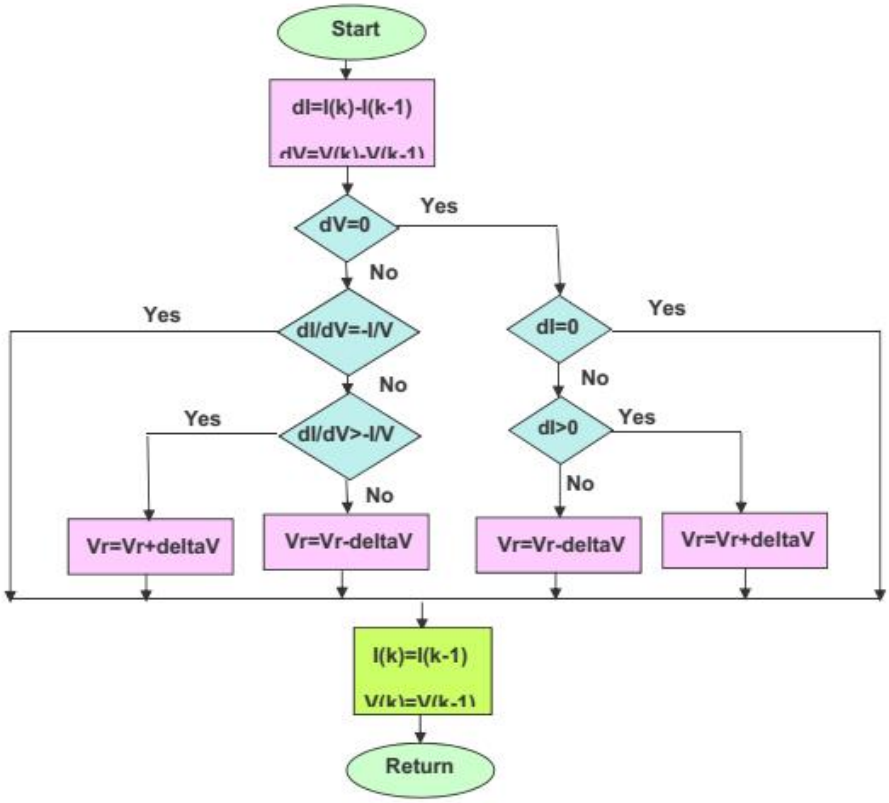

Figure 2.17: Flow chart of IncCond algorithm

- Constant voltage

Constant voltage algorithm makes use of the fact that the MPP voltage changes only slightly with varying irradiances. In this algorithm, the MPPT momentarily sets the PV array current to zero to allow the measurement of the open-circuit voltage V_{oc}. The operating voltage is set to a fixed percentage of the open-circuit voltage. Although the ratio between the MPP voltage and the open-circuit voltage (V_{mp}/V_{oc}) depends on the solar array parameters, a commonly used value for crystalline silicon panels is 76%. This operating point is maintained for a fixed amount of time, after which the cycle is repeated. The main problem with this algorithm is that energy is wasted while the open-circuit voltage is measured, and the MPP voltage V_{mp} is not always at the fixed 76% of the V_{oc} [49], [44].

- Constant current

This algorithm is similar to constant voltage. It operates with current instead of voltage and makes use of the fact that the MPP current is a fixed ratio of the short-circuit current, with a value of $k \approx 0.92$. The tracker sets then periodically the open-circuit voltage of the PV array to zero in order to measure the short-circuit current and then sets the operating point according to this measurement [49], [44].

- Parasitic capacitance

The parasitic capacitance algorithm is a refinement of the incremental conductance algorithm that takes into account the parasitic capacitances of the solar cells in the PV array. To account for the parasitic capacitance, the average ripple in the array power and voltage generated by the switching frequency are measured using a series of filters and multipliers and then used to calculate the array conductance. The incremental conductance algorithm is then used to determine the direction to move the operating point of the MPPT. One disadvantage of this algorithm is that the parasitic capacitance in each module is very small, and will only come into play in large PV arrays with several module strings in parallel. Also, the input capacitor of a DC/DC converter may mask the overall effects of the parasitic capacitance of the PV array [49], [44].

- Fuzzy logic and other semi-heuristic algorithms

Since the PV array exhibits a non-linear $I-V$ and $P-V$ characteristic, its MPP varies with the irradiance and temperature. Some algorithms such as fuzzy logic or artificial neural network control with non-linear and adaptive nature fit the PV control. By knowledge-based fuzzy rules, fuzzy control can track maximum power point by searching the corresponding control of the captured operating values out of a pre-established logic rule table. A neural network control operates like a black box model, requiring no detailed information about the PV system. After learning relation between V_{mp} and V_{oc} or irradiance and temperature, the neural network control can track the maximum power point online. The disadvantage of these controls is the high cost of implementation owing to complex algorithms that usually need a DSP as their computing platform [49], [44].

MPPT Implementation

The algorithm used in this thesis is Incremental Conductance (IncCond) that is as commonly used as Perturb and Observe in the photovoltaic and offers better performance than Perturb and Observe.

Another advantage to be developed of IncCond algorithm is that it is possible to change the tracking speed of reference operating voltage Δv. When the operating point is far from MPP, a faster regulation of MPPT, which means a bigger Δv is used to increase the speed of attaining MPP. When the operating point is around the MPP, a smaller Δv is used to increase the accuracy of the tracking. As the location of the operating point on the $P-V$ curve can be well tracked by IncCond algorithm, the distance to MPP can be determined as well. Thus, it's possible to develop the regulation of Δv . In this thesis, only constant variation of reference operating voltage Δv is applied. The simulation results of MPPT will be presented in the following simulation chapters.

2.10.4 Braking Energy Recovery System

Introduction

Most trains are now equipped with a regenerative braking system that converts the braking energy into electrical energy. This electrical energy can be either stored on board or injected back into the overhead lines. For trains running on DC power this energy cannot be returned to the grid as the AC/DC power supply systems are unidirectional. So in case there's no other train close by, which consumes this energy or the on board energy storage system is full, than it will automatically switch over to rheostatic braking (i.e. the generated electrical power is dissipated as heat in brake grid resistors).
It is then interesting to provide a system that allows the regenerative braking system to return the energy back to the grid or to be stored in a fixed Energy Storage System (EES) in order to avoid wasting this energy ([2], [8]).

Braking Energy Recovery System - Grid

The braking energy recovery system consists basically of a DC/AC converter which can be connected in parallel to an existing substation.

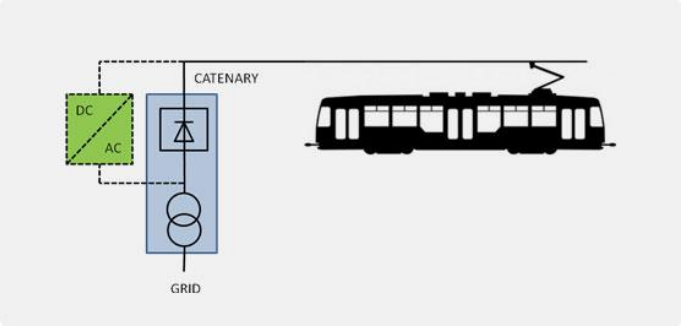

Figure 2.18: braking energy recovery system

Another configuration is a system that consists of a DC/DC converter with an Energy Storage System which permits to store the energy locally instead of returning the energy back to the grid.

When installed in traction substations, its reversibility is possible, allowing for the transmission of recovered energy to the main distribution grid into the storage system [50]. Studies carried out show that a saving of 30% to 50% of the energy consumed by the system can be achieved.

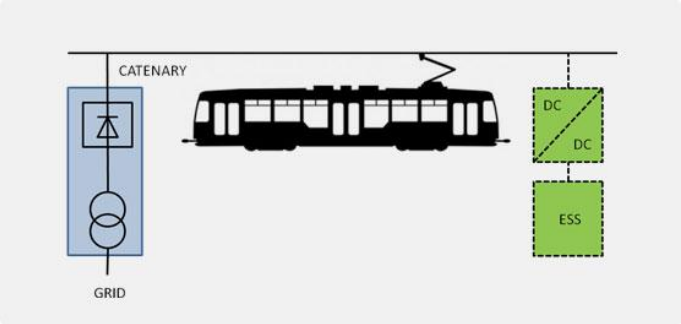

Figure 2.19: braking energy recovery system with storage

The train residual braking energy shown in figure 2.20 is strongly time-varying with several high peaks, and needs to be dealt with properly to ensure that electrical devices connected to the grid don't receive too few or too much power [51].

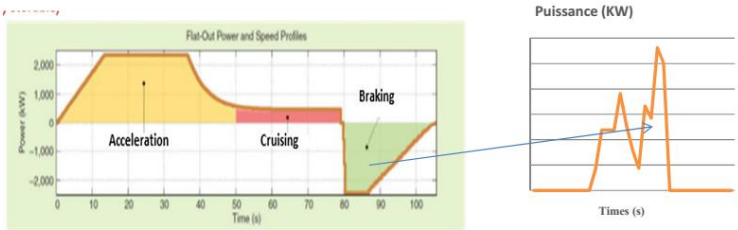

Figure 2.20: Power Profile of braking energy recovery system

2.10.5 Energy Storage System

Storage: Characteristics, Uses

It is desired to clipping consumption by optimizing the use of photovoltaic by integrating a storage element. The power mismatch between generation and demand must be stored or delivered. It varies to a large extend, therefore the Energy Storage System will act as a slack-node, which means that it will cover the difference. This is limited to the capacities of the system [52]. The characteristics that classify an ESS are [53]:

- Energy Density/Capacity
- Power Rating/Capability
- Duration of effective operation/Rate of discharge

The selection of a certain type of device suiting a given need must be done according to those cited above. Some advantages of each energy storage device will be briefly described but not discussed further in details.

2.10.6 Energy storage technologies

Supercapacitors

They're built up with modules of single cells connected in series and packed with adjacent modules connected in parallel [53]. The capacitance and energy density of these devices is thousands of times larger than electrolytic capacitors [54].

$$W_C = \frac{1}{2}CV^2 \tag{2.3}$$

Advantages:

- Very high rates of charge and discharge
- Light weight and low toxicity
- No charge/discharge memory effects, therefore it has good reversibility and high cycle efficiency, allowing hundreds of thousands of cycles.

Disadvantages:

- Low energy density
- The cell voltage is a function of the energy stored

Superconducting Magnetic Energy Storage - SMES

Superconducting Magnetic Energy Storage (SMES) systems store energy in the magnetic field created by the flow of direct current in a superconducting coil which has been cryogenically cooled to a temperature below its superconducting critical temperature. A typical SMES system includes three parts: superconducting coil, power conditioning system and cryogenically cooled refrigerator. Once the superconducting coil is charged, the current will not decay and the magnetic energy can be stored indefinitely. The stored

energy can be released back to the network by discharging the coil [55].

Advantages:

- Capable of storing and discharging large amount of power.
- High efficiency.
- Quick response time.
- Completely static and robust construction.
- Very low maintenance.

Disadvantages:

- Need large amount of power to keep the coil at low temperature.
- The initial setup cost is high.
- Mechanical stability problem.

Flywheel Energy Storage System (FESS)

Flywheels store energy in the form of the angular momentum of a spinning mass, called a rotor. Flywheels store energy in a rotating mass.

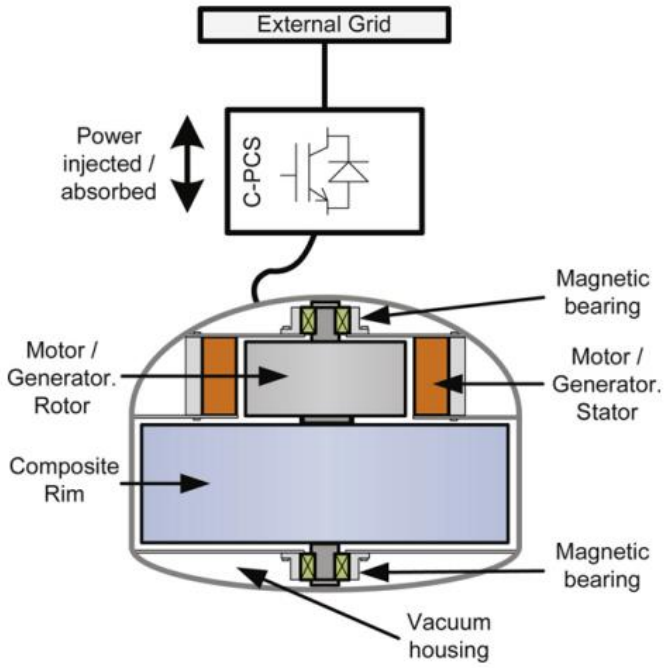

Figure 2.21: Topology of Flywheel Energy Storage System

The work done to spin the mass is stored in the form of kinetic energy. A flywheel system transfers kinetic energy into electric power through the use of controls and power conversion systems. Flywheels can respond rapidly, both as a source and sink for electricity, making them a valuable resource for frequency regulation in electric power grids.

Flywheels are one of the most cost effective storage technologies for high power (rapid discharge) applications, where they compete directly with batteries [55].

The rapid charging and discharging characteristics of flywheels, and their ability to cycle hundreds of thousands of times with minimal performance degradation, make them ideally suited to provide power quality and frequency regulation to electric grids [56].

Electrochemical storage,Battery

1. Lead Acid Battery The Lead Acid Battery (LAB) will be mentioned in the study as, even if they will not be used, they have been used deeply in the past, and remain the base of further research. Its functioning has been mastered over a century of development. In the Lead-Acid type, the charge process leads to a reform of the sulfuric acid of the electrolyte as follows [57]:

   $$SO_4 + 2H^+ \Rightarrow H_2SO_4$$

   The equation for the recharge reaction is as follows:

   $$2PbSO_4 + 2H_2O \Rightarrow PbO_2 + 2H_2SO_4 + Pb$$

   Valid for both plates and electrolyte.
   Advantages:

   - Robust (tolerant to abuse)
   - Tolerant to overcharging
   - Low internal impedance
   - Able to deliver very high currents

   Disadvantages:

   - They're quite heavy and bulky
   - Limited efficiency
   - Danger of overheating during charging
   - Not suitable for fast charging
   - Sulfating process

2. Sodium–Sulfur battery - NAS
   The placement of the electrodes in the battery is as follows, sulfur at the positive electrode and as outer layer while the interior that will be the negative electrode is made up by sodium. These two will be separated by the beta alumina tube that, while being ceramic, allows the conduction of sodium ions. The battery is hermetically sealed under the condition that the active materials at both electrodes are liquid and its electrolyte is solid.

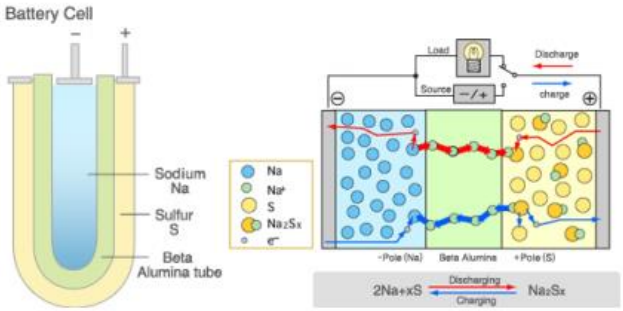

Figure 2.22: NAS Diagram

Manufacturing of such top performance isolators is one of the main characteristics of the Japanese provider [58].

If a load is connected to the terminals, electric power is discharged through the load. During the discharge, sodium ions converted from sodium in a negative electrode pass through solid electrolyte then reach to sulfur in positive electrode. The electrons finally flow to outside circuits. The electric power is generated by such current flow. With the progress of the discharge, sodium polysulfide is formed in positive electrode; on the contrary, sodium in negative electrode will decrease by consumption. During the charge, the electric power supplied from the outside will form sodium in the negative electrode and sulfur in the positive one by following the reverse process of the discharge. The energy will then be restored in the battery. By applying Beta alumina for its solid electrolyte, the NAS battery is free from secondary reaction due to charge/discharge. In addition, the thermal energy loss caused by internal resistance is used to keep the battery warm. As a result, the NAS battery can obtain high efficiency [56].

3. Nickel-Cadmium battery Ni-Cd
   It uses nickel hydroxide as the active material for the positive plate and cadmium hydroxide for the negative plate.

   A potassium hydroxide aqueous solution is used as electrolyte. It contains small quantities of lithium hydroxide to improve life cycle and high temperature operation.

   This electrolyte is only used for ion transfer; it is not chemically changed or degraded during the charging cycles, The support structure of both plates is steel, which is unaffected by the electrolyte and does not corrode.

   On the charge process, a water loss occurs until the cell potential rises to a level where hydrogen is evolved at the negative plate and oxygen at the positive plate.

   Unlike LAB, little change in the electrolyte density occurs during charge and discharge. Therefore, large reserves of electrolyte can be used without inconvenience to the electrochemistry of the couple, leading to a more stable behavior, longer life, and a greater resistance against adverse conditions.

   Ni-Cd batteries have a higher energy density and longer life cycle than lead acid batteries but are inferior to chemistries such as Li-ion and Ni-MH [56].

4. Lithium battery Li
   The lithium ions move between the anode and cathode to produce a current flow [56]. The cathode in these batteries is a lithiated metal oxide and the anode is made of graphitic carbon with a layer structure. The electrolyte is made up of lithium salts dissolved in organic carbonates. When the battery is being charged, the lithium atoms in the cathode become ions and migrate through the electrolyte toward the carbon anode where it combines with external electrons and are deposited between carbon layers as lithium atoms. This process is reversed during discharge [58].
   The cell of this battery can be operated with higher current level than other cells, but some problems have to be solved. The internal resistance can produce internal heat-up and failure. Therefore, to ensure safe operation, it is mandatory to use a battery management system to at least provide overvoltage, undervoltage, overtemperature, and overcurrent protection [56].
   Advantages:
   - Weight much lower than Ni-Cd or Ni-Mh.
   - Low-polluting and recyclable
   - High Voltage
   - High energy density
   - No memory effect

   Disadvantages:
   - Cost

5. Flow Batteries
   Flow batteries store and release energy through a reversible electrochemical reaction between two electrolytes. There are four types of flow battery currently being produced or in the late stages of development; zinc bromine, vanadium redox (VRB), polysulphide bromide and cerium zinc. The zinc-bromine system - developed by ZBB Energy Corp in the USA - represents a type of hybrid flow battery. A leading form of the vanadium redox flow battery is a system by VRB Power Systems Inc in Canada. These systems feature the separation of chemical reactants from the electrochemical cells through which charging and discharging take place. The storage capacity is dependent upon the size of the electrolyte tanks whilst the power output is dependent upon the size of the fuel cell. The vanadium redox system has an advantage over the hybrid system as the discharge time at full power can be varied.

   Energy Density Discharge Time: VRBs can be fully discharged without reducing life expectancy. A VRB in Sapporo, Japan has undergone around 14000 discharge cycles, this gives it a competitive advantage over many other storage technologies [59].

   The main advantages of the technology include the following:
   - high power and energy capacity;

- fast recharge by replacing exhaust electrolyte;
- long life enabled by easy electrolyte replacement;
- full discharge capability;
- use of nontoxic materials;
- low-temperature operation.

The main disadvantage of the system is the need for moving mechanical parts such as pumping systems that make system miniaturization difficult. Therefore, the commercial uptake to date has been limited.

6. Metal-Air Batteries
   In common with other advanced battery systems, metal-air batteries are electrochemical cells. Metal-air batteries are the most compact batteries available according to the Energy Storage Association [(ESA, 2007)].
   The advantage of Metal-Air Batteries are the Energy Density and Discharge Time. Energy densities for metal air batteries can be high covering the range $110-420 Wh/kg$. The most significant disadvantage of metal-air batteries is the inefficient electrical recharging leading to a typical charge/discharge efficiency of around 50%.

Comparison

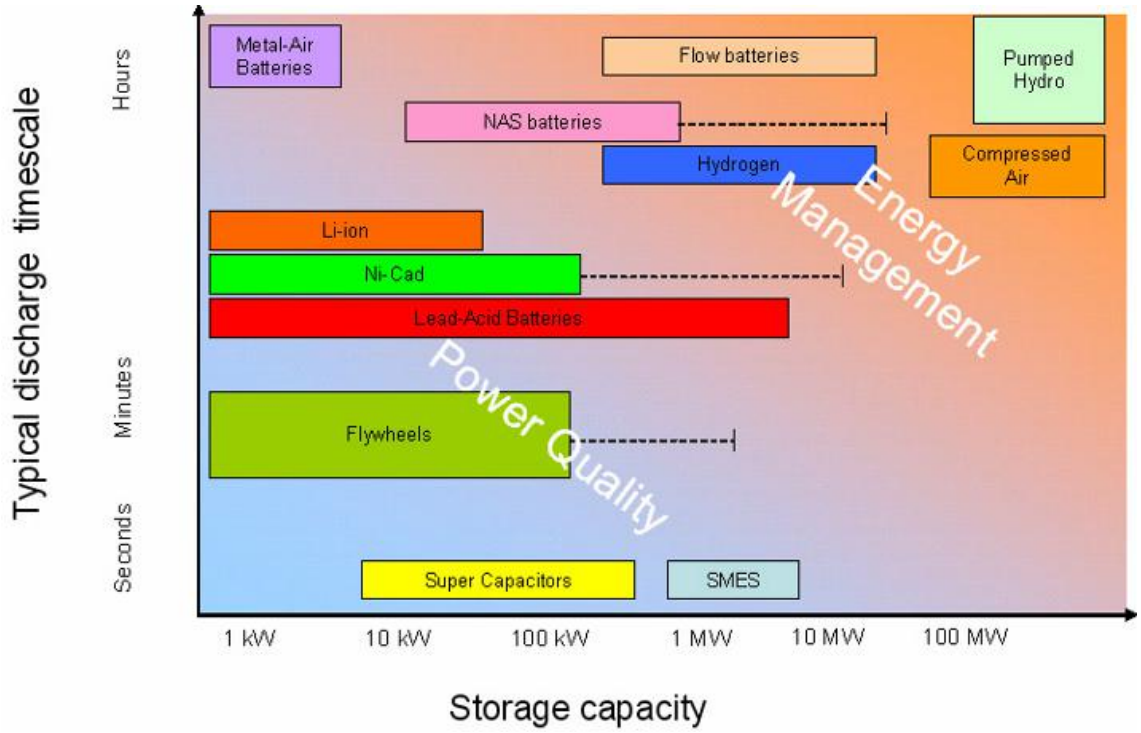

Figure 2.23: Typical storage capacity versus discharge

Batteries are a worldwide well known component with many suppliers which makes prices more competitive and can even be designed to supply a short-duration and a high

power load. This won't be the approach, as supercapacitors are rather used for that, knowing that a reduction in the remaining capacity and lifetime would take place when a battery is operating under high fluctuations.

Nevertheless, the main principle for designing high-power batteries would be to consider that these batteries discharge a high percentage of their stored energy in a short period of time. In contrast, batteries of a lower power can deliver more energy but only if they are discharged during a long period of time. The Peukert's Law describes the phenomenon:

$$C_P = I^N t$$

where C_p is the nominal capacity $[Ah]$, I is the discharge current $[A]$, t is the time of discharge $[h]$, and N is the Peukert's constant w. The ideal value is 1, that would mean that the actual capacity was independent from the current.

Technology	Lead Acid Batteries	NaS Batteries	Supercapacitor
Charge Time Scale	$1-5h.$ $5-20h.$	$30s$ to $7h.$	0.3 to $30s.$
Life Cycle	$500-1000$ times	$+4500$ times	1 million times
Operating Temperature	-20 to $+65^0C$	$+300^0C$	-40 to $+75^0C$
Cell Operating Voltage	1.25 to $3.6V$	$2V$	$2.5V$
Capacitance	N/A	N/A	$0.1-1000F$ $350-2700F$
Power Density	0.005 to $0.4KW/kg$	$0.01KW/kg$	0.01 to $10.3KW/kg$
Energy Density	8 to $600Wh/kg$	170 to $400Wh/kg$	0.05 to $10Wh/kg$
Round Trip Efficiency	$63-80\%$	$89-95\%$	$85-98\%$
Pulse Load	0.5 to $50A$	20 to $80A$	0.1 to $100A$

Table 2.1: Bateries and Supercapacitors Characteristics Comparison

in view what was cited previously the energy Density, Power Rating and Rate of discharge of the storage device depends on their technology, this is why we choose two different technologies, one that ensures energy Density, the second assure Power Rating as battery and Supercapacitor.

2.10.7 Power electronic converters

The role of power electronic converters is to provide power to the user in a suitable form at high efficiency. Power electronic converters are needed in PV systems to convert DC voltage to the required values and to convert from DC to AC and vice versa [47], [60], [61], [62]. In addition they control the charging and discharging of batteries in systems where batteries are storage elements.

Buck converter

A Buck converter is a step down DC/DC converter consisting mainly of an inductance and two switches (usually a transistor and a diode) for controlling the inductance. It switches between connection of inductance to source voltage to accumulate energy and then discharging the inductance's energy to the load [63].

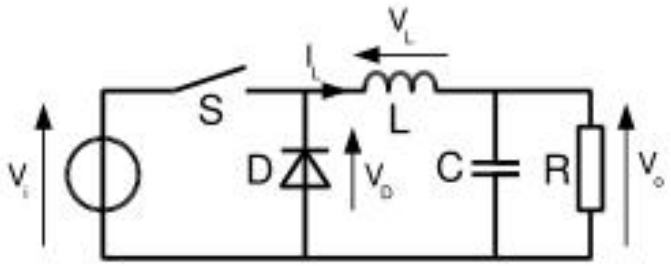

Figure 2.24: Functional circuit of a buck converter

When the switch pictured above is closed (i.e. On-state), the voltage across the inductance is:

$$V_L = V_1 - V_0 \tag{2.4}$$

The current flowing through the inductance linearly rises. The diode doesn't allow current to flow through it, since it is reverse-biased by voltage V.

For Off Case (i.e. when switch pictured above is opened), diode is forward biased and voltage is $V_L = -V_0$ (neglecting drop across diode) across inductance. The inductance current which was rising in ON case, now decreases.
Computing the integral of the inductance voltage over one time period to zero yields.

$$\int_T^0 V_L dt = \int_{t.on}^0 V_L dt + \int_{t.off}^0 V_L dt = 0 \tag{2.5}$$

$$\int_{t.on}^0 (V_1 - V_0) dt + \int_{t.off}^0 (-V_0) dt = 0 \tag{2.6}$$

$$(V_1 - V_0)\alpha T + (-V_0)(1-\alpha)T = 0 \leftrightarrow V_0 = \alpha V_1 \tag{2.7}$$

where α is the duty cycle.

From this equation, it can be seen that the output voltage of the converter varies linearly with the duty cycle for a given input voltage. As the duty cycle α is equal to the ratio between t_{on} and the period T, it cannot be more than 1. This is why this converter is referred to as step-down converter.

Boost converter

A boost converter (step-up converter), as its name suggests steps up the input DC voltage value to the output. This converter contains basically a diode and a transistor as switches and at least one energy storage element. Capacitors are generally added to output so as to perform the function of removing output voltage ripple and sometimes inductances are also combined with [63].

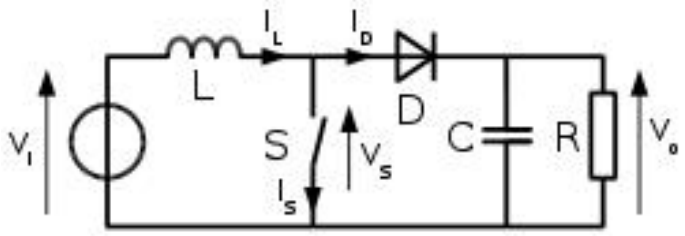

Figure 2.25: Functional circuit of a boost converter

The basic principle of a Boost converter consists of two distinct states - in the On-state, the switch S is closed, resulting in an increase in the inductor current and then $V_L = V_1$. In the Off-state, the switch is open and the only path offered to inductor current is through the flyback diode D, the capacitor C and the load R. This results in transferring the energy accumulated during the On-state into the capacitor, and then $V_L = V_1 - V_0$. Equating the integral of the inductor voltage over one time period to zero yields.

$$\int_T^0 V_L dt = \int_{t.on}^0 V_L dt + \int_{t.off}^0 V_L dt = 0 \tag{2.8}$$

$$\int_{t.on}^0 (V_1) dt + \int_{t.off}^0 (V_1 - V_0) dt = 0 \tag{2.9}$$

$$(V_1)\alpha T + (V_1 - V_0)(1-\alpha)T = 0 \leftrightarrow V_0 = \frac{1}{(1-\alpha)} V_1 \tag{2.10}$$

where α is the duty cycle. From the above expression it can be seen that the output voltage is always higher than the input voltage as the duty cycle goes from 0 to 1, and that it increases with α, theoretically to infinity as α approaches 1. This is why this converter is sometimes referred to as a step-up converter.

Inverters

Inverters are electrical devices that convert direct current to alternating current, which may be single or multi-phase. Several topologies exist for both single phase and multi-phase

inverters [63].

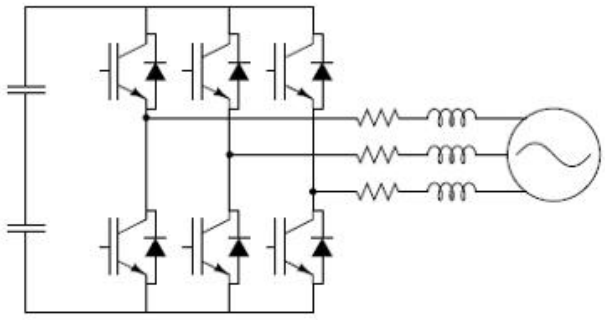

Figure 2.26: Functional circuit of inverter

The converted AC can be at any required voltage and frequency with the use of appropriate transformers, switching, and control circuits. A basic three-phase inverter consists of three single-phase inverter switches each connected to one of the three load terminals. For the most basic control scheme, the operation of the three switches is coordinated so that one switch operates at each 60^0.

2.11 Conclusion

In this Chapter an overview of MicroGrids concept is provided, the existing architectures are detailed An introduction about the problematic of integration distribued generation in the grid are discussed, as well as a description of the different pieces of MicroGrid ,the Photovoltaic systems are discussed, different technologies of storage component are developed ,function of power electronics interface module are explained .and the utilized controls strategies in MicroGrids are detailed. And finally we have introduced the components of the considered MicroGrid. This chapter makes preparations for the system modeling in the following chapter.

Chapter 3

Modeling of MicroGrid

3.1 Introduction

A MicroGrid as seen in previous chapter is composed by different elements. In general, one can classify them among sources, loads, storage and interconnection to other grids. In this thesis the main focus is on urban MicroGrids, so the main considered source will be photovoltaic panels (PV).

This chapter will give methodology of appropriate modelling of DC MicroGrid in order to design control synthesis and stability analysis.

The different components of a MicroGrid will be mathematically modelled and the operating principles of DC/DC converters will be described. For this we will use the averaging modelling approach to develop the dynamical model of the system. Finally it will be presented the validation of the models of different operational components by Matlab/Simulink simulations.
The complete model of a classical MicroGrid based on photovoltaic arrays, their Maximum Power Point Tracking (MPPT) algorithms, the different technologies for storage systems using different time scales and the different topologies of power converters will be analyzed in order to design control algorithms that will be able to assure stability of the overal system.

3.2 Photovoltaic System

3.2.1 Solar cell modeling

Introduction

To determine the characteristics of the solar cell, the power vs. voltage (PV) and current vs. voltage (IV) curves must be constructed. Current is measured at the output when the cell is short-circuited. From these curves the maximum power point (MPP) can be ascertained [41], [64], [65], [66].

Solar cell model

This model is composed by a current source, a parallel diode, a shunt resistance and a series resistance. A current generator is used for modeling the incident luminous flux, a single diode for the cell polarization phenomena, and two resistors for the losses. The model of an individual cell has been depicted in Figure 3.1, where:

- I_{ph} is the photocurrent generated by solar irradiance (A)
- I_d is the current passing through diode (A)
- I_{sh} is the current passing through parallel resistance (A)
- I is the output current of solar cell (A)
- V is the output voltage of solar cell (V)
- R_{sh} represents the loss of dissipative effect of the cell (Ω)
- R_s represents the junction resistance (Ω)

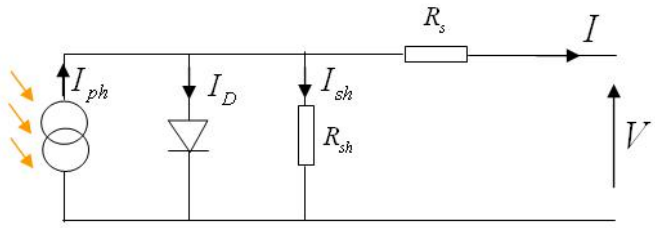

Figure 3.1: Equivalent circuit model of solar cell

The characteristic equation of the real cell is then given by:

$$I = Iph - I_d - I_{sh} \tag{3.1}$$

- Photocurrent I_{ph}, [67], [68]

The photocurrent mainly depends on the solar irradiance and the cell's working temperature, which is described as:

$$Iph = [I_{sc} + K_0(T - T_{nom})]\frac{G}{G_{nom}} \tag{3.2}$$

where:

- I_{sc} is the short-circuit current (A) given by the solar cell supplier at standard condition (25^0C and $1000W/m^2$)
- T_{nom} is the cell's reference temperature which is 25^0C at standard condition
- $G_{nom}$is the cell's reference working irradiance which is $1000W/m^2$ at standard condition
- T is the cell's working temperature (^0C) that depends on both the ambient temperature (T_a) and the local irradiance (G) explained in Equation (3.3)
- G is the local irradiance on the cell surface

- K_0 is an experimental coefficient given by $K_0 = 3mA/^0C$, which explains that for a constant irradiance, the short-circuit current increases $3mA$ for 1^0C increment of the ambient temperature

The proposed experimental relation between short-circuit current and environmental conditions shows that for an uniform ambient temperature, the photocurrent I_{ph} varies proportionately with the local irradiance G while the influence of ambient temperature is limited for an uniform irradiance.

Cell's working temperature is different from the ambient temperature and is calculated by the ambient temperature and the local irradiance as below:

$$T - T_a = (\frac{T_{fn} - 20}{800})G \tag{3.3}$$

where:

- T_a is the ambient temperature (^0C)
- T_{fn} is the nominal working temperature given by solar cell suppliers (normally 45^0C)

- Shunt current I_{sh}

The shunt current passing through parallel resistance is easily computed according to Kirchhoff's circuit laws:

$$I_{sh} = \frac{V_p + R_s I_p}{R_{sh}} \tag{3.4}$$

- Bypass current I_d

The current on the diode is calculated according to the Shockley diode ideal equation I_d, modeled as follows:

$$I_d = I_0[e^{(\frac{q(V_p + R_s I_p}{nkT}} - 1] \tag{3.5}$$

where:

- I_0 is the diode saturation current that depends on open circuit voltage $V_{OC}^{'}$ (calculated according to V_{OC} for standard conditions and to local environmental conditions), short circuit current $I_{sc}^{'}$ (given by the cell supplier) and cell working temperature, illustrated by the Equation (3.3)
- n is the ideal factor representing how closely the diode follows the ideal diode equation which depends on the manufacturing, in many cases $n$is assumed to be approximately equal to 1
- k is Boltzman's constant and $k = 1.3810^{-23}J/K$
- q is an electron's charge: $q = 1,610^{-19}C$
- T is the cell's working temperature (^0C)

Moreover, the inverse saturation current of the diode can be defined as shown in equations below:

$$I_0 = \frac{I_{sc}}{\frac{qV_{oc}}{e^{knT}} - 1} \tag{3.6}$$

$$I_0 = I_0(T_1)(\frac{T}{T_1})^{\frac{3}{n}} e^{(\frac{qV_q(T_1)}{nk(\frac{1}{T} - \frac{1}{T_1})})} \tag{3.7}$$

$$I_0(T_1) = \frac{I_{sc}(T_1)}{e^{\frac{qV_{oc}(T_1)}{nkT_1}} - 1} \tag{3.8}$$

The term V_{oc} is obtained by assuming the output current equal to zero, which means that $I = 0$ in Equation (3.6).

- Output current I_p and I_{ph} [67], [68]

Replacing equations (3.4), (3.5) and (3.8) in general equation (3.2) establishes a unique model of the solar cell represented by equation (3.9).

$$I = I_{ph} - I_0[e^{\frac{(V+R_sI)q}{nkT}} - 1] - \frac{(V + R_sI)}{R_{sh}} \tag{3.9}$$

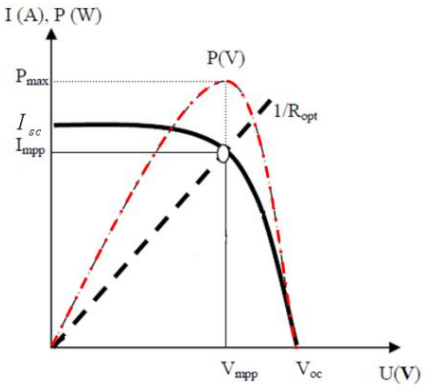

Figure 3.2: Solar cell characteristics

The non-linear characteristics of the output current of a photovoltaic cell are illustrated by the curve $I = f(V)$ in figure (3.2), where: I is given by equation (3.9) and V is the output voltage given by the load.

Series and parallel connection of solar cells

As the output power of a single solar cell of $1m^2$ is around $100W$, it needs to connect several solar cells in series and/or parallel to form a solar panel that is able to achieve the range of desired power output.

Figure (3.3) illustrates the equivalent model of a solar panel with N_S solar cells, whose circuit model is illustrated in Figure (3.1) in series on one branch and N_p branches in parallel. The series connection of solar cells multiplies the output voltage dimension while

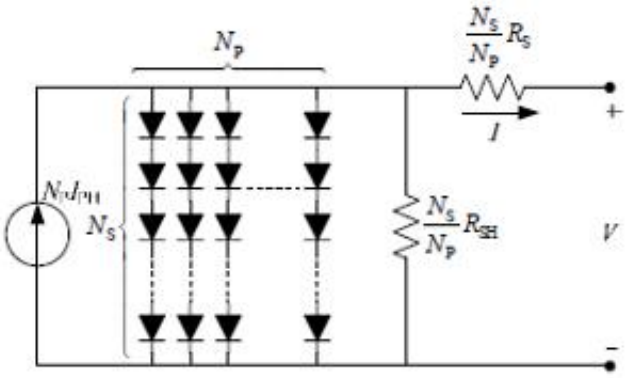

Figure 3.3: Series and parallel connection of solar cells

the parallel connection of solar cells multiplies the output current dimension. The series-parallel connection enables a desired high power of the solar panel [67].

When there are N_S solar cells in series on one branch, the equivalent series resistance of each branch equals $N_S R_S$ and the equivalent resistance of a panel with N_p in parallel equals $\frac{N_S R_S}{N_p}$.

It goes the same for shunt resistance, the equivalent of which is $\frac{N_S R_{sh}}{N_p}$. According to the equivalence of resistance, the complete solar panel model with series-parallel connection is presented as follows:

$$I_{PV} = N_P I_{ph} - N_P I_0 [e^{\frac{(V_{PV} + \frac{N_S R_S}{N_P} I_{PV}) q}{nkT}} - 1] - \frac{V_{PV} + I_{PV} \frac{N_S R_S}{N_P}}{\frac{N_S R_{sh}}{N_P}} \tag{3.10}$$

Given the presented solar panel model, the characteristics of photovoltaic panels are easy to be simulated in Matlab/Simulink. Once the panel is installed or its physical parameters are decided, the output current depends only on three external inputs of the panel: load voltage (V), ambient temperature (T) and irradiance (G).

3.2.2 Constitution of a photovoltaic generator (PVG)

The combination of several PV cells in series / parallel results in a PVG. If the cells are connected in series, the voltages of each cell are added, increasing the total voltage of the generator. On the other hand, if the cells are connected in parallel, the current will increase [68].

Most commercial PV panels are made up of sub-networks of cells connected in series. Each of these sub-networks is itself made up of a group of PV cells connected in series. The number of cells per sub-networks is the result of a compromise between protection and economic losses of an important part of PVG in the event of partial fault [67].

The transition from one module to a panel is made by adding protection diodes, in series to prevent reverse current flow and in parallel, called by-pass diode, which act in case of imbalance in a set of cells to limit the reverse voltage across the terminals of this set and minimize the consequent loss of production.

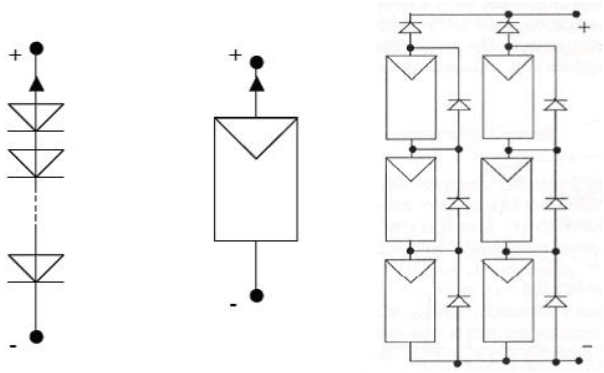

Figure 3.4: PV Array

3.2.3 Maximum power point tracking

Maximum power point tracking, frequently refereed as MPPT, is an optimization algorithm that frequently adjusts the electrical operating point of the modules so that the photovoltaic modules are able to deliver maximum available power [43],[44].

MPPT (Incremental Conductance) Implementation

The algorithm used in this thesis is Incremental Conductance (IncCond) that is as commonly used as Perturb and Observe in the photovoltaic and offers better performance than Perturb and Observe.

Another advantage to be developed of IncCond algorithm is that it is possible to change the tracking speed of reference operating voltage Δv. When the operating point is far from MPP, a faster regulation of MPPT, which means a bigger Δv is used to increase the speed of attaining MPP. When the operating point is around the MPP, a smaller Δv is used to increase the accuracy of the tracking. As the location of the operating point on the $P-V$ curve can be well tracked by IncCond algorithm, the distance to MPP can be determined as well. Thus, it's possible to develop the regulation of Δv . In this thesis, only constant variation of reference operating voltage Δv is applied. The simulation results of MPPT will be presented in the simulation chapters that follow.

We use MPPT in order to extract maximum power from PV array all time. the reference of the PV voltage given by MPPT will be used as the control target.

3.3 Braking Energy Recovery System

Here we introduce the railway electrification system, and the elements used to supply electrical energy to multiple units in the rail station and the railway.

3.3.1 Standard voltages

The range of voltages allowed for rail supply are stated in standards $BSEN50163$ and $IEC60850$ (as seen in [50]).

Electrification System	Lowest non permanent voltage	Lowest permanent voltage	Nominal voltage	Highest permanent voltage	Highest non permanent voltage
$600VDC$	$400V$	$400V$	$600V$	$720V$	$800V$
$750VDC$	$500V$	$500V$	$750V$	$900V$	$1kV$
$1500VDC$	$1000V$	$1000V$	$1500V$	$1800V$	$1950V$
$3kVDC$	$2kV$	$2kV$	$2kV$	$3kV$	$3kV$
$15kVAC$ $16.7HZ$	$11kV$	$12kV$	$15kV$	$17.25kV$	$18kV$
$25kVAC$ $50HZ$	$17.5kV$	$19kV$	$25kV$	$27.5kV$	$29kV$

Table 3.1: Standardized voltages

3.3.2 Contact System

Urban rail systems are powered by electricity either by the use of catenaries (overhead lines) or a third rail placed along the track.

Figure 3.5: Third rail System

Figure 3.6: Overhead line

3.3.3 energy-saving techniques

Figure 3.7 shows some technologies currently used in DC-electrified railway systems to improve energy efficiency by increasing system receptivity. The two main technologies are:

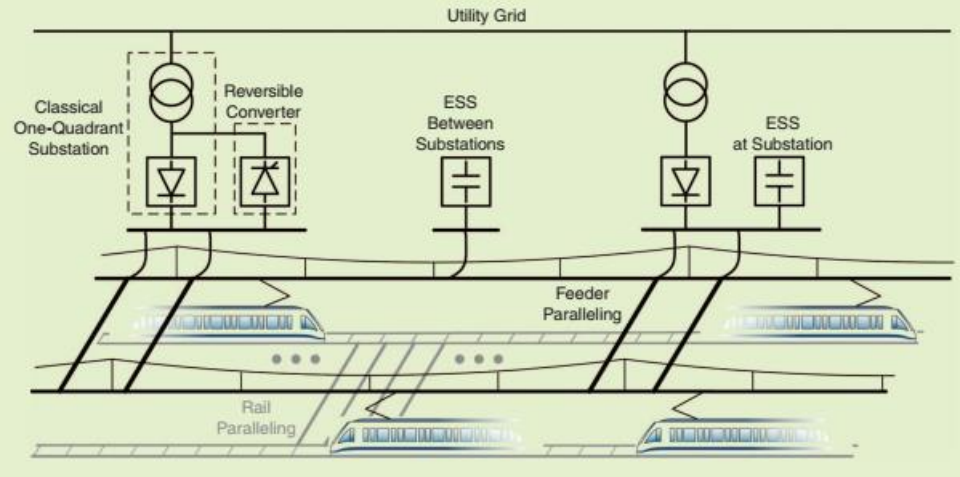

Figure 3.7: Energy-saving techniques in DC-electrified railway systems

- Reversible substations: they make it possible to give occasional energy surpluses back to the utility grid. In practice, this is only useful if the country regulation permits to discount this energy from the total energy bill paid by the railway operator. Indeed, this kind of regulation can be used to promote energy efficiency by using this technique.

- Energy storage System (ESS): they store energy from braking when the system is not receptive and will release it once the network again becomes a power consumer. ESS may be deployed in fixed locations or onboard. Reversible substations may be built using a single bidirectional converter or by adding another converter in parallel with the original one [51].

The braking energy recovery system consists basically of a DC/DC converter which can be connected in parallel to an existing AC/DC one connecting the catenary with the AC grid.

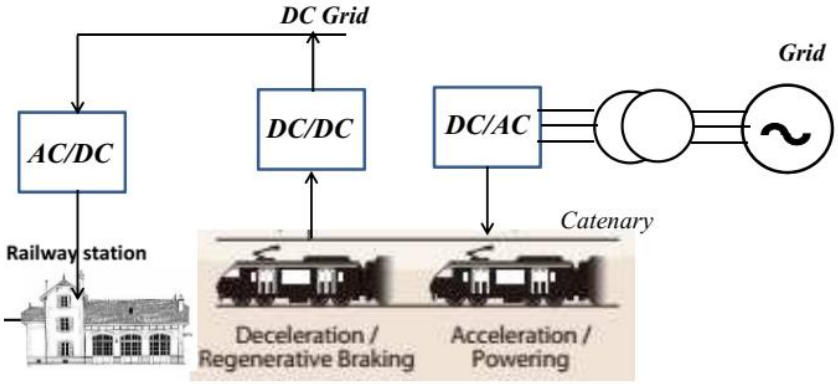

Figure 3.8: Substation Architecture

The train residual braking energy is very time varying with several strong peaks, and need to be dealt with properly to ensure that electrical devices connected to the grid don't receive too little or too much power.

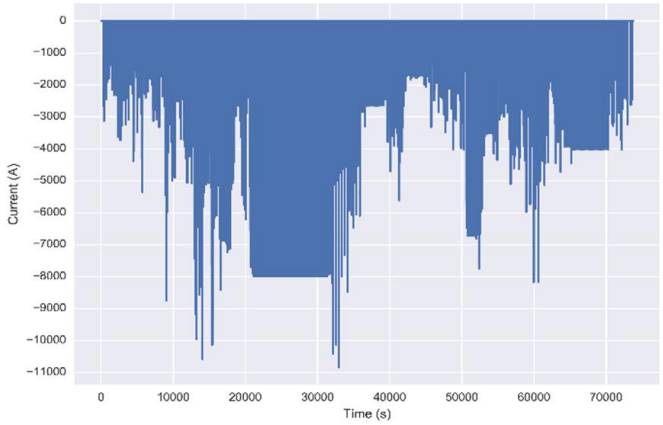

Figure 3.9: Metro line residual braking energy measurement

Figure 3.9 (see [2]) shows measurements on a metro line and gives the power profile versus the running phases of the metro vehicle.

A power peak occurs when the metro is braking, causing a momentary increase of power in the network. The converter role is to recover the exceeding energy from the network

3.4 Energy Storage System

The selection of storage device must take account the energy Density, Power Rating and Rate of discharge.

3.4.1 Hybrid Energy Storage System

Several applications require a combination of energy and power density, but a single energy storage device cannot meet this requirement.

The advantages of the combination of storage devices include:

- Longer battery run time
- Extra backup power
- Easier to meet current specifications
- Allows low/high temperature operation
- Minimizes space requirements and battery size
- Enhances load balancing when used in parallel with a battery

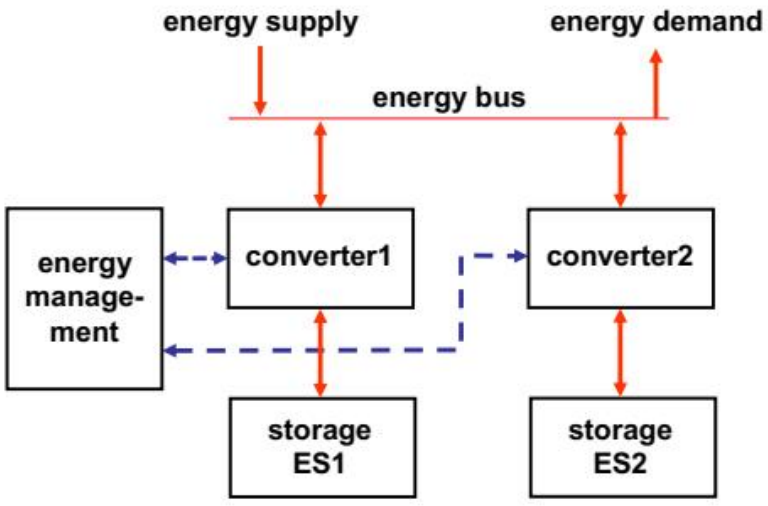

Figure 3.10: Basic structure of a HESS [1].

Two storage systems will be considered in the study: Supercapacitors and Batteries.

3.4.2 Batteries model

Usually, the studies over battery models were led following different hypothesis concerning the internal structure of the battery. Therefore according to each study assumptions, the models of Battery found in the literature are different, what does not mean that they are wrong. The models are empirical; hence there is no "unique" solution in the modeling. The choice of a model depends on which accuracy and which purpose we want to model.

There are many models available for battery modeling, and a few of them are explained here in this section. The merits and demerits of those models and the reason for choosing Thevenin equivalent model are also given in the following.

1. Simple battery model
   The most commonly used battery model is shown in figure (3.11). It consists of an ideal battery with open-circuit voltage V_1, a constant equivalent internal resistance R_{int} and the terminal voltage represented by V_{bat}.
   The battery is known to be a voltage generator. We can see it as a device that absorbs or supplies a user-defined current while always keeping roughly the same voltage. V_{bat} thus acts like a real voltage source.
   The internal resistance accounts for several phenomena:

   - Charge/Discharge resistance: it is associated with the electrolyte resistance, plate resistance, and fluid resistance.
   - Self-discharge resistance: it is the resistance that is associated with the electrolysis of water at high voltage levels and slow leakage across the battery terminal at low voltage.

   The terminal voltage V_{bat} can be obtained from the open circuit measurement, and R_{int} can be measured by connecting a load and measuring both terminal voltage and current, at fully charged condition. While this model seems to be very simple, it does not take into consideration the varying nature of the internal resistance due to temperature, state of charge, and electrolytic concentration. This kind of model is often considered as too rough [69].

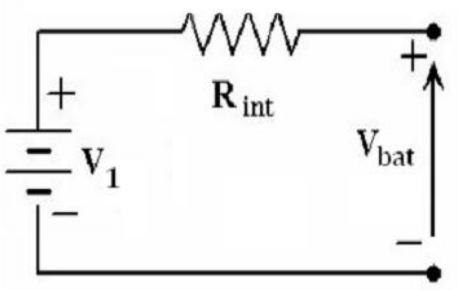

Figure 3.11: Schematic diagram of the Rint model.

2. Resistive Thevenin battery model
   The resistive Thevenin battery model is similar to the model described in the previous subsection but it assumes that the Battery charge and discharge modes are processing a bit differently. This is why two kinds of internal resistances are introduced,R_{ch} and R_{disch}, which are associated with the charging and discharging process of the battery respectively, as it can be seen on figure (3.12).
   These two parameters model all forms of energy loss which include electrical and non-electrical losses. The diodes imply that during charging or discharging, only one

of the resistances R_{ch} or R_{disch} will be used because when one diode is forward biased, the other will be reverse biased. These diodes are present only for modeling purposes and have no physical meaning in the battery (see [69] and [70]). The same thing is done with the open-circuit voltage that is not exactly the same during charge as in the discharge mode.

This model is more complete than the previous one but it does not account for the capacitance effect such as the transient current conditions occurring in the battery [69].

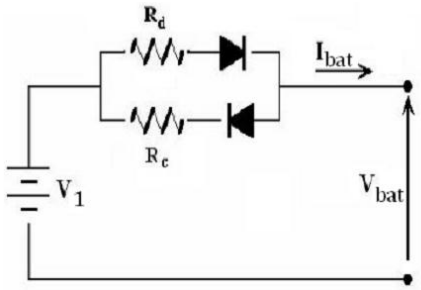

Figure 3.12: Resistive Thevenin battery model scheme

3. Dynamic Thevenin battery model

The transient effects in the battery are taken into account in this dynamic model, figure.(3.13). It shows a polarization capacitance C_{pol}: this is the capacitance due to the chemical diffusion within the battery and does not necessarily represent a purely electrical capacitance. It depends on state of charge, temperature and also the device design [69], [70].

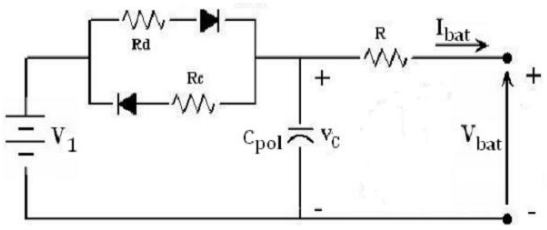

Figure 3.13: Dynamic Thevenin equivalent battery model scheme

The Resistive Thevenin battery model was considered as the best for the type of applications studied in this thesis.

Battery modeling

Simulink model

The chosen model for this study is based on the resistive Thevenin model for the Battery

(3.13). It holds on the estimation of the battery state-of-charge. It differs only in the charge/discharge equivalent resistances.
The central point of battery modeling is to estimate the battery state of charge. Therefore the relation between battery voltage and input current is straightforward.
The Battery is designed like a real voltage generator. The main input quantity is the Battery current I_{bat} and the main output quantity is the Battery voltage V_{bat}. But there is a gap between the knowledge of I_{bat} and V_{bat}. The Battery has a nonlinear relation between these two quantities and the actual state of charge (SOC_n) of the Battery has to be determined first to find the instantaneous value of V_{bat}.
The determination of V_{bat} is done in three steps:

1. first determine the ideal voltage source $V_1 = f(I_{bat}, SOC_{n-1})$
2. at the same time, deduce the output battery voltage $V_{bat} = f(V_1, I_{bat}, R_{int}, SOC_{n-1})$
3. then find the actual real time state of charge $SOC_n = f(V_1, I_{bat}, SOC_{n-1})$.

The algorithm to determine step by step the actual state of charge and terminal voltage of the battery is described in the following scheme:

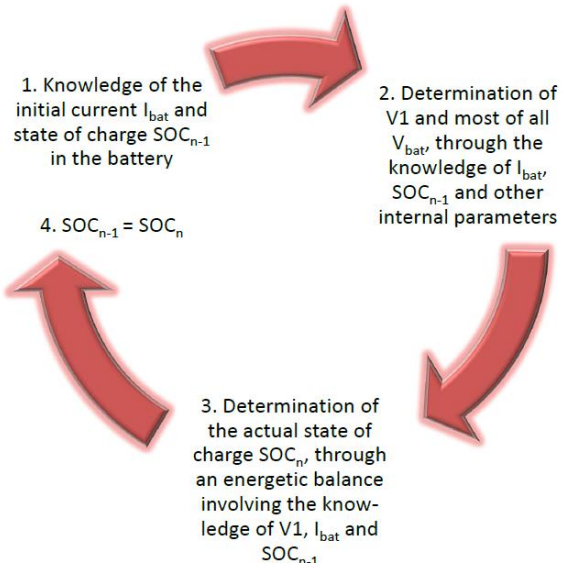

Figure 3.14: Model scheme

The determination is a three step process: [71],[72]

- Step one:
  Voltage delivered by an ideal voltage source V_1. Measures and tests have permitted to give a quite accurate estimation of V_1 as long as we know the actual instant battery state of charge and input current. The equation has to be decomposed in two parts whether: The battery is charging and $V_1 = V_{ch}$.

$$V_{ch} = N_b[1.85{+}0.08SOC{+}(\frac{I_{bat}}{C_{10}})(\frac{6}{1+I_{bat}^{0.86}}{+}\frac{0.48}{1.06-SOC^{1.2}}{+}0.036)(1{-}0.007.\Delta Temp)] \tag{3.11}$$

The battery is discharging and $V_1 = V_{disch}$.

$$V_{disch} = N_b[1.926{+}0.124.SOC{+}(\frac{I_{bat}}{C_{10}})(\frac{4}{1+I_{bat}^{1.3}}{+}\frac{0.27}{1.06-SOC^{1.5}}{+}0.02)(1{-}0.007.\Delta Temp)] \tag{3.12}$$

Where:

- N_b :Number of $2V$ cells in the battery
- SOC_{max} : Maximum battery energy in Wh.
- D : Self-discharge rate of the battery in h^{-1}
- K : Charge/Discharge efficiency of the battery
- Steps/hour: Number of sample periods in an hour ($3600s$.)

- Step two
  State of Charge (SOC) estimation.
  The efficiency of the electromechanical conversion will be taken into account. The energy balance equation is:

$$SOC(t+\Delta t) = SOC(t).(1 - D\frac{\Delta t}{3600}) + K\frac{(V_{bat}.I_{bat} - R_1 I_{bat}^2)}{3600}\Delta t \tag{3.13}$$

  It computes the value of the SOC increment as the energy increment in a differential time, taking into account self-discharge and efficiency.
  The equation can be simplified further by substituting V_{bat} as a function of V_1.

$$SOC(t+\Delta t) = SOC(t).(1 - D\frac{\Delta t}{3600}) + K\frac{(V_{bat}.I_{bat})}{3600}\Delta t \tag{3.14}$$

  Integrating to solve for $SOC(t)$:

$$SOC(t) = SOC(t-1) + \int_t^{t-1} \frac{KV_1 I_{bat}}{3600 SOC_{max}} - \frac{DSOC(u-1)}{3600}du \tag{3.15}$$

  Therefore, the SOC is found through the previous states. Since $SOC(0) = SOC_{init}$, by iteration any $SOC(t)$ can be obtained.

- Step three:

  Expression of V_{bat} This step is an obvious consequence of the two preceding steps. V_{ch} and V_{dich} will come from the same equation from step one. The equations that must be fulfilled are:

$$V_{bat} = V_{ch} + R_{ch} I_{bat} \tag{3.16}$$

$$V_{bat} = V_{disch} + R_{disch} I_{bat} \tag{3.17}$$

Only one of the two expressions must be enabled at a time. That condition will be granted by Charge/Discharge complementary 0 or 1 values out of the I_{bat} relay followed by a NOT logical operator as described in step one.
R_{ch} and R_{disch} are equivalent resistances that model the internal impedance and follow the expressions. Several blocks were used to form the expressions of V_{ch} and V_{dich} as well as R_{ch} and R_{disch}. Resistance expressions are multiplied by I_{bat}. Later on, that product is added to each voltage, which product with the complementary 0/1 coefficient, will uniquely lead to the right value such that when adding both, it will always be the proper voltage plus zero.

3.4.3 Supercapacitor Model

Introduction

The electric behaviour for an electrostatic capacitor is given by equations (3.18) and (3.19).

$$C = \frac{Q}{u_c} = \epsilon \frac{S}{d} \tag{3.18}$$

$$i_c = C \frac{du_C}{dt} \tag{3.19}$$

Where
C is the capacitance of the component in Farads.
Q is the charge in Coulombs.
ϵ is the dielectric constant of the dielectric.
u_c is the electric potential in Volts.
i_c is the current through the capacitor.

These equations describe the electrical behaviour of this component. As we can see on equation (3.18), the voltage applied across the capacitors is directly linked to the charge. And the equation (3.19) shows the link between the current and the voltage across the capacitors. From equation (3.18) we can see that the capacitance is directly linked to the component size. We can define the energy accumulated by the capacitor in eq. (3.20).

$$E_C = \frac{1}{2} C u_c^2 \tag{3.20}$$

Equivalent model

The main work here is to find a simple good model for the supercapacitor behaviour. Models are described by equivalent electrical circuits. Differently from batteries, the supercapacitor model is expressed by electrical equations, easier than batteries.

Supercapacitors as circuit elements
Both engineers and scientists still try to establish electrical schemes and identify their

parameters by identification methods. From the accuracy of these models, it was chosen one in a balance of accuracy and simplicity. An interesting study in [73] details and experiments several models.

- short term model (a few hours)
- long term model (a few days)

These models take into account the dynamic behaviour of the parameters in their environments. However in our case, it was chosen the simplest one. In the following it is provided a list of the different models studied in this thesis.

1. First-order Model

   The first order model designed on (3.15) represents with simplicity the supercapacitor. [73]

   - a single capacitance
   - a parallel resistance

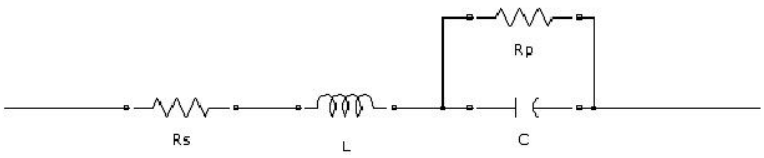

Figure 3.15: Equivalent circuit model of an supercapacitor

   where each element is ideal.

2. Impedance Spectroscopy method
   We can find another model based on complex methods using impedance spectroscopy. In this document it is presented a new approach of modelling the dynamic behaviour of SuperCapacitors. This very accurate method permits to measure the complex impedance of electrochemical cells such as batteries of SuperCapacitors. During the measurement, a small AC current flows through the component and the AC voltage response is measured.
   These experiments take into account the environment during the normal operation of the SuperCapacitor, both temperature and voltage [74].

3. Realistic model
   A simple model for a double-layer capacitor can be represented by a capacitance (C) with an equivalent series resistance (ESR). Even if the previous model could be considered as a realistic model, we can find another one based on transmission line modelling. The following figure shows the equivalent circuit of an supercapacitor using this principle [73]:

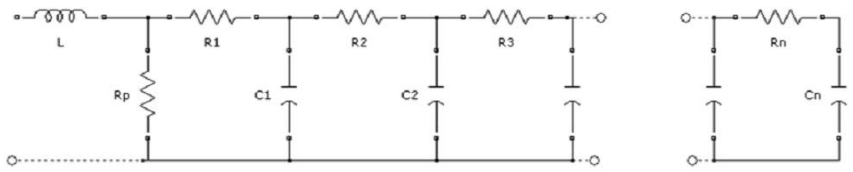

Figure 3.16: Equivalent circuit of an supercapacitor, realistic model

4. The three-branch model

   Extracted from the previous ones some researchers, particularly *Maxwell*, define a model based on transmission line modelling. This three-branch model is 13% more accurate than a Two-branch model. The following figure represents the equivalent circuit of the three-branch model [73]:

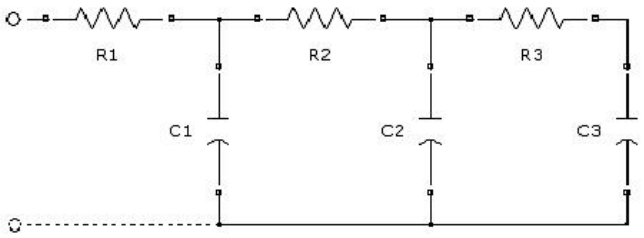

Figure 3.17: Equivalent circuit of a practical supercapacitor, three-branch model

Where:

Parameters	*Values*
R_1	$0.3 \times ESR$
R_2	$0.2 \times ESR$
R_3	$0.5 \times ESR$
C_1	$0.4 \times C$
C_2	$0.414 \times C$
C_3	$0.16 \times C$

Table 3.2: Parameters for the three branch model

5. The chosen model

   We choose the three-branch model (3.17). This model represents a compromise between simplicity and reality [72].

6. Simulink model

   Here it was chosen to develop a model using transfer functions [72]. The three-branch transfer function is:

$$\frac{V_{EES}(S)}{I_{EES}(S)} = \frac{As^2 + BS^2 + Cs + 1}{Cs^3 + Es^2 + Fs} \tag{3.21}$$

Where
$A = C_1C_2C_3R_1R_2R_3$
$B = R_2R_3C_2C_3 + R_1R_3C_1C_3 + R_1R_2C_1C_2 + R_1R_2C_1C_3 + R_1R_3C_2C_3$
$C = C_3R_3 + C_2R_2 + C_1R_1 + C_3R_2 + C_2R_1 + C_3R_1$
$D = C_1C_2C_3R_2R_3$
$E = C_1C_3R_3 + C_1C_2R_2 + C_1C_3R_2 + C_2C_3R_3$
$F = C_1 + C_2 + C_3$

The previous scheme gives us the possibility to obtain the behaviour of the supercapacitor. But it is necessary to integrate the initial conditions of a supercapacitor cell. For this reason it was integrated the initial SOC in the voltage calculation.

First, it is converted the voltage in State Of Charge (image of the voltage) with equation (3.18). It was considered the capacitance as a constant value. Then, it was added this value to the initial SOC, thus obtaining the charge in the supercapacitor. The inverse operation gives the possibility to have the output of the model: the UC voltage.

The model is controlled by power demand. A division by the voltage gives the input value for the model. The supercapacitor behaviour is simpler than batteries, for the U_C, the SOC is directly linked to the voltage, and the voltage is an image of the current through the capacitance.

3.5 Power electronic converters

In this section we will establish the models of the DC/DC converters ,the model of the inverter is not studied it was considered out of the scope of the present thesis.

3.5.1 DC/DC Converter Modeling

DC/DC Converter for PV

Due to the variations of the temperature and solar irradiance, the voltage generated by the PV panel is variable. Thus DC/DC converter is normally needed in a complete photovoltaic system to provide the required voltage by the type of load. To increase the efficiency of the photovoltaic system, it is fundamental that the control of the converter guarantees its operation near to the instantaneous MPP, independent of atmospheric conditions.
In this section, the modelling of a DC/DC converter is presented [75], [76], [77].

Modeling Steps:

- Step1
  A graphical method of constructing an equivalent circuit diagram in MATLAB SIMULINK (Simpower).
- Step 2
  A formal approach (topological model) which consists in extracting the state equations for each possible circuit topology, to create the average model of the converter.

For modeling the switches, it will be considered small resistances (R_{01} and R_{02}) when they are driving, so the conduction losses are taken into account.

Modelling of a BOOST converter
The most commonly used topologies of a DC/DC converter in the PV system are buck and boost converters.in this study we choose boost converter shown in Figure (3.18). It is important to know and control the dynamic behavior of the converter at the varying atmospheric conditions. The major analytical method to model a converter is known as state-variable-averaging method.

The circuit of DC/DC boost converter is presented in Figure (3.18). To further derive the boost converter's mathematical model, it is used the equivalent circuit representation for the two switch states (open and closed switch).

Operating: Considering that the circuit is operating in the first interval, we have the equivalent circuit shown in figure (3.19). When the switch is closed, current flows through the inductance which stores some energy by generating a magnetic field. Polarity of the left side of the inductance is positive.

We select three state variables, the voltages on the capacitors C_1, C_2, and the current in the inductance L_1. Considering that the circuit is functioning in the first interval $[0, u_1T]$,

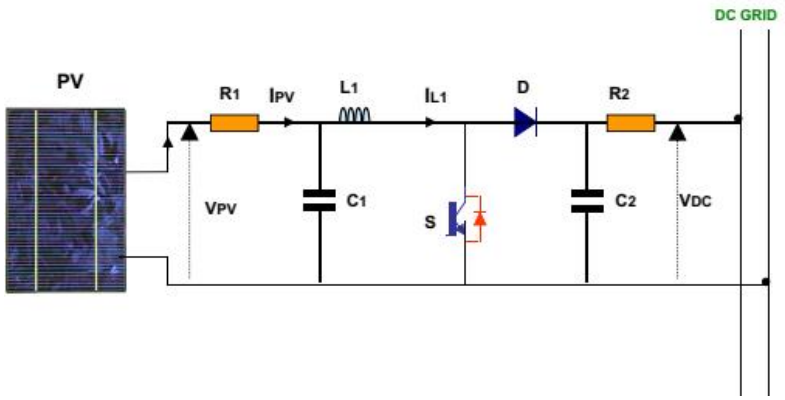

Figure 3.18: DC/DC Boost Converter Circuit

corresponding to duty cycle of PWM driving signal.

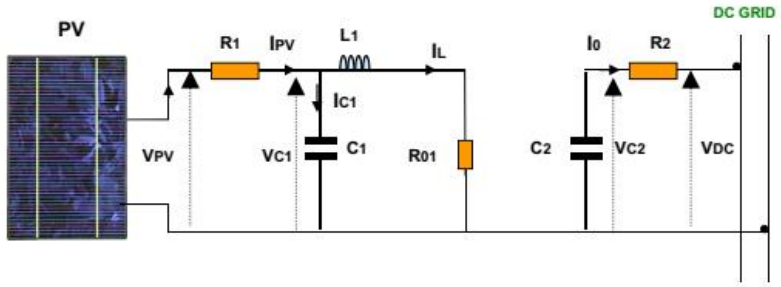

Figure 3.19: The equivalent circuit in interval $[0, u_1 T]$

The following equations can be obtained:

$$\begin{aligned}
\frac{dV_{C1}}{dt} &= -\frac{1}{R_1 C_1} V_{C1} - \frac{1}{C_1} i_{L1} + \frac{1}{R_1 C_1} V_P V \\
\frac{dV_{C2}}{dt} &= -\frac{1}{R_2 C_2} V_{C2} + \frac{1}{R_2 C_2} V_{DC} \\
\frac{di_{L1}}{dt} &= \frac{1}{L_1} V_{C1} - \frac{R_{01} i_{L1}}{L_1}
\end{aligned} \tag{3.22}$$

Therefore, the state space model in the interval $[0, u_1 T]$ can be described by the following equation:

$$\dot{x}(t) = A_1 x + B_1 u \tag{3.23}$$

Where

$$x = \begin{bmatrix} V_{C1} \\ V_{C2} \\ i_{L1} \end{bmatrix} \tag{3.24}$$

$$A_1 = \begin{bmatrix} -\frac{1}{(R_1 C_1)} & 0 & \frac{1}{C_1} \\ 0 & -\frac{1}{(R_2 C_2)} & 0 \\ \frac{1}{L_1} & 0 & \frac{R_{01}}{L_1} \end{bmatrix} \tag{3.25}$$

$$B_1 = \begin{bmatrix} \frac{1}{(R_1C_1)} & 0 \\ 0 & \frac{1}{R_2C_2} \\ 0 & 0 \end{bmatrix} \tag{3.26}$$

$$C_1 = \begin{bmatrix} 0 & 0 & 1 \end{bmatrix} \tag{3.27}$$

In the interval the system's equivalent circuit is depicted in figure (3.20). When the switch is opened, current will be reduced as the impedance is higher. The magnetic field previously created will reduce to maintain the current towards the load. Thus the polarity will be reversed (means left side of inductance will be negative now). As a result, two sources will be in series causing a higher voltage to charge the capacitor through the diode.

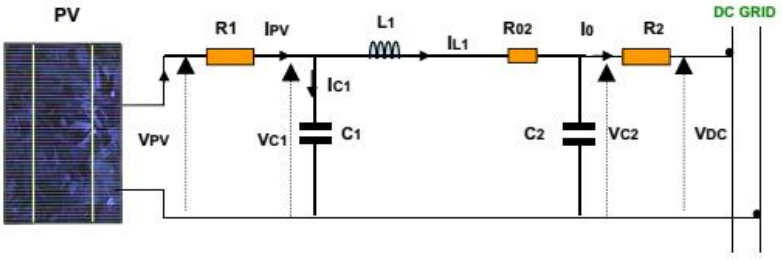

Figure 3.20: The equivalent circuit in interval $[u_1T, T]$

Similarly, the following equations can be obtained:

$$\begin{aligned} \frac{dV_{C1}}{dt} &= -\frac{1}{R_1C_1}V_{C1} - \frac{1}{C_1}i_{L1} + \frac{1}{R_1C_1}V_{PV} \\ \frac{dV_{C2}}{dt} &= -\frac{1}{R_2C_2}V_{C2} + \frac{1}{C_2}i_{L1}\frac{1}{R_2C_2}V_{DC} \\ \frac{di_{L1}}{dt} &= \frac{1}{L_1}V_{C1} - \frac{1}{L_1}V_{C2} - \frac{R_{02}i_{L1}}{L_1} \end{aligned} \tag{3.28}$$

Therefore, the state space model in the interval $[u_1T, T]$ can be described by the following equation:

$$\dot{x}(t) = A_2x + B_2u \tag{3.29}$$

$$A_2 = \begin{bmatrix} -\frac{1}{(R_1C_1)} & 0 & \frac{1}{C_1} \\ 0 & -\frac{1}{(R_2C_2)} & \frac{1}{C_2} \\ \frac{1}{L_1} & -\frac{1}{L_1} & -\frac{R_{02}}{L_1} \end{bmatrix} \tag{3.30}$$

$$B_2 = \begin{bmatrix} \frac{1}{(R_1C_1)} & 0 \\ 0 & \frac{1}{R_2C_2} \\ 0 & 0 \end{bmatrix} \tag{3.31}$$

$$C_2 = \begin{bmatrix} 0 & 0 & 1 \end{bmatrix} \tag{3.32}$$

Finally, based on the power electronics averaging technique [78], the system's state space average model can be expressed as:

$$\begin{aligned}\langle \dot{x} \rangle &= A\langle x \rangle + B\langle U \rangle = [A_1 u + A_2(1-u)]\langle x \rangle + [B_1 U + B_2(1-u)]\langle U \rangle \\ \langle Y \rangle &= C\langle x \rangle = [C_1 u + C_2(1-u)]\langle x \rangle \end{aligned} \tag{3.33}$$

Where $\langle x \rangle$ denotes the system states that have been averaged over one switching cycle. Thus, we have:

$$A = \begin{bmatrix} -\frac{1}{R_1 C_1} & 0 & -\frac{1}{C_1} \\ 0 & -\frac{1}{R_2 C_2} & \frac{(1-u_1)}{C_1} \\ \frac{1}{L_1} & \frac{1}{L_1} & \frac{-u_1 R_{01} - (1-u_1) R_{02}}{L_1} \end{bmatrix} \tag{3.34}$$

$$B = \begin{bmatrix} \frac{1}{R_1 C_1} & 0 \\ 0 & \frac{1}{R_2 C_2} \\ 0 & 0 \end{bmatrix} \tag{3.35}$$

$$C = \begin{bmatrix} 0 & 0 & 1 \end{bmatrix} \tag{3.36}$$

the following equations can be obtained:

$$\begin{aligned} \frac{dV_{C1}}{dt} &= -\frac{1}{R_1 C_1} V_{C1} - \frac{1}{C_1} i_{L1} + \frac{1}{R_1 C_1} V_{PV} \\ \frac{dV_{C2}}{dt} &= -\frac{1}{R_2 C_2} V_{C2} + \frac{1-u_1}{C_2} i_{L1} + \frac{1}{R_2 C_2} V_{DC} \\ \frac{di_{L1}}{dt} &= \frac{1}{L_1} V_{C1} - \frac{1}{L_1} V_{C2} - \frac{u_1 R_{01} + (1-u_1) R_{02}}{L_1} i_{L1} \end{aligned} \tag{3.37}$$

Since the variable duty cycle u_1 is embedded in the matrix A, thus the derived model is a nonlinear state space averaged model.

Verification of the state space average model

To verify the state space model, first let's create a file in SIMULINK to simulate the DC DC BOOST converter. Then create the model and compare the results.

All this is shown in Figure (3.21).

The convergence between the two curves justify mathematical model. The simulation values are listed in following Table:

R_{01}	$interneResistanceofT_1$	0.001Ω
R_{02}	$interneResistanceofD$	0.0012Ω
R_1	$Resistanceofsource$	0.01Ω
R_2	$Resistanceofsource$	0.01Ω
C_1	$ParallelCapacitance$	$0.1F$
C_2	$ParallelCapacitance$	$0.01F$
L_1	$Inductance$	$0.0033H$
V_{PV}	$PVVoltage$	$1000V$
V_{DC}	$MicrigridVoltage$	$1000V$

Table 3.3: Values of simulation of PV converter

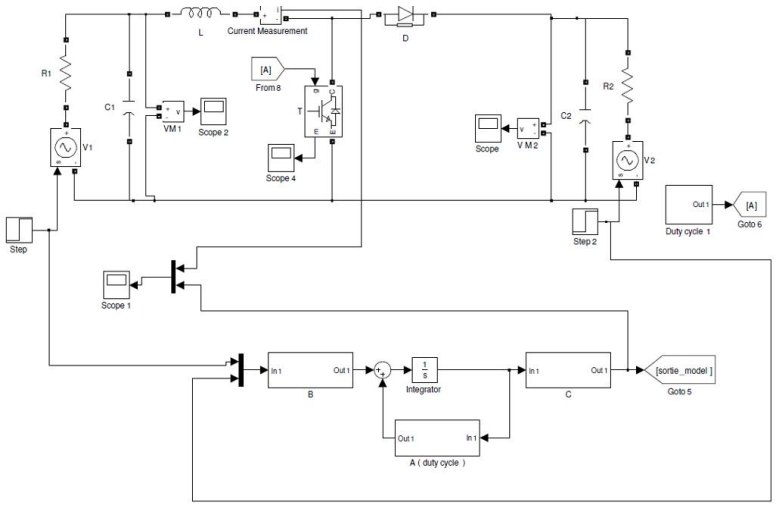

Figure 3.21: The BOOST converter and corresponding state space nonlinear average model

The comparison results between the real circuit and the non-linear average model is shown in the following figure (3.22).

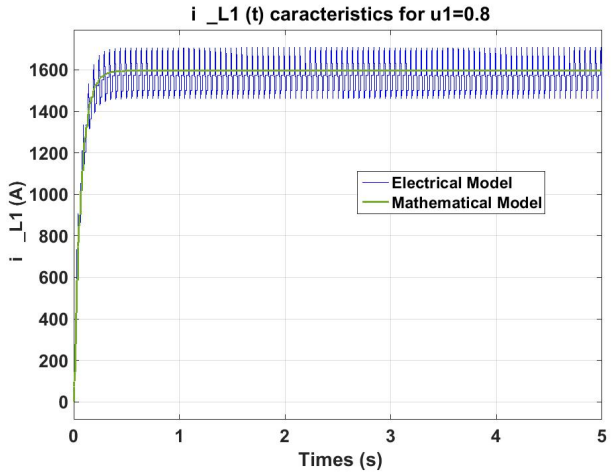

Figure 3.22: Current characteristics for $u_1 = 0.8$

As the two curves coincide, this means that we have well fit our model.
Several conclusions can be drawn from the graph. The first is that the current through the inductance behaves as a first order system to step input, as it should be. Another conclusion is that as the current through the inductance is positive, this means that the power goes in the same direction as the direction of current. In this case the low side to high.

DC/DC Converter for battery and Supercapacitor

We study the averaged model of the bidirectional $DC - DC$ Bidirectional Boost Converter [75], [76], [77].

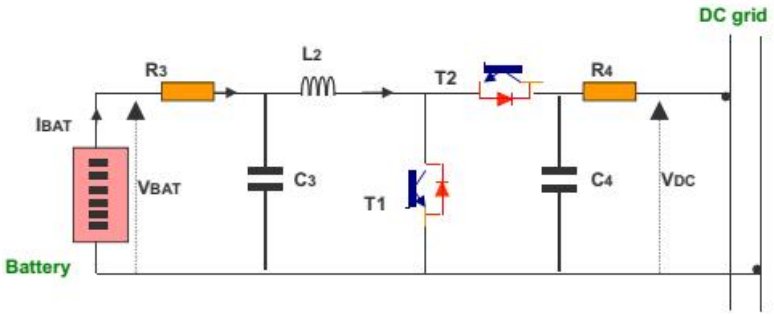

Figure 3.23: DC Bidirectional Converter Circuit

We have two structures for the bidirectional converter. In the first one, the current branch receives energy in a positive voltage. In the second structure, current branch supplies power in a positive voltage. The reversal of power transfer is obtained by changing the direction of the current. Similarly to the PV's DC converter, one superposes the two structures we get the equivalent circuit in Figure (3.23).

Operating rules

- In the first interval T_1 closes and T_2 opens
- In the second interval T_1 opens and T_2 closes

Modeling the switches it will be taken into account small resistances (R_{03} and R_{04}) when they are driving, so the conduction losses are taken into account.
In the following, u_2 denotes the duty ratio of the switches, ON denotes the state switch on and OFF denotes the state switch off.
Noteworthy that these driving modes are such that $0 < u_2 < 0.5$ the power goes low side to high side, and if $0.5 < u_2 < 1$ the power goes the other way.
We select three state variables, the voltages on the capacitors C_3 and C_4 and the current in the inductance L_2.

Modeling Steps:
*Step*1
A graphical method of constructing an equivalent circuit diagram in MATLAB SIMULINK (Simpower).
*Step*2
A formal approach (topological model) which consists in extracting the state equations for each possible circuit topology, to create the averaged model of the converter.

Considering that the circuit is functioning in the first interval $[0, u_2T]$,

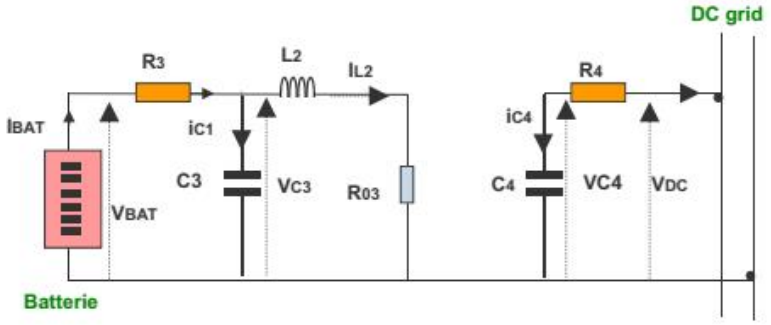

Figure 3.24: The equivalent circuit in interval $[0, u_2T]$

The following equations can be obtained:

$$\begin{aligned}
\frac{dV_{C3}}{dt} &= -\frac{1}{R_3C_3}V_{C3} - \frac{1}{C_3}i_{L2} + \frac{1}{R_3C_3}V_{BAT} \\
\frac{dV_{C4}}{dt} &= -\frac{1}{R_4C_4}V_{C4} + \frac{1}{R_4C_4}V_{DC} \\
\frac{di_{L2}}{dt} &= \frac{1}{L_2}V_{C3} - \frac{R_{03}i_{L2}}{L_2}
\end{aligned} \tag{3.38}$$

Therefore, the state space model in the interval $[0, u_2T]$ can be described by the following equation:

$$\dot{x(t)} = A_1x + B_1u \tag{3.39}$$

Where X denotes the system states that have been averaged over one switching cycle.,Y is the output vector,U is control vector,$A$is state matrix,B is input matrix and C is output matrix. Where:

$$x = \begin{bmatrix} V_{C3} \\ V_{C4} \\ i_{L2} \end{bmatrix} \tag{3.40}$$

and:

$$\dot{x} = \begin{bmatrix} \frac{dV_{C3}}{dt} \\ \frac{dV_{C4}}{dt} \\ \frac{di_{L2}}{dt} \end{bmatrix} \tag{3.41}$$

And the relevant matrices are as follows:

$$A_1 = \begin{bmatrix} = -\frac{1}{(R_3C_3)} & 0 & \frac{1}{C_3} \\ 0 & -\frac{1}{(R_4C4)} & 0 \\ \frac{1}{L_2} & 0 & \frac{R_{03}}{L_2} \end{bmatrix} \tag{3.42}$$

$$B_1 = \begin{bmatrix} = \frac{1}{(R_3C_3)} & 0 \\ 0 & \frac{1}{R_4C_4} \\ 0 & 0 \end{bmatrix} \tag{3.43}$$

and

$$C_1 = \begin{bmatrix} = 0 & 0 & 1 \end{bmatrix} \tag{3.44}$$

In the interval $[u_2T, T]$, we have the equivalent circuit shown in figure (3.25).

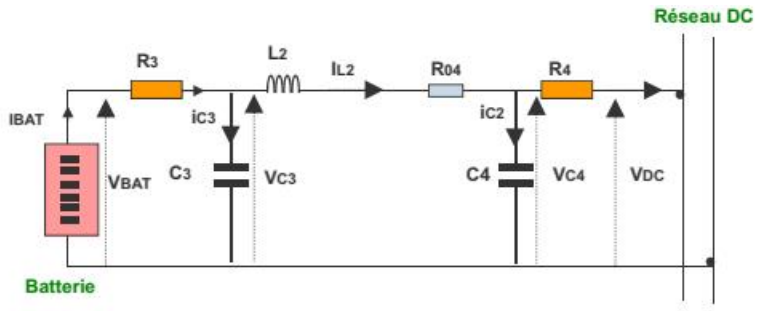

Figure 3.25: Structure convertisseur DC/DC dans l'intervalle $[u_2T, T]$

Similarly, the following equations can be obtained:

$$\begin{aligned}
\frac{dV_{C3}}{dt} &= -\frac{1}{R_3C_3}V_{C3} - \frac{1}{C_3}i_{L2} + \frac{1}{R_3C_3}V_PV \\
\frac{dV_{C4}}{dt} &= -\frac{1}{R_4C_4}V_{C4} + \frac{1}{C_4}i_{L2} + \frac{1}{R_4C_4}V_{DC} \\
\frac{di_{L2}}{dt} &= \frac{1}{L_2}V_{C3} - \frac{1}{L_2}V_{C4} - \frac{R_{04}i_{L2}}{L_2}
\end{aligned} \tag{3.45}$$

Therefore, the state space model in the interval $[u_2T, T]$ can be described by:

$$\dot{x}(t) = A_2x + B_2u \tag{3.46}$$

And the relevant matrices are as follows:

$$A_2 = \begin{bmatrix} = -\frac{1}{(R_3C_3)} & 0 & \frac{1}{C_3} \\ 0 & -\frac{1}{(R_4C_4)} & \frac{1}{C_4} \\ \frac{1}{L_2} & -\frac{1}{L_2} & -\frac{R_{04}}{L_2} \end{bmatrix} \tag{3.47}$$

$$B_2 = \begin{bmatrix} = \frac{1}{(R_3C_3)} & 0 \\ 0 & \frac{1}{R_4C_4} \\ 0 & 0 \end{bmatrix} \tag{3.48}$$

and

$$C_2 = \begin{bmatrix} = 0 & 0 & 1 \end{bmatrix} \tag{3.49}$$

Finally, based on the power electronics averaging technique, the system's state space average model can be expressed as:

$$\begin{aligned}
\langle x \rangle &= A\langle x \rangle + B\langle U \rangle = [A_1u_2 + A_2(1-u_2)]\langle x \rangle + [B_1u_2 + B_2(1-u_2)]\langle U \rangle \\
\langle Y \rangle &= C\langle x \rangle = [C_1u_2 + C_2(1-u_2)]\langle x \rangle
\end{aligned} \tag{3.50}$$

Where $\langle x \rangle$ denotes the system states that have been averaged over one switching cycle.

Thus, we have:

$$A = \begin{bmatrix} -\frac{1}{R_3C_3} & 0 & -\frac{1}{C_3} \\ 0 & -\frac{1}{R_4C_4} & \frac{(1-u_2)}{C_3} \\ \frac{1}{L_2} & \frac{1-u_2}{L_2} & \frac{-u_2R_{03}-(1-u_2)R_{04}}{L_2} \end{bmatrix} \tag{3.51}$$

$$B = \begin{bmatrix} \frac{1}{R_3C_3} & 0 \\ 0 & \frac{1}{R_4C_4} \\ 0 & 0 \end{bmatrix} \tag{3.52}$$

$$C = \begin{bmatrix} 0 & 0 & 1 \end{bmatrix} \tag{3.53}$$

and the following equations can be obtained:

$$\begin{aligned} \frac{dV_{C3}}{dt} &= -\frac{1}{R_3C_3}V_{C3} - \frac{1}{C_3}i_{L2} + \frac{1}{R_3C_3}V_PV \\ \frac{dV_{C42}}{dt} &= -\frac{1}{R_4C_4}V_{C4} + \frac{1-u_2}{C_4}i_{L2} + \frac{1}{R_4C_4}V_{DC} \\ \frac{di_{L2}}{dt} &= \frac{1}{L_2}V_{C3} - \frac{1}{L_2}V_{C4} - \frac{u_2R_{03}+(1-u_2)R_{04}}{L_2}i_{L_2} \end{aligned} \tag{3.54}$$

Since the variable duty cycle is embedded in matrix A, the derived model is a nonlinear state space averaged one.

Verification of the state space averaged model

To verify the state space model, first let's create a file in SIMULINK to simulate the DC DC bidirectional converter. Then create the model and compare the results. All this is shown in the following Figures.

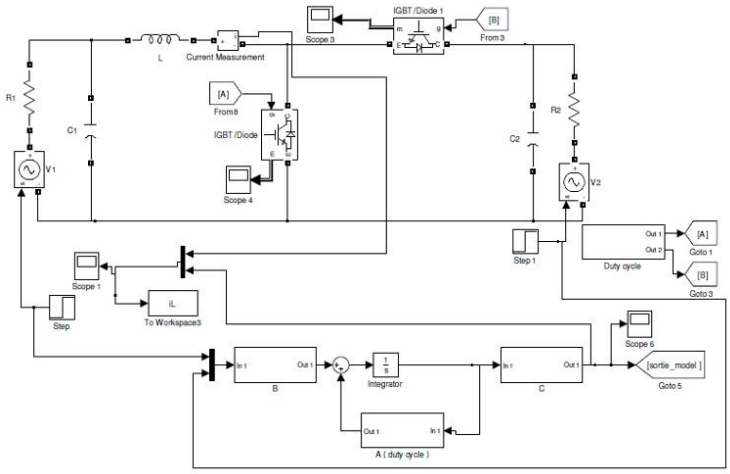

Figure 3.26: The Bidirectional converter and correspond state space nonlinear average model

The simulation values are listed in the following Table:

R_{03}	interne Resistance of T_1	0.001Ω
R_{04}	interne Resistance of T_2	0.0012Ω
R_3	Resistance of source	0.01Ω
R_4	Resistance of source	0.01Ω
C_3	Parallel Capacitance	$0.1F$
C_4	Parallel Capacitance	$0.01F$
L_2	Inductance	$0.0033H$
V_{BAT}	Battery Voltage	$1000V$
V_{DC}	MicroGrid Voltage	$1000V$

Table 3.4: Simulation values for Battery converter

The comparison results between the real circuit and the non-linear average model is shown in the following Figure.

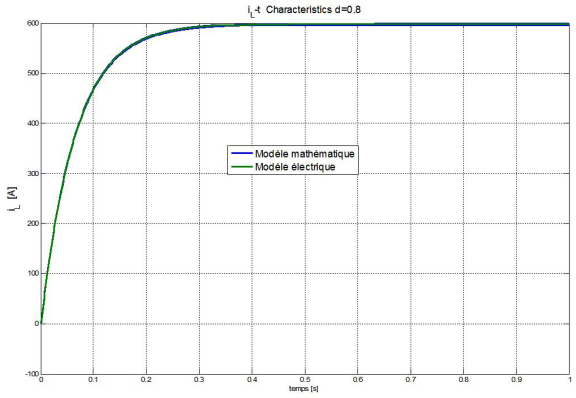

Figure 3.27: The comparison results between the real circuit and average model ($u_2 = 0.8$)

As the two curves coincide, this means that we have sized well our model.

The direction of the current depends on the duty cycle, so if we change to a $u_2 = 0.2$ (the complement of the above) and keep the other parameters we obtain the following Figure.

This result shows that the current has the same absolute value but opposite sign than before (this is because we have chosen a duty cycle complementary to the above). Now the power goes from high side to low.

3.6 MicroGrid Model

DC MicroGrid topology is formed by photovoltaic Panel connected to $DC - DC$ boost converter for the source. Battery and supercapacitor are the components of the storage system, connected through a $DC - DC$ bidirectional boost converter.

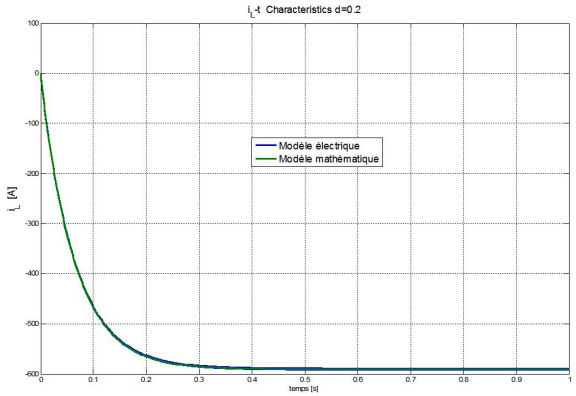

Figure 3.28: Comparison results between the real circuit and the average model ($u_2 = 0.2$)

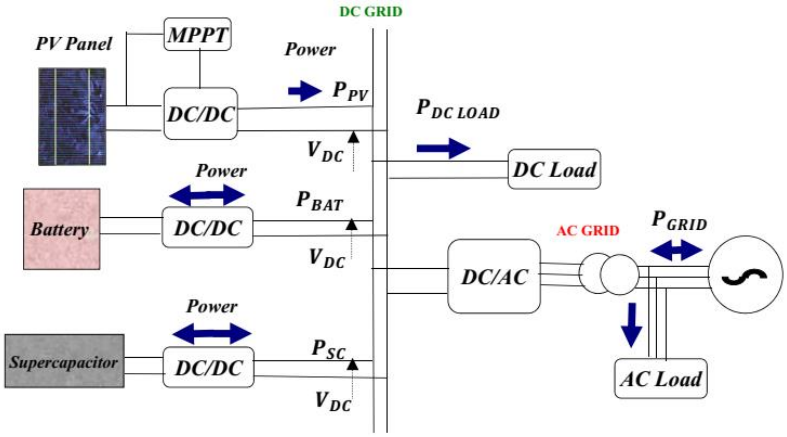

Figure 3.29: DC Microgrid studied topology

3.7 Conclusion

In this chapter, a Microgrid- system operation concept has been established and validated. Besides, each components of a DC Microgrid- system have been modeled , simulated and validated as well in order to establish study of whole systems.

We choose two technologies for the storage system to have larger degree of freedom to control voltage of MicroGrid. The battery for high energy and supercapacitor for high power.

Furthermore, it was explained the operating principles of the converters and a detailed averaged state-space model for DC/DC converter to develop the dynamical model of the system.

And finally we have introduced system configuration of the considered MicroGrid.

Chapter 4

Microgrids Control

4.1 Introduction

Linear control methods have been the mostly used in the field of MicroGrids, but with limited control performances [79], [15], [14]. Developing new control structures is necessary to improve the performance of such systems [10], [9].

In this chapter we design a control scheme based on several assumptions coming from physics of power systems. Such assumptions make the system stable inside a smaller operation region, based on local results, but is able to cope with large disturbances. The control philosophy is based on rigorous analysis of the dynamics interaction through the grid, with the aim to propose a new control strategy able to stabilize the whole system [6]. The proposed control will be based on two control layers. At first, we define the high level controller to give reference values for lower local controllers. Thereafter we developed a distributed control using backstepping technique, feedback linearization and Lyapunov based control laws. In this chapter the power system stability will be analyzed. Lyapunov functions will be provided for each step with the objective to construct a composite Lyapunov function which will be used in the stability analysis.

4.2 Context and Problem Position

The main objective of a DC grid controller is voltage stabilization of the DC MicroGrid, while assuring the balance of power flow for the different energy sources and consumers. The control philosophy is based on the concept of "Think globally and act locally". This is done in a Systems of Systems approach (see [6], [80], [81], [82], [9]). It is important to remark that each brick of the whole system is designed aiming at participating to the stability of the whole DC voltage system. The global control structure is designed with two levels, where the higher level one provide references for the lower level. In this structure, one storage element will be responsible to assure voltage stability, while another will provide power flow completion. In this way, since one node is responsible for the voltage stability, it represent an intermediate layer of master-slave. The local controllers

are implemented at actuators' level represented by the power converters. The references for these local controllers are given by the high level controllers. For the PV source the reference is obtained directly from a MPPT algorithm. However the control supervision can communicate with the PV source DC-DC converter to return power reference in case it is needed (curtailment).

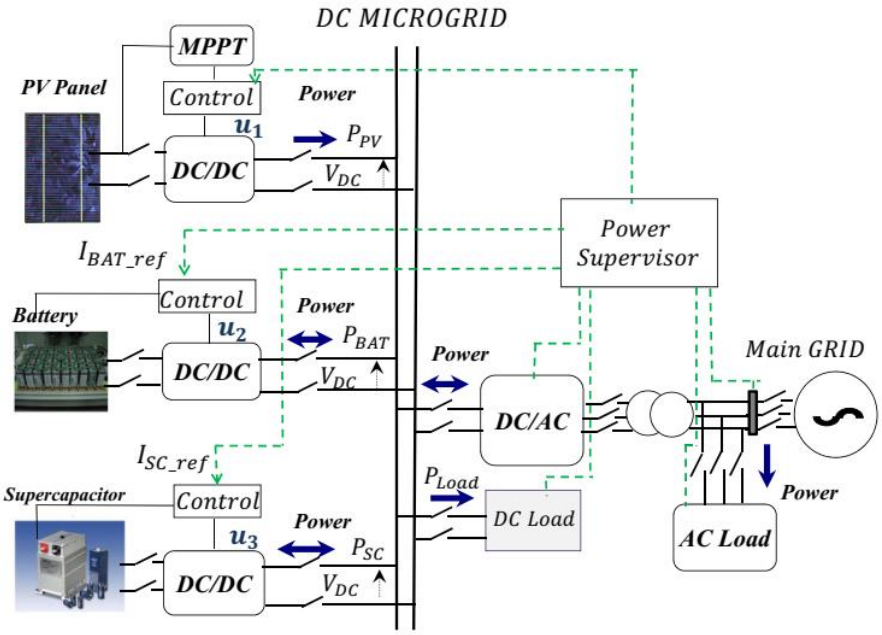

Figure 4.1: DC Microgrid global structure

Figure (4.1) shows the global structure of a DC Microgrid with DG sources,power electronics , differents local controllers and Power supervisor.

4.3 DC MicroGrid Configuration

The photovoltaic (PV) DC-DC boost converter operates following references given by a standard Maximum Power Point Tracking (MPPT) algorithm under varying levels of irradiation and temperature [41], [83] and [47]. A DC/DC unidirectional boost converter is used to control the PV array.

While bidirectional converters are used to charge or discharge the energy storage elements [84]. The load (an electric vehicle charge station for example) is considered as a variable resistance.

4.4 High Level Controller

The high level controller provides a reference to the local controllers. In this section we will define the high level controllers used in this thesis.

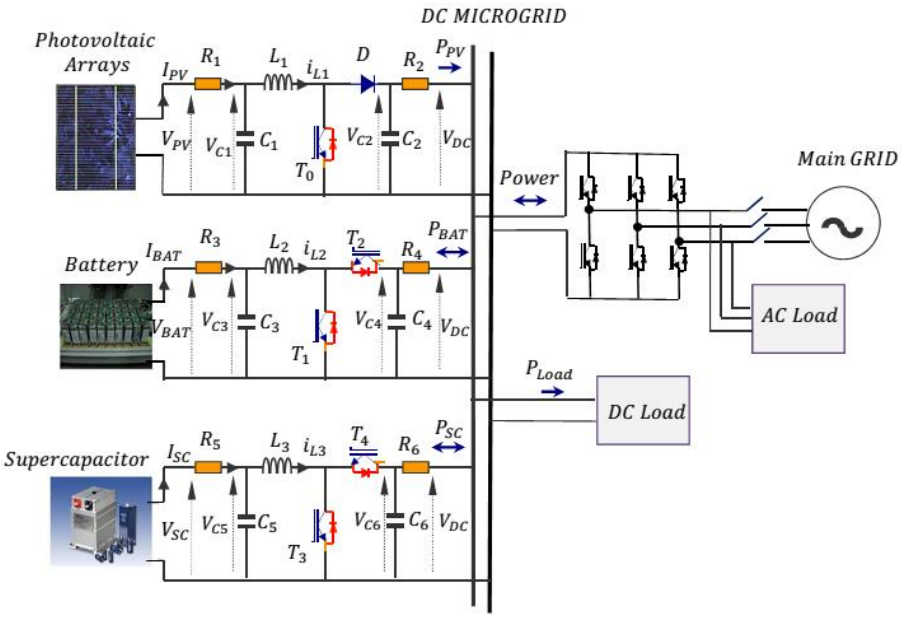

Figure 4.2: DCMicrogrid Configuration

4.4.1 PV Power source

The Maximum Power Point Tracking (MPPT) algorithm is used to extract the maximum power from a photovoltaic array of solar cells. In this thesis, the Incremental Conductance method is applied [85], [83]. To accomplish this task, a V_{C1}^* time varying (piecewise constant) desired voltage reference is provided by the MPPT.

4.4.2 Storage system

The power flow of the components in the proposed DC micro-grid is shown in Figure (4.3). The sum of the output power of the photovoltaic array, and the storage is defined as follows [86]:

$$P_{DC} = P_{PV} + P_L + P_{ST}$$

Where:

- P_{DC}:DC Grid power
- P_{PV}: PV power
- P_Load:Load power
- P_{ST}:Storage system power

and

$$P_{ST} = P_{BAT} + P_{SC} \tag{4.1}$$

- P_{BAT}:Battery power
- P_{SC}: Supercapacitor power

In general the DC MicroGrid is connected to the main AC Grid then $P_{DC} = P_{GRID}$ where P_{GRID} represents the power flowing to the AC grid.
In this case excessive power is supplied to or obtained from the AC Grid.

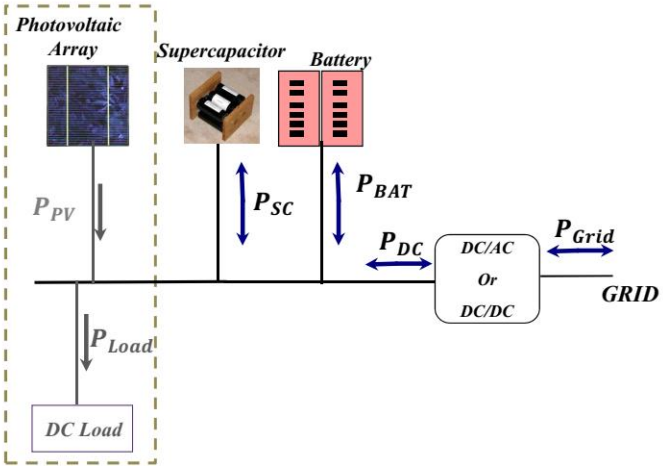

Figure 4.3: Power Flow

- connected Mode

$$P_{DC} = P_{PV} + P_{Load} + P_{ST} \tag{4.2}$$

- Islanded Mode $P_{DC} = 0$

$$P_{PV} + P_{Load} = P_{ST}$$

For this thesis we will study the worst case when the DC MicroGrid is in islanded mode, or that the AC grid is an uncontrollable load, and then it is lumped with the other loads. Following this scheme, the DC grid's voltage will evolve following: from equation 4.2 we can write:

$$C_{DC}\dot{V}_{DC}V_{DC} = [I_{PV} + I_{ST} + I_{Load}]V_{DC} \tag{4.3}$$

$$\dot{V}_{DC} = \frac{1}{C_{DC}}(I_{PV} + I_{ST} + I_{Load}) \tag{4.4}$$

where we define I_{PV} PV current, I_{ST} storage system's current, I_{Load} Load current, I_{DC} DC grid current. The energy storage elements can switch between charge and discharge mode in order to maintain the DC grid power balance. $V_{DC}(t)$ must be kept around its nominal value and inside voltage limitation boundaries with respect to power balance given by equation (4.4).

To attain this goal, the current provided by the battery and the supercapacitor must equal the current error between production and consumption:

$$I_{ST} = I_{PV} - I_{Load}$$

This current error will be considered as a reference for storage system.

4.4.3 Time scales Concept

In this study we designed a control strategy with multilayer control architecture for a system composed by interconnection between several and different subsystems.
The high level control layer is based on MicroGrid's power management, i.e. we can act

on the scale of one day or the scale of a few hours, it gives us the opportunity to clip consumption peaks at end-of-day. In the physical power system, the variation of the power PV source is on the scale of hours or minutes, the variation of the power of the battery is made on the scale of hours or minutes, the variation of the power of the supercapacitor is made on the scale of minutes or seconds, the variation of the power of the capacitors is made on the scale of mili to micro seconds. If one looks from the point of view of current and voltage dynamics it can be observed that the current dynamics can be controlled such as to be much faster than the dynamics of capacitances' voltages. In this way, the system may works in different time scales.

4.4.4 Stabilization strategy

We rely on the storage system (battery + supercapacitor) to act as a buffer to absorb the current (power) variations and ensure a stable voltage. Based on the physical characteristics of the storage components, and in particular on the current limitations from the battery, we propose to decompose (Eq. 4.6) the power reference ($P_{DC_{ref}}$) that will be designed later, in two components, a fast (P_{Fast}) and a slow (P_{Long}) as shown in Fig. 4.4. The slow component will be used as the reference for the battery's power supply, while the fast component will be the reference power for the supercapacitor as in Fig. 4.5.

The two components must be chosen such as to keep sufficient time-scale separation between the lower and higher level control objectives, and to assure that the battery does not need to react faster than its specifications. In this way, the lifespan of the battery is seriously augmented [9].

The purpose is to introduce the basics first order Low pass filter: The transfer function is

$$\frac{Output}{Input} = K\frac{1}{\tau s + 1} \tag{4.5}$$

here:

- s is the Laplace transform variable
- k is the filter gain.
- $\tau$is the filter time constant.

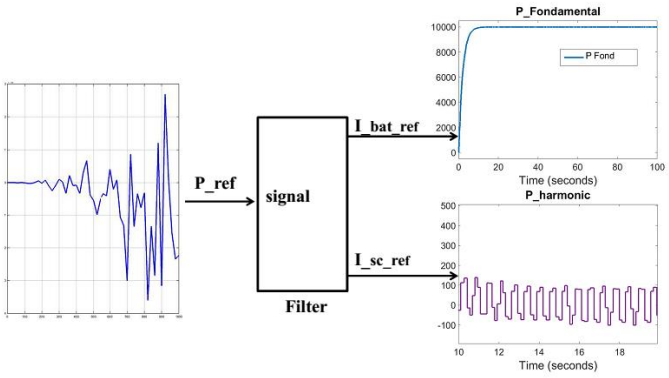

Figure 4.4: Signal decomposition

The choose of cutoff frequency depend of the Dynamic Response of the system. The figure (4.5)represent the strategy control scheme

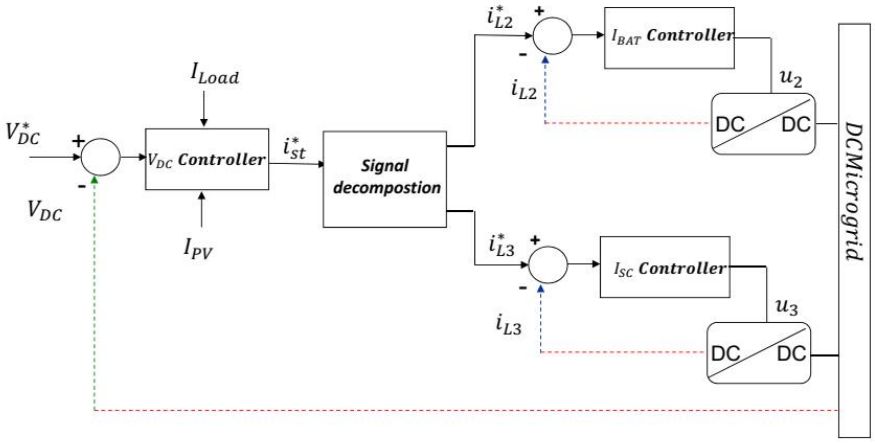

Figure 4.5: Control Strategy

$$P_{DC_{ref}}(t) = P_{Long} + P_{Fast} \tag{4.6}$$

$$I_{BAT_{ref}} = \frac{P_{Long}}{V_{DC}} = i^*_{L2} \tag{4.7}$$

$$I_{SC_{ref}} = \frac{P_{Fast}}{V_{DC}} = i^*_{L3} \tag{4.8}$$

Equation (4.7) acts to maintain the long term balance of power, while equation (4.8) acts to keep voltage stability and to dampen oscillations. These high-frequency oscillations (ripples) are due to the switching of the converter and power electronic used to impose the DC output currents.

High Level Controller for Storage system

First we have to calculate the reference for the storage system. The control target is to stabilise V_{DC} to its nominal value. From equation (4.4) the equation of DC Grid is (remembering that $i^*_{ST} = i^*_{BAT} + i^*_{SC}$ is the current from the storage units):

$$\dot{V}_{DC} = \frac{1}{C_{DC}}[\frac{1}{R_2}(V_{DC} - V_{C2}) + i_{ST} - i_{Load}] \tag{4.9}$$

with:

- i^*_{BAT} the current reference for the Battery
- $i^*_{SC}$the current reference for the Supercapacitor

Thereafter we represent the currents as i_{L2} and i_{L3}:

- i_{L2} is Battery inductor current
- i_{L3} is Supercapacitor inductor current

- i^*_{L2} the current reference for the Battery
- i^*_{L3} the current reference for the Supercapacitor

The reference value for V_{DC} is its constant nominal value V^*_{DC}. In the following, through a backstepping procedure, it will be designed an $i^*_{ST} = i^*_{L2} + i^*_{L3}$, references for i_{L2} and i_{L3} in order to steer V_{DC} to its reference V^*_{DC}.

Lets first define the output tracking errors:

$$e_{V_{DC}} = (V_{DC} - V^*_{DC})$$

and its derivative:

$$\dot{e}_{V_{DC}} = (\dot{V}_{DC} - \dot{V}^*_{DC})$$

The desired dynamics for $e_{V_{DC}}$ is introduced as:

$$\dot{e}_{V_{DC}} = -K_{10} e_{V_{DC}} - \overline{K}_{10} \alpha_{10} \tag{4.10}$$

where α_{10}

represents the integral term assuring zero error in steady state for V_{DC}, and is governed by equation:

$$\dot{\alpha}_{10} = K^{\alpha}_{10} e_{V_{DC}}$$

K_{10}, $\overline{K}_{10}$ and K^{α}_{10} are positive tuning gain parameters such that we can rewrite (4.10) as :

$$\begin{aligned} \dot{e}_{V_{DC}} &= \dot{V}_{DC} - \cancelto{0}{\dot{V}^*_{DC}} = \frac{1}{C_{DC}}\left(\frac{1}{R_2}(V_{DC} - V_{C2}) + i_{ST} - \frac{1}{R_Load} V_{DC}\right) \\ &= -K_{10}(V_{DC} - V^*_{DC}) - \overline{K}_{10}\alpha_{10} \end{aligned} \tag{4.11}$$

and design the following control action:

$$\begin{aligned} &\frac{1}{C_{DC}}\left(\frac{1}{R_2}(V_{DC} - V_{C2}) + i_{ST} - \frac{1}{R_Load} V_{DC}\right) = -K_{10}(V_{DC} - V^*_{DC}) - \overline{K}_{10}\alpha_{10} \\ &i^*_{ST} = \frac{V_{DC}}{R_Load} - \frac{1}{R_2}(V_{DC} - V_{C2}) + C_{DC}(-K_{10}(V_{DC} - V^*_{DC}) - \overline{K}_{10}\alpha_{10}) \end{aligned} \tag{4.12}$$

such as to obtain arbitrary linear dynamics for the states $[\alpha_{10}\ V_{DC}]^T$ for suitable choice of gains $K_{10}, \overline{K}_{10}, K^{\alpha}_{10}$. The closed loop sub-system then becomes:

$$\begin{aligned} \dot{\alpha}_{10} &= K^{\alpha}_{10} e_{V_{DC}} \\ \dot{e}_{V_{DC}} &= -K_{10} e_{V_{DC}} - \overline{K}_{10}\alpha_{10} \end{aligned}$$

We consider an augmented system $\widetilde{V}_{DC}$.

$$\widetilde{V}_{DC} = \begin{bmatrix} V_{DC} - V_{DC}^{*} \\ \alpha_{10} \end{bmatrix} \tag{4.13}$$

Its linear dynamics are here introduced as:

$$\dot{\widetilde{V}}_{DC} = A_{10}\widetilde{V}_{DC} = \begin{bmatrix} -K_{10} & -\overline{K}_{10} \\ K_{10}^{\alpha} & 0 \end{bmatrix} \widetilde{V}_{DC} \tag{4.14}$$

where the eigenvalues of the state matrix can be computed as:

$$\lambda_{11.12} = -\frac{1}{2}(K_{10} \pm \sqrt{(K_{10}^{2} - 4\overline{K}_{10}K_{10}^{\alpha})})$$

By properly selecting positive gains K_{10}, $\overline{K}_{10}$ and K_{10}^{α} both eigenvalues are stable; then the origin is a exponentially stable equilibrium point for the augmented state. As a corollary, there exist $P_{10} = P_{10}^{T} > 0$ such that $P_{10}A_{10} + A_{10}^{T}P_{10} = -I_2$ where I_2 is an identity matrix in $\mathbb{R}^2$.

Now from the control signal 4.12 can be decomposed as:

$$i_{ST}^{*} = i_{BAT}^{*} + i_{SC}^{*} \tag{4.15}$$

with i_{BAT}^{*} being the reference current for local control of the Battery and i_{SC}^{*} the reference current for local control of the Supercapacitor.

Proof. In order to complete the analysis, we introduce the Lyapunov function:

$$V_{10} \quad = \quad ([\alpha_{10}\ e_{V_{DC}}]^{T}\ P_{10}\ [\alpha_{10}\ e_{V_{DC}}]) \tag{4.16}$$

which derivative is then:

$$\dot{V}_{10} = -e_{V_{DC}}^{2} - \alpha_{10}^{2} \tag{4.17}$$

Now using the property (see [87]) :

$$\lambda_{min}(P_{10})\left\|x\right\|^{2} \ \leq \ x^{T}P_{10}x \ \leq \ \lambda_{max}(P_{10})\left\|x\right\|^{2} \tag{4.18}$$

we can then write that (m_{10} is a positive constant):

$$\dot{V}_{10} \leq -\frac{\lambda_{min}(P_{10})}{\lambda_{max}(P_{10})}\left\|x\right\|^{2} \tag{4.19}$$

$$\dot{V}_{10} \leq -\frac{1}{\lambda_{max}(P_{10})}V_{10} \stackrel{\triangle}{=} m_{10}V_{10} \tag{4.20}$$

that implies that:

$$\dot{V}_{10}(t) = e^{-m_{10}t}\ V_{10}(0) \tag{4.21}$$

and then we can conclude that:

$$\lim_{t\to\infty}\left\|\begin{bmatrix} e_{V_{DC}}(t) \\ \alpha_{10}(t) \end{bmatrix}\right\| = 0$$

and that the closed-loop dynamics of V_{DC} are exponentially stable.

□

4.5 Local Control

4.5.1 PV System Component Modeling and Control

The solar array has a characteristic current/voltage profile. This implies that for obtaining the maximum power from it, it is important to keep its output voltage to a given reference. In this thesis this reference is provided by an Incremental Conductance algorithm based on differentiation of PV power to its voltage and on condition of zero slope of P-V curve in maximum power point [88], [89].

PV connected DC/DC BOOST converter

The mathematical model for the DC/DC boost converter that interconnects the PV to the DC grid is obtained based on power electronics averaging technique [76], [75], [77].

$$\dot{V}_{C1} = -\frac{1}{R_1 C_1} V_{C1} - \frac{1}{C_1} i_{L1} + \frac{1}{R_1 C_1} V_{PV} \tag{4.22a}$$

$$\dot{V}_{C2} = -\frac{1}{R_2 C_2} V_{C2} + \frac{(1-u_1)}{C_2} i_{L1} + \frac{1}{R_2 C_2} V_{DC} \tag{4.22b}$$

$$\dot{i}_{L1} = \frac{1}{L_1} V_{C1} - \frac{([(R_{01} - R_{02})u_1 + R_{02}]i_{L1})}{L_1} - \frac{(1-u_1)}{L_1} V_{C2} \tag{4.22c}$$

where R_1, L_1, C_1, C_2 and C_{DC} are known positive values of resistances, capacitors and inductors. For modelling the switches there are small resistances (R_{01} and R_{02}) when they are driving, so the conduction losses are taken into account. V_{PV}, and V_{DC} are the photovoltaic panel and DC Microgrid voltages respectively. The measurement state is V_{C1}, V_{C2}, i_{L1} and V_{DC}. u_1 will be the control input which define the duty cycle of the converter.

Nonlinear control law and system's stability analysis

In this part the control target is to stabilize voltage on capacitor C_1, therefor we have to assigned V_{C1} to V_{C1}^*, the time varying (piecewise constant) reference provided by the MPPT algorithm.

In the following, it is used the assumption that the current can be set to have much faster dynamics than the capacitances' voltages (see [9]). The current and voltage regulation consists in a cascade control: there will be an inner current loop and an outer voltage loop as in Fig. 4.6.

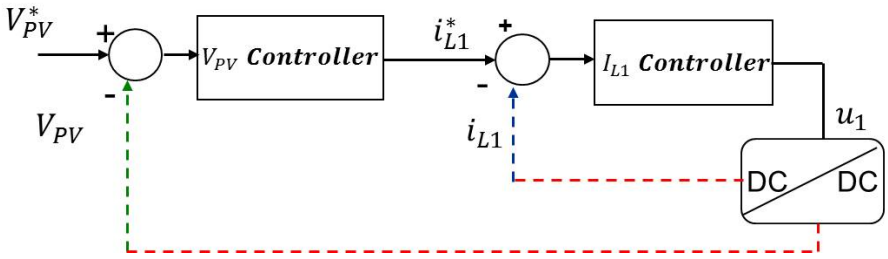

Figure 4.6: DC/Control of PV system

Following a backstepping procedure, i^*_{L1} reference for i_{L1} will be designed in order to steer V_{C1} to its reference V^*_{C1}.

Lets first define the output tracking errors:

$$e_{V_{C1}} = (V_{C1} - V^*_{C1})$$

$$e_{i_{L1}} = (i_{L1} - i^*_{L1})$$

and their derivatives:

$$\dot{e}_{V_{C1}} = (\dot{V}_{C1} - \dot{V}^*_{C1})$$
$$\dot{e}_{i_{L1}} = (\dot{i}_{L1} - \dot{i}^*_{L1})$$

We are now going to determined the control law by backstepping. The desired dynamics for V_{C1} are introduced as:

$$\dot{V}_{C1} = -K_1 e_{V_{C1}} - \overline{K_1}\alpha_1 \tag{4.23}$$

We can then design:

$$i^*_{L1} = \frac{1}{R_1}(V_{PV} - V_{C1}) + C_1 K_1 (V_{C1} - V^*_{C1}) + C_1 \overline{K}_1 \alpha_1 \tag{4.24}$$

where α_1 represents the integral term assuring zero error in steady state for the dynamics of V_{C1}, now defined as an extended state governed by equation:

$$\dot{\alpha}_1 = K^\alpha_1 e_{V_{C1}}$$

and K_1, $\overline{K}_1$ and K^α_1 are positive tuning gain parameters such that we can rewrite (4.23) as :

$$\begin{aligned} \dot{e}_{V_{C1}} &= \dot{V}_{C1} - \cancel{\dot{V}^*_{C1}}^{\,0} = -\frac{1}{R_1 C_1} V_{C1} - \frac{1}{C_1} i^*_{L1} + \frac{1}{R_1 C_1} V_{PV} \\ &= -K_1 (V_{C1} - V^*_{C1}) - \overline{K}_1 \alpha_1 \end{aligned} \tag{4.25}$$

such as to obtain an arbitrary linear system for the states $[\alpha_1\ V_{C1}]^T$ for suitable choice of gains $K_1, \overline{K}_1, K_1^\alpha$. The closed loop sub-system becomes:

$$\begin{aligned}\dot{\alpha}_1 &= K_1^\alpha e_{V_{C1}} \\ \dot{e}_{V_{C1}} &= -K_1 e_{V_{C1}} - \overline{K}_1 \alpha_1\end{aligned}$$

We consider an augmented system $\widetilde{V}_{C1}$

$$\widetilde{V}_{C1} = \begin{bmatrix} \alpha_1 \\ V_{C1} - V_{C1}^* \end{bmatrix}$$

Its closed loop (linear) dynamics is here defined with the eigenvalues

$$\dot{\widetilde{V}}_{C1} = A_1 \widetilde{V}_{C1} = \begin{bmatrix} 0 & K_1^\alpha \\ -\overline{K}_1 & -K_1 \end{bmatrix}$$

$$\lambda_{1.2} = -\frac{1}{2}(K_1 \pm \sqrt{(K_1^2 - 4\overline{K}_1 K_1^\alpha)})$$

By properly selecting positive gains K_1,$\overline{K}_1$ and K_1^α both eigenvalues are stable; then the origin is a stable equilibrium point for the augmented state. As state above for a similar case, there exist $P_1 = P_1^T > 0$ such that $P_1 A_1 + A_1^T P_1 = -I_2$ where I_2 is an identity matrix in $\mathbb{R}^2$.

As next step, we need to design a control law u_1 (shown below at Equation (4.29)) such as to steer i_{L1} towards its reference i_{L1}^*. As before, one may impose a desired dynamic behaviour:

$$\dot{e}_{i_{L1}} = -K_3 e_{i_{L1}} - \overline{K_3}\alpha_3 \tag{4.26}$$

where α_3 represents the integral term, now defined as an extended state governed by equation:

$$\dot{\alpha}_3 = \overline{K}_3 e_{i_{L1}} \tag{4.27}$$

we can then rewrite $\dot{i}_{L1}$ as

$$\begin{aligned}\dot{i}_{L1} &= \frac{1}{L_1}V_{C1} - \frac{([(R_{01} - R_{02})u_1 + R_{02}]i_{L1})}{L_1} - \frac{(1-u_1)}{L_1}V_{C2} \\ &= \frac{1}{L_1}V_{C1} - \frac{(R_{01} - R_{02})i_{L1}u_1}{L_1} - \frac{R_{02}i_{L1}}{L_1} - \frac{V_{C2}}{L_1} + \frac{u_1 V_{C2}}{L_1} \\ &= \frac{1}{L_1}(V_{C1} - V_{C2}) - \frac{R_{02}}{L_1}i_{L1} + [-\frac{(R_{01} - R_{02})i_{L1}}{L_1} + \frac{V_{C2}}{L_1}]u_1\end{aligned}$$

And then, in order to impose desired dynamics:

$$\dot{i}_{L1} - \dot{i}_{L1}^* = -K_3 e_{i_{L1}} - \overline{K_3}\alpha_3 \tag{4.28}$$

with the positive tuning gain parametersK_3 , $\overline{K}_3$ and K_3^α we obtain the following control law:

$$\begin{aligned} u_1 &= \frac{1}{(V_{C2}+(R_{02}-R_{01})i_{L1}}\Big[V_{C2}-V_{C1}+R_{02}i_{L1}-L_1(K_3e_{i_{L1}}+\overline{K}_3\alpha_3 \\ &- C_1\overline{K}_1K_1^{\alpha}e_{V_{C1}}+(C_1K_1-\frac{1}{R_1})(K_1e_{V_{C1}}+\overline{K}_1\alpha_1))\Big] \end{aligned} \tag{4.29}$$

where we have computed:

$$\begin{aligned} \dot{i}_{L1}^{*} &= (C_1K_1-\frac{1}{R_1})\dot{V}_{C1}+C_1\overline{K}_1\dot{\alpha}_1 \\ &= (C_1K_1-\frac{1}{R_1})(-\frac{1}{R_1C_1}V_{C1}-\frac{1}{C_1}i_{L1}+\frac{1}{R_1C_1}V_{PV})+C_1\overline{K}_1K_1^{\alpha}e_{V_{C1}} \\ &= (C_1K_1-\frac{1}{R_1})[-K_1e_{V_{C1}}-\overline{K}_1\alpha_1+C_1\overline{K}_1K_1^{\alpha}e_{V_{C1}}] \end{aligned}$$

With condition

$$V_{C2}+(R_{02}-R_{01})i_{L1}\neq 0 \tag{4.30}$$

such as to obtain an arbitrary linear system for the states $[\alpha_3\ i_{L1}]^T$ for suitable choice of gains $K_3, \overline{K}_3, K_3^{\alpha}$. The closed loop sub-system becomes:

$$\begin{aligned} \dot{\alpha}_3 &= K_3^{\alpha}e_{i_{L1}} \\ \dot{e}_{i_{L1}} &= -K_3e_{i_{L1}}-\overline{K}_3\alpha_3 \end{aligned}$$

We consider an augmented system $\widetilde{i}_{L1}$

$$\widetilde{i}_{L1}=\begin{bmatrix}\alpha_3\\ i_{L1}-i_{L1}^{*}\end{bmatrix}$$

Its closed loop (linear) dynamic is here defined by the eigenvalues:

$$\dot{\widetilde{i}}_{L1}=A_3\widetilde{i}_{L1}=\begin{bmatrix}0 & K_3^{\alpha}\\ -\overline{K}_3 & -K_3\end{bmatrix}$$

$$\lambda_{3.4}=-\frac{1}{2}(K_3\pm\sqrt{(K_3^2-4\overline{K}_3K_3^{\alpha})})$$

By properly selecting positive gains K_3,$\overline{K}_3$ and K_3^{α} both eigenvalues are stable; then the origin is a stable equilibrium point for the augmented state. We can then state that the control input u_1 feedback linearizes the dynamics of V_{C1} and i_{L1}. Again one can find $P_3=P_3^T>0$ such that $P_3A_3+A_3^TP_3=-I_2$ where I_2 is an identity matrix in $\mathbb{R}^2$.

Let us consider the extended system:

$$\dot{V}_{C1} = -\frac{1}{R_1 C_1} V_{C1} - \frac{1}{C_1} i_{L1} + \frac{1}{R_1 C_1} V_{PV} \tag{4.31a}$$

$$\dot{\alpha}_1 = \overline{K}_1 e_{V_{C1}} \tag{4.31b}$$

$$\dot{V}_{C2} = -\frac{1}{R_2 C_2} V_{C2} + \frac{(1-u_1)}{C_2} i_{L1} + \frac{1}{R_2 C_2} V_{DC} \tag{4.31c}$$

$$\dot{i}_{L1} = \frac{1}{L_1} V_{C1} - \frac{([(R_{01} - R_{02})u_1 + R_{02}] i_{L1})}{L_1} - \frac{(1-u_1)}{L_1} V_{C2} \tag{4.31d}$$

$$\dot{\alpha}_3 = \overline{K}_3 e_{i_{L1}} \tag{4.31e}$$

Lemma 4.5.1. *Under control law (4.29), and suitable control gains* K_1, $\overline{K}_1$, K_1^α, K_3, $\overline{K}_3$ *and* $K_3^\alpha > 0$ *, the closed-loop system (4.22),(4.31) has an equilibrium point. Any evolution starting from initial conditions inside the attraction region, exponentially converges to the equilibrium point, under the condition* $V_{C2} + (R_{02} - R_{01}) i_{L1} \neq 0$ *that defines the attraction region.*

Proof. We introduce the Lyapunov function

$$V_{1,3} = ([\alpha_1 \; e_{V_{C1}}]^T \; P_1 \; [\alpha_1 \; e_{V_{C1}}]) \; + \; ([\alpha_3 \; e_{i_{L1}}]^T \; P_3 \; [\alpha_3 \; e_{i_{L1}}]) \tag{4.32}$$

It's derivative is then:

$$\dot{V}_{1,3} = [\dot{\alpha}_1 \; \dot{e}_{V_{C1}}]^T \; P_1 \; [\alpha_1 \; e_{V_{C1}}] + [\alpha_1 \; e_{V_{C1}}]^T \; P_1 \; [\dot{\alpha}_1 \; \dot{e}_{V_{C1}}] + [\dot{\alpha}_3 \; \dot{e}_{i_{L1}}]^T \; P_3 \; [\alpha_3 \; e_{i_{L1}}] + [\alpha_3 \; e_{i_{L1}}]^T \; P_3 \; [\dot{\alpha}_3 \; \dot{e}_{i_{L1}}]$$

$$\dot{V}_{1,3} = [\alpha_1 \; e_{V_{C1}}]^T \; (A_1^T \; P_1 + P_1 \; A_1) \; [\alpha_1 \; e_{V_{C1}}] \; + \; [\alpha_3 \; e_{i_{L1}}]^T \; (A_3^T \; P_3 + P_3 \; A_3) \; [\alpha_3 \; e_{i_{L1}}]$$

as we know, $P_1 A_1 + A_1^T P_1 = -I_2$ and $P_3 A_3 + A_3^T P_3 = -I_2$, then:

$$\dot{V}_{1.3} \quad = \quad -e_{V_{C1}}^2 - \alpha_1^2 - e_{i_{L1}}^2 - \alpha_3^2 \tag{4.33}$$

we use the inequalities [87] for a quadratic positive definite function $V(x) = x^T P x$:

$$\lambda_{min}(P) \, ||x| \, |^2 \; \leq \; x^T P x \; \leq \; \lambda_{max}(P) \, ||x| \, |^2$$

we can then write:

$$\dot{V}_{1.3} \leq -\frac{1}{\lambda_{max}} V_{1.3} \stackrel{\triangle}{=} -m_{1.3} \, V_{1.3}$$

and then:

$$V_{1.3}(t) = e^{-m_{1.3} t} \, V_{1.3}(0) \tag{4.34}$$

which implies that

$$\lim_{t\to\infty}\left\|\begin{bmatrix} e_{VC1}(t) \\ \alpha_1(t) \\ e_{i_{L1}}(t) \\ \alpha_3(t) \end{bmatrix}\right\| = 0$$

exponentially, and as a consequence this subsystem is exponentially stable.

Therefore considering the desired references, the relative degree of (4.22) in $\mathbb{R}^3$ is 2 (respectively of (4.31) in $\mathbb{R}^5$ is 4), hence we have internal zero dynamics of order 1.
The zero dynamics are defined as the following:

$$y = V_{C1} \equiv V_{C1}^* \tag{4.35}$$

consequently

$$i_{L1} \equiv i_{L1}^* = \frac{V_{PV} - V_{C1}^*}{R_1} \tag{4.36}$$

and

$$\begin{aligned} u_1 &= \frac{1}{(V_{C2} + (R_{02} - R_{01})i_{L1})}\Big[V_{C2} - V_{C1} + R_{02}i_{L1} - L_1(K_3 e_{i_{L1}} + \overline{K}_3\alpha_3 \\ &- C_1\overline{K}_1 K_1^{\alpha} e_{V_{C1}} + (C_1K_1 - \frac{1}{R_1})(K_1 e_{V_{C1}} + \overline{K}_1\alpha_1))\Big] \end{aligned}$$

we can rewrite the zero dynamics equation as:

$$
\begin{aligned}
\dot{V}_{C2} &= \frac{1}{R_2C_2}(V_{DC}-V_{C2})+\frac{(1-u_1)}{C_2}i_{L1} \\
&= \frac{1}{R_2C_2}(V_{DC}-V_{C2}) \\
&\quad +(1-\left(\frac{R_1(V_{C2}-V_{C1}^*)+R_{02}(V_{PV}-V_{C1}^*)}{(R_1V_{C2}+(R_{02}-R_{01})(V_{PV}-V_{C1}^*))}\right)) \\
&\quad \frac{V_{PV}-V_{C1}^*}{R_1C_2} \\
&= \frac{1}{R_2C_2}(V_{DC}-V_{C2}) \\
&\quad +\frac{1}{(R_1V_{C2}+(R_{02}-R_{01})(V_{PV}-V_{C1}^*))} \\
&\quad ((\cancel{R_1V_{C2}}+(\cancel{R_{02}}-R_{01})(V_{PV}-V_{C1}^*))-(R_1(\cancel{V_{C2}}-V_{C1}^*)+\cancel{R_{02}}(V_{PV}-V_{C1}^*))) \\
&\quad \frac{V_{PV}-V_{C1}^*}{R_1C_2} \\
&= \frac{1}{R_2C_2}(V_{DC}-V_{C2})+\frac{(R_1V_{C1}^*-R_{01}(V_{PV}-V_{C1}^*))}{(R_1V_{C2}+(R_{02}-R_{01})(V_{PV}-V_{C1}^*))}\frac{V_{PV}-V_{C1}^*}{R_1C_2} \\
&= \frac{1}{R_2C_2}(V_{DC}-V_{C2})+\frac{1}{C_2}[\frac{\mu}{(V_{C2}+\frac{(R_{02}-R_{01})}{R_1}(V_{PV}-V_{C1}^*)}]
\end{aligned}
$$

where

$$\mu=\frac{1}{R_1}(V_{PV}-V_{C1}^*)[V_{C1}^*-\frac{R_{01}}{R_1}(V_{PV}-V_{C1}^*)]$$

Now we must study the stability of this Zero Dynamic. For this, we consider it around the equilibrium points.

The equilibrium points of zero dynamics V_{C2} are the solutions of:

$$a_1V_{C2}^2+a_2V_{C2}+a_3=0 \tag{4.37}$$

with:

$$a_1=-\frac{1}{R_2C_2} \tag{4.38}$$

$$a_2=\frac{V_{DC}}{R_2C_2}-\frac{(R_{02}-R_{01})}{R_1}(V_{PV}-V_{C1}^*) \tag{4.39}$$

$$a_3=\frac{V_{DC}}{R_2C_2}-\frac{(R_{02}-R_{01})}{R_1}(V_{PV}-V_{C1}^*)+\frac{1}{R_2C_2}\frac{(V_{PV}-V_{C1}^*)}{R_1}[V_{C1}^*-\frac{R_{01}}{R_1}(V_{PV}-V_{C1}^*)] \tag{4.40}$$

Providing the results:

$$V_{C2_{1.2}}^*=\frac{-a_2\pm\sqrt{a_2^2-4a_1a_3}}{2a_1} \tag{4.41}$$

We can study the stability of these zero dynamics by taking the tangent linearization of V_{C2} dynamical equation as $J_{V_{C2}}$.

$$\begin{aligned} J_{V_{C2}} &= -\frac{1}{R_2C_2} + \left(\frac{1}{C_2}\mu * \left((V_{C2} + \frac{(R_{02}-R_{01})}{R_1}(V_{PV} - V_{C1}^*)\right)^{-1}\right)' \\ &= -\frac{1}{R_2C_2} - \frac{1}{C_2}\mu * \left((V_{C2} + \frac{(R_{02}-R_{01})}{R_1}(V_{PV} - V_{C1}^*)\right)^{-2} \\ &= -\frac{1}{R_2C_2} - \frac{1}{C_2}\frac{\mu}{(V_{C2} + \frac{(R_{02}-R_{01})}{R_1}(V_{PV} - V_{C1}^*))^2} \end{aligned}$$

According to that, stability of the equilibrium points will depend on sign of μ. Before the discussion about their possible values, it must be noticed that in the PV case the current will go from the PV to the grid only: the considered case will then impose $(V_{PV} - V_{C1}^*) > 0$. Let us now take into account the possible cases:

1. $\mu > 0$: the Jacobian is always negative and then the system is always stable. In order to have such positive μ the only possible case is

$$(V_{PV} - V_{C1}^*) > 0 \text{ and } (V_{C1}^* - \frac{R_{01}}{R_1}(V_{PV} - V_{C1}^*)) > 0$$

then

$$\frac{R_{01}}{R_1 + R_{01}}V_{PV} < V_{C1}^* < V_{PV} \tag{4.42}$$

2. $\mu = 0$: in this case zero dynamics are a linear asymptotically stable system. One of the following conditions will then take place:

$$V_{PV} = V_{C1}^* \text{ or } V_{C1}^* = \frac{R_{01}}{R_1 + R_{01}}V_{PV} \tag{4.43}$$

3. $\mu < 0$: in this case, depending on values of states and parameters, there would exist stable and unstable operating regions. Nevertheless, such case needs that:

$$\begin{aligned} \mu &= \frac{1}{R_1}(V_{PV} - V_{C1}^*)[V_{C1}^* - \frac{R_{01}}{R_1}(V_{PV} - V_{C1}^*)] < 0 \\ & (R_1 + R_{01})V_{C1}^* - R_{01}V_{PV} < 0 \\ & V_{C1}^* < \frac{R_{01}V_{PV}}{R_1 + R_{01}} \end{aligned}$$

that for technological reasons (much smaller value of R_{01} than that of R_1) wold not be feasible. So, in order to theoretically avoid such possibility, it is sufficient to require that:

$$V_{C1}^* > \frac{R_{01}V_{PV}}{R_1 + R_{01}} \tag{4.44}$$

Under conditions (4.30) and requirement (4.44), we can state that the system is always stable and converge to the calculated equilibrium point.

□

4.5.2 Storage System Local Control

The hybrid storage system (battery-supercapacitor) adopts the advantages of both technologies, high power density from the supercapacitor and high energy density from the battery, and consists of a lead acid battery and a supercapacitor like in [84], [90], [71] and [91]. The control target is to stabilize V_{DC} to its nominal value.

We define the output tracking errors:

$$e_{i_{L2}} = (i_{L2} - i^*_{L2})$$

$$e_{i_{L3}} = (i_{L3} - i^*_{L3})$$

We need to design a control law u_2 and u_3 such as to steer i_{L2} and i_{L3} towards their references i^*_{L2} and i^*_{L3} respectevely.

Bidirectional Boost Converter

The bidirectional boost converter controlling the battery is modeled based on the voltages on the capacitors C_3, C_4 and the current in the inductance i_{L2} [76],[75],[77].

For modeling the switches T_1 and T_2 the conduction losses are taken into account by considering small resistances R_{03} and R_{04}. We select 3 state variables for each converter, capacitors' voltage V_{C3} and $V_{C4} \in \mathbb{R}^+$ and inductor's current $i_{L2} \in \mathbb{R}$.

The Mathematical model is given based on power electronics averaging method.

$$\begin{aligned}
\dot{V}_{C3} &= -\frac{1}{R_3 C_3} V_{C3} - \frac{1}{C_3} i_{L2} + \frac{1}{R_3 C_3} V_{BAT} \\
\dot{V}_{C4} &= -\frac{1}{R_4 C_4} V_{C4} + \frac{(1-u_2)}{C_4} i_{L2} + \frac{1}{R_4 C_4} V_{DC} \\
\dot{i}_{L2} &= \frac{1}{L_2} V_{C3} - \frac{([(R_{03} - R_{04})u_2 + R_{04}]i_{L2})}{L_2} - \frac{(1-u_2)}{L_2} V_{C4}
\end{aligned} \tag{4.45}$$

Control strategy

To design correctly the control law, it is necessary to take two steps. The first is to respond to the need of a power transfer from the network to the storage systems and vice-versa. The first objective in this step is to regulate the DC MicroGrid voltage .

it is done under assumption The state of the charge for the battery (SOC) must be kept inside $40\% < SOC < 80\%$.

In the following, it is used the assumption that the current can be set to have much faster dynamic than the capacitances' voltages [9]. storage current and voltage regulation consists in a cascade control: there will be an inner current loop and an outer voltage loop. The dynamics can be designed such as to present two time scales. The capacitance's voltage for the dc microgrid will get assigned to have slow dynamics.

we consider the inner current loop and deal with the control of the converter that directly acts on the network. This step is used when the state of charge (SOC) is between 40% and 80% .

The outer voltage loop is used to extract the reference for current regulation ,it was done in by High level controller we seen before.

Current Control law for the battery

We need to assign the i_{L2}^* reference value to i_{L2} in order to obtain convergence to the desired equilibrium DC grid's voltage. This is done by input/output feedback linearization as follows. First we define an extended state α_6 governed by equation:

$$\dot{\alpha}_6 = K_6^{\alpha} e_{i_{L2}} \tag{4.46}$$

we need to design a control law u_2 such as to steer i_{L2} towards its reference i_{L2}^* by imposing new desired dynamics:

$$\dot{e}_{i_{L2}} = -K_6 e_{i_{L2}} - \overline{K_6}\alpha_6 \tag{4.47}$$

Then considering the third equation of (4.45) we can rewrite $\dot{i}_{L2}$ as:

$$\begin{aligned} \dot{i}_{L2} &= \frac{1}{L_2}V_{C3} - \frac{([(R_{03}-R_{04})u_2 + R_{04}]i_{L2})}{L_2} - \frac{(1-u_2)}{L_2}V_{C4} \\ &= \frac{1}{L_2}\left((V_{C3}-V_{C4}) - R_{04}i_{L2} + (V_{C4} + (R_{04}-R_{03})i_{L2})u_2\right) \end{aligned}$$

and we may obtain the following control law:

$$u_2 = \frac{1}{(V_{C4} + (R_{04}-R_{03})i_{L2}}\Big)[-(V_{C3}-V_{C4}) + R_{04}i_{L2} - L_2(K_6(i_{L2}-i_{L2}^*) + \overline{K}_6\alpha_6) + \dot{i}_{L2}^*] \tag{4.48}$$

with condition:

$$V_{C4} + (R_{04}-R_{03})i_{L2} \neq 0 \tag{4.49}$$

such as to obtain an arbitrary linear system for the states $[\alpha_6\ i_{L2}]^T$ for suitable choice of gains $K_6, \overline{K}_6, K_6^{\alpha}$. The closed loop sub-system becomes:

$$\begin{aligned} \dot{\alpha}_6 &= K_6^{\alpha} e_{i_{L2}} \\ \dot{e}_{i_{L2}} &= -K_6 e_{i_{L2}} - \overline{K}_6\alpha_6 \end{aligned}$$

We consider an augmented system $\widetilde{i}_{L2}$:

$$\widetilde{i}_{L2} = \begin{bmatrix} \alpha_6 \\ i_{L2} - i_{L2}^* \end{bmatrix}$$

Its closed loop (linear) dynamics is here defined with the eigenvalues:

$$\dot{\widetilde{i}}_{L2} = A_6\widetilde{i}_{L2} = \begin{bmatrix} 0 & K_6^{\alpha} \\ -\overline{K}_6 & -K_6 \end{bmatrix}$$

$$\lambda_{7.8} = -\frac{1}{2}(K_6 \pm \sqrt{(K_6^2 - 4\overline{K}_6 K_6^\alpha)})$$

By properly selecting positive gains K_6, $\overline{K}_6$ and K_6^α both eigenvalues are stable; then the origin is a stable equilibrium point for the augmented state, and we can state that the control input u_2 feedback linearizes the dynamics of V_{DC} and i_{L2}. As a corollary, there exists $P_6 = P_6^T > 0$ such that $P_6 A_6 + A_6^T P_6 = -I_2$ where I_2 is an identity matrix in $\mathbb{R}^2$.

- Stability study

$$\begin{aligned}
\dot{V}_{C3} &= -\frac{1}{R_3 C_3} V_{C3} - \frac{1}{C_3} i_{L2} + \frac{1}{R_3 C_3} V_{BAT} \\
\dot{V}_{C4} &= -\frac{1}{R_4 C_4} V_{C4} + \frac{(1-u_2)}{C_4} i_{L2} + \frac{1}{R_4 C_4} V_{DC} \\
\dot{i}_{L2} &= \frac{1}{L_2} V_{C3} - \frac{([(R_{03} - R_{04})u_2 + R_{04}]i_{L2})}{L_2} - \frac{(1-u_2)}{L_2} V_{C4} \\
\dot{\alpha}_6 &= \overline{K}_6 e_{i_{L1}}
\end{aligned} \tag{4.50}$$

Lemma 4.5.2. *Under control law (4.48), and suitable control gains K_6, $\overline{K}_6$ and K_6^α, the closed-loop system (4.50) has one equilibrium point. Any evolution starting from initial conditions satisfying the condition $V_{C4} + (R_{04} - R_{03})i_{L2} \neq 0$, exponentially converges to this equilibrium point.*

Proof. We introduce the Lyapunov function

$$V_{6,10} = ([\alpha_{10}\ e_{V_{DC}}]^T\ P_{10}\ [\alpha_{10}\ e_{V_{DC}}])\ +\ ([\alpha_6\ e_{i_{L2}}]^T\ P_6\ [\alpha_6\ e_{i_{L2}}]) \tag{4.51}$$

It's derivative is then:

$$\begin{aligned}
\dot{V}_{10,6} &= [\dot{\alpha}_{10}\ \dot{e}_{V_{DC}}]^T\ P_{10}\ [\alpha_{10}\ e_{V_{DC}}] + [\alpha_{10}\ e_{V_{DC}}]^T\ P_{10}\ [\dot{\alpha}_{10}\ \dot{e}_{V_{DC}}] \\
&+ [\dot{\alpha}_6\ \dot{e}_{i_{L2}}]^T\ P_6\ [\alpha_6\ e_{i_{L2}}] + [\alpha_6\ e_{i_{L2}}]^T\ P_6\ [\dot{\alpha}_6\ \dot{e}_{i_{L2}}]
\end{aligned}$$

$$\dot{V}_{10,6} = [\alpha_{10}\ e_{V_{DC}}]^T\ (A_{10}^T\ P_{10} + P_{10}\ A_{10})\ [\alpha_{10}\ e_{V_{DC}}]\ +\ [\alpha_6\ e_{i_{L2}}]^T\ (A_6^T\ P_6 + P_6\ A_6)\ [\alpha_6\ e_{i_{L2}}] \tag{4.52}$$

We now that $P_{10}A_{10} + A_{10}^T P_{10} = -I_2$ and $P_6 A_6 + A_6^T P_6 = -I_2$.
Then

$$\dot{V}_{10.6} = -e_{V_{DC}}^2 - \alpha_{10}^2 - e_{i_{L2}}^2 - \alpha_6^2 \tag{4.53}$$

For the quadratic positive definite function $V(x) = x^T P x$ ([87]):

$$\lambda_{min}(P)\,||x||^2\ \leq\ x^T P x\ \leq\ \lambda_{max}(P)\,||x||^2 \tag{4.54}$$

and we can write:

$$\dot{V}_{10.6} \leq -\frac{1}{\lambda_{max}} V_{10.6} \stackrel{\triangle}{=} -m_2\ V_{10.6} \tag{4.55}$$

$$V_{6,10}(t) = e^{-m_{6,10}t}\, V_{6,10}(0) \tag{4.56}$$

$$\lim_{t\to\infty} \left\| \begin{bmatrix} e_{VDC}(t) \\ \alpha_{10}(t) \\ e_{i_{L2}}(t) \\ \alpha_6(t) \end{bmatrix} \right\| = 0$$

and the system is exponentially stable.

Let us now move the focus to the remaining zero dynamics. They are defined following:

$$y_2 = i_{L2} = i^*_{L2} \tag{4.57}$$

Let us rewrite equation 2 of (4.45) as:

$$\begin{aligned}
\dot{V}_{C4} &= -\frac{1}{R_4C_4}V_{C4} + \frac{(1-u_2)}{C_4}i_{L2} + \frac{1}{R_4C_4}V_{DC} \\
&= -\frac{1}{R_4C_4}V_{C4} + \frac{1}{C_4}i_{L2} + \frac{1}{R_4C_4}V_{DC} - \frac{i_{L2}}{C_4}u_2 \\
&= -\frac{1}{R_4C_4}V_{C4} + \frac{1}{R_4C_4}V_{DC} + \frac{1}{C_4}i^*_{L2} - \frac{i^*_{L2}}{C_4}\left(\frac{1}{(V_{C4}+(R_{04}-R_{03})i^*_{L2}}\right)[-(V_{C3}-V_{C4}) + R_{04}i^*_{L2})]\Big) \\
&= -\frac{1}{R_4C_4}(V_{C4}-V_{DC}) + \frac{1}{C_4(V_{C4}+(R_{04}-R_{03})i^*_{L2})} \\
&\quad (i^*_{L2}(V_{C4}+(R_{04}-R_{03})i^*_{L2}) - i^*_{L2}\left([-(V_{C3}-V_{C4}) + R_{04}i^*_{L2}]\right)) \\
&= -\frac{1}{R_4C_4}(V_{C4}-V_{DC}) + \frac{1}{C_4(V_{C4}+(R_{04}-R_{03})i^*_{L2})} \\
&\quad (i^*_{L2}(-R_{03})i^*_{L2}) - i^*_{L2}\left([-(V_{C3}))]\right)) \\
&= -\frac{1}{R_4C_4}(V_{C4}-V_{DC}) + \frac{1}{C_4(V_{C4}+(R_{04}-R_{03})i^*_{L2})} \\
&\quad i^*_{L2}\left(V_{C3} - R_{03}i^*_{L2}\right)
\end{aligned}$$

$$\dot{V}_{C4} = \frac{1}{R_4C_4}(V_{DC}-V_{C4}) + \frac{1}{C_4}[\frac{i^*_{L2}(V_{C3}-R_{03}i^*_{L2})}{V_{C4}+(R_{04}-R_{03})i^*_{L2}}] \tag{4.58}$$

We can then define:

$$\kappa = i^*_{L2}(R_{03}i^*_{L2} - V^*_{C3}) \tag{4.59}$$

we analyze now its behaviour around the equilibrium points. We can rewrite the equilibrium value for the control as:

$$u^*_2 = \frac{(-V_{C3}+V_{C4}+R_{04}i_{L2})}{(V_{C4}+(R_{04}-R_{03})i_{L2})} \tag{4.60}$$

The equilibrium points of V_{C4} are the solutions of:

$$b_1 V_{C4}^2 + b_2 V_{C4} + b_3 = 0 \tag{4.61}$$

with:

$$b_1 = -\frac{1}{R_4 C_4} \tag{4.62}$$

$$b_2 = \frac{1}{R_4 C_4}(V_{DC} - (R_{04} - R_{03}) i_{L2}^*) \tag{4.63}$$

$$b_3 = [\frac{V_{DC}}{R_4 C_4}(R_{04} - R_{03}) i_{L2}^*)] + \frac{1}{C_4} i_{L2}^* (V_{C3} - R_{03} i_{L2}^*) \tag{4.64}$$

Providing the results:

$$V_{C4_{1.2}}^* = \frac{-b_2 \pm \sqrt{b_2^2 - 4 b_1 b_3}}{2 b_1} \tag{4.65}$$

Finally we can state that the system in (4.45) has the following equilibria when we want to assign the dynamics i_{L2} to the value i_{L2}^* :

$$x^e = \begin{bmatrix} V_{C3}^e \\ V_{C4}^e \\ i_{L2}^e \\ \alpha_6^e \end{bmatrix} = \begin{bmatrix} V_{BAT} - R_3 iL2^* \\ R_4 i_{L2}^* (1 - u_2^*) \\ \frac{1}{R_3}(V_{BAT} - V_{C3}^*) \\ 0 \end{bmatrix}; \qquad u_2^e = \frac{(-V_{C3} + V_{C4} + R_{04} i_{L2})}{(V_{C4} + (R_{04} - R_{03}) i_{L2})} \tag{4.66}$$

We can study the stability of the zero dynamics by taking the tangent linearization of V_{C3} and V_{C4} dynamical equations as $J_{V_{C3},V_{C4}}$ as follows. First, the Equations for zero dynamics are:

$$\begin{aligned} \dot{V}_{C3} &= -\frac{1}{R_3 C_3} V_{C3} - \frac{1}{C_3} i_{L2} + \frac{1}{R_3 C_3} V_{BAT} \\ \dot{V}_{C4} &= -\frac{1}{R_4 C_4} V_{C4} + \frac{(1 - u_2)}{C_4} i_{L2} + \frac{1}{R_4 C_4} V_{DC} \end{aligned} \tag{4.67}$$

we can rewrite:

$$\begin{aligned} \dot{V}_{C3} &= -\frac{1}{R_3 C_3} V_{C3} - \frac{1}{C_3} i_{L2} + \frac{1}{R_3 C_3} V_{BAT} \\ \dot{V}_{C4} &= \frac{1}{R_4 C_4}(V_{DC} - V_{C4}) + \frac{1}{C_4}[\frac{i_{L2}^*(V_{C3} - R_{03} i_{L2}^*)}{V_{C4} + (R_{04} - R_{03}) i_{L2}^*}] \end{aligned} \tag{4.68}$$

$$\begin{aligned} \dot{V}_{C3} &= -\frac{1}{R_3 C_3} V_{C3} - \frac{1}{C_3} i_{L2} + \frac{1}{R_3 C_3} V_{BAT} \qquad (4.69) \\ \dot{V}_{C4} &= +\frac{1}{C_4}[\frac{i_{L2}^*(V_{C3}}{V_{C4} + (R_{04} - R_{03}) i_{L2}^*}] - \frac{1}{R_4 C_4} V_{C4} - \frac{1}{C_4}[\frac{i_{L2}^{2*} R_{03}}{V_{C4} + (R_{04} - R_{03}) i_{L2}^*}] + \frac{1}{R_4 C_4} V_{DC} \end{aligned}$$

The analysis is performed using the linearization around the equilibrium point. Matrix J_3 below is the Jacobian linearization matrix around V_{C3}^* and V_{C4}^*:

$$J_{V_{C3},V_{C4}} = \begin{bmatrix} -\frac{1}{R_3C_3} & 0 \\ \frac{1}{C_4}\left[\frac{i_{L2}^*}{V_{C4}^*+(R_{04}-R_{03})i_{L2}^*}\right] & -\frac{1}{R_4C_4} - \frac{i_{L2}^*(V_{C3}-R_{03}i_{L2}^*)}{C_4(V_{C4}+(R_{04}-R_{03})i_{L2}^*)^2} \end{bmatrix} \tag{4.70}$$

where

$$\kappa = i_{L2}^*(V_{C3} - R_{03}i_{L2}^*)$$

To establish the stability of the zero dynamics, it is computed the eigenvalues $\lambda_{V_{C3},V_{C4}}$ that can be written as:

$$\lambda_{V_{C3}} = -\frac{1}{R_3C_3}$$

$$\lambda_{V_{C4}} = -\frac{1}{R_4C_4} - \frac{\kappa}{C_4(V_{C4} + (R_{04} - R_{03})i_{L2}^*)^2}$$

Now, we can analyse the different cases. where

$$\kappa = \frac{1}{R_1}(V_{PV} - V_{C1}^*)[V_{C1}^* - \frac{R_{01}}{R_1}(V_{PV} - V_{C1}^*)]$$

1. $\kappa > 0$ the Jacobian is always negative and then the system is always stable. In order to have such negative κ the possibilities are either $i_{L2}^* < 0$ and $(R_{03}i_{L2}^* - V_{C3}^*) < 0$, or $i_{L2}^* > 0$ and $(R_{03}i_{L2}^* - V_{C3}^*) > 0$ and a consequence we obtain the conditions:

$$i_{L2}^* < 0 \quad and \quad i_{L2}^* < \frac{V_{C3}^*}{R_{03}} \tag{4.71}$$

$$i_{L2}^* > 0 \quad and \quad i_{L2}^* > \frac{V_{C3}^*}{R_{03}} \tag{4.72}$$

2. $\kappa = 0$ the Jacobian is always negative and then the system is always stable.

3. $\kappa < 0$, the system will be stable while the condition below holds:

$$\frac{(V_{C4} + (R_{04} - R_{03})i_{L2}^*)^2}{R_4} > \kappa \tag{4.73}$$

what implies that :

$$\frac{(V_{C4} + (R_{04} - R_{03})i_{L2}^*)^2}{R_4} > i_{L2}^{2*}R_{03} - i_{L2}^*V_{C3}^* \tag{4.74}$$

$$\frac{(V_{C4} + (R_{04} - R_{03})i_{L2}^*)^2}{R_4} + i_{L2}^*V_{C3}^* > i_{L2}^{2*}R_{03} \tag{4.75}$$

The term $i_{L2}^{2*}R_{03}$ represents power losses in interrupter, it is very small and the condition is always fulfilled in practice.

We can then state that the Jacobian is always negative and then in real operating conditions the system is always asymptotically stable.

□

Supercapacitor

- Bidirectional Boost Converter's Model

The bidirectional boost converter controlling the supercapacitor is modeled based on the voltages on the capacitors C_5, C_6 and the current in the inductance L_3 [76],[75],[77].

$$\begin{aligned}
\dot{V}_{C5} &= -\frac{1}{R_5C_5}V_{C5} - \frac{1}{C_5}i_{L3} + \frac{1}{R_5C_5}V_{SC} \\
\dot{V}_{C6} &= -\frac{1}{R_6C_6}V_{C6} + \frac{(1-u_3)}{C_6}i_{L3} + \frac{1}{R_6C_6}V_{DC} \\
\dot{i}_{L3} &= \frac{1}{L_3}V_{C5} - \frac{([(R_{05}-R_{06})u_3 + R_{06}]i_{L3})}{L_3} - \frac{(1-u_3)}{L_3}V_{C6}
\end{aligned} \tag{4.76}$$

Current Control law for the supercapacitor

We need to assign the i^*_{L3} reference value to i_{L3} in order to obtain convergence to the desired equilibrium DC grid's voltage. This is done by input/output feedback linearization as follows. First we define an extended state α_9 governed by equation:

$$\dot{\alpha}_9 = K^{\alpha}_9 e_{i_{L3}} \tag{4.77}$$

we need to design a control law u_3 such as to steer i_{L3} towards its reference i^*_{L3} . As before, there is also a desired dynamic behaviour to impose:

$$\dot{e}_{i_{L3}} = -K_9 e_{i_{L3}} - \overline{K_9}\alpha_9 \tag{4.78}$$

The first step constitutes to rewrite the last equation of (4.76) as:

$$\begin{aligned}
\dot{i}_{L3} &= \frac{1}{L_3}V_{C5} - \frac{([(R_{05}-R_{06})u_3 + R_{06}]i_{L3})}{L_3} - \frac{(1-u_3)}{L_3}V_{C6} \\
\dot{i}_{L3} &= \frac{1}{L_3}V_{C5} - \frac{1}{L_3}\left(((R_{05}-R_{06})u_3 i_{L3} + R_{06}i_{L3}) - V_{C6} + u_3 V_{C6}\right) \\
\dot{i}_{L3} &= \frac{1}{L_3}V_{C5} - \frac{1}{L_3}\left(+R_{06}i_{L3} - V_{C6} + [(R_{05}-R_{06})i_{L3} + V_{C6}]u_3\right)
\end{aligned} \tag{4.79}$$

with the positive tuning gain parameters K_9, $\overline{K}_9$ and K^{α}_9, we obtain the following control law:

$$u_3 = \frac{1}{(V_{C6} + (R_{06}-R_{05})i_{L3}}\Big)[-V_{C5} + V_{C6} + R_{05}i_{L3} - L_3(K_9(i_{L3} - i^*_{L3}) + \overline{K}_9\alpha_9 + i^*_{L3})] \tag{4.80}$$

With condition :

$$V_{C6} + (R_{06} - R_{05})i_{L3} \neq 0 \tag{4.81}$$

such as to obtain an arbitrary linear system for the states $[\alpha_9\ i_{L3}]^T$ for suitable choice of gains $K_9, \overline{K}_9, K_9^\alpha$. The closed loop sub-system becomes:

$$\begin{aligned}\dot{\alpha}_9 &= K_9^\alpha e_{i_{L3}} \\ \dot{e}_{i_{L3}} &= -K_9 e_{i_{L3}} - \overline{K}_9 \alpha_9\end{aligned}$$

Again we consider an augmented system $\widetilde{i}_{L3}$:

$$\widetilde{i}_{L3} = \begin{bmatrix} \alpha_9 \\ i_{L3} - i_{L3}^* \end{bmatrix}$$

Its closed loop (linear) dynamics are here defined with their eigenvalues:

$$\dot{\widetilde{i}}_{L3} = A_9 \widetilde{i}_{L3} \triangleq \begin{bmatrix} 0 & K_9^\alpha \\ -\overline{K}_9 & -K_9 \end{bmatrix} \widetilde{i}_{L3}$$

$$\lambda_{9.10} = -\frac{1}{2}(K_9 \pm \sqrt{(K_9^2 - 4\overline{K}_9 K_9^\alpha)})$$

By properly selecting positive gains K_9, $\overline{K}_9$ and K_9^α both eigenvalues are stable; then the origin is a asymptotic stable equilibrium point for the augmented state. As a corollary, there exist $P_9 = P_9^T > 0$ such that $P_9 A_9 + A_9^T P_9 = -I_2$ where I_2 is an identity matrix in $\mathbb{R}^2$.

Let us consider the system

$$\begin{aligned}\dot{V}_{C5} &= -\frac{1}{R_5 C_5} V_{C5} - \frac{1}{C_5} i_{L3} + \frac{1}{R_5 C_5} V_{SC} \\ \dot{V}_{C5} &= -\frac{1}{R_6 C_6} V_{C6} + \frac{(1-u_3)}{C_6} i_{L3} + \frac{1}{R_6 C_6} V_{DC} \\ \dot{i}_{L3} &= \frac{1}{L_3} V_{C5} - \frac{([(R_{05} - R_{06})u_3 + R_{06}]i_{L3})}{L_3} - \frac{(1-u_3)}{L_3} V_{C6} \\ \dot{\alpha}_9 &= K_9^\alpha e_{i_{L3}} \qquad (4.82)\end{aligned}$$

(4.83)

Lemma 4.5.3. *Under control law (4.80), and suitable control gains K_1, $\overline{K}_1$, K_1^α, K_3, $\overline{K}_3$ and $K_3^\alpha > 0$, the closed-loop system (4.76), (4.83) has an equilibrium point. Any evolution starting from initial conditions respecting $V_{C2} + (R_{02} - R_{01}) i_{L1} \neq 0$ asymptotically converges to this equilibrium point.*

Proof. We introduce the Lyapunov function

$$V_9 = ([\alpha_9\ e_{i_{L3}}]^T\ P_9\ [\alpha_9\ e_{i_{L3}}]) \qquad (4.84)$$

It's derivative is then:

$$\dot{V}_9 = [\dot{\alpha}_9\ \dot{e}_{i_{L3}}]^T\ P_9\ [\alpha_9\ e_{i_{L3}}] + [\alpha_9\ e_{i_{L3}}]^T\ P_9\ [\dot{\alpha}_9\ \dot{e}_{i_{L3}}] \qquad (4.85)$$

$$\dot{V}_9 = [\alpha_9 \; e_{i_{L3}}]^T \; (A_9^T \; P_9 + P_9 \; A_9) \; [\alpha_9 \; e_{i_{L3}}] \tag{4.86}$$

we know that $P_9 A_9 + A_9^T P_9 = -I_2$, then:

$$\dot{V}_9 \;\; = \;\; -e_{i_{L3}}^2 - \alpha_9^2 \tag{4.87}$$

again we use the inequalities:

$$\dot{V}_9 \leq -\frac{1}{\lambda_{max}(P_9)} V_9 \stackrel{\triangle}{=} \dot{V}_9 \leq -m_9 \; V_9 \tag{4.88}$$

which implies that:

$$V_9(t) = e^{-m_9 t} \; V_9(0) \tag{4.89}$$

$$\lim_{t \to \infty} \left\| \begin{bmatrix} e_{i_{L3}}(t) \\ \alpha_9(t) \end{bmatrix} \right\| = 0$$

and the subsystem is exponentially stable.

Let us now move the focus to the remaining zero dynamics. They are defined following:

$$y_3 = i_{L3} = i_{L3}^* \tag{4.90}$$

The first step constitutes to rewrite the last equation of (4.76) as:

$$\begin{aligned}
\dot{i}_{L3} &= \frac{1}{L_3} V_{C5} - \frac{([(R_{05} - R_{06})u_3 + R_{06}]i_{L3})}{L_3} - \frac{(1 - u_3)}{L_3} V_{C6} \\
\dot{i}_{L3} &= \frac{1}{L_3} V_{C5} - \frac{1}{L_3} \left(((R_{05} - R_{06})u_3 i_{L3} + R_{06} i_{L3}) - V_{C6} + u_3 V_{C6} \right) \\
\dot{i}_{L3} &= \frac{1}{L_3} V_{C5} - \frac{1}{L_3} \left(+ R_{06} i_{L3} - V_{C6} + [(R_{05} - R_{06}) i_{L3} + V_{C6}] u_3 \right) \qquad (4.91) \\
& \qquad\qquad\qquad\qquad\qquad\qquad\qquad\qquad\qquad\qquad\qquad\qquad (4.92)
\end{aligned}$$

we can rewrite the equilibrium point for control as:

$$u_3^* = \frac{(-V_{C5} + V_{C6} + R_{06} i_{L3})}{(V_{C6} + (R_{06} - R_{05}) i_{L3})} \tag{4.93}$$

The equilibrium points for V_{C6} are the solutions of:

$$c_1 V_{C6}^2 + c_2 V_{C6} + c_3 = 0 \tag{4.94}$$

With:

$$c_1 = -\frac{1}{R_6 C_6} \tag{4.95}$$

$$c_2 = \frac{1}{R_6 C_6}(V_{DC} - (R_{06} - R_{05})i^*_{L3}) \tag{4.96}$$

$$c_3 = [\frac{V_{DC}}{R_6 C_6}(R_{06} - R_{05})i^*_{L3})] + \frac{1}{C_6} i^*_{L3}(V_{C5} - R_{05} i^*_{L3}) \tag{4.97}$$

Providing the results

$$V^*_{C6_{1.2}} = \frac{-c_2 \pm \sqrt{c_2^2 - 4b_1 c_3}}{2c_1} \tag{4.98}$$

Finally we can state that the system in (4.76) has the following equilibria when we want to assign the dynamics i_{L3} to the value i^*_{L3} :

$$x^e = \begin{bmatrix} V^e_{C5} \\ V^e_{C6} \\ i^e_{L3} \\ \alpha^e_9 \end{bmatrix} = \begin{bmatrix} V_{SC} \\ R_6 i_{L3}(1 - u^*_3) \\ \frac{1}{R_5}(V_{SC} - V^*_{C5}) \\ 0 \end{bmatrix}; \qquad u^e_3 = \frac{(-V_{C5} + V_{C6} + R_{06} i_{L3})}{(V_{C6} + (R_{06} - R_{05})i_{L3})} \tag{4.99}$$

The equations for the zero dynamics are:

$$\begin{aligned} \dot{V}_{C5} &= -\frac{1}{R_5 C_5} V_{C5} - \frac{1}{C_5} i^*_{L3} + \frac{1}{R_5 C_5} V_{SC} \\ \dot{V}_{C6} &= -\frac{1}{R_6 C_6} V_{C6} + \frac{(1 - u_3)}{C_6} i^*_{L3} + \frac{1}{R_6 C_6} V_{DC} \end{aligned} \tag{4.100}$$

and then:

$$\begin{aligned}
\dot{V}_{C6} &= -\frac{1}{R_6 C_6} V_{C6} + \frac{(1 - u_3)}{C_6} i^*_{L3} + \frac{1}{R_6 C_6} V_{DC} \\
\dot{V}_{C6} &= \frac{1}{R_6 C_6}(V_{DC} - V_{C6}) + \frac{i^*_{L3}}{C_6} - \frac{u_3 i^*_{L3}}{C_6} \\
\dot{V}_{C6} &= \frac{1}{R_6 C_6}(V_{DC} - V_{C6}) + \frac{i^*_{L3}}{C_6} - \frac{i^*_{L3}}{C_6}\left(\frac{1}{(V_{C6} + (R_{06} - R_{05})i_{L3}}\right)[-V_{C5} + V_{C6} + R_{06} i^*_{L3}]\Big) \\
\dot{V}_{C6} &= \frac{1}{R_6 C_6}(V_{DC} - V_{C6}) + \frac{i^*_{L3}}{C_6}\frac{1}{(V_{C6} + (R_{06} - R_{05})i^*_{L3}}\,(V_{C6} + (R_{06} - R_{05})i^*_{L3} + V_{C5} - V_{C6} - R_{06} i^*_{L3}) \\
\dot{V}_{C6} &= \frac{1}{R_6 C_6}(V_{DC} - V_{C6}) + \frac{i^*_{L3}}{C_6}\frac{1}{(V_{C6} + (R_{06} - R_{06})i^*_{L3}}\,(+(R_{06} - R_{05})i^*_{L3} + V_{C5} - R_{05} i^*_{L3}) \\
\dot{V}_{C6} &= \frac{1}{R_6 C_6}(V_{DC} - V_{C6}) + \frac{1}{C_6}[\frac{i^*_{L3}(V_{C5} - (R_{05})i^*_{L3})}{V_{C6} + (R_{06} - R_{05})i^*_{L3}}] \\
\dot{V}_{C6} &= \frac{1}{R_6 C_6}(V_{DC} - V_{C6}) + \frac{1}{C_6}[\frac{i^*_{L3}(V_{C5} - (R_{05})i^*_{L3})}{V_{C6} + (R_{06} - R_{05})i^*_{L3}}] \\
\dot{V}_{C6} &= \frac{1}{C_6}[\frac{i^*_{L3} V_{C5}}{V_{C6} + (R_{06} - R_{05})i^*_{L3}}] - \frac{1}{R_6 C_6} V_{C6} + \frac{1}{C_6}[\frac{i^*_{L3}(-(R_{05})i^*_{L3})}{V_{C6} + (R_{06} - R_{05})i^*_{L3}}] + \frac{1}{R_6 C_6} V_{DC}
\end{aligned}$$

The analysis of these zero dynamics is performed using the linearization around the equilibrium points in order to check stability. Matrix J_4 below is the Jacobian linearization Matrix:

$$J_{v_{C5},V_{C6}} = \begin{bmatrix} -\frac{1}{R_5 C_5} & 0 \\ \frac{1}{C_6}\left[\frac{i^*_{L3}}{V^*_{C6}+(R_{06}-R_{05})i^*_{L3}}\right] & -\frac{1}{R_6 C_6} - \frac{\gamma}{C_6(V^*_{C6}+(R_{06}-R_{05})i^*_{L3})^2} \end{bmatrix} \tag{4.101}$$

Where:

$$\gamma = i^*_{L3}(V^*_{C5} + (R_{06} - 2R_{05})i^*_{L3}) \tag{4.102}$$

To study the stability of such zero dynamics, one must analyse the eigenvalues $\lambda_{V_{C5},V_{C6}}$ that can be written as:

$$\begin{aligned} \lambda V_{C5} &= -\frac{1}{R_5 C_5} \\ \lambda_{V_{C3}} &= -\frac{1}{R_6 C_6} - \frac{\gamma}{C_6(V_{C6} + (R_{06} - R_{05})i^*_{L3})^2} \end{aligned} \tag{4.103}$$

The stability will be given by the following cases:

1. $\gamma > 0$ the Jacobian is always negative and then the system is always stable. In order to have such negative γ the possibilities are:

   $i^*_{L3} < 0$ and $(R_{05} i^*_{L3} - V^*_{C5}) < 0$

   $$i^*_{L3} < 0 \quad and \quad i^*_{L3} < \frac{V^*_{C5}}{R_{05}} \tag{4.104}$$

   $i^*_{L2} > 0$ and $(R_{03} i^*_{L2} - V^*_{C3}) > 0$

   $$i^*_{L3} > 0 \quad and \quad i^*_{L32} > \frac{V^*_{C5}}{R_{05}} \tag{4.105}$$

2. $\gamma = 0$ the Jacobian is always negative and then the system is always stable.

3. $\gamma < 0$, the system will be stable while the condition below holds:

   $$\frac{(V_{C6} + (R_{06} - R_{05})i^*_{L3})^2}{R_6} > \gamma \tag{4.106}$$

   So, it is needed to be respected in order to assure stability the relations:

   $$\frac{(V_{C6} + (R_{06} - R_{05})i^*_{L3})^2}{R_6} > i^{2*}_{L3} R_{05} - i^*_{L3} V^*_{C5} \tag{4.107}$$

   $$\frac{(V_{C6} + (R_{06} - R_{05})i^*_{L3})^2}{R_6} + i^*_{L3} V^*_{C5} > i^{2*}_{L3} R_{05} \tag{4.108}$$

   $i^{2*}_{L3} R_{05}$ represent power loss in interrupter,it is very small.

Then in real operating conditions the Jacobian is always negative and then in this case the full system is asymptotically stable

□

4.6 Stability study of interconnected System

Let us now analyze the interconnected MicroGrid system. Its mathematical model is obtained considering a DC grid, a DC/DC boost converter interfacing a PV, and DC/DC boost Bidirectional converters for the Battery and supercapacitor as shown in Figure (4.2), [92],[78],[76],[93].

$$\begin{aligned}
\dot{V}_{C1} &= -\frac{1}{R_1C_1}V_{C1} - \frac{1}{C_1}i_{L1} + \frac{1}{R_1C_1}V_{PV} \\
\dot{V}_{C2} &= -\frac{1}{R_2C_2}V_{C2} + \frac{(1-u_1)}{C_2}i_{L1} + \frac{1}{R_2C_2}V_{DC} \\
\dot{i}_{L1} &= \frac{1}{L_1}V_{C1} - \frac{([(R_{01}-R_{02})u_1 + R_{02}]i_{L1})}{L_1} - \frac{(1-u_1)}{L_1}V_{C2} \\
\dot{V}_{C3} &= -\frac{1}{R_3C_3}V_{C3} - \frac{1}{C_3}i_{L2} + \frac{1}{R_3C_3}V_{BAT} \\
\dot{V}_{C4} &= -\frac{1}{R_4C_4}V_{C4} + \frac{(1-u_2)}{C_4}i_{L2} + \frac{1}{R_4C_4}V_{DC} \\
\dot{i}_{L2} &= \frac{1}{L_2}V_{C3} - \frac{([(R_{03}-R_{04})u_2 + R_{04}]i_{L2})}{L_2} - \frac{(1-u_2)}{L_2}V_{C4} \\
\dot{V}_{C5} &= -\frac{1}{R_5C_5}V_{C5} - \frac{1}{C_5}i_{L3} + \frac{1}{R_5C_5}V_{SC} \\
\dot{V}_{C6} &= -\frac{1}{R_6C_6}V_{C6} + \frac{(1-u_3)}{C_6}i_{L3} + \frac{1}{R_6C_6}V_{DC} \\
\dot{i}_{L3} &= \frac{1}{L_3}V_{C5} - \frac{([(R_{05}-R_{06})u_3 + R_{06}]i_{L3})}{L_3} - \frac{(1-u_3)}{L_3}V_{C6} \\
\dot{V}_{DC} &= \frac{1}{C_{DC}}[\frac{1}{R_2}(V_{C2}-V_{DC}) + \frac{1}{R_4}(V_{C4}-V_{DC}) + \frac{1}{R_6}(V_{C6}-V_{DC}) - \frac{V_{DC}}{R_{Load}} \qquad (4.109)
\end{aligned}$$

with V_{C1}, V_{C2} V_{C3}, V_{C4} V_{C5}, V_{C6} and V_{DC} $\mathbb{R} \to \mathbb{R}^+$, i_{L1}, i_{L2} and $i_{L3} \in \mathbb{R}$
The equilibrium point of the system (4.109) is:

$$x^e = \begin{bmatrix} V_{C1}^e \\ V_{C2}^e \\ V_{C3}^e \\ V_{C4}^e \\ V_{C5}^e \\ V_{C6}^e \\ i_{L1}^e \\ i_{L2}^e \\ i_{L3}^e \\ V_{DC}^e \end{bmatrix} = \begin{bmatrix} V_{C1}^* \\ R_2 i_{L1}(1-u_1^* \\ V_{BAT} - R_3 i_{L2}^* \\ R_4 i_{L2}^*(1-u_2^*) \\ V_{SC} - R_3 i_{L3}^* \\ R_6 i_{L3}^*(1-u_3^*) \\ i_{L1}^* \\ i_{L2}^* \\ i_{L3}^* \\ V_{DC}^* \end{bmatrix} \qquad (4.110)$$

where V_{C1}^* ,V_{C2}^* ,V_{C3}^* ,V_{C4}^* V_{C5}^* ,V_{C6}^* ,V_{DC}^* , i_{L1}^*, i_{L2}^* and i_{L3}^* have already been defined.

$$x^e = \begin{bmatrix} V_{C1}^e \\ V_{C2}^e \\ V_{C3}^e \\ V_{C4}^e \\ V_{C5}^e \\ V_{C6}^e \\ i_{L1}^e \\ i_{L2}^e \\ i_{L3}^e \\ V_{DC}^e \end{bmatrix} = f(V_{C1}^*, i_{L1}^*, i_{L2}^*, i_{L3}^*, V_{DC}^*) \tag{4.111}$$

Lemma 4.6.1. *Under the assumption that for each t conditions (4.30), (4.49) and (4.81) are verified, there exist control laws u_1, u_2 and u_3 such that the system (4.109) has in closed loop an equilibrium point x_e, and any initial condition exponentially converges to it.*

Proof. The proof is based on the use of a Lyapunov function V which is a composition of different Lyapunov functions, the control inputs u_1, u_2 and u_3 already defined for controlling dynamics of V_{C1}, i_{L1}, i_{L2}, i_{L3} and V_{DC}. They are proven to be stable by the Lyapunov functions $V_{1.3}$,V_6,V_9 and V_{10}. A control input u_2 and u_3 are calculated in the following to ensure voltage grid stability and to assign a desired transient with respect to the disturbance. The Lyapunov functions provided for each steps will be used for the entire system treatment: at the end the result is a study of composite Lyapunov functions. The Lyapunov function V is defined as

$$V = V_{1.3} + V_6 + V_9 + V_{10} + V_{2.4.5.7.8} \tag{4.112}$$

where $V_{1.3}$, V_6, V_9 and V_{10} have already been introduced and $V_{2.4.5.7.8}$ must be found.

The function $V_{2.4.5.7.8}$ refers to dynamics V_{C2}, V_{C3}, V_{C4}, V_{C5} and V_{C6}. Introducing the errors e_2, e_4, e_5, e_7 and e_8 between the dynamics and their equilibrium points as:

$$\begin{aligned} e_{V_{C2}} &= V_{C2} - V_{C2}^* \\ e_{V_{C3}} &= V_{C3} - V_{C3}^* \\ e_{V_{C4}} &= V_{C4} - V_{C4}^* \\ e_{V_{C5}} &= V_{C5} - V_{C5}^* \\ e_{V_{C6}} &= V_{C6} - V_{C6}^* \end{aligned}$$

that can be rewritten as:

$$\begin{aligned} V_{C2} &= e_{V_{C2}} + V^*_{C2} \\ V_{C3} &= e_{V_{C3}} + V^*_{C3} \\ V_{C4} &= e_{V_{C4}} + V^*_{C4} \\ V_{C5} &= e_{V_{C5}} + V^*_{C5} \\ V_{C6} &= e_{V_{C6}} + V^*_{C6} \end{aligned}$$

Their derivatives are:

$$\begin{aligned} \dot{e}_{V_{C2}} &= \frac{1}{R_2C_2}(V_{DC} - e_2 - V^*_{C2}) + \frac{(1-u_1)}{C_2} i_{L1} \\ \dot{e}_{V_{C3}} &= \frac{1}{R_3C_3}(V_{BAT} - e_3 - V^*_{C3}) - \frac{1}{C_3} i_{L2} \\ \dot{e}_{V_{C4}} &= \frac{1}{R_4C_4}(V_{DC} - e_4 - V^*_{C4}) + \frac{(1-u_2)}{C_4} i_{L2} \\ \dot{e}_{V_{C5}} &= \frac{1}{R_5C_5}(V_{BAT} - e_5 - V^*_{C5}) - \frac{1}{C_5} i_{L3} \\ \dot{e}_{V_{C6}} &= \frac{1}{R_6C_6}(V_{DC} - e_6 - V^*_{C6}) + \frac{(1-u_3)}{C_3} i_{L3} \end{aligned} \tag{4.113}$$

and the $V_{2.4.5.7.8}$ can be defined as:

$$V_{2.4.5.7.8} = \frac{R_2C_2}{2} e^2_{V_{C2}} + \frac{R_3C_3}{2} e^2_{V_{C3}} + \frac{R_4C_4}{2} e^2_{V_{C4}} + \frac{R_5C_5}{2} e^2_{V_{C5}} + \frac{R_6C_6}{2} e^2_{V_{C6}} \tag{4.114}$$

We can compute its derivative as:

$$\dot{V}_{2.4.5.7.8} = R_2C_2 e_{V_{C2}} \dot{e}_{V_{C2}} + R_3C_3 e_{V_{C3}} \dot{e}_{V_{C3}} + R_4C_4 e_{V_{C4}} \dot{e}_{V_{C4}} + R_5C_5 e_{V_{C5}} \dot{e}_{V_{C5}} + R_6C_6 e_{V_{C6}} \dot{e}_{V_{C6}} \tag{4.115}$$

$$\begin{aligned} \dot{V}_{2.4.5.7.8} &= R_2C_2 e_{V_{C2}} (\frac{1}{R_2C_2}(V_{DC} - e_{V_{C2}} - V^*_{C2}) + \frac{(1-u_1)}{C_2} i_{L1}) \\ &+ R_3C_3 e_{V_{C3}} (\frac{1}{R_3C_3}(V_{BAT} - e_{V_{C3}} - V^*_{C3}) - \frac{1}{C_3} i_{L2}) \\ &+ R_4C_4 e_{V_{C4}} (\frac{1}{R_4C_4}(V_{DC} - e_{V_{C4}} - V^*_{C4}) + \frac{(1-u_2)}{C_4} i_{L2}) \\ &+ R_5C_5 e_{V_{C5}} (\frac{1}{R_5C_5}(V_{BAT} - e_{V_{C5}} - V^*_{C5}) - \frac{1}{C_5} i_{L3}) \\ &+ R_6C_6 e_{V_{C6}} (\frac{1}{R_6C_6}(V_{DC} - e_{V_{C6}} - V^*_{C6}) + \frac{(1-u_3)}{C_3} i_{L3}) \end{aligned}$$

$$\dot{V}_{2.4.5.7.8} = -e^2_{V_{C2}} - e^2_{V_{C3}} - e^2_{V_{C4}} - e^2_{V_{C5}} - e^2_{V_{C6}} \tag{4.116}$$

The full Lyapunov function is

$$V = V_{1.3} + V_6 + V_9 + V_{10} + \frac{R_2C_2}{2} e^2_{V_{C2}} + \frac{R_3C_3}{2} e^2_{V_{C3}} + \frac{R_4C_4}{2} e^2_{V_{C4}} + \frac{R_5C_5}{2} e^2_{V_{C5}} + \frac{R_6C_6}{2} e^2_{V_{C6}} \tag{4.117}$$

We can finally state the constructive Lyapunov function for the whole system $V_{1,2,3,4,5,6,7,8,9,10} = V_1 + V_2 + V_3 + V_4 + V_5 + V_6 + V_7 + V_8 + V_9 + V_{10}$ as follows:

$$\begin{aligned} V_{1\cdots10} &= ([\alpha_1\ e_{V_{C1}}]^T\ P_1[\alpha_1 e_{V_{C1}}]) + ([\alpha_3 e_{i_{L1}}]^T P_3[\alpha_3 e_{i_{L1}}]) \\ &+\frac{R_2C_2}{2}e_{V_{C2}}^2 + \frac{R_3C_3}{2}e_{V_{C3}}^2 + \frac{R_4C_4}{2}e_{V_{C4}}^2\ ([\alpha_6\ e_{i_{L2}}]^T\ P_6\ [\alpha_6 e_{i_{L2}}]) + \frac{R_5C_5}{2}e_{V_{C5}}^2 + \frac{R_6C_6}{2}e_{V_{C6}}^2 \\ &+([\alpha_9\ e_{i_{L3}}]^T\ P_9[\alpha_9 e_{i_{L3}}]) + ([\alpha_{10}\ e_{V_{DC}}]^T\ P_{10}[\alpha_{10}\ e_{V_{DC}}]) \end{aligned} \tag{4.118}$$

It's derivative is then:

$$\begin{aligned} \dot{V}_{1\cdots10} &= -e_{V_{C1}}^2 - \alpha_1^2 - e_{i_{L1}}^2 - \alpha_3^2 - e_{V_{C2}}^2 - e_{V_{C3}}^2 - e_{V_{C4}}^2 \\ &-e_{i_{L2}}^2 - \alpha_6^2 - e_{V_{C5}}^2 - e_{V_{C6}}^2 - e_{i_{L3}}^2 - \alpha_9^2 - e_{V_{DC}}^2 - \alpha_{10}^2 \end{aligned} \tag{4.119}$$

which implies that:

$$V_{1\cdots10} = e^{-m_{1-10}t}\ V_{1\cdots10}(0) \tag{4.120}$$

This in its turn assures again the exponential convergence of all states of the interconnected system towards their equilibrium points.

□

Remark 1. *To perform the decomposition of the reference signal, we use a first order low pass filter, that represents a first order stable linear system.*

The decomposed signal was used as reference for both control levels. The frequency of such filter will impose dynamics for both levels, and its choice must take into account the possible dynamics both levels may assure, in particular the battery. Its impacts in the system's performance is further investigated in section (6.5). A deeper mathematical study on the interactions of this point was considered out of the scope of the present thesis, and was left for future works.

4.7 Simulations Result

In this section, we present some simulations that show the results obtained using Matlab Simulink.
The simulations are done in two steps, the first step we did simulations in 300s to observe power characteristics and the energy behaviour of the system. the second step we did simulations in 50s to observe dynamic performance of proposed control.

Shunt resistance of a single solar cell	$R_{sh} = 415.4k\Omega$
Series resistance of a single solar cell	$R_s = 0.22\Omega$
Standard short-circuit current	$I_{sh} = 8.21A$
Standard open-circuit voltage	$V_{oc} = 32.9V$
Number of cells in series of a series-module	$N_S = 38 * 54$
Number of series-modules in parallel	$N_P = 122$

Table 4.1: Solar panel simulation parameters

R_{01}	0.001Ω		R_1	0.1Ω		C_1	$0.1F$
R_{02}	0.002Ω		R_2	0.001Ω		C_2	$0.01F$
R_{03}	0.001Ω		R_3	0.5Ω		C_3	$0.1F$
R_{04}	0.0015Ω		R_4	0.01Ω		C_4	$0.01F$
R_{05}	0.001Ω		R_5	0.4Ω		C_5	$0.1F$
R_{06}	0.0015Ω		R_6	0.01Ω		C_6	$0.01F$
L_1	$0.0033H$		L_2	$0.0033H$		L_3	$0.0033H$
V_{PV}	$1000V$		P_n	$1MW$		V_{DC}	$1000V$
V_{SC}	$500V$		V_{BAT}	$500V$		V_{DC}	$1000V$

Table 4.2: Parameter values used in simulations

V_{cell}	$2V$
Nominal power	$1MW$
C_{10}	$3000A$
I_{10}	$300A$
LAB Electrochemical process efficiency	$K = 0.75$
LAB self-discharge rate	$D = 1e^{-}5$
$Step_sec$	3600
Nb_serie	250

Table 4.3: Battery simulation parameters

R_{1C}	$0.3 * ESR$
R_{2C}	$0.2 * ESR$
R_{3C}	$0.5 * ESR$
C_{1C}	$0.4 * C$
C_{2C}	$0.414 * C$
C_{3C}	$0.16 * C$
ESR	$0.35m\Omega$
Voltage across the SC	$500V$ to $1000V$
Discharge Ratio Desired/Limit	$d = 50\%$
Required Demanded Power	$1MW$ to $2MW$
$P_{required}$	$1MW$
Capacitance	$2700F$
Stable Operating Voltage	$2.7V$
Time Constant	0.9
Thermal Operating Conditions	-40^oC to 70^oC

Table 4.4: Supercapacitor simulation parameters

K_1	870.963	$\overline{K}_1$	620.83^2	K_1^α	1
K_3	8796.3	$\overline{K}_3$	6283.1^2	K_3^α	1
K_6	8796.2	$\overline{K}_6$	6283^2	K_6^α	1
K_9	87963.4	$\overline{K}_9$	62831^2	K_9^α	1
K_{10}	87.963	$\overline{K}_{10}$	62.83^2	K_{10}^α	1

Table 4.5: Control parameters

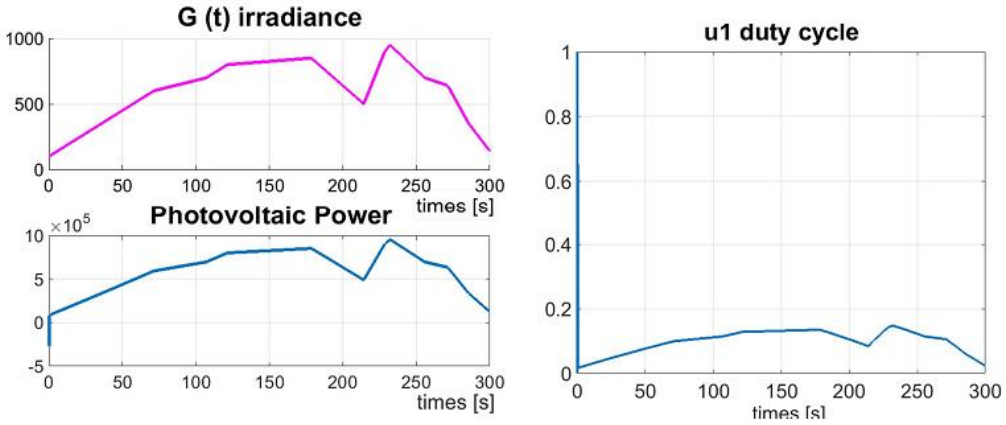

Figure 4.7: PV power with Varying Irradiance

Figure 4.7 in the left shows the characteristic Power curves of this PV system with varying irradiance. It can be seen that when the irradiance varies the output power varies.

Figure 4.7 in the righ shows the control input u_1, which is bounded between zero and one. These simulations illustrate that the local controller makes the PV work in maximum Power Point.

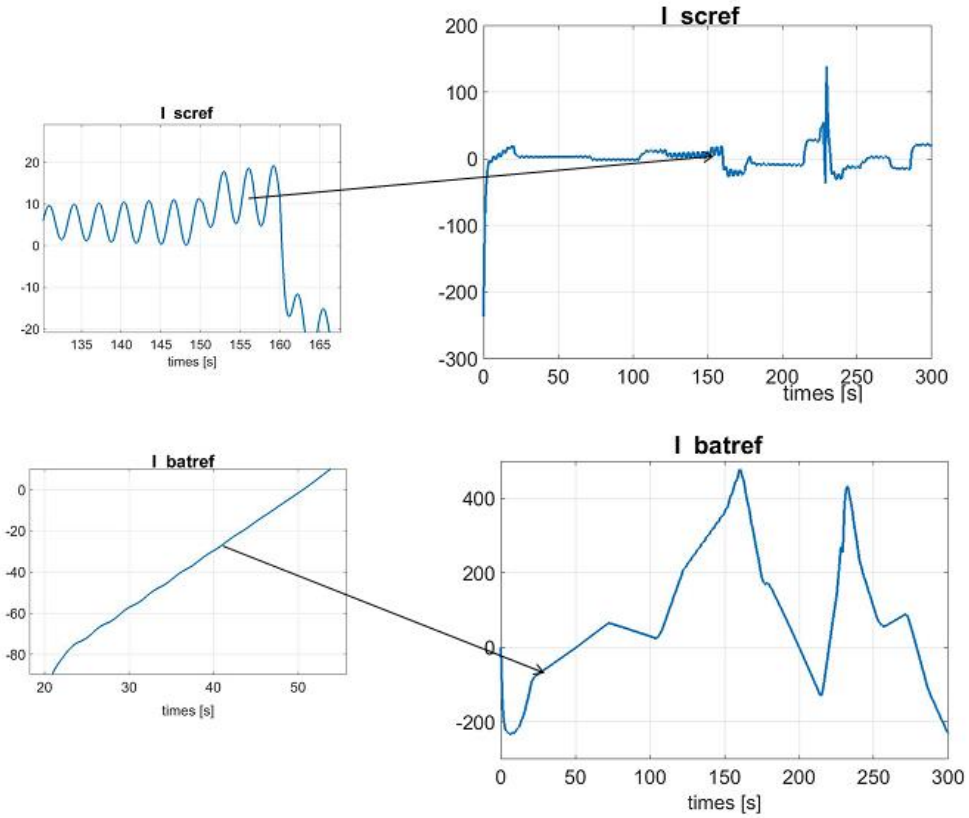

Figure 4.8: Reference power components

Figure 4.8 shows the signal decomposition into the two time scales. The fast reference is shown in the figure at the top and the slow reference in the figure at the bottom.

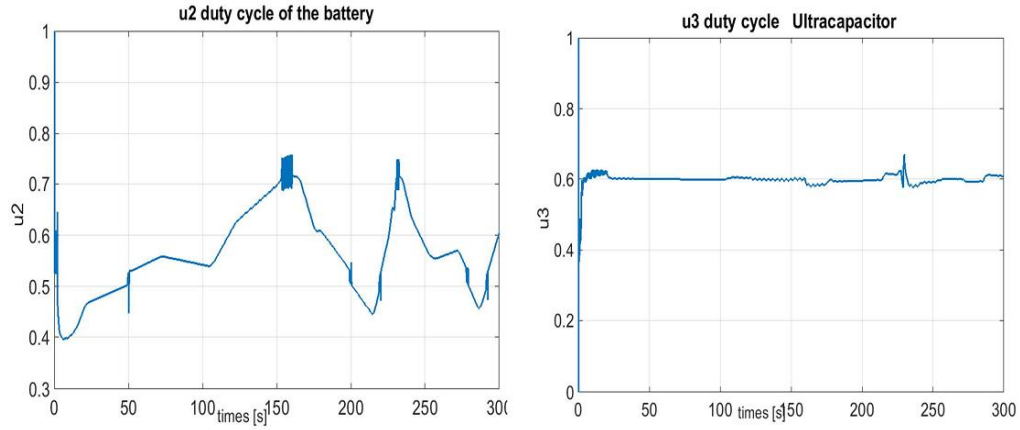

Figure 4.9: Control inputs u_2 and u_3

Figure 4.9 shows control inputs u_2 and u_3 which are bounded between zero and one.

The control inputs are smooth except in the case of fast power variations of differents elements of the DC MicroGrid.

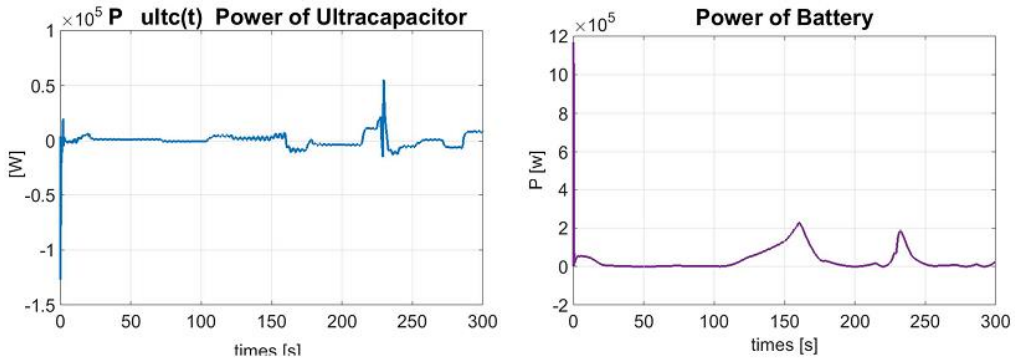

Figure 4.10: Output power of battery and supercapacitor

Figure 4.10 shows the output power of the battery and supercapacitor.

The fast time-varying signal is instantaneously absorbed by the supercapacitor P_{SC}, such that the battery can remain rather unchanged during fast perturbations. This is capital to assure a long lifespan for the battery. This one can then provide most of the energy demanded by the load, allowing long term planning, and the use of weather forecast and load predictions in the higher level algorithms.

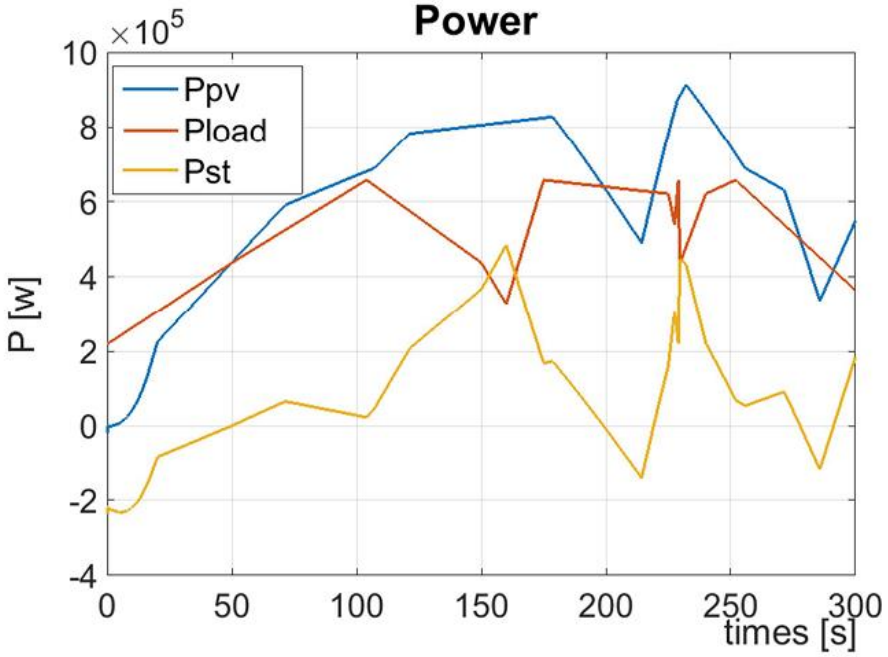

Figure 4.11: Output Power

Figure 4.11 shows output power of different elements of DC MicroGrid. We can remark the variation of the stored power, that follows the variations of PV and load powers. One can then conclude that the references designed for grid Voltage stabilisation fit the power

grid fluctuation.

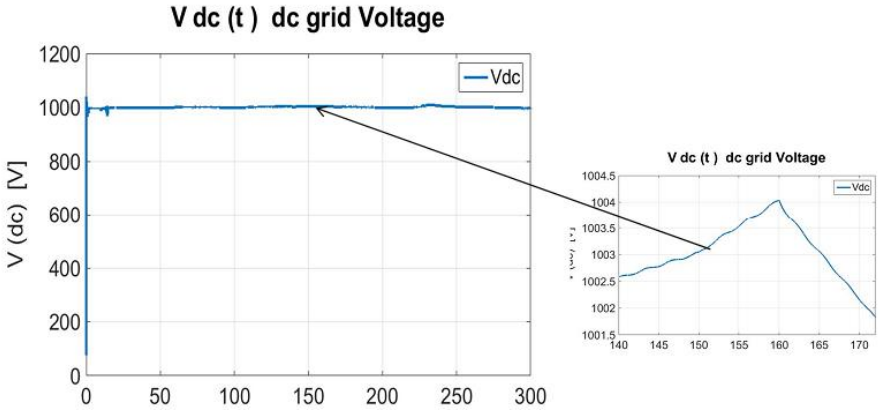

Figure 4.12: DC MicroGrid voltage

We can see in Figure 4.12 that the controller keeps V_{DC} close to its nominal value. The control strategy is then shown to successfully operate in a wide range of situations.Thanks to the designed control, the storage system manage to keep the DC MicroGrid voltage stable.

We can see in Figure (4.12) that the controller always keeps V_DC close to its nominal value. The control strategy is then shown to successfully operate in a wide range of situations.Thanks to storage the DC Microgrid voltage remains stable.

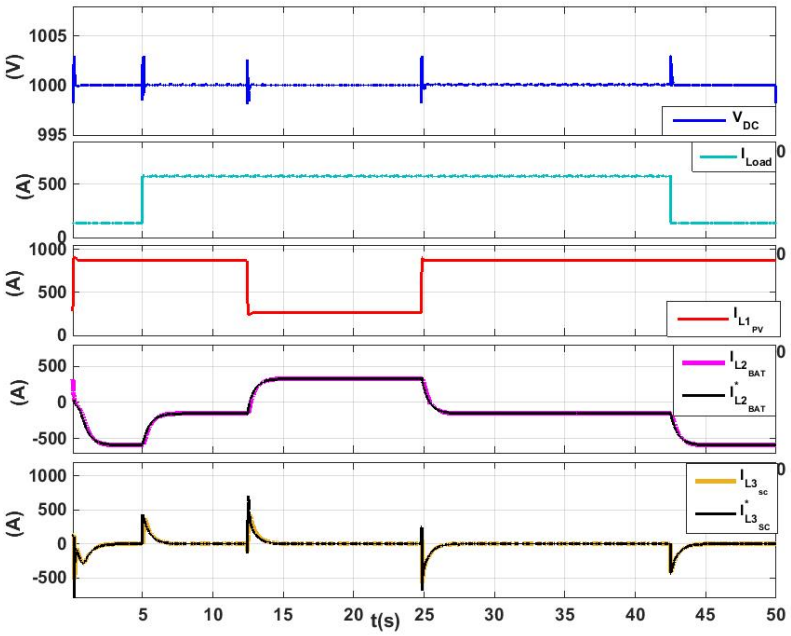

Figure 4.13: Dynamic response of the system

Figure (4.13) shows how the DC bus voltage (top) varies as the load current and PV current (following screens) vary. The load current is equal to $576A$ for $5s < t < 42.8s$

and is equal to $138A$ elsewhere. The solar irradiance was rated to $1000W/m^2$ one for $t < 12.4s$ and $t > 24.8s$, and equal to $300W/m^2$ otherwise. There, one sees that the DC bus voltage varies briefly following the transients, quickly recovering and stabilizing at the rated ($1000V$) DC bus voltage in about $10ms$. The maximum DC bus voltage error is equal to $4V$.

This is achieved by the action of the proposed control scheme making use of the battery and supercapacitor interfaces. The reference and actual waveforms of the former are shown in the fourth screen from the top. The reference signal varies slowly and the actual waveform follows it with a small switching frequency ripple. Besides, the battery current is the one required to balance the power in the DC microgrid in steady-state.
The reference and actual waveforms of the supercapacitor unit are shown in the fifth screen from the top. This reference varies fast, following PV generation and load demand variations, returning to $0A$ after transitory.

These results confirm that the proposed scheme is effective in achieving the goals defined for this application.

4.8 Comparison with PI control

In order to demonstrate the performance of the proposed control strategy, it is compared with PI linear control . State space averaging method is used to obtain a Small Signal model for the converter, see ([94, 95, 96]). The model is derived under the assumption that all the converter elements are ideal. The PI controllers are designed using method cited in ([97, 98]).

Figure (4.14) presents a comparison on DC MicroGrid voltage dynamics between a classical linear PI controller and the proposed nonlinear controller. There one sees that the DC bus voltage varies following the transients, recovering and stabilizing at the rated ($1000V$). The maximum DC bus voltage error is equal to $55V$ for linear control in blue.
In the PI linear control, the voltage V_{DC} oscillates for $2,2s$ before reaching steady state while the steady-state response time for the proposed nonlinear control is reached at $10ms$ as designed (it could be chosen to be faster though).
For the battery, the reference and actual waveforms are shown in the fourth screen from the top. The reference signal varies slowly and the actual waveform follows it with a small switching frequency ripple.
For the SuperCapacitor, its reference and actual waveforms are shown in the last screen from the top. The reference signal varies fast and the actual waveform follows it, following PV generation, load demand variations, and V_{DC} oscillations, converging to $0A$ in steady state.
It can be concluded that the PI linear control response have bigger overshoots in transients and a slower response speed.

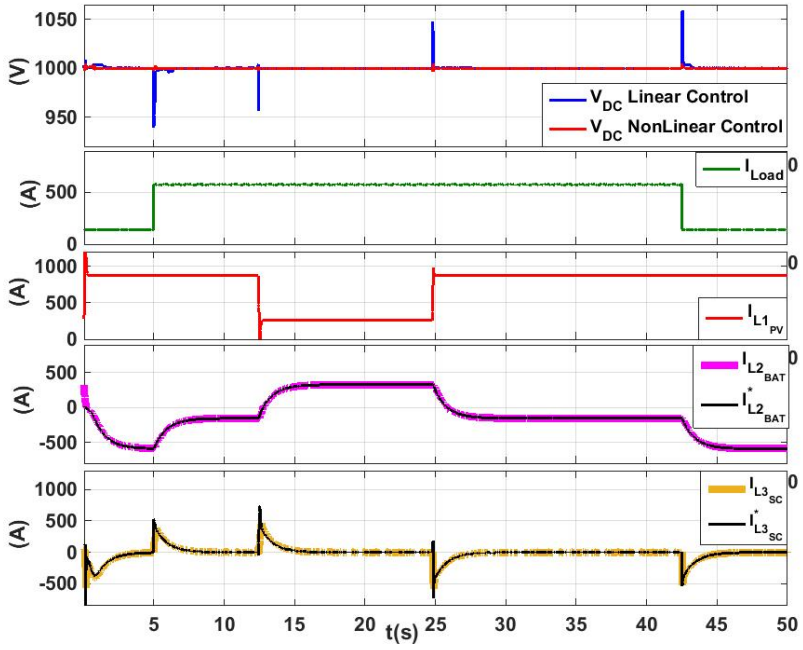

Figure 4.14: Comparison of the V_{DC} dynamics by applying nonlinear control in red and classical PI control in blue

4.9 Conclusion

In this chapter, the model for the DC MicroGrid is provided. We then have developed the controller of each brick of the system using backstepping technique. Their dynamics are then studied aiming at proposing a power management and hierarchical control strategy able to absorb maximum available power, while providing desired power to the loads and keeping the DC grid's voltage stable. Furthermore, the control strategy must respect physical constraints in order to guarantee a suitable lifespan for the battery.

The storage elements are used to stabilise the DC voltage and guarantee the balance between energy production and consumption; this is obtained by an algorithm applied in these storage elements that tracks the produced and consumed power, compute the difference and split the reference into a fast and slow terms to be followed by the supercapacitor and the battery respectively.

Simulation results corroborate our claims, and illustrate the good behaviour of each element and the overall interconnected system. Compared to other results in the literature, this paper is based on realistic characteristics of the grid's element, and was focused on proposing easily implementable control algorithms. The results perfectly respect the operating margin of plus or minus 5% in the DC grid's voltage, and in simulations were around 1%.

Chapter 5

Braking Energy Recovery power

5.1 Introduction

In this chapter we will replace photovoltaic power source by another distributed generation known as Braking Energy Recovery power. A Braking Energy Recovery System (BERS) is an important energy efficiency issue that recovers the kinetic energy a train has, back into electric energy. During the last decade, considerable progress has been made on electric traction due to evolving of Power Electronics. These innovations have made it possible a large range of regeneration of the train braking energy, and offer a very attractive way to reduce the energy consumption of urban railway stations. However, the electricity production from these sources is strongly variable with very high transients (see [2] [99] [100]). This energy is naturally available when the train uses electric brakes to slow down its engines, instead of using mechanical brakes. From the high transients it is then necessary to design a hybrid Storage System to limit power losses and store the excess of braking energy. Furthermore, this system must take into account several operating constraints (see [99] and [43]). The stored energy can then be used to supply the railway station load for many hours.

The energy coming from urban trains is available in a DC grid, the storage system being also DC, it is then natural to develop a control strategy in a DC node (see [99] and [101]). In this study the model of each component of the DC MicroGrid has to be developed. we propose through a power electronics study to analyze the dynamic behaviour of the system and to simulate the electric power flow and to optimize the storage device size, lifetime and control algorithm (see [99] and [102]).

This chapter describes the Braking Energy Recovery System scheme; the model of the source and associated power electronics; the Energy storage system (lithium ion battery and supercapacitor) where all aspects related to control and integration are addressed. Finally, simulation results are provided in the end of the chapter.

5.2 Braking energy recovery system scheme

The braking energy recovery system consists of a DC/DC converter which is connected in parallel to an existing substation, with an Energy Storage System (ESS) which permits to store the energy [8].
As said before, since all elements are in DC, we have chosen to build a DC grid. As shown in Figure (5.1), the proposed system consists of train residual braking energy as source, energy storage elements such as super-capacitors and batteries, DC loads and grid-tied converter [8]. The train residual braking energy converter is an $1MW$ buck converter. Energy storage elements play an important role for the entire power management of the DC micro-grid. They ensure a secured grid, provide high quality power and maintain common DC grid voltage constant [43]. Bidirectional converters are used to charge or discharge the energy storage elements, while an inverter is used to feed railway station [86], [80].

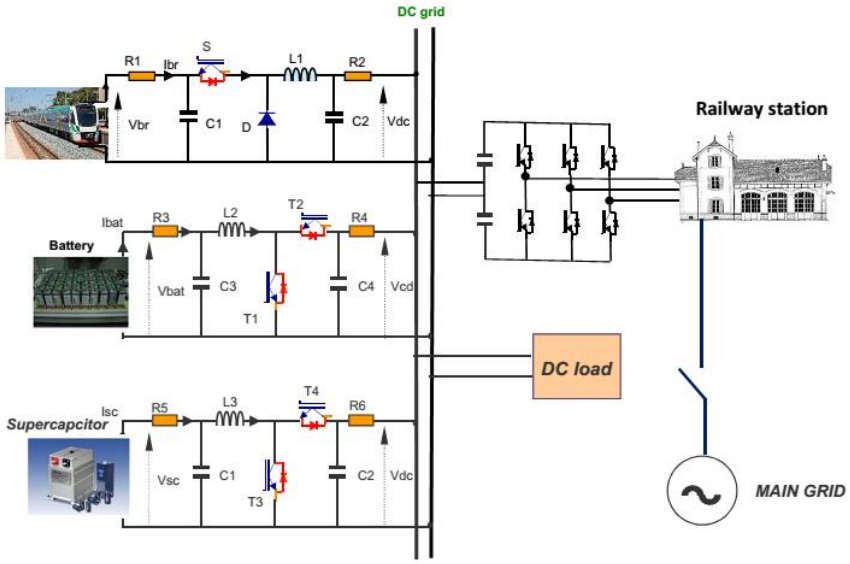

Figure 5.1: System Configuration

For modeling the converters' switches it will be included small resistances $R_{o1}, R_{o2}, R_{o3}, R_{o4}, R_{o5}$ and $Ro6$ when they are driving, so the conduction losses are taken into account.

5.3 High Level Controller for storage system

The power flow in the MicroGrid is shown in Figure (5.2). It is the sum of the output power of the train residual braking energy, the consumption and the storage. It is defined as follows.

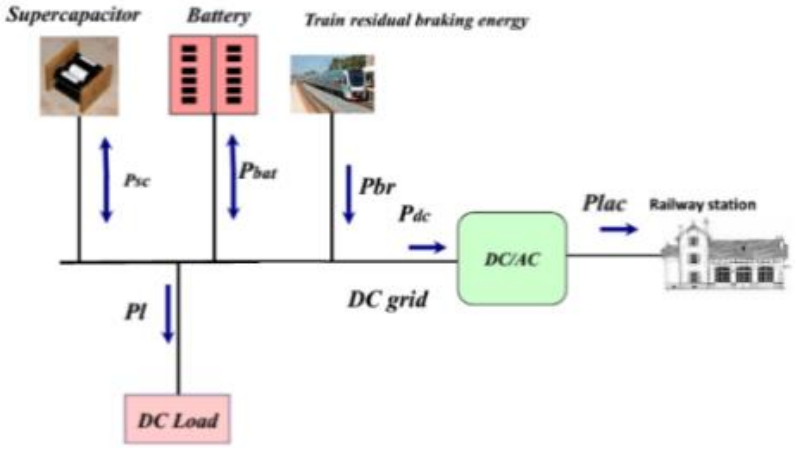

Figure 5.2: Power Flow of DC MicroGrid

With:

$$P_{DC} = P_{BR} + P_L + |P_{ST}| \tag{5.1}$$

$$P_{ST} = P_{BAT} + P_{SC} \tag{5.2}$$

and:

- P_{BR}: Breaking recovery power
- P_{ST}: Storage system power
- P_{BAT}: Battery power
- P_{SC}: Supercapacitor power
- P_{Load}: Load power
- P_{DC}: DC grid power

This power flow will directly affect the DC MicroGrid's voltage following:

$$\frac{dV_{DC}}{dt} = C_{DC}[I_{BR} + I_{ST} + I_{Load}] \tag{5.3}$$

It is then obvious that it is necessary a controller to provide references to accomplish power balance. The residual braking energy is used to supply the train station through a converter. The energy storage elements can switch between charge and discharge mode in order to maintain the DC grid power balance.

The Supercapacitor is meant to undertake the sudden peaks of power while the battery supplies the demands of large amounts of power for long time periods. In this work strong currents are minimized in the battery aiming at maximizing its lifetime. The strategy control is the same as in previous chapter.

5.3.1 High level control for Power source

The desired voltage reference is given by the metro company as the nominal voltage of the grid, $V_N = 750V$ in the case of this thesis. As shown in figure (5.3) the voltage rise during the braking,it means that the train rejects the power on the grid.

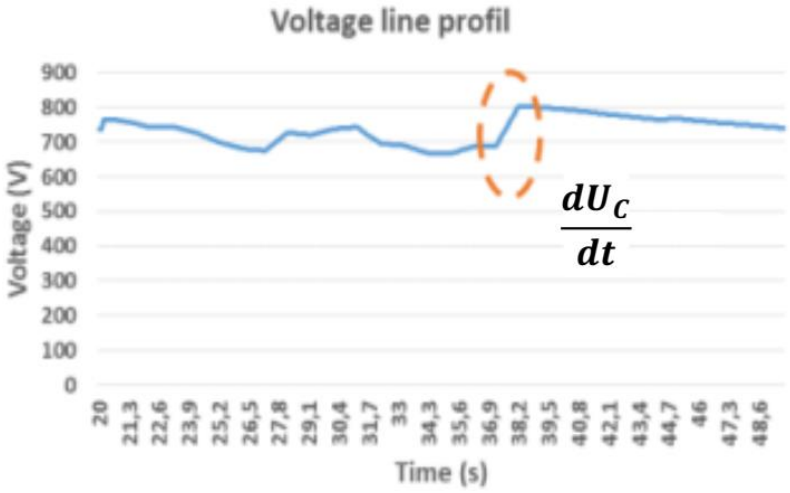

Figure 5.3: Voltage metro profiles measurements [2]

The objective is to absorb Any variation beyond a nominal value ($V_N = 750V$) will be absorbed to the DC MicroGrid via DC converter..

5.4 Control for the source

The considered railway system works in $750V$, and it is wanted to recover energy by regenerative braking [50]. The converter integrates a LC filter due to very fluctuating current as shown below.

DC/DC buck Converter

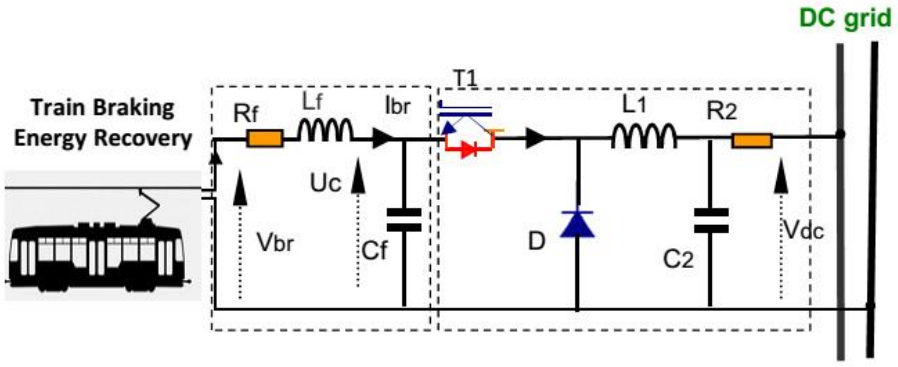

Figure 5.4: DC/DC buck Converter

The DC/DC converter topology used is the buck (Figure 5.4), which is modeled by a state-variable-averaging method [75], [76], that can be expressed as: the equivalent circuit representation for the the Buck converter can be expressed using a state space average model.

Four state variables are needed for the system model: The capacitor voltages $U_C\,\mathbb{R} \to \mathbb{R}^+$ and $V_{C2}\,\mathbb{R} \to \mathbb{R}^+$ The inductor currents $i_{Lf}\,\mathbb{R} \to \mathbb{R}$ and $i_{L1}\,\mathbb{R} \to \mathbb{R}$

$$\begin{bmatrix} U_C \\ i_{Lf} \\ V_{C2} \\ i_{L1} \end{bmatrix} = \begin{bmatrix} U_C capacitor voltage \\ i_{Lf} inductor current \\ V_{C2} capacitor voltage \\ i_{L1} inductor current \end{bmatrix} \tag{5.4}$$

$$\begin{aligned} \dot{U}_C &= \frac{1}{C_f} i_{Lf} - \frac{u_1}{C_f} i_{L1} \\ \dot{i}_{Lf} &= -\frac{R_f}{L_f} i_{Lf} - \frac{1}{L_f} U_C + \frac{1}{L_f} V_{BR} \\ \dot{V}_{C2} &= -\frac{1}{R_2 C_2} V_{C2} + \frac{1}{C_2} i_{L1} + \frac{1}{R_2 C_2} V_{DC} \\ \dot{i}_{L1} &= \frac{1}{L_1} U_C - \frac{[(R_{01} - R_{02})u_1 + R_{02}] i_{L1}}{L_1} - \frac{u_1}{L_1} V_{C2} \end{aligned} \tag{5.5}$$

Nonlinear control law and system stability's analysis

Here the control target is to stabilize voltage at C_f capacitor V_{Cf}. The reference value for V_{Cf} the nominal value of the rail voltage; it will be taken as a desired equilibrium point for the first equation of system (5.5), $V^*_{Cf} = 750V$. Following a backstepping procedure, it is necessary to design an i^*_{LF} reference for i_{Lf} in order to steer V_{Cf} towards its reference V^*_{Cf}.

The braking of the train increases the energy of the train's grid, and therefore an over voltage in the catenary. The control strategy is to reduce this voltage to its nominal value of $(750V)$ by recovering this supplementary energy through the converter. Here the control target is to control voltage U_c , [8].

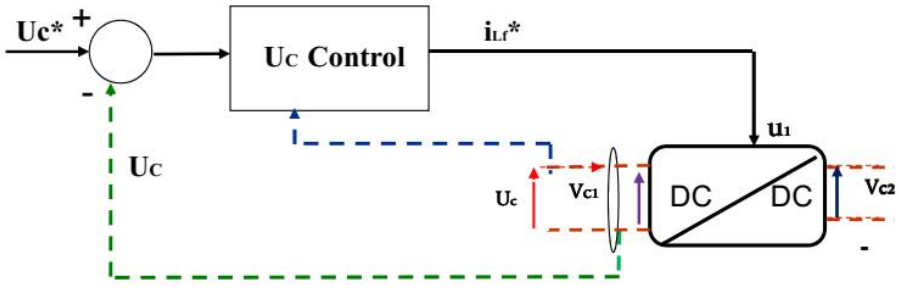

Figure 5.5: DC/DC Buck Converter Control

As said before, in order to assign U^*_C reference to U_C, an i^*_{Lf} reference is designed by a backstepping procedure as follows. First we define the output tracking errors as:

$$e_{U_C} = (U_C - U^*_C) \tag{5.6}$$

$$e_{i_{Lf}} = (i_{Lf} - i^*_{Lf}) \tag{5.7}$$

We are now going to design the control law by backstepping. The desired dynamics for e_{U_C} are introduced as:

$$\begin{aligned} \dot{\alpha}_1 &= K_1^{\alpha} e_{V_{C1}} && (5.8) \\ \dot{e_{U_c}} &= -K_1 e_{U_C} - \overline{K_1}\alpha_1 && (5.9) \end{aligned}$$

where α_1 represents the integral term assuring zero error in steady state, and with the positive tuning gain parameters K_1, K_1^{α} and $\overline{K}_1$. We can then design :

$$i_{Lf}^* = u_1 i_{L1} - K_1 C_f (U_C - V_n^*) - C_f \overline{K}_1 \alpha_1 \tag{5.10}$$

such that we can rewrite (5.9) as :

$$\begin{aligned} \dot{e}_{U_C} &= \dot{U}_C - \cancelto{0}{\dot{U}_C^*} = \frac{1}{C_f} i_{Lf} - \frac{u_1}{C_f} i_{L1} \\ &= -K_1 (U_C - U_C^*) - \overline{K}_1 \alpha_1 \end{aligned} \tag{5.11}$$

such as to obtain an arbitrary linear system for the states $[\alpha_1 \; U_C]^T$ for suitable choice of gains $K_1, \overline{K}_1, K_1^{\alpha}$. The closed loop sub-system becomes:

$$\begin{aligned} \dot{\alpha}_1 &= K_1^{\alpha} e_{U_C} \\ \dot{e}_{U_C} &= -K_1 e_{U_C} - \overline{K}_1 \alpha_1 \end{aligned}$$

We consider an augmented system $\widetilde{U}_C$

$$\widetilde{U}_C = \begin{bmatrix} \alpha_1 \\ V_{C1} - U_C^* \end{bmatrix}$$

Its closed loop (linear) dynamics is here defined with the eigenvalues

$$\dot{\widetilde{U}}_C = A_1 \widetilde{U}_C = \begin{bmatrix} 0 & K_1^{\alpha} \\ -\overline{K}_1 & -K_1 \end{bmatrix}$$

$$\lambda_{1.2} = -\frac{K_1}{2} \pm \frac{1}{2}\sqrt{(K_1^2 - 4\overline{K}_1 K_1^{\alpha})}$$

By properly selecting positive gains K_1,$\overline{K}_1$ and K_1^{α} both eigenvalues are stable; then the origin is an exponentially stable equilibrium point for the augmented state.

As a corollary, there exists $P_1 = P_1^T > 0$ such that $P_1 A_1 + A_1^T P_1 = -I_2$ where I_2 is an identity matrix in $\mathbb{R}^2$.

As next step, we need to design a control law u_1 such as to steer i_{Lf} towards its reference i_{Lf}^*. As above, there is a desired dynamic behavior to impose:

$$\dot{e}_{i_{Lf}} = -K_2 e_{i_{Lf}} - \overline{K_2}\alpha_2 \tag{5.12}$$

where α_2 represents the integral term and is now defined as an extended state governed by equation:

$$\dot{\alpha}_2 = \overline{K}_2 e_{i_{Lf}} \tag{5.13}$$

and the positive tuning gain parameters K_2, $\overline{K}_2$ and K_2^α. We can then obtain the following control law:

$$u_1 = \frac{1}{K_2 i_{L1}}[(K_2 - \frac{R_f}{L_f})i_{Lf} + K_1 K_2 C_f (U_C - U_C^*) - \frac{1}{L_f}(U_C - V_{BR}) + \overline{K}_1 K_2 C_f \alpha_1 + \overline{K}_2 \alpha_2 - \dot{i}_{Lf}^* \tag{5.14}$$

With condition:

$$K_2 i_{L1} \neq 0 \tag{5.15}$$

We operate in Continuous Conduction Mode, and we may design the control such as to only operate when $i_{Lf}^* \neq 0$ and then condition 5.15 will be satisfied.

We can then obtain an arbitrary linear system for the states $[\alpha_2 \; i_{Lf}]^T$ for suitable choice of gains $K_2, \overline{K}_2, K_2^\alpha$. The closed loop sub-system becomes:

$$\begin{aligned} \dot{\alpha}_2 &= K_2^\alpha e_{i_{Lf}} \\ \dot{e}_{i_{Lf}} &= -K_2 e_{i_{Lf}} - \overline{K}_2 \alpha_2 \end{aligned}$$

We consider an augmented system $\widetilde{i}_{L2}$

$$\widetilde{i}_{Lf} = \begin{bmatrix} \alpha_2 \\ i_{Lf} - i_{Lf}^* \end{bmatrix}$$

Its closed loop (linear) dynamics is here defined with the eigenvalues

$$\dot{\widetilde{i}}_{Lf} = A_2 \widetilde{i}_{Lf} = \begin{bmatrix} 0 & K_2^\alpha \\ -\overline{K}_2 & -K_2 \end{bmatrix}$$

$$\lambda_{3.4} = -\frac{1}{2}(K_2 \pm \sqrt{(K_2^2 - 4\overline{K}_2 K_2^\alpha)})$$

By properly selecting positive gains K_2,$\overline{K}_2$ and K_2^α both eigenvalues are stable; then the origin is a stable equilibrium point for the augmented state. The control input u_1 feedback linearizes the dynamics of U_C and i_{Lf}. As a corollary, there exists $P_2 = P_2^T > 0$ such that $P_2 A_2 + A_2^T P_2 = -I_2$ where I_2 is was defined above. Let us consider the system:

$$\begin{aligned}
\dot{U}_C &= \frac{1}{C_f} i_{Lf} - \frac{u_1}{C_f} i_{L1} \\
\dot{\alpha}_1 &= \overline{K}_1 e_{V_{C1}} \\
\dot{i}_{Lf} &= \frac{R_f}{L_f} i_{Lf} - \frac{1}{L_f} U_C - \frac{1}{L_f} V_{BR} \\
\dot{\alpha}_2 &= \overline{K}_2 e_{i_{Lf}} \\
\dot{V}_{C2} &= -\frac{1}{R_2 C_2} V_{C2} + \frac{1}{C_2} i_{L1} + \frac{1}{R_2 C_2} V_{DC} \\
\dot{i}_{L1} &= \frac{1}{L_1} U_C - \frac{[(R_{01} - R_{02})u_1 + R_{02}] i_{L1}}{L_1} - \frac{u_1}{L_1} V_{C2}
\end{aligned} \tag{5.16}$$

Lemma 5.4.1. *Under control law (5.14), and suitable control gains K_1, $\overline{K}_1$, K_1^α, K_2, $\overline{K}_2$ and $K_2^\alpha > 0$, the closed-loop system (5.5), (5.16) asymptotically converges to its equilibrium point, under the condition $K_2 i_{L1} \neq 0$.*

Proof. We introduce the Lyapunov function

$$V_{1,2} = ([\alpha_1 \; e_{U_C}]^T \; P_1 \; [\alpha_1 \; e_{U_C}]) \; + \; ([\alpha_2 \; e_{i_{Lf}}]^T \; P_2 \; [\alpha_2 \; e_{i_{Lf}}]) \tag{5.17}$$

It's derivative is then:

$$\dot{V}_{1,2} = [\dot{\alpha}_1 \; \dot{e}_{U_C}]^T \; P_1 \; [\alpha_1 \; e_{U_C}] + [\alpha_1 \; e_{U_C}]^T \; P_1 \; [\dot{\alpha}_1 \; \dot{e}_{U_C}] + [\dot{\alpha}_2 \; \dot{e}_{i_{Lf}}]^T \; P_2 \; [\alpha_2 \; e_{i_{Lf}}] + [\alpha_2 \; e_{i_{Lf}}]^T \; P_2 \; [\dot{\alpha}_2 \; \dot{e}_{i_{Lf}}] \tag{5.18}$$

$$\dot{V}_{1,2} = [\alpha_1 \; e_{U_C}]^T \; (A_1^T \; P_1 + P_1 \; A_1) \; [\alpha_1 \; e_{U_C}] \; + \; [\alpha_2 \; e_{i_{Lf}}]^T \; (A_2^T \; P_2 + P_2 \; A_2) \; [\alpha_2 \; e_{i_{Lf}}] \tag{5.19}$$

where it was defined above that $P_1 A_1 + A_1^T P_1 = -I_2$ and $P_2 A_2 + A_2^T P_2 = -I_2$. Then :

$$\dot{V}_{1.2} \;\; = \;\; -e_{U_C}^2 - \alpha_1^2 - e_{i_{Lf}}^2 - \alpha_2^2 \tag{5.20}$$

For the quadratic positive definite function $V(x) = x^T P x$

$$\lambda_{min}(P) \, ||x| \, |^2 \; \leq \; x^T P x \; \leq \; \lambda_{max}(P) \, ||x| \, |^2 \tag{5.21}$$

we can write:

$$\dot{V}_{1.2} \leq -\frac{1}{\lambda_{max}} V_{1.2} \tag{5.22}$$

$$\dot{V}_{1.2} \leq -m_{1.2} \, V_{1.2} \tag{5.23}$$

$$V_{1.2}(t) = e^{-m_{1.2} t} \, V_{1.2}(0) \tag{5.24}$$

which implies that:

$$\lim_{t\to\infty}\left\|\begin{bmatrix} e_{UC}(t) \\ \alpha_1(t) \\ e_{i_{Lf}}(t) \\ \alpha_2(t) \end{bmatrix}\right\| = 0$$

and this subsystem is then exponentially stable.

Therefore the relative degree of (5.5) is 2 in $\mathbb{R}^4$,and hence we have internal dynamics of order 2. Let us now move the focus to these remaining zero dynamics. They are defined following:

$$y = U_C \equiv U_C^* \tag{5.25}$$

The V_{C2} and i_{L1}variables will compose the zero dynamics, which will be chosen to converge to a Desired Set. Taking the current i_{L1} and the DC grid voltage value V_{DC}:

$$\begin{aligned} \dot{V}_{C2} &= -\frac{1}{R_2C_2}V_{C2} + \frac{1}{C_2}i_{L1} + \frac{1}{R_2C_2}V_{DC} \\ \dot{i}_{L1} &= \frac{1}{L_1}U_C - \frac{([(R_{01}-R_{02})u_1 + R_{02}]i_{L1})}{L_1} - \frac{u_1}{L_1}V_{C2} \end{aligned} \tag{5.26}$$

From:

$$u_1^* = \frac{1}{i_{L1}^* R_f}(V_{BR} - U_C^*) \tag{5.27}$$

we can rewrite:

$$\dot{i}_{L1} = \frac{1}{L_1}U_C - \frac{(R_{01}-R_{02})(V_{BR}-U_C^*)}{R_fL_1} - \frac{(R_{02}+R_2)}{L_1}i_{L1}^* - \frac{1}{i_{L1}^*L_1R_f}(V_{BR}-U_C^*)V_{DC} \tag{5.28}$$

we can rewrite the zero dynamics equations of (5.26) as:

$$\dot{i}_{L1} = \frac{1}{L_1}U_C - \frac{(R_{01}-R_{02})(V_{BR}-U_C^*)}{R_fL_1} - \frac{(R_{02}+R_2)}{L_1}i_{L1}^* - \frac{\delta}{i_{L1}^*L_1} \tag{5.29}$$

with:

$$\delta = \frac{(V_{BR}-U_C^*)V_{DC}}{R_f} \tag{5.30}$$

$$\begin{aligned} \dot{V}_{C2} &= -\frac{1}{R_2C_2}V_{C2} + \frac{1}{C_2}i_{L1} + \frac{1}{R_2C_2}V_{DC} \\ \dot{i}_{L1} &= \frac{1}{L_1}U_C - \frac{(R_{01}-R_{02})(V_{BR}-U_C^*)}{R_fL_1} - \frac{(R_{02}+R_2)}{L_1}i_{L1}^* - \frac{\delta}{i_{L1}^*L_1} \end{aligned} \tag{5.31}$$

The analysis is performed using the linearization around the equilibrium points in order to check stability. The matrix ξ is the Jacobian linearization matrix:

$$\xi = \begin{bmatrix} -\frac{(R_{02}+R_2)}{L_1} - \frac{\delta}{i_L{1^*}^2L_1} & 0 \\ \frac{1}{C_2} & -\frac{1}{C_2R_2} \end{bmatrix} \tag{5.32}$$

To determinate the stability of this system, it is calculated the determinant of $(\lambda I - \xi)$, such that the eigenvalues of ξ can be written:

$$det(\lambda I - A) = (\lambda + \frac{1}{(R_2 C_2)})(\lambda + \frac{(R_{02} + R_2)}{L_1} + \frac{\delta}{{i^*_{L1}}^2 L_1}) \tag{5.33}$$

with:

$$\lambda_a = -\frac{1}{(R_2 C_2)} \qquad \lambda_b = -\frac{(R_{02} + R_2)}{L_1} - \frac{\delta}{{i^*_{L1}}^2 L_1} \tag{5.34}$$

It is important to remark that $\delta \geq 0$ because $(V_{BR} - U_C)V_{DC} \geq 0$. For this reason, the Jacobian is always negative and then the system is always stable. Then we can state that the full system is asymptotic stable.

□

5.5 Storage System Control

The hybrid system (battery-supercapacitor) adopts the advantages of both technologies, high power density from the supercapacitor and high energy density from the battery. see previous chapter.

5.5.1 Calculation of High Level Controller

First we have to compute the references for the storage system for the battery and supercapacitor. The control target is to stabilize V_{DC} to its nominal value.

$$\dot{V}_{DC} = \frac{1}{C_{DC}}[\frac{1}{R_2}(V_{DC} - V_{C2}) + i_{ST} - i_{Load}] \tag{5.35}$$

The reference value for V_{DC} is its constant nominal value V^*_{DC}. In the following, throught a backstepping procedure, it will be designed an $i^*_{ST} = i^*_{L2} + i^*_{L3}$, references for i_{L2} and i_{L3} in order to steer V_{DC} to its reference V^*_{DC}.

Lets first define the output tracking errors:

$$\begin{aligned} e_{V_{DC}} &= (V_{DC} - V^*_{DC}) \\ e_{i_{L2}} &= (i_{L2} - i^*_{L2}) \\ e_{i_{L3}} &= (i_{L3} - i^*_{L3}) \end{aligned}$$

and their derivatives:

$$\begin{aligned} \dot{e}_{V_{DC}} &= (\dot{V}_{DC} - \dot{V}^*_{DC}) \\ \dot{e}_{i_{L2}} &= (\dot{i}_{L2} - \dot{i}^*_{L2}) \\ \dot{e}_{i_{L3}} &= (\dot{i}_{L3} - \dot{i}^*_{L3}) \end{aligned}$$

We are now going to determined the control law by backstepping. The desired dynamics for V_{DC} is introduced as:

$$\dot{V}_{DC} = -K_{11} e_{V_{DC}} - \overline{K}_{11} \alpha_{11} \tag{5.36}$$

where α_{11}, α_7 and α_{10} represent the integral terms assuring zero error in steady state between the dynamics of V_{DC}, i_{L2} and i_{L3}. α_{11} is governed by equation:

$$\dot{\alpha}_{11} = K_{11}^{\alpha} e_{V_{DC}}$$

and K_{11}, $\overline{K}_{11}$ and K_{11}^{α} the positive tuning gain parameters. Now the objective is to rewrite (5.36) as:

$$\begin{aligned} \dot{e}_{V_{DC}} &= \dot{V}_{DC} - \cancelto{0}{\dot{V}_{DC}^{*}} = \frac{1}{C_{DC}}\left(\frac{1}{R_2}(V_{DC} - V_{C2}) + i_{ST} - \frac{1}{R_Load} V_{DC}\right) \\ &= -K_{11}(V_{DC} - V_{DC}^{*}) - \overline{K}_{11}\alpha_{11} \end{aligned} \tag{5.37}$$

To attain this goal, we design the control action:

$$\frac{1}{C_{DC}}\left(\frac{1}{R_2}(V_{DC} - V_{C2}) + i_{ST} - \frac{1}{R_{Load}} V_{DC}\right) = -K_{11}(V_{DC} - V_{DC}^{*}) - \overline{K}_{11}\alpha_{11}$$

such as to obtain arbitrary linear system for the states $[\alpha_{11}\ V_{DC}]^T$ for suitable choice of gains $K_{11}, \overline{K}_{11}, K_{11}^{\alpha}$. The closed loop sub-system becomes:

$$\begin{aligned} \dot{\alpha}_{11} &= K_{11}^{\alpha} e_{V_{DC}} \\ \dot{e}_{V_{DC}} &= -K_{11} e_{V_{DC}} - \overline{K}_{11}\alpha_{11} \end{aligned}$$

We consider an augmented system $\widetilde{V}_{DC}$:

$$\widetilde{V}_{DC} = \begin{bmatrix} V_{DC} - V_{DC}^{*} \\ \alpha_{11} \end{bmatrix} \tag{5.38}$$

with the linear dynamics:

$$\dot{\widetilde{V}}_{DC} = A_{11}\widetilde{V}_{DC} \triangleq \begin{bmatrix} -K_{11} & -\overline{K}_{11} \\ K_{11}^{\alpha} & 0 \end{bmatrix} \widetilde{V}_{DC} \tag{5.39}$$

with its eigenvalues given by:

$$\lambda_{5.6} = -\frac{1}{2}(K_{10} \pm \sqrt{(K_{10}^2 - 4\overline{K}_{11})K_{10}^{\alpha})})$$

As before, by properly selecting positive gains K_{11}, $\overline{K}_{11}$ and K_{11}^{α} both eigenvalues are stable; then the origin is a exponentially stable equilibrium point for the augmented state, as a corollary, there exist $P_{11} = P_{11}^T > 0$ such that $P_{11}A_{11} + A_{11}^T P_{11} = -I_2$ with I_2 defined as before, and with the control action defined as:

$$i_{ST}^{*} = -C_{DC}K_{11}(V_{DC} - V_{DC}^{*}) - C_{DC}\overline{K}_{11}\alpha_{11} - \frac{1}{R_2}(V_{DC} - V_{C2}) + \frac{V_{DC}}{R_{Load}} \tag{5.40}$$

We present as before the decomposition

$$i^*_{ST} = i^*_{BAT} + i^*_{SC} = i^*_{L2} + i^*_{L3} \tag{5.41}$$

with i^*_{BAT} being the reference current for the local controller of the Battery and i^*_{SC} the reference current for the local controller of the Supercapacitor, where the signal decomposition is done by a first-order low pass filter as the previous chapter

5.5.2 Current Control Law for the battery

In this section the control laws for the battery is designed similarly to the previous chapter.

$$\begin{aligned}
\dot{V}_{C3} &= -\frac{1}{R_3 C_3} V_{C3} - \frac{1}{C_3} i_{L2} + \frac{1}{R_3 C_3} V_{BAT} \\
\dot{V}_{C4} &= -\frac{1}{R_4 C_4} V_{C4} + \frac{(1-u_2)}{C_4} i_{L2} + \frac{1}{R_4 C_4} V_{DC} \\
\dot{i}_{L2} &= \frac{1}{L_2} V_{C3} - \frac{([(R_{03}-R_{04})u_2 + R_{04}]i_{L2})}{L_2} - \frac{(1-u_2)}{L_2} V_{C4}
\end{aligned} \tag{5.42}$$

We need to assign an i^*_{L2} reference value for i_{L2} in order to obtain convergence to the desired equilibrium DC grid's voltage. This is done by input/output feedback linearization as before, by setting a desired dynamic behaviour:

$$\dot{e}_{i_{L2}} = -K_7 e_{i_{L2}} - \overline{K_7}\alpha_7 \tag{5.43}$$

and:

$$\dot{\alpha}_7 = K^\alpha_7 e_{i_{L2}} \tag{5.44}$$

we obtain then the following control law:

$$u_2 = \frac{1}{(V_{C4} + (R_{04} - R_{03})i_{L2}}) [-(V_{C3} - V_{C4}) + R_{04} i_{L2} - L_2 (K_7 (i_{L2} - i^*_{L2}) + \overline{K}_7 \alpha_7) + \dot{i}^*_{L2}] \tag{5.45}$$

with condition:

$$V_{C4} + (R_{04} - R_{03}) i_{L2} \neq 0 \tag{5.46}$$

such as to obtain an arbitrary linear system for the states $[\alpha_7 \; i_{L2}]^T$ for suitable choice of gains $K_7, \overline{K}_7, K^\alpha_7$. The closed loop sub-system becomes:

$$\begin{aligned}
\dot{\alpha}_7 &= K^\alpha_7 e_{i_{L2}} \\
\dot{e}_{i_{L2}} &= -K_7 e_{i_{L2}} - \overline{K}_7 \alpha_7
\end{aligned}$$

We consider an augmented system $\widetilde{i}_{L2}$:

$$\widetilde{i}_{L2} = \begin{bmatrix} \alpha_7 \\ i_{L2} - i^*_{L2} \end{bmatrix}$$

Its closed loop (linear) dynamics is here defined with their eigenvalues:

$$\dot{\widetilde{i}}_{L2} = A_7 \widetilde{i}_{L2} = \begin{bmatrix} 0 & K_7^\alpha \\ -\overline{K}_7 & -K_7 \end{bmatrix}$$

$$\lambda_{7.8} = -\frac{1}{2}(K_7 \pm \sqrt{(K_7^2 - 4\overline{K}_7 K_7^\alpha)})$$

By properly selecting positive gains K_7, $\overline{K}_7$ and K_7^α both eigenvalues are stable; then the origin is a stable equilibrium point for the augmented state. The control input u_2 feedback linearizes the dynamics of V_{DC} and i_{L2}. As a corollary, there exists $P_7 = P_7^T > 0$ such that $P_7 A_7 + A_7^T P_7 = -I_2$.

5.5.3 Current Control Law for the Supercapacitor

The bidirectional boost converter controlling the supercapacitor is modeled as follow:

$$\begin{aligned} \dot{V}_{C5} &= -\frac{1}{R_5 C_5} V_{C5} - \frac{1}{C_5} i_{L3} + \frac{1}{R_5 C_5} V_{SC} \\ \dot{V}_{C6} &= -\frac{1}{R_6 C_6} V_{C6} + \frac{(1-u_3)}{C_6} i_{L3} + \frac{1}{R_6 C_6} V_{DC} \\ \dot{I}_{L3} &= \frac{1}{L_3} V_{C5} - \frac{([(R_{05} - R_{06})u_3 + R_{06}]i_{L3})}{L_3} - \frac{(1-u_3)}{L_3} V_{C6} \end{aligned} \tag{5.47}$$

We need to design a control law u_3 such as to steer i_{L3} towards its reference i^*_{L3}. As before, there is a desired dynamic behaviour to impose:

$$\dot{e_{i_{L3}}} = -K_{10} e_{i_{L3}} - \overline{K_{10}} \alpha_{10} \tag{5.48}$$

$$\dot{\alpha}_{10} = K_{10}^\alpha e_{i_{L3}} \tag{5.49}$$

with the positive tuning gain parameters K_{10}, $\overline{K}_{10}$ and K_{10}^α, where we obtain the following control law:

$$u_3 = \frac{1}{(V_{C6} + (R_{06} - R_{05})i_{L3}}) [-V_{C5} + V_{C6} + R_{05} i_{L3} - L_3(K_{10}(i_{L3} - i^*_{L3}) + \overline{K}_{10}\alpha_{10} + i^*_{L3})] \tag{5.50}$$

with condition:

$$V_{C6} + (R_{06} - R_{05}) i_{L3} \neq 0 \tag{5.51}$$

such as to obtain an arbitrary linear system for the states $[\alpha_{10}\ i_{L3}]^T$ for suitable choice of gains $K_{10}, \overline{K}_{10}, K_{10}^\alpha$. The closed loop sub-system becomes:

$$\begin{aligned}\dot{\alpha}_{10} &= K^{\alpha}_{10} e_{i_{L3}} \\ \dot{e}_{i_{L3}} &= -K_{10} e_{i_{L3}} - \overline{K}_{10}\alpha_{10}\end{aligned}$$

We consider an augmented system $\widetilde{i}_{L3}$:

$$\widetilde{i}_{L3} = \begin{bmatrix} \alpha_{10} \\ i_{L3} - i^{*}_{L3} \end{bmatrix}$$

Its closed loop (linear) dynamics is here defined with their eigenvalues:

$$\dot{\widetilde{i}}_{L3} = A_9 \widetilde{i}_{L3} = \begin{bmatrix} 0 & K^{\alpha}_{10} \\ -\overline{K}_{10} & -K_{10} \end{bmatrix}$$

$$\lambda_{9.10} = -\frac{1}{2}(K_{10} \pm \sqrt{(K^2_{10} - 4\overline{K}_{10})K^{\alpha}_{10})})$$

By properly selecting positive gains K_{10}, $\overline{K}_{10}$ and K^{α}_{10} both eigenvalues are stable; then the origin is a stable equilibrium point for the augmented state. The control input u_3 feedback linearizes the dynamics of V_{DC} and i_{L3}. As a corollary, there exists $P_{10} = P^T_{10} > 0$ such that $P_{10}A_{10} + A^T_{10}P_{10} = -I_2$.

Let us now consider the system:

$$\begin{aligned}\dot{V}_{DC} &= \frac{1}{C_{DC}}[\frac{1}{R_2}(V_{DC} - V_{C2}) + i_{ST} - i_{Load}] \\ \dot{\alpha}_{11} &= K^{\alpha}_{11} e_{V_{DC}} \\ \dot{i}_{L2} &= \frac{1}{L_2}V_{C3} - \frac{([(R_{03} - R_{04})u_2 + R_{04}]i_{L2})}{L_2} - \frac{(1-u_2)}{L_2}V_{C4} \\ \dot{\alpha}_7 &= K^{\alpha}_7 e_{i_{L2}} \\ \dot{i}_{L3} &= \frac{1}{L_3}V_{C5} - \frac{([(R_{05} - R_{06})u_3 + R_{06}]i_{L3})}{L_3} - \frac{(1-u_3)}{L_3}V_{C6} \\ \dot{\alpha}_{10} &= K^{\alpha}_{10} e_{i_{L3}}\end{aligned} \tag{5.52}$$

5.5.4 stability of storage system

Lemma 5.5.1. *Under control laws (5.45), (5.50), and suitable control gains* $K_7, \overline{K}_7, K^{\alpha}_7, K_{10}, \overline{K}_{10}, K^{\alpha}_{10}, K_{11}, \overline{K}_{11} and K^{\alpha}_{11} > 0$ *the closed-loop system (5.52) has an equilibrium point given by references (5.41). Any evolution starting from the initials conditions, asymptotically converges to the equilibrium point, under the conditions* $V_{C4} + (R_{04} - R_{03})i_{L2} \neq 0$ *and* $V_{C6} + (R_{06} - R_{05})i_{L3} \neq 0$.

Proof. We introduce the Lyapunov function:

$$\begin{aligned}V_{7.10.11} &= ([\alpha_{11}\ e_{V_{DC}}]^T\ P_{11}\ [\alpha_{11}\ e_{V_{DC}}]) \\ &+ ([\alpha_7\ e_{i_{L2}}]^T\ P_7\ [\alpha_7\ e_{i_{L2}}]) \\ &+ ([\alpha_{10}\ e_{i_{L3}}]^T\ P_{10}\ [\alpha_{10}\ e_{i_{L3}}])\end{aligned} \tag{5.53}$$

It's derivative is then:

$$\begin{aligned}\dot{V}_{7.10.11} &= [\dot{\alpha}_{11}\ \dot{e}_{V_{DC}}]^T\ P_{11}\ [\alpha_{11}\ e_{V_{DC}}] + [\alpha_{11}\ e_{V_{DC}}]^T\ P_{11}\ [\dot{\alpha}_{11}\ \dot{e}_{VDC}] \\ &+ [\dot{\alpha}_7\ \dot{e}_{i_{L2}}]^T\ P_7\ [\alpha_7\ e_{i_{L2}}] + [\alpha_7\ e_{i_{L2}}]^T\ P_7\ [\dot{\alpha}_7\ \dot{e}_{i_{L2}}] \\ &+ [\dot{\alpha}_{10}\ \dot{e}_{i_{L3}}]^T\ P_{10}\ [\alpha_{10}\ e_{i_{L3}}] + [\alpha_{10}\ e_{i_{L3}}]^T\ P_{10}\ [\dot{\alpha}_{10}\ \dot{e}_{i_{L3}}] \end{aligned} \tag{5.54}$$

$$\begin{aligned}\dot{V}_{7.10.11} &= [\alpha_7\ e_{i_{L2}}]^T\ (A_7^T\ P_7 + P_7\ A_7)\ [\alpha_7\ e_{i_{L2}}] \\ &+ [\alpha_{10}\ e_{i_{L3}}]^T\ (A_{10}^T\ P_{10} + P_{10}\ A_{10})\ [\alpha_{10}\ e_{i_{L3}}] \\ &+ [\alpha_{11}\ e_{V_{DC}}]^T\ (A_{11}^T\ P_{11} + P_{11}\ A_{11})\ [\alpha_{11}\ e_{V_{DC}}] \end{aligned} \tag{5.55}$$

We now that $P_7A_7 + A_7^TP_7 = -I_2$, $P_{10}A_{10} + A_{10}^TP_{10} = -I_2$ and $P_{10}A_{11} + A_{11}^TP_{11} = -I_2$ Then:

$$\dot{V}_{7.10.11} = -e_{i_{L2}}^2 - \alpha_7^2 - e_{i_{L3}}^2 - \alpha_{10}^2 - e_{V_{DC}}^2 - \alpha_{11}^2 \tag{5.56}$$

It is well known ([87]) that for a quadratic positive definite function $V(x) = x^TPx$:

$$\lambda_{min}(P)\,||x||^2 \ \leq\ x^TPx\ \leq\ \lambda_{max}(P)\,||x||^2 \tag{5.57}$$

we can write:

$$\dot{V}_{7.10.11} \leq -\frac{1}{\lambda_{max}} V_{7.10.11} \tag{5.58}$$

$$\dot{V}_{7.10.11} \leq -m_{7.10.11}\ V_{7.10.11} \tag{5.59}$$

$$V_{7.10.11}(t) = e^{-m_{7.10.11}t}\ V_{7.10.11}(0) \tag{5.60}$$

which implies that:

$$\lim_{t\to\infty} \left\| \begin{bmatrix} e_{V_{DC}}(t) \\ \alpha_{11}(t) \\ e_{i_{L2}}(t) \\ \alpha_7(t) \\ e_{i_{L3}}(t) \\ \alpha_{10}(t) \end{bmatrix} \right\| = 0$$

and then the closed loop system (5.52) is exponentially stable.

□

5.6 Stability study of interconnected System

Let's now introduce the analysis of the interconnected Microgrid system whose dynamics are as follows.

The mathematical model is as follow

$$\dot{x}(t) = f(x(t)) + g(x(t), u(t), d(t)) \tag{5.61}$$

$$x = [U_C\ V_{C2}\ V_{C3}\ V_{C4}\ V_{C5}\ V_{C6}\ i_{L1}\ i_{L2}\ i_{L3}\ V_{DC}]^T \tag{5.62}$$

$$u = [u_1\ u_3\ u_3]^T \tag{5.63}$$

$$d = [V_{BR}\ V_{BAT}\ V_{SC}\ \frac{1}{R_{Load}}]^T \tag{5.64}$$

U_C, V_{C2} V_{C3}, V_{C4} V_{C5}, V_{C6} and $V_{DC} \in \mathbb{R}^+$, i_{L1}, i_{L2} and $i_{L3} \in \mathbb{R}$.

$$\begin{aligned}
\dot{U}_C &= \frac{1}{C_f} i_{Lf} - \frac{u_1}{C_f} i_{L1} \\
\dot{i}_{Lf} &= -\frac{R_f}{L_f} i_{Lf} - \frac{1}{L_f} U_C + \frac{1}{L_f} V_{BR} \\
\dot{V}_{C2} &= -\frac{1}{R_2 C_2} V_{C2} + \frac{1}{C_2} i_{L1} + \frac{1}{R_2 C_2} V_{DC} \\
\dot{i}_{L1} &= \frac{1}{L_1} U_C - \frac{[(R_{01} - R_{02})u_1 + R_{02}] i_{L1}}{L_1} - \frac{u_1}{L_1} V_{C2} \\
\dot{V}_{C3} &= -\frac{1}{R_3 C_3} V_{C3} - \frac{1}{C_3} i_{L2} + \frac{1}{R_3 C_3} V_{BAT} \\
\dot{V}_{C4} &= -\frac{1}{R_4 C_4} V_{C4} + \frac{(1 - u_2)}{C_4} i_{L2} + \frac{1}{R_4 C_4} V_{DC} \\
\dot{i}_{L2} &= \frac{1}{L_2} V_{C3} - \frac{([(R_{03} - R_{04})u_2 + R_{04}] i_{L2})}{L_2} - \frac{(1 - u_2)}{L_2} V_{C4} \\
\dot{V}_{C5} &= -\frac{1}{R_5 C_5} V_{C5} - \frac{1}{C_5} i_{L3} + \frac{1}{R_5 C_5} V_{SC} \\
\dot{V}_{C6} &= -\frac{1}{R_6 C_6} V_{C6} + \frac{(1 - u_3)}{C_6} i_{L3} + \frac{1}{R_6 C_6} V_{DC} \\
\dot{i}_{L3} &= \frac{1}{L_3} V_{C5} - \frac{([(R_{05} - R_{06})u_3 + R_{06}] i_{L3})}{L_3} - \frac{(1 - u_3)}{L_3} V_{C6} \\
\dot{V}_{DC} &= \frac{1}{C_{DC}} [\frac{1}{R_2}(V_{C2} - V_{DC}) + \frac{1}{R_4}(V_{C4} - V_{DC}) + \frac{1}{R_6}(V_{C6} - V_{DC}) - \frac{V_{DC}}{R_{Load}}
\end{aligned} \tag{5.65}$$

We remark that the relative degrees of (5.65) is 5 in $\mathbb{R}^1$1, and hence we have internal dynamics of order 7.

It is possible to split the states into controlled variables $U_C^e, i_{Lf}^e\, i_{L2}\, i_{L3}$ and V_{DC} and the zero dynamics (uncontrolled variables) $V_{C2}\, V_{C3}\, V_{C4}\, V_{C5}\, V_{C6}$ and i_{L1}:

$$\begin{bmatrix} U_C^e \\ i_{Lf}^e \\ V_{C2}^e \\ V_{C3}^e \\ V_{C4}^e \\ V_{C5}^e \\ V_{C6}^e \\ i_{L1}^e \\ i_{L2}^e \\ i_{L3}^e \\ V_{DC}^e \end{bmatrix} = \begin{bmatrix} Controlled\ dynamics \\ Controlled\ dynamics \\ Zero\ dynamics \\ Zero\ dynamics \\ Zero\ dynamics \\ Zero\ dynamics \\ Zero\ dynamics \\ Zero\ dynamics \\ Controlled\ dynamics \\ Controlled\ dynamics \\ Controlled\ dynamics \end{bmatrix} \tag{5.66}$$

Let us now move the focus to the zero dynamics. We can rewrite the zero dynamics equations of system (5.65) as:

$$\begin{aligned} \dot{V}_{C2} &= -\frac{1}{R_2C_2}V_{C2} + \frac{1}{C_2}i_{L1} + \frac{1}{R_2C_2}V_{DC} \\ \dot{i}_{L1} &= \frac{1}{L_1}U_C - \frac{[(R_{01}-R_{02})u_1 + R_{02}]i_{L1}}{L_1} - \frac{u_1}{L_1}V_{C2} \\ \dot{V}_{C3} &= -\frac{1}{R_3C_3}V_{C3} - \frac{1}{C_3}i_{L2} + \frac{1}{R_3C_3}V_{BAT} \\ \dot{V}_{C4} &= -\frac{1}{R_4C_4}V_{C4} + \frac{(1-u_2)}{C_4}i_{L2} + \frac{1}{R_4C_4}V_{DC} \\ \dot{V}_{C5} &= -\frac{1}{R_5C_5}V_{C5} - \frac{1}{C_5}i_{L3} + \frac{1}{R_5C_5}V_{SC} \\ \dot{V}_{C6} &= -\frac{1}{R_6C_6}V_{C6} + \frac{(1-u_3)}{C_6}i_{L3} + \frac{1}{R_6C_6}V_{DC} \end{aligned} \tag{5.67}$$

and we can compute $V_{C2}^e\, V_{C3}^e\, V_{C4}^e\, V_{C3}^e\, V_{C5}^e\, V_{C6}^e$ and i_{L1}^e their equilibrium points:

$$\begin{aligned} 0 &= -\frac{1}{R_2C_2}V_{C2} + \frac{1}{C_2}i_{L1} + \frac{1}{R_2C_2}V_{DC} \\ 0 &= \frac{1}{L_1}U_C - \frac{[(R_{01}-R_{02})u_1 + R_{02}]i_{L1}}{L_1} - \frac{u_1}{L_1}V_{C2} \\ 0 &= -\frac{1}{R_3C_3}V_{C3} - \frac{1}{C_3}i_{L2} + \frac{1}{R_3C_3}V_{BAT} \\ 0 &= -\frac{1}{R_4C_4}V_{C4} + \frac{(1-u_2)}{C_4}i_{L2} + \frac{1}{R_4C_4}V_{DC} \\ 0 &= -\frac{1}{R_5C_5}V_{C5} - \frac{1}{C_5}i_{L3} + \frac{1}{R_5C_5}V_{SC} \\ 0 &= -\frac{1}{R_6C_6}V_{C6} + \frac{(1-u_3)}{C_6}i_{L3} + \frac{1}{R_6C_6}V_{DC} \end{aligned} \tag{5.68}$$

then define the complete equilibrium vector:

$$x^e = \begin{bmatrix} U_C^e \\ i_{Lf}^e \\ V_{C2}^e \\ V_{C3}^e \\ V_{C4}^e \\ V_{C5}^e \\ V_{C6}^e \\ i_{L1}^e \\ i_{L2}^e \\ i_{L3}^e \\ V_{DC}^e \end{bmatrix} \tag{5.69}$$

Lemma 5.6.1. *Under the assumption that for each t conditions 5.15 5.46 and 5.51 are verified; there exist control lawsu*$_1$, u_2 *and* u_3 *such that the system (5.65) has in closed loop an equilibrium point* x_e *(5.70), and any initial condition exponentially converges to it.*

$$x^e = \begin{bmatrix} U_C^e \\ i_{Lf}^e \\ V_{C2}^e \\ V_{C3}^e \\ V_{C4}^e \\ V_{C5}^e \\ V_{C6}^e \\ i_{L1}^e \\ i_{L2}^e \\ i_{L3}^e \\ V_{DC}^e \end{bmatrix} = \begin{bmatrix} U_C^* \\ i_{Lf}^* \\ R_2 i_{L1}(1 - u_1^* \\ V_{BAT} - R_3 i_{L2}^* \\ R_4 i_{L2}^*(1 - u_2^*) \\ V_{SC} - R_3 i_{L3}^* \\ R_6 i_{L3}^*(1 - u_3^*) \\ \frac{1}{u_1} i_{f1} \\ i_{L2}^* \\ i_{L3}^* \\ V_{DC}^* \end{bmatrix} \tag{5.70}$$

where U_C^*, V_{C2}^*, V_{C3}^*, V_{C4}^*, V_{C5}^*, V_{C6}^*, V_{DC}^*, i_{L1}^*, i_{L2}^* *and* i_{L3}^* *have already been defined .*

Proof. The equilibrium point is function of the reference values of U_C i_{Lf} i_{L1}, i_{L2}, i_{L3} and V_{DC}:

$$x^e = \begin{bmatrix} U_C^e \\ i_{Lf}^e \\ V_{C2}^e \\ V_{C3}^e \\ V_{C4}^e \\ V_{C5}^e \\ V_{C6}^e \\ i_{L1}^e \\ i_{L2}^e \\ i_{L3}^e \\ V_{DC}^e \end{bmatrix} = f(U_C^*, i_{Lf}^*, i_{L2}^*, i_{L3}^*, V_{DC}^*) \tag{5.71}$$

The proof is based on the use of a Lyapunov function V which is a composition of different Lyapunov functions, the control inputs u_1, u_2 and u_3 were already defined for controlling the dynamics of U_C, i_{Lf}, i_{L2}, i_{L3} and V_{DC}. They are proven to be stable by the Lyapunov functions $V_{1.2}$ and $V_{7.10.11}$. The Lyapunov function V is now defined as:

$$V = V_{1.2} + V_{7.10.11} + V_{3.4.5.6.8.9} \tag{5.72}$$

where $V_{1.2}$ and $V_{7.10.11}$, have already been introduced and $V_{3.4.5.6.8.9}$ must be studied.

The function $V_{3.4.5.6.8.9}$ refers to dynamics i_{L1}, V_{C2}, V_{C3}, V_{C4}, V_5 and V_{C6} introducing the errors e_2, e_4, e_5, e_7 and e_8 between the dynamics and their equilibrium points as:

$$\begin{aligned} e_{V_{C2}} &= V_{C2} - V_{C2}^* \\ e_{i_{L1}} &= i_{L1} - i_{L1}^* \\ e_{V_{C3}} &= V_{C3} - V_{C3}^* \\ e_{V_{C4}} &= V_{C4} - V_{C4}^* \\ e_{V_{C5}} &= V_{C5} - V_{C5}^* \\ e_{V_{C6}} &= V_{C6} - V_{C6}^* \end{aligned}$$

that can be rewritten as:

$$\begin{aligned} V_{C2} &= e_{V_{C2}} + V_{C2}^* \\ i_{L1} &= e_{i_{L1}} + i_{L1}^* \\ V_{C3} &= e_{V_{C3}} + V_{C3}^* \\ V_{C4} &= e_{V_{C4}} + V_{C4}^* \\ V_{C5} &= e_{V_{C53}} + V_{C5}^* \\ V_{C6} &= e_{V_{C6}} + V_{C6}^* \end{aligned}$$

Their derivative is:

$$\begin{aligned}
\dot{e}_{V_{C2}} &= \frac{1}{R_2C_2}(V_{DC} - e_{V_{C2}} - V^*_{C2}) + \frac{(1-u_1)}{C_2} i_{L1} \\
\dot{e}_{i_{L1}} &= \frac{1}{L_1} U_C - \frac{[(R_{01} - R_{02})u_1 + R_{02}]i_{L1}}{L_1} - \frac{u_1}{L_1} V_{C2} - e_{i_{L1}} \\
\dot{e}_{V_{C3}} &= \frac{1}{R_3C_3}(V_{BAT} - e_{V_{C3}} - V^*_{C3}) - \frac{1}{C_3} i_{L2} \\
\dot{e}_{V_{C4}} &= \frac{1}{R_4C_4}(V_{DC} - e_{V_{C4}} - V^*_{C4}) + \frac{(1-u_2)}{C_4} i_{L2} \\
\dot{e}_{V_{C5}} &= \frac{1}{R_5C_5}(V_{BAT} - e_{V_{C5}} - V^*_{C5}) - \frac{1}{C_5} i_{L3} \\
\dot{e}_{V_{C6}} &= \frac{1}{R_6C_6}(V_{DC} - e_{V_{C6}} - V^*_{C6}) + \frac{(1-u_3)}{C_3} i_{L3}
\end{aligned} \tag{5.73}$$

and $V_{3.4.5.6.8.9}$ can be defined as:

$$V_{3.4.5.6.8.9} = \frac{R_2C_2}{2} e^2_{V_{C2}} + \frac{L_1}{2} e^2_{i_{L1}} + \frac{R_3C_3}{2} e^2_{V_{C3}} + \frac{R_4C_4}{2} e^2_{V_{C4}} + \frac{R_5C_5}{2} e^2_{V_{C5}} + \frac{R_6C_6}{2} e^2_{V_{C6}} \tag{5.74}$$

which derivative can be computed as:

$$\begin{aligned}
\dot{V}_{3.4.5.6.8.9} &= R_2C_2 e_{V_{C2}} (\frac{1}{R_2C_2}(V_{DC} - e_{V_{C2}} - V^*_{C2}) + \frac{(1-u_1)}{C_2} i_{L1}) \\
&\quad + L_1 e_{i_{L1}} (\frac{1}{L_1} U_C - \frac{[(R_{01} - R_{02})u_1 + R_{02}]i_{L1}}{L_1} - \frac{u_1}{L_1} V_{C2} - e_{i_{L1}}) \\
&\quad + R_3C_3 e_{V_{C3}} (\frac{1}{R_3C_3}(V_{BAT} - e_{V_{C3}} - V^*_{C3}) - \frac{1}{C_3} i_{L2}) \\
&\quad + R_4C_4 e_{V_{C4}} (\frac{1}{R_4C_4}(V_{DC} - e_{V_{C4}} - V^*_{C4}) + \frac{(1-u_2)}{C_4} i_{L2}) \\
&\quad + R_5C_5 e_{V_{C5}} (\frac{1}{R_5C_5}(V_{BAT} - e_{V_{C5}} - V^*_{C5}) - \frac{1}{C_5} i_{L3}) \\
&\quad + R_6C_6 e_{V_{C6}} (\frac{1}{R_6C_6}(V_{DC} - e_{V_{C6}} - V^*_{C6}) + \frac{(1-u_3)}{C_3} i_{L3})
\end{aligned}$$

$$\dot{V}_{3.4.5.6.8.9} = -e^2_{V_{C2}} - e^2_{i_{L1}} - e^2_{V_{C3}} - e^2_{V_{C4}} - e^2_{V_{C5}} - e^2_{V_{C6}} \tag{5.75}$$

We can finally state the constructive Lyapunov function for the whole system: as follows:

$$\begin{aligned}
V_{1\cdots11} &= ([\alpha_1\ e_{U_C}]^T\ P_1[\alpha_1 e_{U_C}]) + ([\alpha_2 e_{i_{Lf}}]^T P_2[\alpha_2 e_{i_{LF}}]) + \frac{R_2C_2}{2} e^2_{V_{C2}} \frac{L_1}{2} e^2_{i_{L1}} \\
&+ \frac{R_3C_3}{2} e^2_{V_{C3}} + \frac{R_4C_4}{2} e^2_{V_{C4}} + \frac{R_5C_5}{2} e^2_{V_{C5}} + \frac{R_6C_6}{2} e^2_{V_{C6}} + \ ([\alpha_7\ e_{i_{L2}}]^T\ P_7\ [\alpha_7 e_{i_{L2}}]) \\
&+ ([\alpha_{10}\ e_{i_{L3}}]^T\ P_{10}[\alpha_{10} e_{i_{L3}}]) + ([\alpha_{11}\ e_{V_{DC}}]^T\ P_{11}[\alpha_{11}\ e_{V_{DC}}])
\end{aligned} \tag{5.76}$$

It's derivative is then:

$$\begin{aligned}
\dot{V}_{1\cdots11} &= -e^2_{U_C} - \alpha^2_1 - e^2_{i_{Lf}} - \alpha^2_2 - e^2_{V_{C2}} - e^2_{i_{L1}} - e^2_{V_{C3}} - e^2_{V_{C4}} \\
&- e^2_{V_{C5}} - e^2_{V_{C6}} - e^2_{i_{L2}} - \alpha^2_7 - e^2_{i_{L3}} - \alpha^2_{10} - e^2_{V_{DC}} - \alpha^2_{11}
\end{aligned} \tag{5.77}$$

Then

$$V_{1\cdots11}(t) = e^{-m_{1\cdots11}t}\, V_{1\cdots11}(0) \tag{5.78}$$

This in its turn assures again the exponential convergence of all states of the interconnected system towards their equilibrium points.

□

5.7 Simulations result

In this section, we present some simulations that show the results obtained using Matlab Simulink. The objective of the simulations is to stabilize the DC MicroGrid voltage in spite of the variations of the production and consumption in the grid.

R_{01}	0.001Ω	R_1	0.2Ω	C_1	$0.1F$
R_{02}	0.002Ω	R_2	0.015Ω	C_2	$0.001F$
R_{03}	0.001Ω	R_3	0.5Ω	C_3	$0.01F$
R_{04}	0.0015Ω	R_4	0.01Ω	C_4	$0.001F$
R_{05}	0.001Ω	R_5	0.4Ω	C_5	$0.01F$
R_{06}	0.0015Ω	R_6	0.01Ω	C_6	$0.001F$
L_1	$0.005H$	L_2	$0.0033H$	L_3	$0.0033H$
V_N	$75V$	P_n	$1MW$	L_f	$0.004H$
V_{SC}	$200V$	V_{BAT}	$200V$	V_{DC}	$560V$

Table 5.1: Values of simulation

V_{cell}	$2V$
Nominal power	$1MW$
C_{10}	$5000A$
I_{10}	$500A$
LAB Electrochemical process efficiency	$K = 0.75$
LAB self-discharge rate	$D = 1e^{-}5$
$Step_sec$	3600
Nb_serie	100

Table 5.2: Battery simulation parameters

R_{1C}	$0.3 * ESR$
R_{2C}	$0.2 * ESR$
R_{3C}	$0.5 * ESR$
C_{1C}	$0.4 * C$
C_{2C}	$0.414 * C$
C_{3C}	$0.16 * C$
ESR	$0.35m\Omega$
Voltage across the SC	$150V to 250V$
Discharge Ratio Desired/Limit	$d = 50\%$
Required Demanded Power	$1MW$ to over $2MW$
$P_{required}$	$1MW$
Capacitance	$2700F$
Stable Operating Voltage	$2.7V$
Time Constant	0.9
Thermal Operating Conditions	-40^oc to $+70^oc$

Table 5.3: Supercapacitor simulation parameters

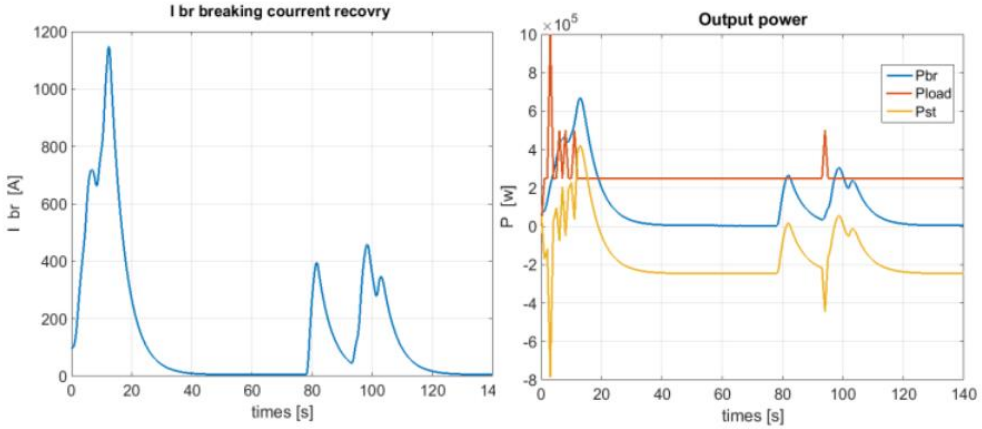

Figure 5.6: Output current and Output Power

In Figure (5.6) one can see the strong power (right) and respective current (left) from the braking. This power shape is instantaneously absorbed by the supercapacitor (P_{SC}), such that the battery can stay rather unchanged during the whole time. As a consequence its lifespan is significantly increased. The battery can then provide most of the energy demanded by the load, allowing long term planning, and the use of weather forecast and load predictions in the higher level algorithms.

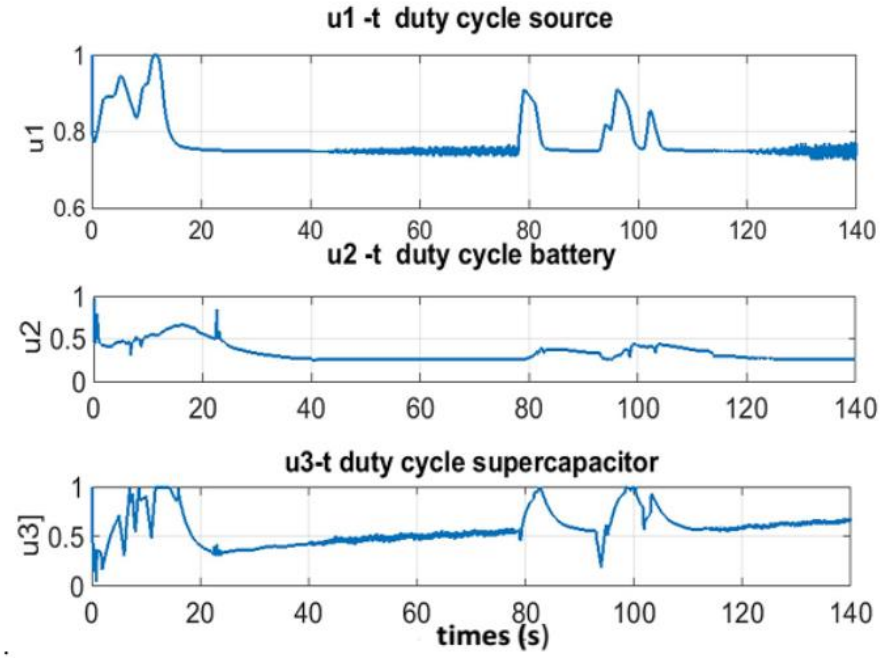

Figure 5.7: Control inputs u_1, u_2 and u_3

The control inputs (shown in Figure 5.7) are smooth except in the case of fast power variations of different elements of the DC MicroGrid.

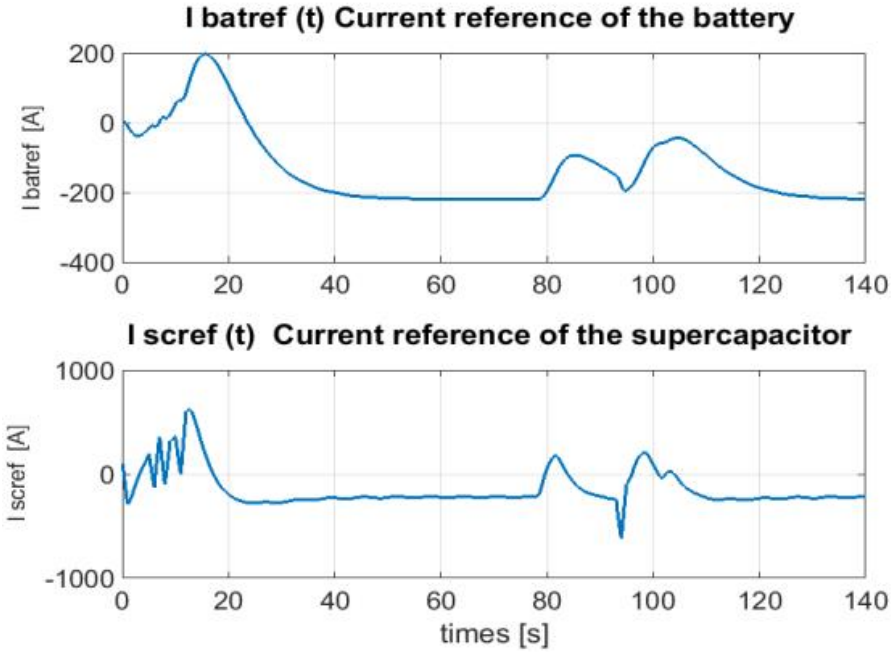

Figure 5.8: Current references

In Figure (5.8) it can be seen the variations of the two components of the power reference provided to storage, the slow and the fast references.

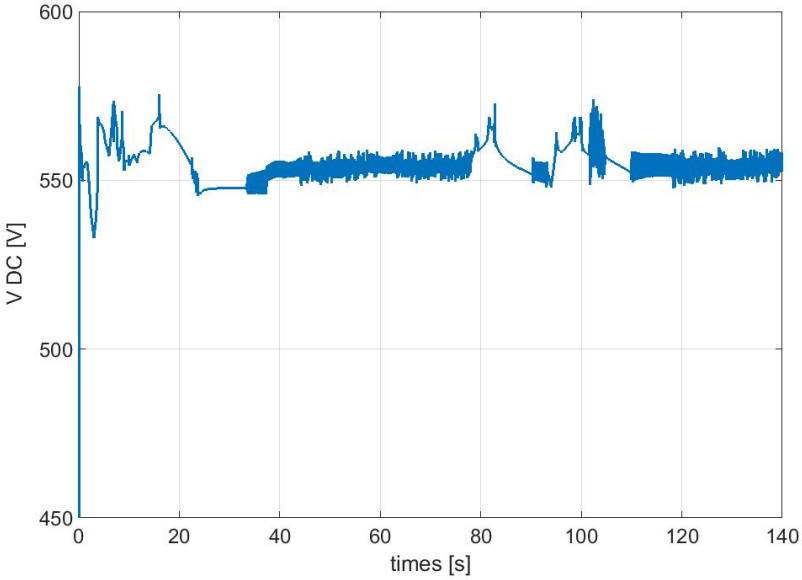

Figure 5.9: DC MicroGrid voltage

We can see in Figure (5.9) that the controller always keeps Vdc close to its nominal value. The control strategy is then shown to successfully operate in a wide range of situations.

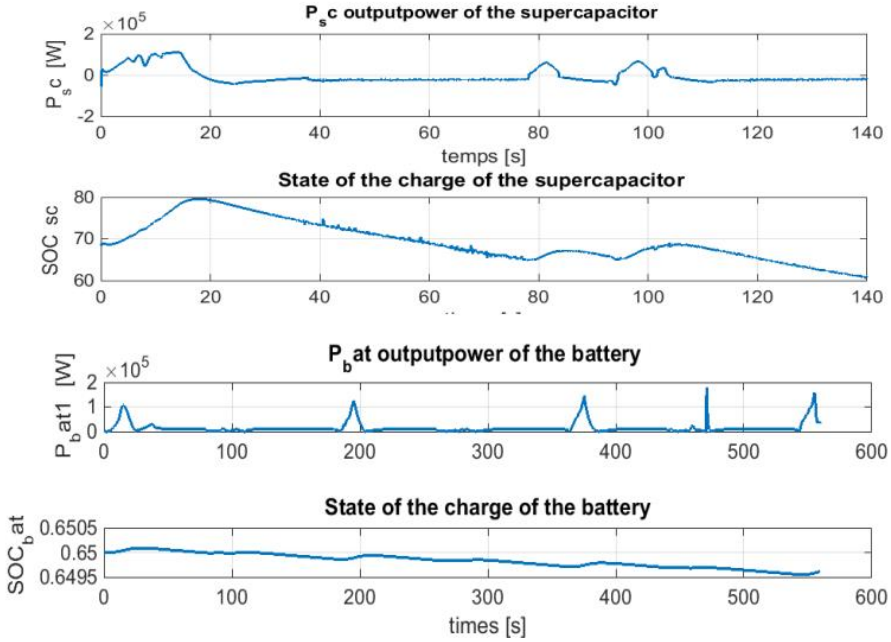

Figure 5.10: Output power and state of the charge of the battery and supercapacitor

Figure (5.10) illustrates provided power and the state of charge (SOC) for the battery and supercapacitor, we can see the supercapacitor charge and discharge very fast to meet a peak power demand and battery discharge slowly to secure power balance and to maintain voltage in dc grid.

5.8 Conclusion

In this chapter it is studied the design of a braking energy recovery system for rail, through a DC MicroGrid, aiming to be used in a station (rail, metro, tramway), such that trains can use electric brakes instead of mechanical ones, and the grid can extract a maximum power from this braking.

The power management strategy and the nonlinear control are developed for the DC distribution system recovering the DC train braking energy. The regulated sources (storage) are used to keep the DC voltage and guarantee the balance between generation and energy consumption; this is obtained by an algorithm applied in these storage elements that tracks the DC voltage, and injects electric power into the DC network. Simulation results illustrate our claims, and the good behavior of each element and the overall interconnected system. In this chapter the control law is designed for each converter and stability of the dynamics of the whole system is proved.

Chapter 6

Control Application

6.1 Introduction

In previous chapters, we have discussed and analysed DC MicroGrid structure with different sources. We established control philosophy and stabilising algorithms, and we confirmed our results by simulations in Matlab Simulink.

Now in this chapter we present experiments made on test bed to validate the control design and stability study. The experimental part have been realized in the laboratory of Concordia University in Montreal. It was necessary to adapt the theoretical study for the existing test platform. A Three-Input DC–DC Boost Converter Circuit is modeled and the control approach was redesigned to fit to this topology. I a firs step, simulations were performed to test the control design. Then the control algorithms were tested on the real system.

As before, the main task of the controller is to manage the power flow of the whole DC MicroGrid and to keep grid voltage around its reference value.

6.2 System Configuration

The structure of the DC MicroGrid is shown in figure (6.1). It is composed by the PV array, battery and supercapacitor connected through the Three-Input DC–DC Boost Converter. One unidirectional leg is used for the PV input as source, while two bidirectional legs were used for the storage elements, while the load is connected to the DC MicroGrid.

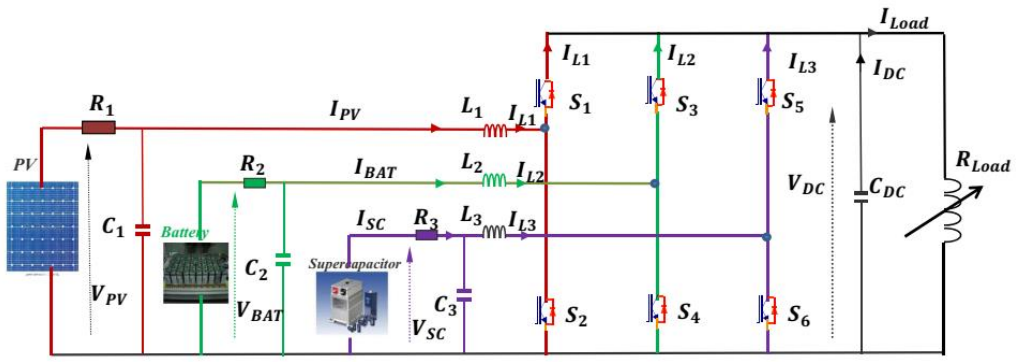

Figure 6.1: Three-Input DC–DC Boost Converter Circuit

6.2.1 Model of Three-Input DC–DC Boost Converter

This converter consists of three-Input DC–DC Boost Converter with six switches connected in parallel per phase. Six power switches are independently controlled with three different duty cycles. Using these duty cycle to controlling the power flow among the PV, storage and the load. The mathematical model is given, based on power electronics averaging technique, the state variables are the capacitor voltages V_{C1}, V_{C2}, V_{C3}, inductor currents i_{L1}, i_{L2}, i_{L3} and DC MicroGrid voltage V_{DC}, where V_{C1}, V_{C2} V_{C3} and $V_{DC} \in \mathbb{R}^+$, i_{L1} i_{L2} $i_{L3} \in \mathbb{R}$

The model is written as follows:

$$\begin{aligned}
\dot{V}_{C1} &= -\frac{1}{R_1 C_1} V_{C1} - \frac{1}{C_1} i_{L1} + \frac{1}{R_1 C_1} V_{PV} \\
\dot{i}_{L1} &= \frac{1}{L_1} V_{C1} - \frac{[(R_{01} - R_{02})u_1 + R_{02}] i_{L1}}{L_1} - \frac{(1-u_1)}{L_1} V_{DC} \\
\dot{V}_{C2} &= -\frac{1}{R_2 C_2} V_{C2} - \frac{1}{C_2} i_{L2} + \frac{1}{R_2 C_2} V_{BAT} \\
\dot{i}_{L2} &= \frac{1}{L_2} V_{C2} - \frac{[(R_{03} - R_{04})u_2 + R_{04}] i_{L2}}{L_2} - \frac{(1-u_2)}{L_2} V_{DC} \\
\dot{V}_{C3} &= -\frac{1}{R_3 C_3} V_{C3} - \frac{1}{C_3} i_{L3} + \frac{1}{R_3 C_3} V_{SC} \\
\dot{i}_{L3} &= \frac{1}{L_3} V_{C3} - \frac{[(R_{05} - R_{06})u_3 + R_{06}] i_{L3}}{L_3} - \frac{(1-u_3)}{L_3} V_{DC} \\
\dot{V}_{DC} &= \frac{1}{C_{DC}} [(1-u_1) i_{L1} + i_{Storage} - i_{Load}]
\end{aligned} \tag{6.1}$$

$R_1, R_2, R_3, L_1, L_2, L_3, C_1, C_2, C_3$ and C_{DC} are known positive values of resistances, capacitors and inductors. For modeling the switches there are small resistances (R_{01}, R_{02}, R_{03}, R_{04}, R_{05} and R_{06}) when they are driving, so the conduction losses are taken into account. V_{PV}, V_{BAT}, V_{SC} and V_{DC} are the photovoltaic panel, battery, supercapacitor and DC MicroGrid voltages respectively. The measurement state is composed by $V_{C1}, V_{C2}, V_{C3}, i_{L1}, i_{L2}, i_{L3}$ and V_{DC}. u_1, u_2 and u_3 will be the control inputs which define the duty cycle of the converter.

6.3 Grid Control Strategy

The objective of this work is to keep DC MicroGrid voltage in its nominal value and to assure stability of the whole system. To attain this goal, high level controllers provide references for the local ones. This higher level task is split in different objectives. The high level controller for the PV follows a MPPT algorithm. The high level controller for the storage system is given by a power flow management in DC MicroGrid. In this part, the DC MicroGrid voltage V_{DC} is compared to its reference value V_{DC}^*, then it is computed the total current required to be provided/absorbed by the storage such as to fulfill the power flow and steer the DC grid voltage to its reference. We use a low-pass filter to split this current into two references. The average (low frequency) component of the signal is the reference for the battery current control. The dynamic (higher frequency) component becomes the reference for the supercapacitor current control.

The objective of this control strategy is to use each storage element in a different time scale; the role of the battery is to support slow transitory flow, while the supercapacitor supports fast transitory flows.

6.3.1 High level controller

Control for the Power Source

In order to maximize the solar panel's producing capability, it is necessary to control its operating point to draw the maximum power from it. The algorithm of Maximum Power Point Tracking (MPPT) used in this work is an Incremental Conductance (IncCond) which delivers a reference voltage V_{C1}^* to be tracked by the lower level controller.

Control for the storage connected DC/DC converter

The proposed Hybrid storage consists of a Li-Ion Battery and a supercapacitor. The target of the control is to charge/discharge the storage component and to provide grid voltage stability during transients. The power needed to fulfill the power flow is represented by a current flowing from/to the storage to/from the DC-link capacitance.
As seen in previous chapters:

$$i_{ST}^* = i_{L2}^* + i_{L3}^* \tag{6.2}$$

The reference value for V_{DC} is the constant V_{DC}^*, a backstepping procedure is then adopted such as to design an $i_{ST} = i_{L2}^* + i_{L3}^*$ reference for i_{L2} and i_{L3} that will provide new desired dynamics for the DC bus voltage.

Lets first define the output tracking error:

$$e_{V_{DC}} = (V_{DC} - V_{DC}^*)$$

and the desired dynamic of V_{DC} as:

$$\begin{aligned} \dot{\alpha}_7 &= K_7^{\alpha} e_{V_{DC}} \\ \dot{e}_{V_{DC}} &= -K_7(V_{DC} - V_{DC}^*) - \overline{K}_7 \alpha_7 \end{aligned} \tag{6.3}$$

where α_7 is now defined as an extended state (integral term).

From (6.1) we have equation:

$$\dot{V}_{DC} = \frac{1}{C_{DC}}[(1-u_1)i_{L1} + i_{Storage} - \frac{V_{DC}}{R_{Load}}] \tag{6.4}$$

From (4.11) and (6.4) we can design:

$$\begin{aligned} i_{ST}^* &= -K_7 C_{DC}(V_{DC} - V_{DC}^*) - \overline{K}_7 C_{DC}\alpha_7 \\ &\quad -(1-u_1)i_{L1} + \frac{V_{DC}}{R_{Load}} \end{aligned} \tag{6.5}$$

with $K_7, \overline{K}_7$ and K_7^{α}, positive gains that are used to impose desired dynamics to the closed loop system as:

$$\dot{\widetilde{V}}_{DC} = \begin{bmatrix} \dot{\alpha}_7 \\ \dot{e}_{V_{DC}} \end{bmatrix} = \begin{bmatrix} 0 & K_7^{\alpha} \\ -\overline{K}_7 & -K_7 \end{bmatrix} \widetilde{V}_{DC} \tag{6.6}$$

which closed loop (linear) dynamics present the eigenvalues:

$$\lambda_{7.\alpha_7} = -\frac{1}{2}(K_7 \pm \sqrt{(K_7^2 - 4\overline{K}_7 K_7^{\alpha})})$$

As a corollary, there exists $P_7 = P_7^T > 0$ such that $P_7 A_7 + A_7^T P_7 = -I_2$ where I_2 is the identity matrix in $\mathbb{R}^2$[1].

We introduce now the Lyapunov function:

$$V_7 = ([\alpha_7 \; e_{V_{DC}}]^T \; P_7 \; [\alpha_7 \; e_{V_{DC}}]) \tag{6.7}$$

It's derivative is then:

$$\dot{V}_7 = -e_{V_{DC}}^2 - \alpha_7^2 \tag{6.8}$$

Here again we follow the procedure used in the previous chapter, using the property (see [87]) :

$$\lambda_{min}(P_7)\,\|x\|^2 \;\leq\; x^T P_7 x \;\leq\; \lambda_{max}(P_7)\,\|x\|^2 \tag{6.9}$$

we can then write that (m_7 is a positive constant):

$$\dot{V}_7 \leq -\frac{1}{\lambda_{max}(P_7)} V_7 \stackrel{\triangle}{=} -m_7 \; V_7 \tag{6.10}$$

[1]Such matrix always exist because of the stable poles assigned by the tunning gains.

that implies that:

$$V_7(t) = e^{-m_7 t}\, V_7(0) \tag{6.11}$$

and then we can conclude that:

$$\lim_{t\to\infty} \left\| \begin{bmatrix} e_{V_{DC}}(t) \\ \alpha_7(t) \end{bmatrix} \right\| = 0$$

and that the closed-loop dynamics of V_{DC} are exponentially stable.

Now, the reference (6.5) in its turn is split into a Fast and Slow terms by a low pass filter shown in Fig. 6.2.

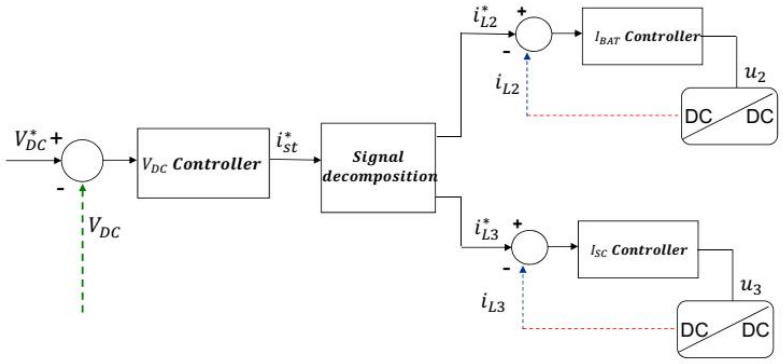

Figure 6.2: Signal Decompostion

such that:

$$i^*_{ST} = i^*_{L2} + i^*_{L3} \tag{6.12}$$

and then i^*_{L2} provided to the battery acts to maintain the balance of power and i^*_{L3} provided to the supercapacitor acts to dampen fast transitory and oscillations.

In our study, the system is sized such that the battery and supercapacitor stay in $40\% < SOC < 80\%$, so we work in the linear phase of the battery and supercapacitor.

6.4 Non linear Control

6.4.1 Control law of PV

Let us first focus on the control u_1 which is dedicated to dynamics V_{C1} and i_{L1}:

$$\begin{aligned} \dot{V}_{C1} &= -\frac{1}{R_1 C_1} V_{C1} - \frac{1}{C_1} i_{L1} + \frac{1}{R_1 C_1} V_{PV} \\ \dot{i}_{L1} &= \frac{1}{L_1} V_{C1} - \frac{[(R_{01} - R_{02})u_1 + R_{02}] i_{L1}}{L_1} - \frac{(1-u_1)}{L_1} V_{DC} \end{aligned} \tag{6.13}$$

The control law is developed by using a backstepping technique. We need to assign the i_{L1}^* reference to i_{L1} in order to assign V_{C1}^* reference to V_{C1}. Lets first define the output tracking errors:

$$e_{V_{C1}} = (V_{C1} - V_{C1}^*)$$

$$e_{i_{L1}} = (i_{L1} - i_{L1}^*)$$

and their derivatives:

$$\dot{e}_{V_{C1}} = (\dot{V}_{C1} - \dot{V}_{C1}^*)$$
$$\dot{e}_{i_{L1}} = (\dot{i}_{L1} - \dot{i}_{L1}^*)$$

The desired dynamics for V_{C1} is introduced as:

$$\dot{\alpha}_1 = K_1^{\alpha} e_{V_{C1}}$$

$$\dot{e}_{V_{C1}} = -K_1 e_{V_{C1}} - \overline{K_1}\alpha_1 \tag{6.14}$$

where α_1 represents the integral term assuring zero error in steady state between the dynamics of V_{C1}. We can then design:

$$i_{L1}^* = \frac{1}{R_1}(V_{PV} - V_{C1}) + C_1 K_1 (V_{C1} - V_{C1}^*) + C_1 \overline{K}_1 \alpha_1 \tag{6.15}$$

with the positive tuning gain parameters K_1,$\overline{K}_1$ and K_1^{α} such that we can rewrite $\dot{e}_{V_{C1}}$ as :

$$\dot{e}_{V_{C1}} = \dot{V}_{C1} - \cancelto{0}{\dot{V}_{C1}^*} = -\frac{1}{R_1 C_1} V_{C1} - \frac{1}{C_1} i_{L1}^* + \frac{1}{R_1 C_1} V_{PV} \tag{6.16}$$

$$\dot{e}_{V_{C1}} = -K_1 (V_{C1} - V_{C1}^*) - \overline{K}_1 \alpha_1 \tag{6.17}$$

We consider an augmented system $\widetilde{V}_{C1}$:

$$\widetilde{V}_{C1} = \begin{bmatrix} \alpha_1 \\ V_{C1} - V_{C1}^* \end{bmatrix}$$

As above, its closed loop (linear) dynamics is here defined with their eigenvalues:

$$\dot{\widetilde{V}}_{C1} = A_1 \widetilde{V}_{C1} = \begin{bmatrix} 0 & K_1^{\alpha} \\ -\overline{K}_1 & -K_1 \end{bmatrix}$$

$$\lambda_{1.2} = -\frac{1}{2}(K_1 \pm \sqrt{(K_1^2 - 4\overline{K}_1 K_1^\alpha)})$$

By properly selecting positive gains K_1,$\overline{K}_1$ and K_1^α both eigenvalues are stable; then the origin is an exponentially stable equilibrium point for the augmented state, and we can then define $P_1 = P_1^T > 0$ such that $P_1 A_1 + A_1^T P_1 = -I_2$.

As next step, we need to design a control law u_1 such as to steer i_{L1} towards its reference i_{L1}^*, as before through a desired dynamic behaviour:

$$\dot{e}_{i_{L1}} = -K_2 e_{i_{L1}} - \overline{K_2}\alpha_2 \tag{6.18}$$

where α_2 is now defined as an extended state governed by equation:

$$\dot{\alpha}_2 = K_2^\alpha e_{i_{L1}} \tag{6.19}$$

We can rewrite $\dot{i}_{L1}$ as

$$\begin{aligned}
\dot{i}_{L1} &= \frac{1}{L_1}V_{C1} - \frac{([(R_{01} - R_{02})u_1 + R_{02}]i_{L1})}{L_1} - \frac{(1-u_1)}{L_1}V_{DC} \\
&= \frac{1}{L_1}V_{C1} - \frac{(R_{01} - R_{02})i_{L1}u_1}{L_1} - \frac{R_{02}i_{L1}}{L_1} - \frac{V_{DC}}{L_1} + \frac{u_1 V_{DC}}{L_1} \\
&= \frac{1}{L_1}(V_{C1} - V_{DC}) - \frac{R_{02}}{L_1}i_{L1} + [-\frac{(R_{01} - R_{02})i_{L1}}{L_1} + \frac{V_{DC}}{L_1}]u_1
\end{aligned}$$

with the positive tuning gain parameters K_2, $\overline{K}_2$ and K_2^α, we obtain the following control law.

$$\begin{aligned}
u_1 &= \frac{1}{(V_{DC} + (R_{02} - R_{01})i_{L1}} \Big[V_{DC} - V_{C1} + R_{02}i_{L1} - L_1(K_2 e_{i_{L1}} + \overline{K}_2\alpha_2 \\
- &\quad C_1\overline{K}_1 K_1^\alpha e_{V_{C1}} + (C_1 K_1 - \frac{1}{R_1})(K_1 e_{V_{C1}} + \overline{K}_1\alpha_1))\Big]
\end{aligned} \tag{6.20}$$

where we have computed:

$$\begin{aligned}
\dot{i}_{L1}^* &= (C_1 K_1 - \frac{1}{R_1})\dot{V}_{C1} + C_1\overline{K}_1\dot{\alpha}_1 \\
&= (C_1 K_1 - \frac{1}{R_1})(-\frac{1}{R_1 C_1}V_{C1} - \frac{1}{C_1}i_{L1} + \frac{1}{R_1 C_1}V_{PV}) + C_1\overline{K}_1 K_1^\alpha e_{V_{C1}} \\
&= (C_1 K_1 - \frac{1}{R_1})[-K_1 e_{V_{C1}} - \overline{K}_1\alpha_1 + C_1\overline{K}_1 K_1^\alpha e_{V_{C1}}]
\end{aligned}$$

With condition:

$$V_{DC} + (R_{02} - R_{01})i_{L1} \neq 0 \tag{6.21}$$

We consider an augmented system $\widetilde{i}_{L1}$:

$$\widetilde{i}_{L1} = \begin{bmatrix} \alpha_2 \\ i_{L1} - i_{L1}^* \end{bmatrix}$$

Its closed loop (linear) dynamics is here defined with their eigenvalues:

$$\dot{\tilde{i}}_{L1} = \begin{bmatrix} 0 & K_2^{\alpha} \\ -\overline{K}_2 & -K_2 \end{bmatrix} \tilde{i}_{L1}$$

$$\lambda_{3.4} = -\frac{1}{2}(K_2 \pm \sqrt{(K_2^2 - 4\overline{K}_2 K_2^{\alpha})})$$

By properly selecting positive gains K_2,$\overline{K}_2$ and K_2^{α} both eigenvalues are stable; then the origin is an exponentially stable equilibrium point for the augmented state, and we define $P_2 = P_2^T > 0$ such that $P_2 A_2 + A_2^T P_2 = -I_2$.

We introduce the Lyapunov function

$$V_{1,2} = [\alpha_1 \; e_{V_{C1}}]^T \; P_1 \; [\alpha_1 \; e_{V_{C1}}] \; + \; [\alpha_2 \; e_{i_{L1}}]^T \; P_2 \; [\alpha_2 \; e_{i_{L1}}] \tag{6.22}$$

It's derivative is then:

$$\dot{V}_{1,2} = [\dot{\alpha}_1 \; \dot{e}_{V_{C1}}]^T \; P_1 \; [\alpha_1 \; e_{V_{C1}}] + [\alpha_1 \; e_{V_{C1}}]^T \; P_1 \; [\dot{\alpha}_1 \; \dot{e}_{V_{C1}}] + [\dot{\alpha}_2 \; \dot{e}_{i_{L1}}]^T \; P_2 \; [\alpha_2 \; e_{i_{L1}}] + [\alpha_2 \; e_{i_{L1}}]^T \; P_2 \; [\dot{\alpha}_2 \; \dot{e}_{i_{L1}}] \tag{6.23}$$

$$\dot{V}_{1,2} = [\alpha_1 \; e_{V_{C1}}]^T \; (A_1^T \; P_1 + P_1 \; A_1) \; [\alpha_1 \; e_{V_{C1}}] \; + \; [\alpha_2 \; e_{i_{L1}}]^T \; (A_2^T \; P_2 + P_2 \; A_2) \; [\alpha_2 \; e_{i_{L1}}] \tag{6.24}$$

we now that $P_1 A_1 + A_1^T P_1 = -I_2$ and $P_2 A_2 + A_2^T P_2 = -I_2$, then:

$$\dot{V}_{1.2} \;\; = \;\; -e_{V_{C1}}^2 - \alpha_1^2 - e_{i_{L1}}^2 - \alpha_2^2 \tag{6.25}$$

As in the previous section, we can state that:
For the quadratic positive definite function $V(x) = x^T P x$

$$\lambda_{min}(P) \, ||x| \, |^2 \; \leq \; x^T P x \; \leq \; \lambda_{max}(P) \, ||x| \, |^2 \tag{6.26}$$

we can write:

$$\dot{V}_{1.2} \leq -\frac{1}{\lambda_{max}} V_{1.2} \tag{6.27}$$

$$\dot{V}_{1.2} \leq -m_{1.2} \; V_{1.2} \tag{6.28}$$

$$V_{1.2}(t) = e^{-m_{1.2} t} \; V_{1.2}(0) \tag{6.29}$$

which implies that

$$\lim_{t \to \infty} \left\| \begin{bmatrix} e_{VC1}(t) \\ \alpha_1(t) \\ e_{i_{L1}}(t) \\ \alpha_2(t) \end{bmatrix} \right\| = 0$$

and that the closed-loop system (6.13) is exponentially stable.

6.4.2 Storage System Control

Lets first define the output tracking errors towards the references computed in equation (6.12):

$$e_{i_{L2}} = (i_{L2} - i^*_{L2})$$

$$e_{i_{L3}} = (i_{L3} - i^*_{L3})$$

Local Control for the Battery

The control input u_2 is dedicated to control the dynamics i_{L2} and to ensure a desired charge/discharge of the battery.

$$\dot{e}_{i_{L2}} = -K_4 e_{i_{L2}} - \overline{K_4}\alpha_4 \tag{6.30}$$

where α_4 is now defined as an extended state governed by equation:

$$\dot{\alpha}_4 = K_4^{\alpha} e_{i_{L2}} \tag{6.31}$$

with the positive tuning gain parameters K_4, $\overline{K}_4$ and K_4^{α}. We can rewrite $\dot{i}_{L2}$:

$$\begin{aligned}
\dot{i}_{L2} &= \frac{1}{L_2}V_{C2} - \frac{([(R_{03}-R_{04})u_2 + R_{04}]i_{L2})}{L_2} - \frac{(1-u_2)}{L_2}V_{DC} \\
&= \frac{1}{L_2}V_{C2} - \frac{(R_{03}-R_{04})i_{L2}u_2}{L_2} - \frac{R_{04}i_{L2}}{L_2} - \frac{V_{DC}}{L_2} + \frac{u_2 V_{DC}}{L_2} \\
&= \frac{1}{L_2}(V_{C2} - V_{DC}) - \frac{R_{04}}{L_2}i_{L2} + [-\frac{(R_{03}-R_{04})i_{L2}}{L_2} + \frac{V_{DC}}{L_2}]u_2
\end{aligned}$$

to obtain the following control law:

$$u_2 = \frac{1}{(V_{DC} + (R_{04} - R_{03})i_{L2}}[V_{DC} - V_{C2} + R_{04}i_{L2} - L_2(K_4 e_{i_{L2}} + \overline{K}_4\alpha_4 + \dot{i_{L2}}*_4)] \tag{6.32}$$

With condition $V_{DC}+(R_{04}-R_{03})i_{L2} \neq 0$, to obtain arbitrary linear system for the states $[\alpha_4\ i_{L2}]^T$ for suitable choice of gains $K_4, \overline{K}_4, K_4^{\alpha}$. The closed loop sub-system becomes:

$$\begin{aligned}
\dot{\alpha}_4 &= K_4^{\alpha} e_{i_{L2}} \\
\dot{e}_{i_{L2}} &= K_4 e_{i_{L6}} + \overline{K}_4\alpha_4
\end{aligned}$$

We consider an augmented system $\widetilde{i}_{L2}$:

$$\widetilde{i}_{L2} = \begin{bmatrix} \alpha_4 \\ i_{L2} - i^*_{L2} \end{bmatrix} \tag{6.33}$$

Its closed loop (linear) dynamics is here defined with their eigenvalues:

$$\dot{\tilde{i}}_{L2} = \begin{bmatrix} 0 & K_4^{\alpha} \\ -\overline{K}_4 & -K_4 \end{bmatrix} \tilde{i}_{L2}$$

$$\lambda_{7.8} = -\frac{K_4}{2} \pm \sqrt{(K_4^2 - 4\overline{K}_4 K_4^{\alpha})}$$

By properly selecting positive gains K_4, $\overline{K}_4$ and K_4^{α} both eigenvalues are stable; then the origin is a exponential stable equilibrium point for the augmented state, and we define $P_4 = P_4^T > 0$ such that $P_4 A_4 + A_4^T P_4 = -I_2$.

Choice of control parameters (see [103, 104])

Several ways may be used for choosing control parameters, like LQR, pole placement, etc. In the following it is presented an industrial standard for tuning.

The transfer function for (6.33) is:

$$H_4(s) = k_4 \frac{\omega_4^2}{s^2 + 2\zeta_4\omega_4 s + \omega_4^2} \tag{6.34}$$

with damping (ζ_4), frequency (ω_4) and k_4 being the static gain. One can then compare with the design parameters:

$$H_4(s) = \frac{K_4^{\alpha}}{s^2 + K_4 s + \overline{K}_4 K_4^{\alpha}} \tag{6.35}$$

A trivial tuning is then to set $K_4^{\alpha} = 1$, such that $k_4 = \frac{1}{\omega_4^2}$. One can then use a simple identification to know the value of the K_4 and $\overline{K}_4$ parameters.

$$\zeta_4 = \frac{K_4}{2\sqrt{\overline{K}_4}}$$

$$\omega_4 = \sqrt{\overline{K}_4}$$

It is known that a battery cannot respond very fast; its time constant is between $1ms$ and $10ms$. That is why it was chosen $\tau_4 = 0.001s$ and $\omega_4 = \frac{2\pi}{\tau_4} = \frac{2\pi}{0.001} = 6283rad/s$. It was also chosen $\zeta_4 = 0.7$ since it provides a quick response without much overshoot. τ_4 is time constant for the battery. With those values one gets:

$$\overline{K}_4 = \omega_4^2 = (6283)^2$$

$$K_4 = 1.4x\,\omega_4 = 1.4\,(6283)$$

The same procedure is repeated for the Supercapacitor, the PV and for the outer voltage loop, imposing new dynamics as above. The computed values will be summarised in Table 6.2.

Local Control for Supercapacitor

The control input u_3 is dedicated to control the dynamics i_{L3} and to ensure a desired charge/discharge of the supercapacitor.

First we define an extended state α_6 governed by equation:

$$\dot{\alpha}_6 = K_6^{\alpha} e_{i_{L3}} \tag{6.36}$$

$$\dot{e_{i_{L3}}} = -K_6 e_{i_{L3}} - \overline{K_6}\alpha_6 \tag{6.37}$$

We rewrite $\dot{i}_{L3}$ as:

$$\begin{aligned}
\dot{i}_{L3} &= \frac{1}{L_3}V_{C3} - \frac{([(R_{05}-R_{06})u_3 + R_{06}]i_{L3})}{L_3} - \frac{(1-u_3)}{L_3}V_{DC} \\
&= \frac{1}{L_3}V_{C3} - \frac{(R_{05}-R_{06})i_{L3}u_3}{L_3} - \frac{R_{06}i_{L3}}{L_3} - \frac{V_{DC}}{L_3} + \frac{u_3 V_{DC}}{L_3} \\
&= \frac{1}{L_3}(V_{C3}-V_{DC}) - \frac{R_{06}}{L_3}i_{L3} + [-\frac{(R_{05}-R_{06})i_{L3}}{L_3} + \frac{V_{DC}}{L_3}]u_3
\end{aligned}$$

with the positive tuning gain parametersK_6 and $\overline{K}_6$, we obtain the following control law:

$$u_3 = \frac{1}{(V_{DC}+(R_{06}-R_{05})i_{L3}}[V_{DC} - V_{C3} + R_{06}i_{L3} - L_3(K_6 e_{i_{L3}} + \overline{K}_6\alpha_6 + \dot{i_{L3}}*)] \tag{6.38}$$

With condition $V_{DC} + (R_{06} - R_{05})i_{L3} \neq 0$ such as to obtain arbitrary linear system for the states $[\alpha_6 \ i_{L3}]^T$ for suitable choice of gains $K_6, \overline{K}_6, K_6^{\alpha}$. The closed loop sub-system becomes:

$$\begin{aligned}
\dot{\alpha}_6 &= K_6^{\alpha} e_{i_{L3}} \\
\dot{e}_{i_{L3}} &= -K_6 e_{i_{L3}} - \overline{K}_6\alpha_6
\end{aligned}$$

We consider an augmented system $\widetilde{i}_{L3}$

$$\widetilde{i}_{L3} = \begin{bmatrix} \alpha_6 \\ i_{L3} - i_{L3}^* \end{bmatrix}$$

Its closed loop (linear) dynamics is here defined with their eigenvalues:

$$\dot{\widetilde{i}}_{L3} = \begin{bmatrix} 0 & K_6^{\alpha} \\ -\overline{K}_6 & -K_6 \end{bmatrix} \widetilde{i}_{L3}$$

$$\lambda_{9.10} = -\frac{1}{2}(K_6 \pm \sqrt{(K_6^2 - 4\overline{K}_6 K_6^{\alpha})})$$

By properly selecting positive gains K_6,$\overline{K}_6$ and K_9^{α} the origin is an exponential stable equilibrium point for the augmented state and there exist $P_6 = P_6^T > 0$ such that $P_6 A_6 + A_6^T P_6 = -I_2$.

We introduce the Lyapunov function:

$$V_{4,6,7} = [\alpha_4\ e_{i_{L2}}]^T\ P_4[\alpha_4\ e_{i_{L2}}] + [\alpha_6\ e_{i_{L3}}]^T\ P_6[\alpha_6\ e_{i_{L3}}] + ([\alpha_7\ e_{V_{DC}}]^T\ P_7[\alpha_7\ e_{V_{DC}}]) \quad (6.39)$$

It's derivative is then:

$$\dot{V}_{4.6} = [\dot{\alpha}_4\dot{e}_{i_{L2}}]^T P_4[\alpha_4 e_{i_{L2}}] + [\alpha_4 e_{i_{L2}}]^T\ P_4[\dot{\alpha}_4\ \dot{e}_{i_{L2}}] + [\dot{\alpha}_6\dot{e}_{i_{L3}}]^T P_6[\alpha_6 e_{i_{L3}}] + [\alpha_6 e_{i_{L3}}]^T P_6[\dot{\alpha}_6\dot{e}_{i_{L3}}] \quad (6.40)$$

$$\dot{V}_{4.6} = [\alpha_4\ e_{i_{L2}}]^T\ (A_4^T\ P_4 + P_4\ A_4)\ [\alpha_4\ e_{i_{L2}}] +\ [\alpha_6\ e_{i_{L3}}]^T\ (A_6^T\ P_6 + P_6\ A_6)\ [\alpha_6\ e_{i_{L3}}] \quad (6.41)$$

we now that $P_4A_4 + A_4^TP_4 = -I_2$ and $P_6A_6 + A_6^TP_6 = -I_2$, then:

$$\dot{V}_{4,6} = -e_{i_{L2}}^2 - \alpha_4^2 - e_{i_{L3}}^2 - \alpha_6^2 \quad (6.42)$$

and as before, the closed loop system

Choice of control parameters for supercapacitor (see [103, 104])

The time constant $0.1ms$. That is why it was chosen $\tau_6 = 0.00001s$ and $\omega_6 = \frac{2\pi}{\tau_6} = \frac{2\pi}{0.0001} = 6283rad/s$. It was also chosen $\zeta_4 = 0.7$ since it provides a quick response without much overshoot. $\tau_6 = 0.0001s$ is time constant for the supercapacitor.

6.4.3 Stability Study for the Interconnected System

From the previous sections, we remark that the relative degrees of (6.1) is 5 in $\mathbb{R}^7$, and hence we have internal dynamics of order 2.

It is possible to split the states into controlled variables $V_{C1}, i_{L1}, i_{L2}, i_{L3}$ and V_{DC} and the zero dynamics (uncontrolled variables) V_{C2} and V_{C3}:

$$\begin{bmatrix} V_{C1} \\ i_{L1} \\ V_{C2} \\ i_{L2} \\ V_{C3} \\ i_{L3} \\ V_{DC} \end{bmatrix} = \begin{bmatrix} Controlled\ dynamics \\ Controlled\ dynamics \\ Zero\ dynamics \\ Controlled\ dynamics \\ Zero\ dynamics \\ Controlled\ dynamics \\ Controlled\ dynamics \end{bmatrix} \quad (6.43)$$

Let us now move the focus to the zero dynamics. We can rewrite the zero dynamics equations of system (6.1) as:

$$\begin{aligned} \dot{V}_{C2} &= -\frac{1}{R_2C_2}V_{C2} - \frac{1}{C_2}i_{L2} + \frac{1}{R_2C_2}V_{BAT} \\ \dot{V}_{C3} &= -\frac{1}{R_3C_3}V_{C3} - \frac{1}{C_3}i_{L3} + \frac{1}{R_3C_3}V_{SC} \end{aligned} \quad (6.44)$$

and we can compute V_{C2}^e and V_{C3}^e their equilibrium points:

$$\begin{aligned} 0 &= -\frac{1}{R_2C_2}V_{C2} - \frac{1}{C_2}i^*_{L2} + \frac{1}{R_2C_2}V_{BAT} \\ 0 &= -\frac{1}{R_3C_3}V_{C3} - \frac{1}{C_3}i^*_{L3} + \frac{1}{R_3C_3}V_{SC} \end{aligned} \tag{6.45}$$

For the battery:
$V_{BAT_{MIN}} \leq V^e_{C2} \leq V_{BAT_{MAX}}$

For the Supercapacitor

$V_{SC_{MIN}} \leq V^e_{C3} \leq V_{SC_{MAX}}$

and then define the complete equilibrium vector:

$$x^e = \begin{bmatrix} V^*_{C1} \\ i^*_{L1} \\ V^e_{C2} \\ i^*_{L2} \\ V^e_{C3} \\ i^*_{L3} \\ V^*_{DC} \end{bmatrix} \tag{6.46}$$

We define a Lyapunov candidate function $V_{3,5}$ for the state V_{C2} and V_{C3}

$$V_{3,5} = \frac{R_2C_2}{2}e^2_{V_{C2}} + \frac{R_3C_3}{2}e^2_{V_{C3}} \tag{6.47}$$

using the errors $e_{V_{C2}}$ and $e_{V_{C3}}$ as:

$$e_{V_{C2}} = (V_{C2} - V^e_{C2})$$

$$e_{V_{C3}} = (V_{C3} - V^e_{C3})$$

The Lyapunov function time derivative is:

$$\dot{V}_{3,5} = -e^2_{V_{C2}} - e^2_{V_{C3}} \tag{6.48}$$

that again assures exponential stability of the zero dynamics.

We can now regroup these partial results in the form of the following theorem that establish the overall stability property.

theorem 6.4.1. *: Consider system (6.1) and its equilibrium point (6.46). Under the assumption that for each time the conditions:*

$$\begin{aligned} V_{DC} + (R_{02} - R_{01})i_{L1} \neq 0 \\ V_{DC} + (R_{04} - R_{03})i_{L2} \neq 0 \\ V_{DC} + (R_{06} - R_{05})i_{L3} \neq 0 \end{aligned}$$

hold, then there exist control laws u_1, u_2 *and* u_3 *given respectively by (6.20), (6.32) and (6.38); positive design parameters* K_1, $\overline{K}_1$, K_1^α, K_2, $\overline{K}_2$, K_2^α,K_4, $\overline{K}_4$, K_4^α, K_6, $\overline{K}_6$ *and* K_6^α, K_7, $\overline{K}_7$ *and* K_7^α, *such that the closed loop system is exponentially stable.*

Proof. We can finally state the constructive Lyapunov function for the whole system $V_{1,2,3,4,5,6,7} = V_1 + V_2 + V_3 + V_4 + V_5 + V_6 + V_7$ as follows:

$$\begin{aligned}
&V_{1\cdots7} = ([\alpha_1\ e_{V_{C1}}]^T\ P_1[\alpha_1 e_{V_{C1}}]) + ([\alpha_2 e_{i_{L1}}]^T P_2[\alpha_2 e_{i_{L1}}]) \\
&+\frac{R_2C_2}{2}e_{V_{C2}}^2 + \ ([\alpha_4\ e_{i_{L2}}]^T\ P_4\ [\alpha_4 e_{i_{L2}}]) + \frac{R_3C_3}{2}e_{V_{C3}}^2 \\
&+([\alpha_6\ e_{i_{L3}}]^T\ P_6[\alpha_6 e_{i_{L3}}]) + ([\alpha_7\ e_{V_{DC}}]^T\ P_7[\alpha_7\ e_{V_{DC}}])
\end{aligned} \tag{6.49}$$

It's derivative is then:

$$\begin{aligned}
&\dot{V}_{1\cdots7} = -e_{V_{C1}}^2 - \alpha_1^2 - e_{i_{L1}}^2 - \alpha_2^2 - e_{V_{C2}}^2 - e_{i_{L2}}^2 - \alpha_4^2 - e_{V_{C3}}^2 \\
&-e_{i_{L3}}^2 - \alpha_6^2 - e_{V_{DC}}^2 - \alpha_7^2 - e_{V_{C2}}e_{i_{L2}} - e_{V_{C3}}e_{i_{L3}}
\end{aligned} \tag{6.50}$$

that completing the squares can be rewritten as:

$$\begin{aligned}
&\dot{V}_{1,\ldots,7} = -e_{V_{C1}}^2 - \alpha_1^2 - e_{i_{L1}}^2 - \alpha_2^2 - e_{V_{C2}}^2 - e_{i_{L2}}^2 - \alpha_4^2 \\
&-e_{V_{C3}}^2 - e_{i_{L3}}^2 - \alpha_6^2 - e_{V_{DC}}^2 - \alpha_7^2 - e_{V_{C2}}e_{i_{L2}} - e_{V_{C3}}e_{i_{L3}} \\
&\dot{V}_{1,\ldots,7} = -e_{V_{C1}}^2 - \alpha_1^2 - e_{i_{L1}}^2 - \alpha_2^2 - \alpha_4^2 - \alpha_6^2 - e_{V_{DC}}^2 - \alpha_7^2 \\
&-e_{V_{C2}}^2 - e_{i_{L2}}^2 - e_{V_{C2}}e_{i_{L2}} - e_{V_{C3}}e_{i_{L3}} - e_{V_{C3}}^2 - e_{i_{L3}}^2 \\
&= -e_{V_{C1}}^2 - \alpha_1^2 - e_{i_{L1}}^2 - \alpha_2^2 - \alpha_4^2 - \alpha_6^2 - e_{V_{DC}}^2 - \alpha_7^2 \\
&-(1-\frac{1}{\sqrt{2}})e_{V_{C2}}^2 - (1-\frac{1}{\sqrt{2}})e_{i_{L2}}^2 \\
&-\frac{1}{\sqrt{2}}e_{V_{C2}}^2 - 2\frac{1}{\sqrt{2}}\frac{1}{\sqrt{2}}e_{V_{C2}}e_{i_{L2}} - \frac{1}{\sqrt{2}}e_{i_{L2}}^2 \\
&-(1-\frac{1}{\sqrt{2}})e_{V_{C3}}^2 - (1-\frac{1}{\sqrt{2}})e_{i_{L3}}^2 \\
&-\frac{1}{\sqrt{2}}e_{V_{C3}}^2 - 2\frac{1}{\sqrt{2}}\frac{1}{\sqrt{2}}e_{V_{C3}}e_{i_{L3}} - \frac{1}{\sqrt{2}}e_{i_{L3}}^2 \\
&= -e_{V_{C1}}^2 - \alpha_1^2 - e_{i_{L1}}^2 - \alpha_2^2 - \alpha_4^2 - \alpha_6^2 - e_{V_{DC}}^2 - \alpha_7^2 \\
&-\left(1-\frac{1}{\sqrt{2}}\right)e_{V_{C2}}^2 - \left(1-\frac{1}{\sqrt{2}}\right)e_{i_{L2}}^2 \\
&-\left(1-\frac{1}{\sqrt{2}}\right)e_{V_{C3}}^2 - \left(1-\frac{1}{\sqrt{2}}\right)e_{i_{L3}}^2 \\
&-\left(\frac{1}{\sqrt[4]{2}}e_{V_{C2}} - \frac{1}{\sqrt[4]{2}}e_{i_{L2}}\right)^2 - \left(\frac{1}{\sqrt[4]{2}}e_{V_{C3}} - \frac{1}{\sqrt[4]{2}}e_{i_{L3}}\right)^2 \\
&\leq -e_{V_{C1}}^2 - \alpha_1^2 - e_{i_{L1}}^2 - \alpha_2^2 - \alpha_4^2 - \alpha_6^2 - e_{V_{DC}}^2 - \alpha_7^2 \\
&-\left(1-\frac{1}{\sqrt{2}}\right)e_{V_{C2}}^2 - \left(1-\frac{1}{\sqrt{2}}\right)e_{i_{L2}}^2 \\
&-\left(1-\frac{1}{\sqrt{2}}\right)e_{V_{C3}}^2 - \left(1-\frac{1}{\sqrt{2}}\right)e_{i_{L3}}^2
\end{aligned} \tag{6.51}$$

$$\dot{V}_{1\cdots7} \leq -e_{V_{C1}}^2 - \alpha_1^2 - e_{i_{L1}}^2 - \alpha_2^2 - \alpha_4^2 - \alpha_6^2 - e_{V_{DC}}^2 - \alpha_7^2 + \left(1 - \frac{1}{\sqrt{2}}\right)(-e_{V_{C2}}^2 - e_{i_{L2}}^2 - e_{V_{C3}}^2 - e_{i_{L3}}^2) \tag{6.52}$$

This in its turn assures again the exponential convergence of all states of the interconnected system towards their equilibrium points.

□

Choice of control parameters for Outer voltage loop (see [103, 104])

Following the same procedure, for the battery:

$$\dot{V}_{DC} = \frac{1}{C_{DC}}[(1-u_1)i_{L1} + i_{Storage} - i_{Load}] \tag{6.53}$$

The reference value for V_{DC} is the constant V^*_{DC}, a backstepping procedure is then adopted such as to design an $i_{ST} = i^*_{L2} + i^*_{L3}$ reference for i_{L2} and i_{L3} that will provide new desired dynamics for the DC bus voltage. Following the backstepping technique, the desired dynamics for i_{L2} are introduced as:

$$\begin{aligned} \dot{\alpha}_7 &= K^{\alpha}_7 e_{V_{DC}} \\ \dot{e}_{V_{DC}} &= \dot{V}_{DC} - \dot{V}^*_{DC} = -K_7 e_{V_{DC}} - \overline{K_7}\alpha_7 \end{aligned} \tag{6.54}$$

The outer voltage loop is to control the V_{DC} voltage ,

We wanted to dissociate the current controller and the voltage controller so that a simple and efficient control system could be set. In order to achieve it, we decided to separate the time constants of the controllers; this is why we decided to have a ratio of 100 between $\tau_{icurrent}$ and $\tau_{ivoltage}$(that is true experimentally: the current variations are really quicker than the voltage variations). With the same method of calculation $\omega_7 = \frac{2\pi}{\tau_7} = \frac{2\pi}{0.1} = 62.831 rad/s$ I also chose $\zeta_7 = 0.7$ since

$$\overline{K}_7 = \omega_7^2 = (62.831)^2$$

$$K_7 = 1.4\,\omega_7 = 1.4\,(62.831)$$

$\tau_7 = 0.1s$ is time constant for the supercapacitor. Frequency choice of Low Pass Filter subsubsection Low Pass Filter τ_7 is the time constant of the outer loop voltage control for V_{DC}. Then, $\omega_7 = \frac{2\pi}{\tau_7}$ with $\tau_7 = 0.1s$. In the same way, τ_F is the time constant for the Low Pass Filter. The time constants τ_F and τ_7 define the dynamic response for the whole system. In order to minimise the impact of the low pass filter response on the system, we have to set $\tau_F < \tau_7$. For this reason it was used $\tau_F = 0.05s\, or\, f_c = 20Hz$. $\tau_1 = 0.1s$ is time constant of the of Outer voltage loop for the photovoltaic system.

$\tau_2 = 0.01s$ is time constant of the of inner current loop for the photovoltaic system.

τ_1 and τ_2 is determined by the same procedure as the storage system.

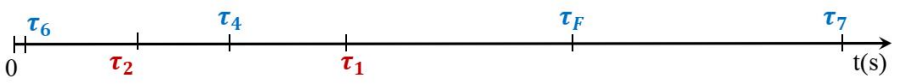

Figure 6.3: Time scale presentation

6.5 Simulation Result

MATLAB/Simulink is used for simulation studies of a DC MicroGrid consisting of solar PV, battery and supercapacitor units supplying a variable resistive load. The system configuration is as shown in Figure (6.1) and the parameters were discussed in Section two. The model parameters' values are depicted in table (6.1):

R_{02},R_{04},R_{06}	0.045Ω
R_{01},R_{03},R_{05}	0.044Ω
R_1,R_2,R_3	0.14Ω
C_1,C_2,C_3	$4700e^{-6}F$
C_{DC}	$1500e^{-6}F$
L_1,L_2,L_3	$100e^{-6}H$
V_{DC}	$50V$

Table 6.1: DC Microgrid paramaters

K_1	870.963	$\overline{K}_1$	620.83^2	K_1^α	1
K_2	8796.3	$\overline{K}_2$	6283.1^2	K_2^α	1
K_4	8796.2	$\overline{K}_4$	6283^2	K_4^α	1
K_6	87963.4	$\overline{K}_6$	62831^2	K_6^α	1
K_7	87.963	$\overline{K}_7$	62.83^2	K_7^α	1

Table 6.2: Control parameters

The main goal is to demonstrate that the proposed strategy provides good results for cases of varying solar irradiance as well as load variations. It is expected to regulate the DC bus voltage with battery and supercapacitor units in such a way that the supercapacitor provides the fast changing components of the required DC bus voltage compensating current while the battery unit provides the slow varying components.
This is achieved with a signal decomposition block with a $20Hz$ LPF first and we did simulation for $f_c = 2Hz$ and $f_c = 100Hz$ in order to study the influence of filter on dynamics of whole system .
As in the section of experimental results, because the voltages in the SC and battery did not vary much, their waveforms are not shown.
During our simulation work we noticed that the dynamic behaviour of the system differs according to the filter cutoff frequency used to provide the references for the battery and the supercapacitor.

6.5.1 Reference split with a $f_c = 20Hz$ Low-pass Filter (LPF)

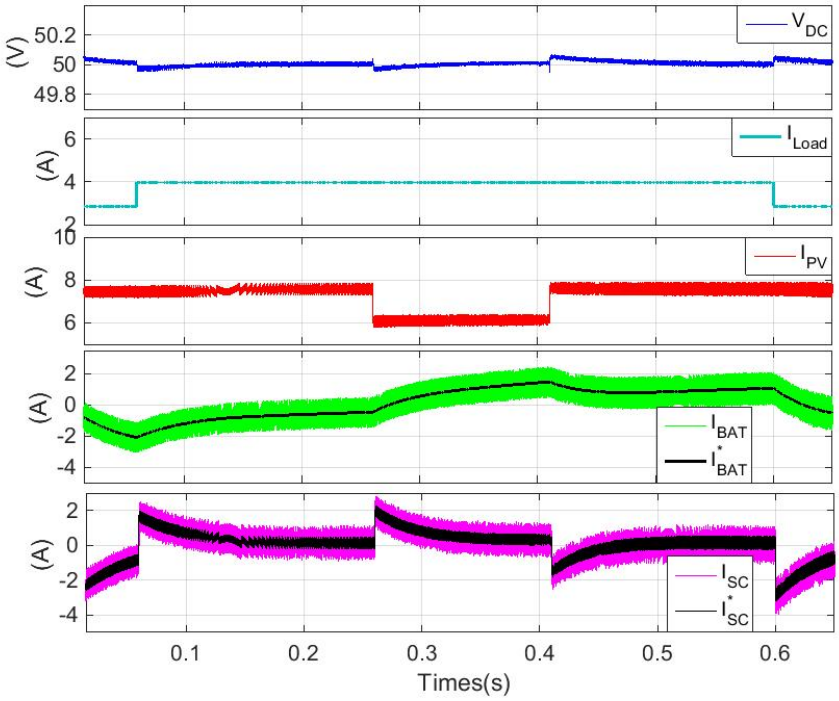

Figure 6.4: Dynamic response of the system

Figure (6.4) shows how the DC bus voltage (top) varies as the load current and PV current (screens just below) vary. The load impedance is equal to 88Ω for $0.06s < t < 0.6s$ and is equal to 44Ω elsewhere.The solar irradiance was rated $1000W/m^2$ for $t < 0.26s$ and $t > 0.4s$, and equal to $800W/m^2$ otherwise. There one sees that the DC bus voltage varies briefly following the transients, quickly recovering and stabilizing at the rated $(50V)$ DC bus voltage in about $30ms$. The maximum DC bus voltage error is equal to $0.07V$.
This is achieved by the action of the proposed control scheme making use of the battery and supercapacitor interfaces. The reference and actual waveforms of the former are shown in the fourth screen from the top. The reference signal varies slowly and the actual waveform follows it with a small switching frequency ripple. Besides, the battery current is the one required to balance the power in the DC microgrid in steady-state. The reference and actual waveforms of the supercapacitor unit are shown in the fifth screen from the top, with the second following closely the first. The SuperCapacitor's response varies fast following PV generation and load demand variations, and tends to stabilize at $0A$.
These results confirm that the proposed scheme is effective in achieving the goals defined for this application. Nevertheless, it is important to remark that the battery is continuously reacting, but much slower than what would happens if it was the only storage element.

6.5.2 Reference split with a $f_c = 2Hz$ Low-pass Filter (LPF)

The variations of load impedance and the solar irradiance are identical to the previous simulation.

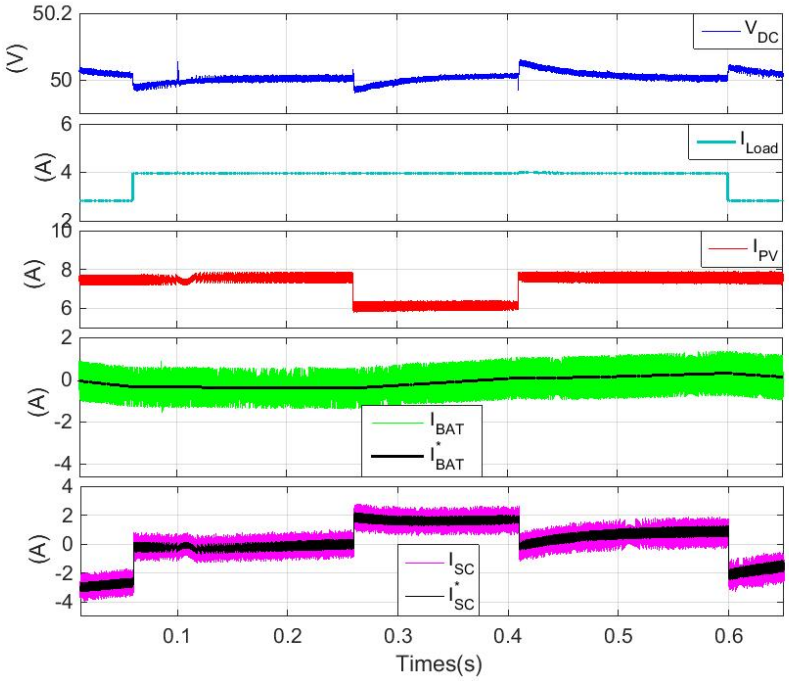

Figure 6.5: Dynamic response of the system

Figure (6.5) shows how the DC bus voltage varies briefly following the transients, quickly recovering and stabilizing at the rated $(50V)$ DC bus voltage in about $45ms$. The maximum DC bus voltage error is equal to $0.06V$.

The battery current change very slowly following its reference, and in some cases, in the short time it doesn't attain balance of power in the DC MicroGrid. As a consequence, Supercapacitor's current has to take this task for a longer time. One can also remark that the Supercapacitor current varies fast following PV generation and load demand variations, and tends to stabilize at $0A$ when battery attain the necessary value to assure power flow.

6.5.3 Reference split with a $f_c = 100Hz$ Low pass Filter (LPF)

The variations of load impedance and the solar irradiance are identical to the previous simulation.

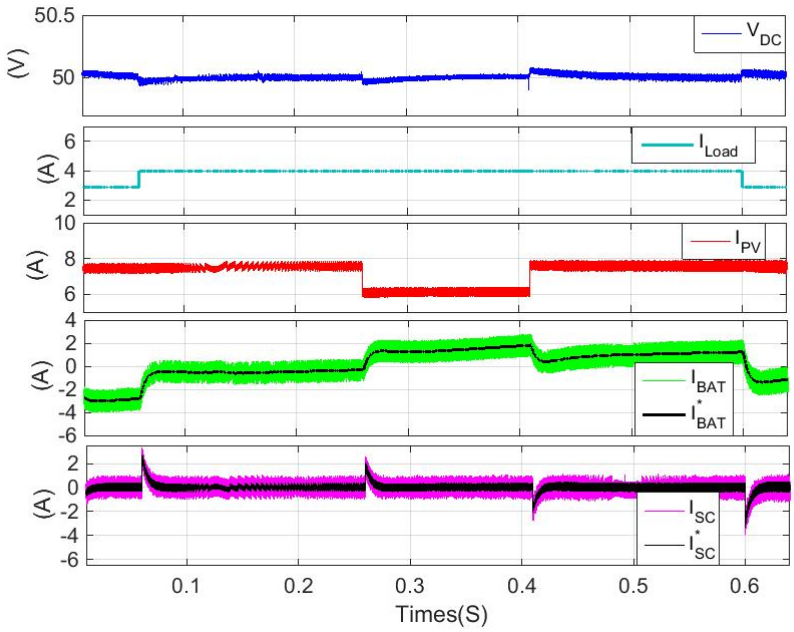

Figure 6.6: Dynamic response of the system

Figure (6.6) shows how the DC bus voltage varies briefly following the transients, quickly recovering and stabilizing at the rated ($50V$) DC bus voltage in about $20ms$. The maximum DC bus voltage error is equal to $0.08V$.

The reference signal varies fast and the actual waveform follows it with switching frequency ripple. The battery reacts much faster than previous cases, and fulfill required power balance in the DC MicroGrid very fast. For this reason, the Supercapacitor current has much less displacement and tends to fast stabilize at $0A$.

These results again support the claim that the proposed scheme is effective in achieving the goals defined for this application, and illustrate the effect of different cut frequency.

Result Analysis

DC MicroGrid receives the required current, where the storage provides the balance of energy and power, shown in figure (6.7).

As said before we use a low-pass filter to divide this current I^*_{ST} to obtain two references.

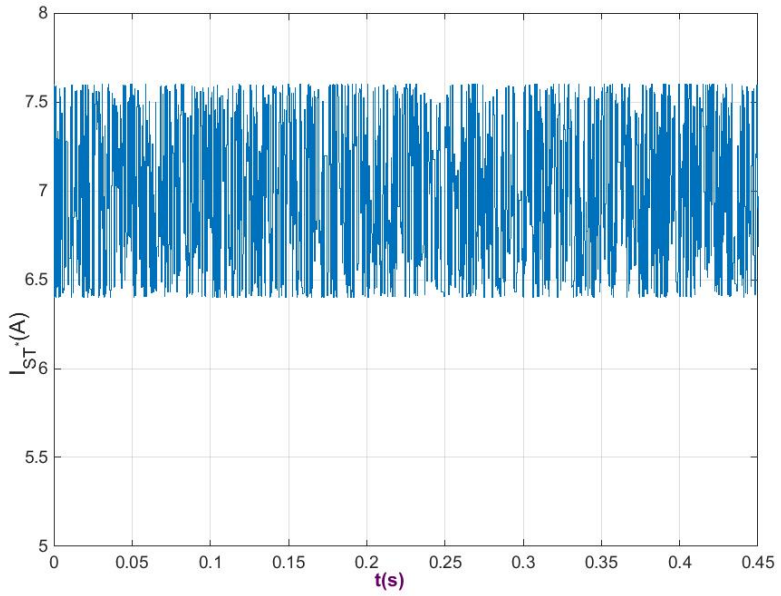

Figure 6.7: Example of the Current reference for the storage

In the different simulations it was noted that the system dynamics depends on the cut-off frequency (time constant) of the filter used to decompose the reference for the storage elements.

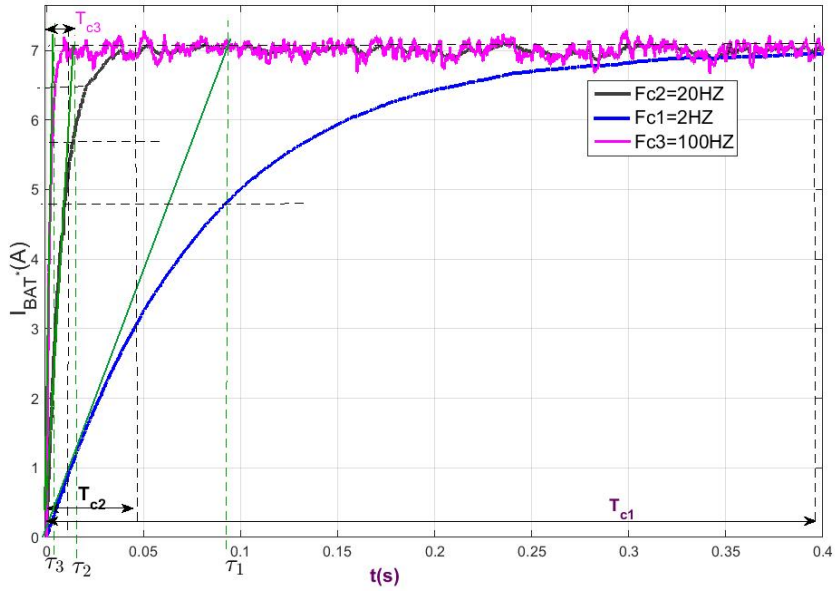

Figure 6.8: Example of reference for the Battery

In figure (6.8), τ_1, τ_2 and τ_3 are the time constants for the filter with respectively cuttoff frequency f_{c1}, f_{c2} and f_{c3}. T_{c1}, T_{c2} and T_{c3} are the time required for the signal to reach

steady state. The average component of the signal is uses as reference for the battery current control, which means that the resulting dynamics of the battery depends on the filter time constant, so the faster the filter is, the more the battery will react.

On the other hand, the dynamic component of this reference is used as the reference for the supercapacitor current control as shown in figure (6.9).

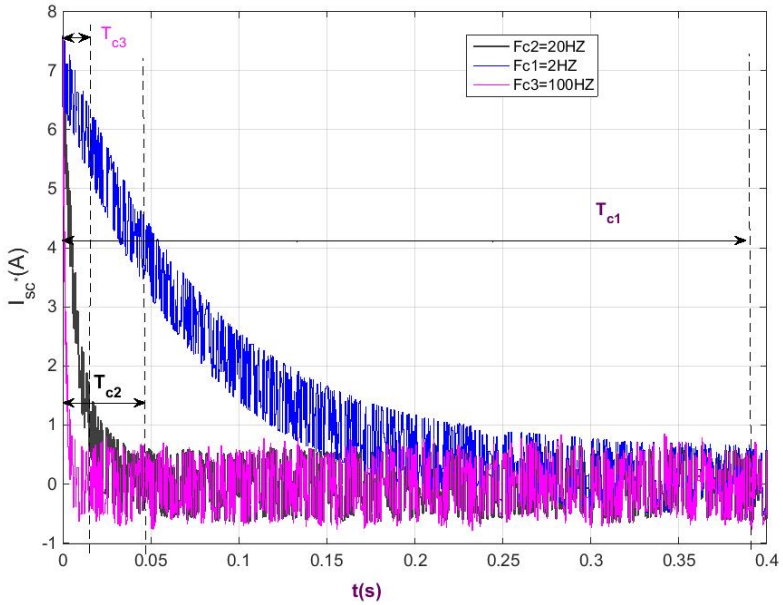

Figure 6.9: Example of the reference for the Battery

Similarly to the battery, the final dynamics of the supercapacitor will depend on the time constants of the filter. In theory the supercapacitor fulfills power balance to cope with PV and Load variations, but if the time constant of the filter is long, supercapacitor will need to supply power for long time.

Conclusion

The control strategy operates successfully in a wide range, in spite of perturbations on the sources and load. The proposed controller always keeps V_{DC} in its nominal value during these variations. The choice of the time constant for the filter depends on desired usage for each element of the Energy Storage System, and in particular this control scheme allows optimal sizing of storage components by splitting the burden among them.

6.6 Experimental investigation and demonstration

A DC MicroGrid composed of a Renewable Energy Source, two energy storage units and a variable load was assembled in laboratory to verify the performance of the proposed control scheme experimentally.

An Agilent Solar Array Simulator $(SAS)(E4350B)$ was used to emulate a solar array. It was programmed to provide a maximum power of $213W$ with $7.35A$ and $29V$ at rated solar

irradiance.
Maxwell supercapacitor modules ($BMOD0165P048$) of $165F$ with a rated voltage of $48V$ were employed for the energy storage units. One is used to simulate a battery and the second is used as a supercapacitor.
Regarding the power electronics interface, a Semikron $MiniSKiiP8$Three-phase $1200V$ Power board, with a MiniSKiiP $83AC$ power module and a $SKHI61$ IGBT driver, was used in this study. One leg of the three-phase inverter is used for each DER. An LC filter ($100\mu H$ and $470\mu F$) is connected between the mid-points of the three-phase inverter legs and the storage and the source elements, to create the classical bi-directional Class C DC-DC converters. A $1500\mu F$ capacitor at the DC bus of the inverter corresponds to the main filter at the DC bus of the Microgrid.
The converters switch at $20kHz$. A $20\mu s$ time step is used in this case. The reference voltage for the DC bus is kept at $50V$. A set of ten parallel switchable 44Ω resistors were used for realizing a variable load, the battery is used in discharge mode in the experiments. A picture of the experimental set-up is shown in the following Figure.

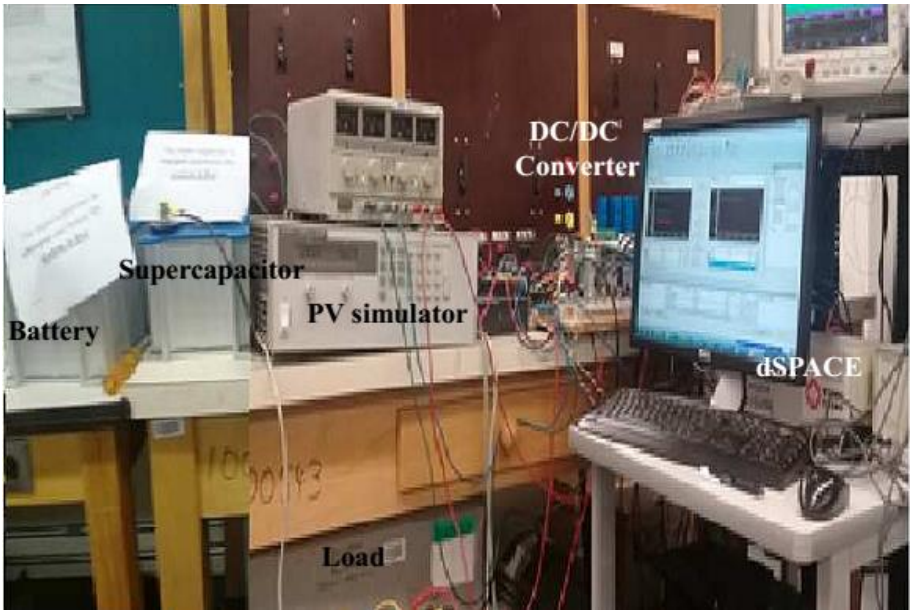

Figure 6.10: Experimental setup

The main objective of these tests is to observe the performance of the system, in particular the regulation of the DC bus voltage; and the split of the required compensating current among the supercapacitor and battery converter units. In this study, the cut-off frequency of the LPF is equal to $2Hz$, $20Hz$ and $100Hz$, as in the simulations. The voltages in the supercapacitor and simulated battery are equal to $24V$ and $28V$, respectively. Considering the short time frames considered in the performance results shown in this study, there should be no noticeable change in their voltage magnitudes, which are not shown in the results presented below.

Figure (6.11) shows a screen shot of the scope with the response of the system (DC bus voltage in blue, battery current in green, PV current in light blue and supercapacitor

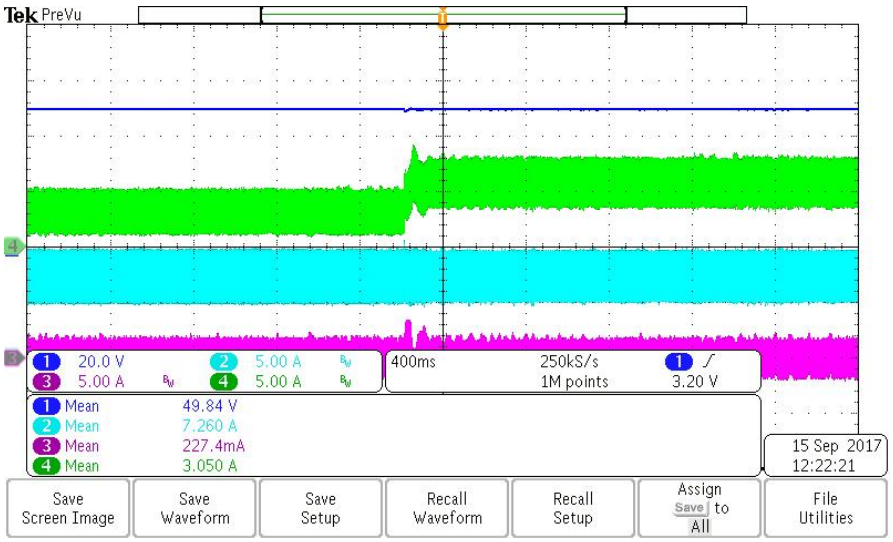

Figure 6.11: Dynamic Response during increasing load with battery discharging

current in pink) to an increase in the power demand, when the load is changed from 8.8Ω (five resistors of 44Ω in parallel) to 7.35Ω (six resistors of 44Ω in parallel). Since it is difficult to see the details of the waveforms, the stored data was sent to MATLAB where it is easier to rescale the waveforms emphasizing their key features for performance analysis.

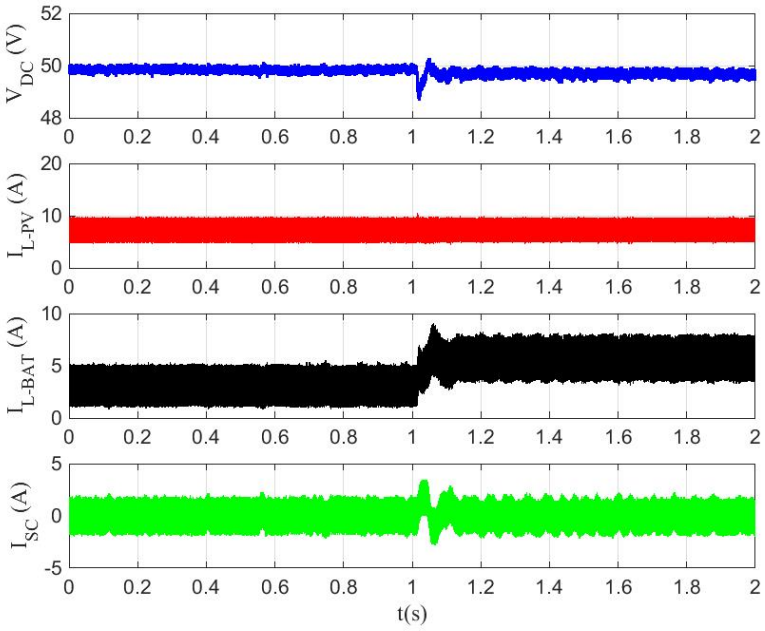

Figure 6.12: Dynamic Response during step increase load with battery discharging

The same result is presented (after rescaling in Matlab) in Figure (6.12). In this case, the load change at $t = 1s$. On the top, one sees that the DC bus is initially equal to $50V$, decreasing briefly by about 0.9 V following the load step, then returning, in about$0.15s$, towards the original value. Just below, the current in the inductor of the PV interface

remains virtually unaffected at the MPPT value. In the pictures below, one sees the inductor currents of the simulated battery and supercapacitor interfaces. The former initially provides about $3.1A$, increasing its output rather slowly, to meet the average value of the step load increase at $t = 1s$. Conversely, in the very bottom, the inductor current of the supercapacitor interface starts at $0A$, showing that it is not providing any average power. Following the load increase, the contribution of the supercapacitor converter increases very fast and returns to an average of about $0A$, as the battery interface takes over the power balancing in the system.

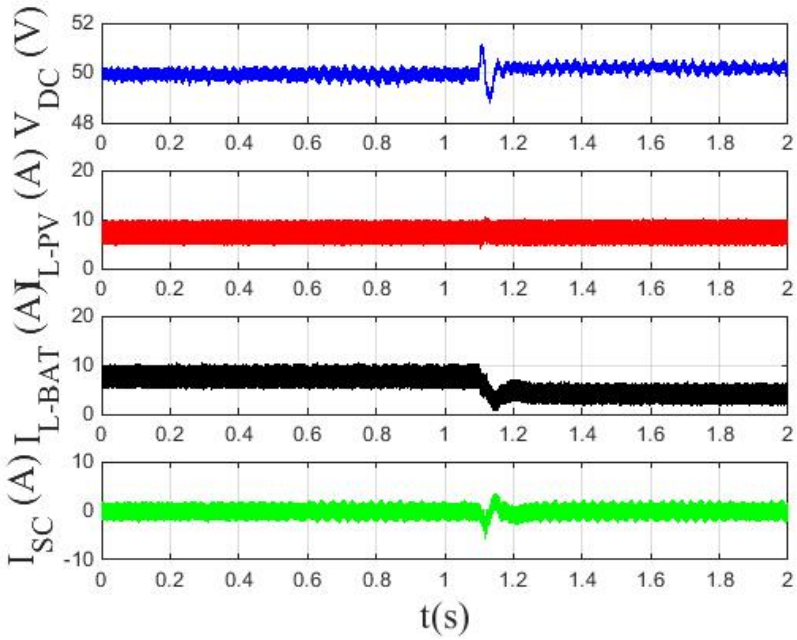

Figure 6.13: Dynamic Response during deacreasing load with battery discharging

Figure (6.13) shows the opposite change: a step load decrease at $t = 0.11s$. In that case, the DC bus voltage will initially increase, by about $0.9V$, then return to its original value as the battery and supercapacitor interfaces adjust their injected powers. As before, the supercapacitor interface reacts faster than the "battery" one, what allows the current in the latter to vary at a lower rate, as desired and expected.

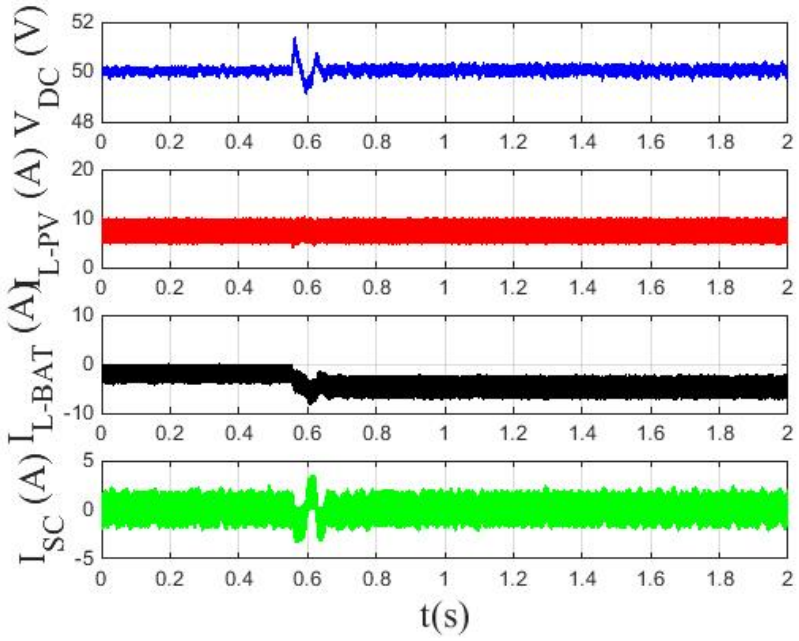

Figure 6.14: Dynamic response during decreasing load with battery charging

Figure (6.14) shows a step load decrease at $t = 0.6s$. The DC bus voltage increase, by about $0.9V$, then return to its original value. The supercapacitor absorbs exceeding power for a very short time while battery adjusts surplus of power.

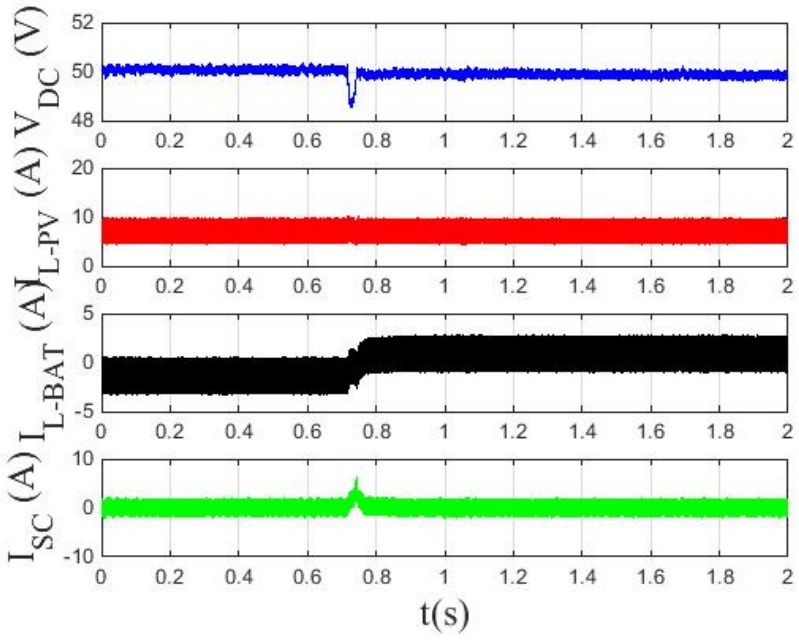

Figure 6.15: Dynamic Response during increasing load with battery charging

Figure (6.15) shows a step load increase at $t = 0.7s$. The DC bus voltage decrease by about $1.1V$, then return to its original value as the battery and supercapacitor interfaces

adjust their injected powers.
As before, the supercapacitor interface reacts faster than the battery one, what allows the current in the latter to vary at a lower rate, as desired and expected.

6.6.1 Reference decomposition with a $f_c = 2Hz$ LPF

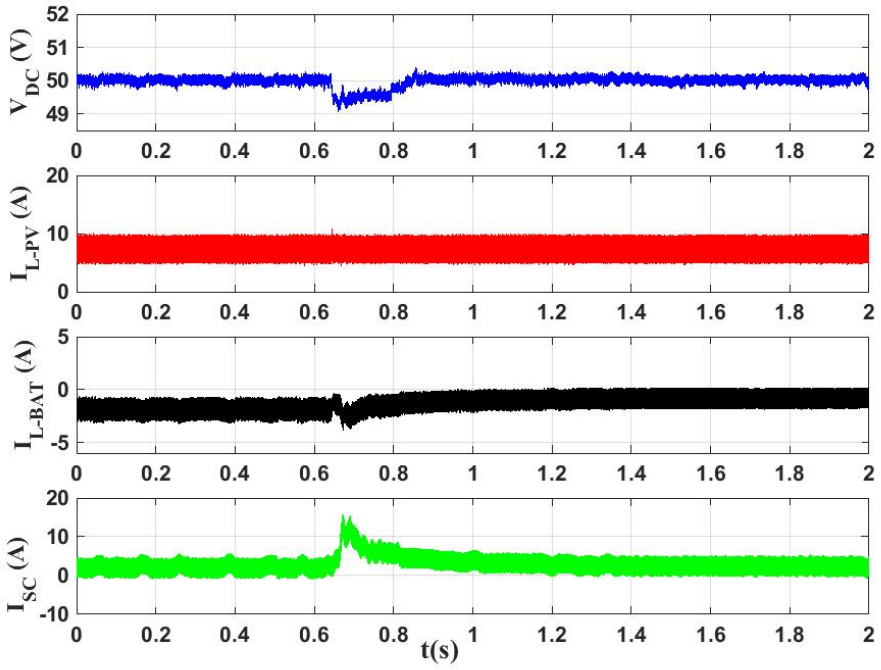

Figure 6.16: Dynamic response during increasing load with battery discharging with $f_c = 2hz$

Figure (6.16) shows Dynamic Response during increasing load with battery charging for $f_c = 2hz$. In such a case, the load increased at $t = 0.66s$. On the top, one sees that the DC bus is initially equal to $50V$, decreasing briefly by about 0.7 V following the load step, then returning in about $2s$ towards the original value.
Just below, the current in the inductor of the PV interface remains virtually unaffected at the MPPT value. Further below, one sees the inductor currents of the "battery" and supercapacitor interfaces.
The Supercapacitor meets the average value of the step load increase momentarily for $1.9s$ and returns to an average of about 0 A.
After this time the battery compensates the load demand and takes over the power balancing in the system.

Figure (6.17): a step load decrease at $t = 0.8s$. In such a case, the DC bus voltage will initially increase, by about $0.7V$, then return to its original value in $1.6s$ as the battery and supercapacitor interfaces adjust their injected powers., The Supercapacitor meets the average value of the step load increase momentarily for $1.8s$ and returns to an average of about 0 A.

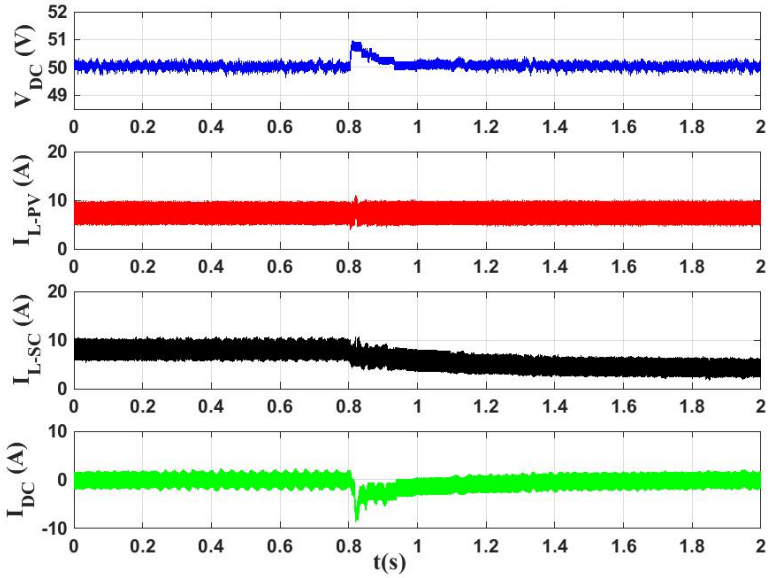

Figure 6.17: Dynamic Response during decreasing load with battery discharging

As planned, one may observe how the supercapacitor interface reacts faster than the "battery" one.

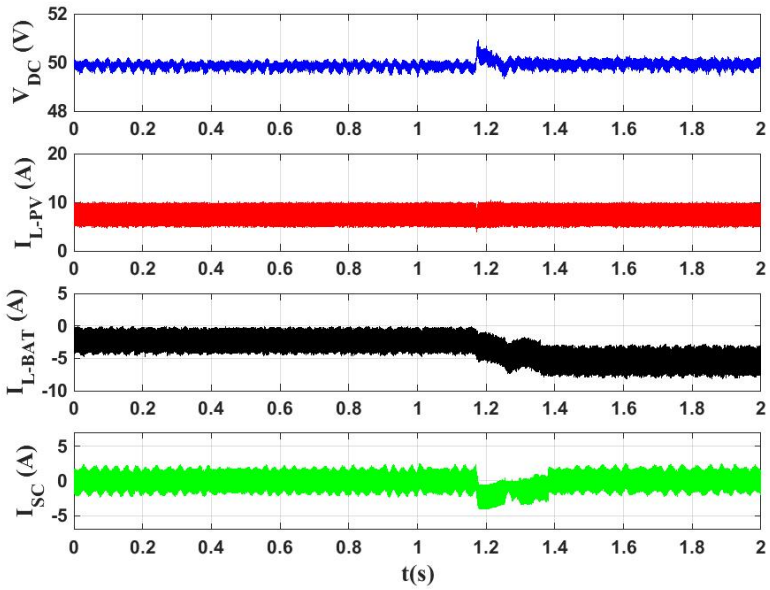

Figure 6.18: Dynamic Response during decreasing load with battery charging

Figure (6.18) shows a step load decrease at $t = 1,15s$. The DC bus voltage increase, by about $0.85V$, then return to its original value $t = 1.4s$. The supercapacitor absorbs exceeding power for a short time while battery adjusts surplus of power

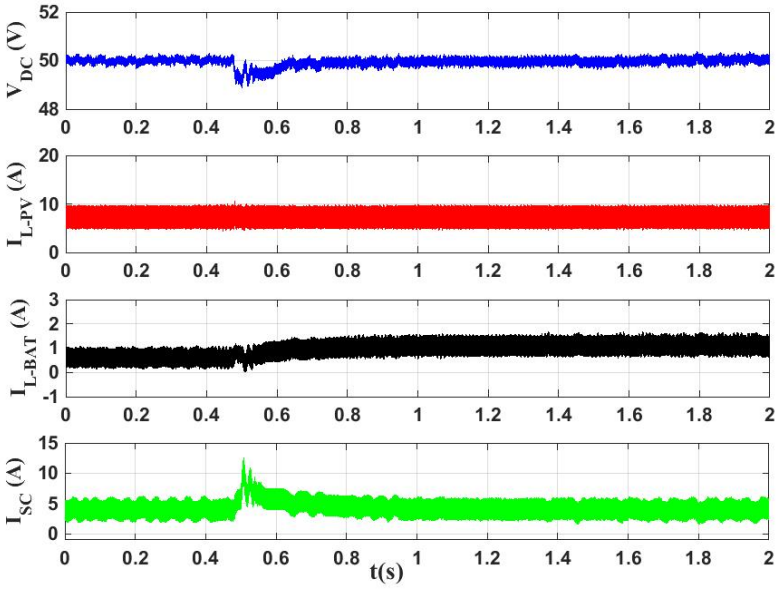

Figure 6.19: Dynamic Response during increasing load with battery charging

Figure (6.19) shows a step load increase at $t = 0.5s$. The DC bus voltage decrease by about $0.9V$, then return to its original value at $t = 1.8s$ as the battery and supercapacitor interfaces adjust their injected powers.
As before, the supercapacitor interface reacts faster than the battery one, what allows the current in the latter to vary at a lower rate, as desired.

6.6.2 Reference decomposition by a $f_c = 100Hz$ LPF

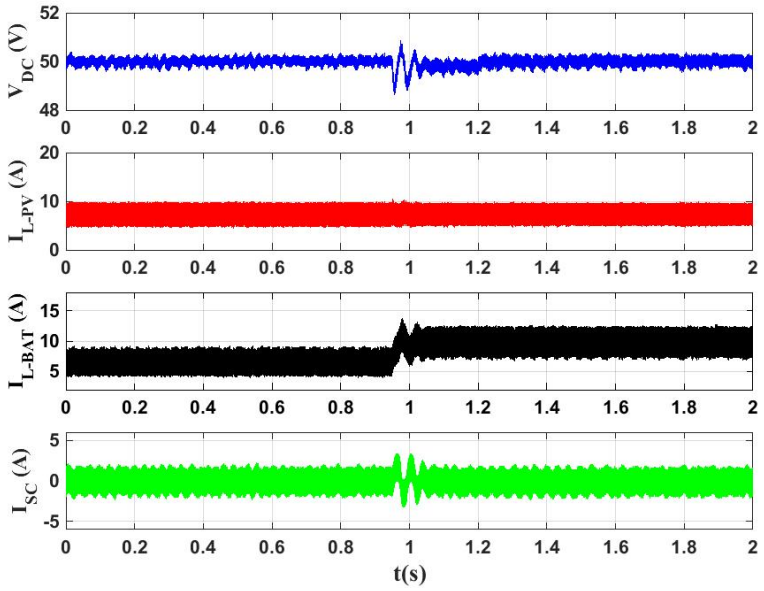

Figure 6.20: Dynamic Response during increasing load with battery discharging with $f_c = 100hz$

Figure (6.20) shows Dynamic Response during increasing load with battery charging for $f_c = 100hz$. The load changed at $t = 0.9s$. On the top, one sees that the DC bus is initially equal to $50V$, decreasing briefly by about 1.1 V following the load step, then returning, in about $0.5s$, towards the original value with little ripple.
Just below, the current in the inductor of the PV interface remains virtually unaffected at the MPPT value. Further below, one sees the inductor currents of the "battery" and supercapacitor interfaces.
Following the load increase, the contribution of the Supercapacitor supplies of exceeding power momentarily for $0.5s$ and returns to an average of about 0 A.
The battery reacts fast to meet the load demand and takes over the power balancing in the system.

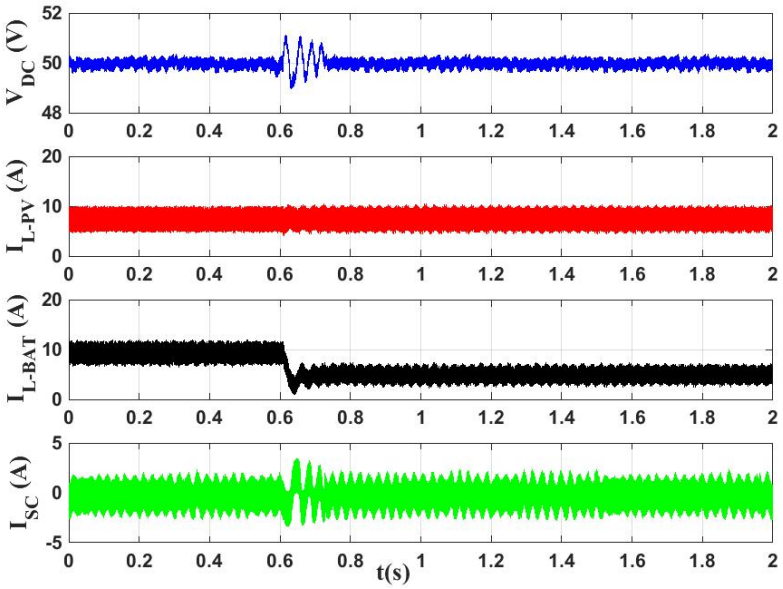

Figure 6.21: Dynamic Response during decreasing load with battery discharging

Figure (6.21) A step load decrease at $t = 0.6s$. In this case, the DC bus voltage will initially increase, by about $1.2V$, then return to its original value in $1.1s$ as the battery and supercapacitor interfaces adjust their injected powers, the supercapacitor interface reacts faster than the "battery" one.

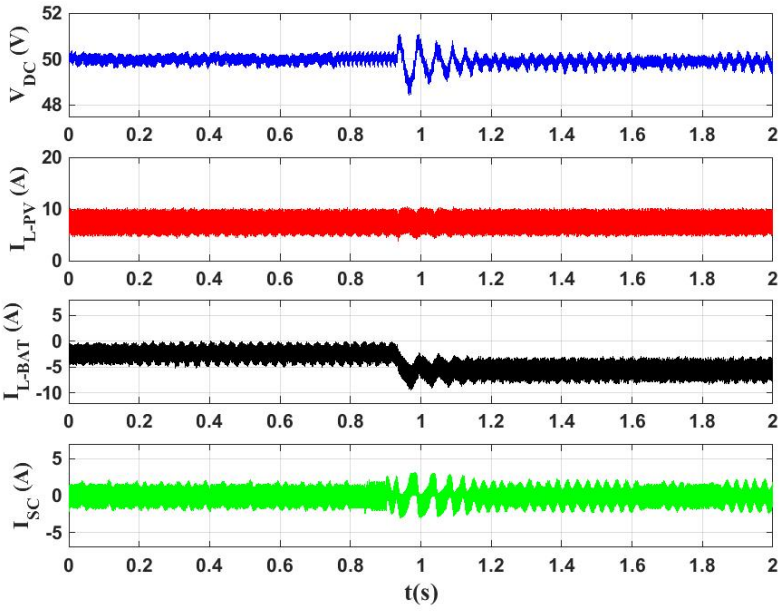

Figure 6.22: Dynamic Response during decreasing load with battery charging

Figure (6.22) shows a step load decrease at $t = 0,95s$. The DC bus voltage increase, by about $1.2V$, then return to its original value in $t = 1.2s$ with ripple. The supercapacitor

absorbs exceeding power for a short time while battery reacts fast to adjust surplus of power

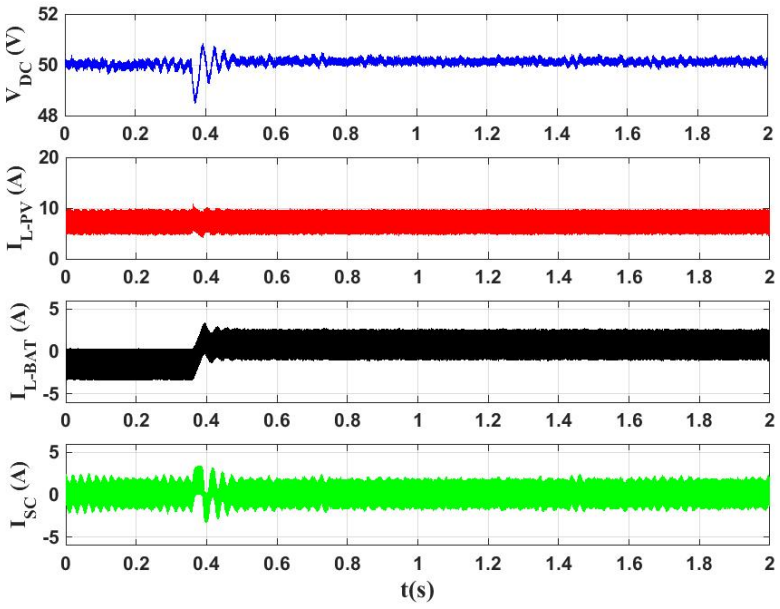

Figure 6.23: Dynamic Response during increasing load with battery charging

Figure (6.23) shows a step load increase at $t = 0.35s$. The DC bus voltage decreases by about $1.3V$, then returns to its original value $t = 1.2s$ with ripple. The supercapacitor reacts fast to meet step load increase and returns to an average of about 0 A. The battery interface reacts fast to adjust its injected power.

Results Analysis As in the simulations, the control strategy operates successfully in a wide range in spite of perturbation on source and load. The controller was always able to keep V_{DC} in its nominal value for step power changes. As in simulations, the dynamics of the system depends of the the time constants of the filter, however when we use a small time constant (cutoff frequency high), the supercapacitor and the battery react simultaneously fast to meet step load change, and cause little ripple in V_{DC} before reaching the steady state. On the other hand, the battery is required to behave much faster, what can be damageable for some technologies. The other result is that the supercapacitor may be smaller, since the battery's support comes faster, demanding less stored energy in the supercapacitor.

As a result of all experiments, the desired voltage for the DC MicroGrid is tightly kept inside desired bounds. The developed control strategy is then shown to successfully operate in a wide range of situations of time-varying load and source, and for big step variations of the references.

6.7 Comparison with PI control

In order to demonstrate the performance of the proposed control strategy, it is compared with PI linear control.
For comparison the simulations have been done for linear control and nonlinear control for the same variations of the load and solar irradiance.

6.7.1 Base results with Nonlinear control

First we present the results using the nonlinear control. In this simulation a succession of variations on load and PV output are presented.

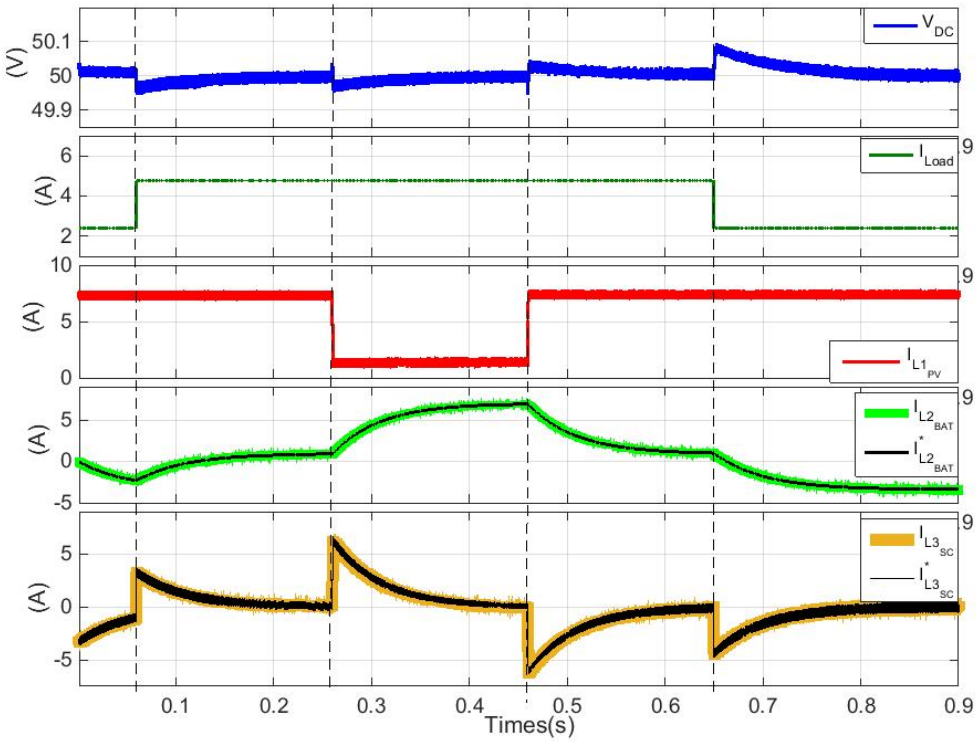

Figure 6.24: Dynamic response of the system for Nonlinear Control

Figure (6.24) shows how the DC bus voltage (top) varies as the load current and PV current (following screens) vary. The load impedance is equal to $10,4\Omega$ for $0.06s < t < 0.65s$ and is equal to 21Ω elsewhere. The solar irradiance was the rated one for $t < 0.22s$ and $t > 0.46s$, and equal to $200W/m^2$ otherwise. There, one sees that the DC bus voltage varies briefly following the transients, quickly recovering and stabilising at the rated $(50V)$ DC bus voltage in about $1ms$. The maximum DC bus voltage error is equal to $0.08V$, when the accepted error is $\pm 5\% = \pm 2.5V$.

6.7.2 Linear control

State space averaging method is used to obtain a Small Signal model for the converter (see [94, 95, 96]). The model is derived under the assumption that all the converter elements are ideal. The PI controllers are designed using methods presented in ([97, 98]).

PI design for storage

The voltage regulation scheme consists of an inner current loop, in blue, and an outer voltage loop, in red, as shown in Figure (6.25).

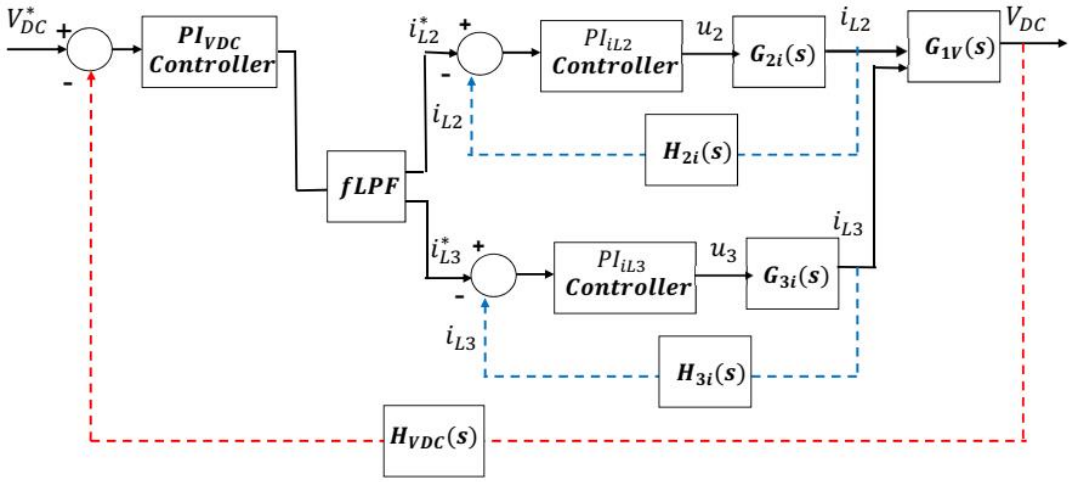

Figure 6.25: Storage Structure Control of Linear Control

Inner current loop for the Battery

The transfer function obtained by Small-Signal modelling, from individual duty cycle to inductor current is:

$$G_{2i}(s) = \frac{\widehat{i}_{L2}}{\widehat{u}_{2_s}} = \frac{C_{DC}V_{DC}s + 2I_{DC}}{L_2C_{DC}s^2 + \frac{L_2}{R}s + (1-u_2)^2} \tag{6.55}$$

A PI controller applied for the battery, has the transfer function:

$$C_{i_{BATi}}(s) = k_{P_{BATi}} + \frac{k_{i_{BATi}}}{s} \tag{6.56}$$

The closed loop transfer function using the current control loop is:

$$G_{2i_{CL}}(s) = \frac{G_{2i}(s)C_{i_{BATi}}(s)}{1 + G_{2i}(s)C_{i_{BATi}}(s)} \tag{6.57}$$

The same current loop can be designed for the battery, supercapacitor and Photovoltaic source. The switching frequency considered in this work is $f_s = 20kHz$. To avoid subharmonic oscillations the inner current loop gain cross over frequency is limited to $f_s/6$ see [98].

The plant parameters used in this work are: $V_{DC} = 50V$, $V_{PV} = 29V$, $V_{BAT} = 28V$,

$V_{SC} = 28V$, $u_1 = 0.42$, $u_2 = 0.44$, $u_3 = 0.44$, $I_{DC} = 4.44A$, $L = 100\mu H$, $C = 1500\mu F$ and $R = 10.8\Omega$. R was selected as the maximum Load that could be supplied by the sources.

For the battery, the PI controller is designed to achieve phase modulation (PM) of 60^0 at $2kHz$ [97]. Then, the PI controller parameters for the battery are computed as $k_{p_{BATi}} = 0.04$ and $k_{i_{BATi}} = 40$.

For the supercapacitor, the PI controller is designed to achieve phase modulation of 60^0 at $3kHz$. The parameters for the supercapacitor are computed as $k_{p_{SCi}} = 0.05$ and $k_{i_{SCi}} = 90$.

For the PV, the PI controller is designed to achieve phase modulation of 60^0 at $2kHz$. Then its parameters are $k_{p_{PVi}} = 0.032$ and $k_{i_{PVi}} = 35$.

Outer voltage loop for the battery and supercapacitor

The transfer function from inductor current to output voltage is given by :

$$G_{2v}(S) = \frac{\widehat{v}_{DC}}{\widehat{i}_s} = \frac{R(1-u_2)(1-\frac{L_2}{R(1-u_2)^2}s)}{2+RC_{DC}s} \tag{6.58}$$

Where $\widehat{v}_{DC}$ and $\widehat{i}_s$ are small perturbations in input current and output voltage of the battery. The PI controller has the transfer function:

$$C_{v_{BATv}}(s) = k_{P_{BATv}} + \frac{k_{i_{BATv}}}{s} \tag{6.59}$$

The closed loop transfer function is then:

$$G_{2v_{CL}}(s) = \frac{G_{2v}(s)C_{i_{BATv}}(s)}{1+G_{2i}(s)C_{i_{BATv}}(s)} \tag{6.60}$$

The PI controller is designed to achieve phase modulation of 60^0 at $3.2kHz$. So, the PI parameters are $k_{p_{BATv}} = 46.8$ and $k_{i_{BATv}} = 974$. It was used $\tau_F = 0.05s$ or $f_c = 20Hz$ for LPF.

Outer Voltage loop for the PV

The PI controller is designed to achieve phase modulation of 60^0 at $3kHz$, with control parameters $k_{p_{PVv}} = 45.9$ and $k_{i_{PVv}} = 970$.

6.7.3 Simulation Results and Comparison

A comparison of the proposed nonlinear control with the classic linear control approach was carried out in the developed MicroGrid.

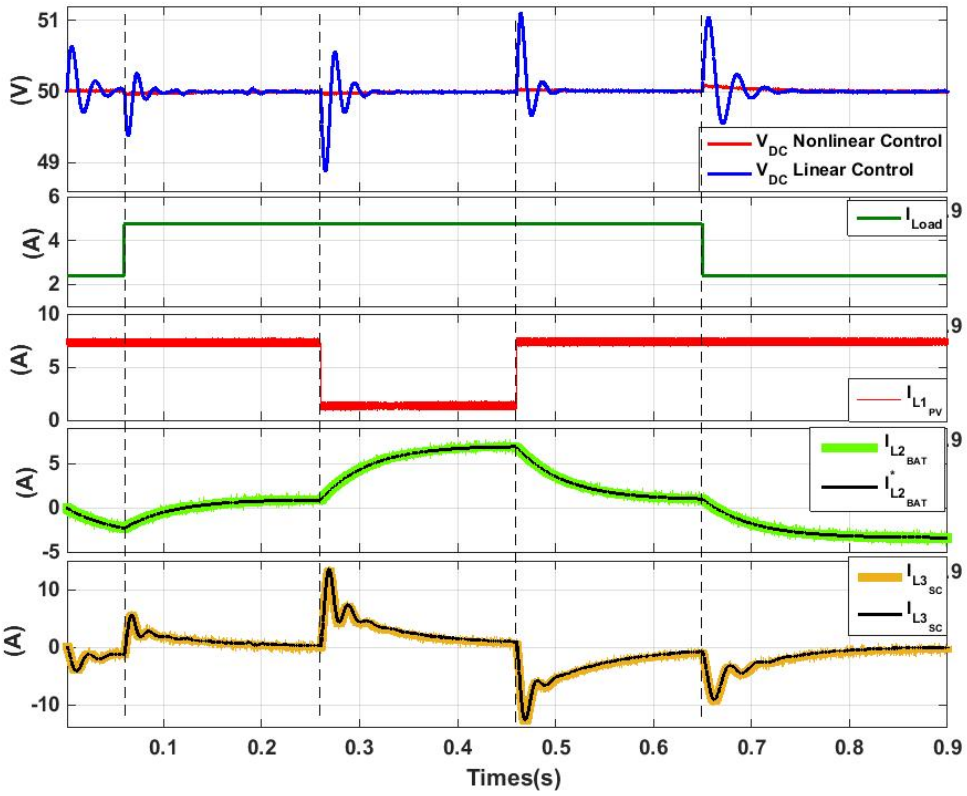

Figure 6.26: Comparison of the V_{DC} dynamics by applying nonlinear control in red and classical PI control in blue

Figure (6.26) shows how the DC bus voltage (top) varies as the load current and PV current (sub-pictures below) vary. The load impedance is equal to 21Ω for $0.06s < t < 0.65s$ and is equal to 10.4Ω elsewhere.
The solar irradiance was rated $1000W/m^2$ for $t < 0.22s$ and $t > 0.46s$, and equal to $200W/m^2$ otherwise.

The reference and actual waveforms for the battery current are shown in the fourth screen from the top. The reference signal varies slowly and the actual waveform follows it with a small switching frequency ripple.
For the SuperCapacitor, its reference and actual waveforms are shown in the last screen. The reference signal varies fast and the actual waveform follows it with a big switching frequency ripple, following PV generation and load demand variations. The result is V_{DC} oscillations that eventually stabilise at $0A$.

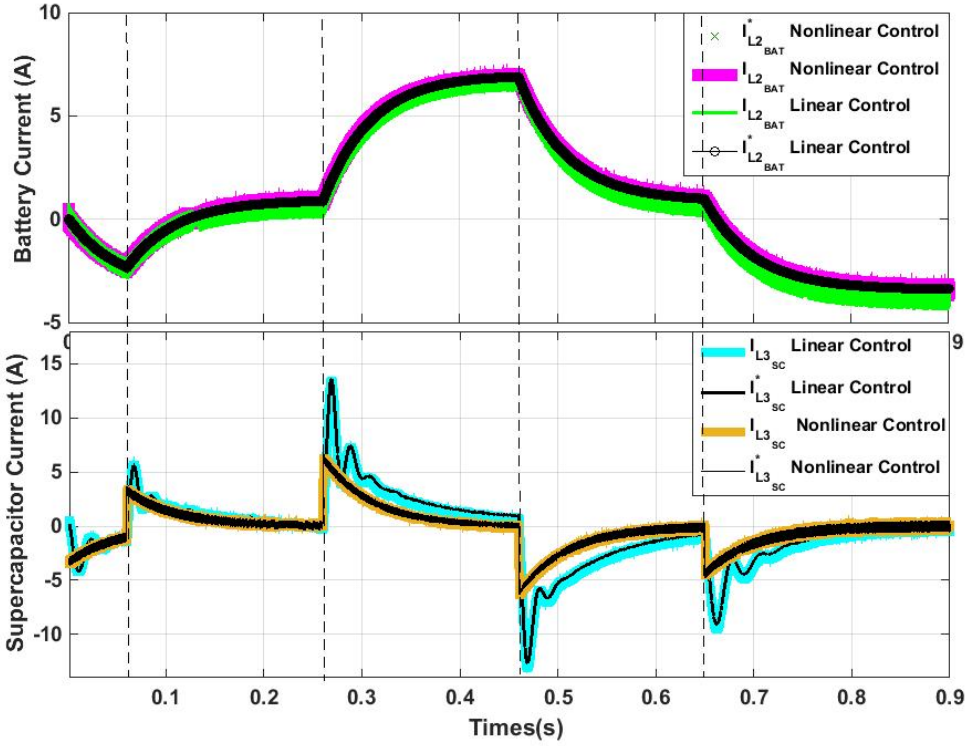

Figure 6.27: Comparison of the Current dynamics by applying nonlinear control and classical PI control

Figure(6.27) shows a comparison between battery and supercapacitor currents for linear and nonlinear control. We can see that for the battery there is not much difference between the two control methods, however, for the supercapacitor that has faster dynamics, we notice several oscillations in high switching frequency in V_{DC}.

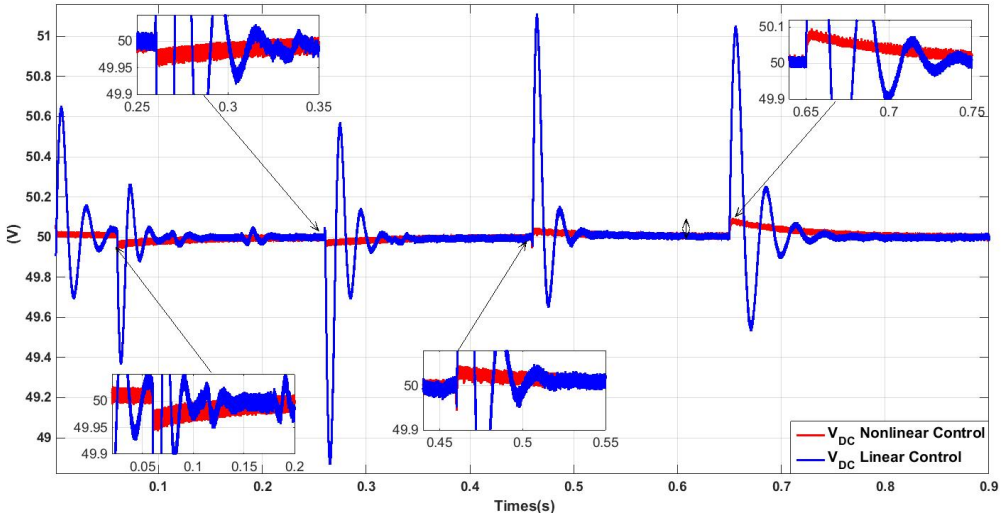

Figure 6.28: Comparison of the V_{DC} dynamics by applying nonlinear control in red and classical PI control in blue

In figure(6.28) one sees that the DC bus voltage varies following the transients, recovering and stabilizing at the rated ($50V$). The maximum DC bus voltage error is equal to $1.2V$ for linear control in blue, while equal to $0.08V$ for Nonlinear control in red. One may conclude that the PI linear control response have bigger overshoots in transients and a slower settling time.

These results confirm that the proposed scheme is effective in achieving the goals defined for this application.

6.8 Conclusion

In this chapter a three legs converter is used to model a DC MicroGrid, and is used to integrate a renewable energy source, a hybrid storage system that can work in two distinct time scales and a load. The proposed scheme is used to test in real experiments the DC MicroGrid studied in this thesis. The proposed control schemes developed in previous chapters are then applied to this scheme, aiming to test in real life the results already obtained in simulations.

This new system is tested either by simulation and by experiments that corroborate the theoretical analysis and show the good performance of the proposed scheme under variations on production and on consumption. The choice of the time constant of the filter will be capital for the final behaviour of the overall system, and its choice depends on the desired use and the technology and sizing of each element of the Energy Storage System. Nevertheless for a very wide range of frequencies, the proposed control strategy assures very good results.

Chapter 7

General Conclusion

7.1 Conclusion

The integration of decentralized energy production, and in particular intermittent sources as solar, will be an important but difficult task in the future; the challenge is to develop flexible integration strategies of such sources to the network based on “Plug and Play" philosophy.
The concept of MicroGrid with storage devices may be the answer for interconnection constraints, and an efficient way to bring such power to the main grid, as well as providing ancillary services as voltage, frequency and inertia support. This intermittent renewables' integration and the self sustainability of such systems imply in the use of storage, as developed in this work. The proposed DC MicroGrid includes a hybrid storage system that can work in two distinct time scales. The physical characteristics of the storage components are used to guarantee equilibrium between power generation and load demand in the time frame of power and energy under variations of production and consumption.
This work was focused on developing control algorithms that can assure the stability of the DC MicroGrid, under sudden and strong variations on production and consumption. The proposed algorithms were meant to be simple enough to be easily implemented in real applications, and to be easier to tune than current methods based on linear control techniques. The proposed schemes are able to supply a load correctly while formally ensuring voltage stability under mild assumptions. The proposed solution is a hierarchical control strategy, which includes local controllers of converters (DC/DC converters), an implicit primary control and a secondary control (based on the power flow).

This thesis starts by providing a literature overview on MicroGrid technology to obtain a good understanding of their topologies, and the different Distributed Generation that may be connected. In the same way, we introduced several existing control structures of MicroGrids in this literature review.

In Chapter two, we study the mathematical model of a MicroGrid composed by renewable sources, load and storage systems. There it is used time-averaged modeling method, which is the most widely used approach in the context of power converters.

In Chapter three the control strategy and the associated stability analysis has been

developed for a DC MicroGrid. A power flow management and a rather complex control strategy becomes mandatory for such systems, and in the present case is composed by a hierarchical control scheme that ensures stability of all variables, in particular the voltage of the DC bus. This control structure is designed with two levels; the low level controller based on nonlinear theory assures exponential stability of each element composing the grid and of the whole system under mild conditions that in their turn define the operation conditions. On top of that, a high level controller provides references to accomplish the power flow. Indeed the overall control strategy implies also in a trivial Master/Slave primary control between these two layers, that is not further explained in this thesis. There is then performed a rigorous stability analysis that takes into account the whole system by a constructive Lyapunov function. The obtained system can then present good dynamic performance and flexibility. The results show the robustness of the adopted control action both during the transient and in steady-state operation mode. Simulations are carried out successfully testing the adopted control strategy.

In Chapter four we have applied the initial MicroGrid structure or a particular case of a rail station (train, metro, tramway...) motivated by industrial collaborations. In this case it is considered the energy recovery from the braking of such trains, what represents a very strong power fluctuation into the MicroGrid through a power converter. In that chapter it was described the Braking Energy Recovery System scheme, the model of the source and associated power electronics, the energy storage system (lithium ion battery and supercapacitor). The same control philosophy was applied to design the control for that system. Finally, simulation results are provided to confirm results.

In Chapter five we have presented experiments made on test bed to validate the control design and stability study. The theoretical study is adapted for the existing test platform. It is presented the average model of a Three-Input DC–DC Boost Converter Circuit used to compose the MicroGrid, followed by a controller redesigned to fit this topology.

The system is tested either by simulation and experiments that corroborate the theoretical analysis and show the robustness and the good performance for the proposed scheme under variations on production and on consumption. Thanks to the real implementation on a test bench it is possible to assure that the proposed control philosophy and the methods developed in this thesis are perfectly valid to operate DC MicroGrids, even in the very difficult case of train's braking energy recovery.

7.2 Main results

The main results of this thesis can be summarized as:

- Non-linear control algorithms for each converter, based on backstepping and Feedback Linearization.
- Controllers are made such as that the system exhibits a multi-time-scale behavior characterized by the presence of fast and slow transients.Furthermore the stabilization is based on splitting tasks between different components of the storage systems (battery and supercapacitor).

- The system's stability is formally mathematically analyzed by constructive Lyapunov functions, that assure exponential stability of the whole system under mild conditions, that in their turn define the operation conditions of the MicroGrid. The obtained system will then guarantee good dynamic performance and flexibility.
- The original scheme designed for renewables integration was then enhanced such as to integrate a difficult problem of braking recovery that was used as an additional renewable source.
- A real DC MicroGrid test bench was built based on a Three-Input DC–DC Boost Converter. There was implemented local and secondary controllers validating the proposed approach.
- The secondary control level was developed based on Low Pass Filters. In this thesis it is given a simple method to chose the cut-off frequency of LPF for signal decomposition. This method allows us to reduce or increase the size of the storage elements (battery and supercapacitor) according to the system performance or economic criteria.

7.3 Perspectives for future work

This thesis has tackled some challenges in the area of DC MicroGrids. However, there still exist many issues to be investigated.

- The stability of DC MicroGrid is based on storage devices working in different timescales. But the addition of other storage units such as fuel cells will make the system more reliable. This will also allow the possibility of including economic aspects and to aim at sustainability in addition to reliability and power quality. In the same way, it is intended to consider the interconnection of the DC MicroGrid to an AC grid. This would help us study the system behaviors and the ancillary services DC could provide to AC. In particular in the case of low inertia AC grids, it would be very interesting to use a DC grid to introduce renewables to costumers in AC.
- Although there are many DC loads in practical daily life, there is still a lack of low cost and commercial DC-DC converters to interface between the DC loads and the DC distribution system. Therefore, DC power conversion is urgently needed for the development of DC distribution system. Furthermore, many questions remain on how such DC distribution system should be, in particular about voltage levels and protection schemes. One of possible further works is to study such topics, in particular mixing control and power electronics to address security and protection issues.
- Finally, it would be important to allow larger systems that could be deployed in a neighborhood geographic spam. This will need some more work in the secondary level and the interaction with a tertiary level.

Bibliography

[1] T. Bocklisch, "Hybrid energy storage systems for renewable energy applications," *Energy Procedia*, vol. 73, pp. 103 – 111, 2015. 9th International Renewable Energy Storage Conference, IRES 2015.

[2] L. G. Dol and A. d. Bernardinis, "Ac or dc grid for railway stations?," in *PCIM Europe 2016; International Exhibition and Conference for Power Electronics, Intelligent Motion, Renewable Energy and Energy Management*, pp. 1–8, 2016.

[3] S. :Infrastructures and C. S. G. Division, "The smart grid by siemens," tech. rep., Siemens, 2012.

[4] C. de régulation de l'énergie, "Appel d'offres de la cre portant sur des installations photovoltaiquessur batiment de puissance crete comprise entre 100 et 250 kw," tech. rep., Commission de régulation de l'énergie (CRE), 2012.

[5] I. Buchmann, *Batteries in a portable world*. Cadex Electronics Inc, 2016.

[6] A. Benchaib, *Advanced Control of AC / DC Power Networks: System of Systems Approach Based on Spatio-temporal Scales*. Wiley-ISTE, 2015.

[7] P. Kundur, J. Paserba, V. Ajjarapu, G. Andersson, A. Bose, C. Canizares, N. Hatziargyriou, D. Hill, A. Stankovic, C. Taylor, T. V. Cutsem, and V. Vittal, "Definition and classification of power system stability $IEEE/CIGRE$ joint task force on stability terms and definitions," *IEEE Transactions on Power Systems*, vol. 19, no. 3, pp. 1387–1401, 2004.

[8] S. Siad, G. Damm, L. G. Dol, and A. d. Bernardinis, "Design and control of a dc grid for railway stations," in *PCIM Europe 2017, International Exhibition and Conference for Power Electronics, Intelligent Motion, Renewable Energy and Energy Management*, pp. 1–8, 2017.

[9] Y. Chen, G. Damm, A. Benchaib, M. Netto, and F. Lamnabhi-Lagarrigue, "Control induced explicit time-scale separation to attain dc voltage stability for a vsc-hvdc terminal," *IFAC Proceedings Volumes*, vol. 47, no. 3, pp. 540 – 545, 2014. 19th IFAC World Congress.

[10] I. Alessio, S. B. Siad, G. Damm, E. D. Santis, and M. D. D. Benedetto, "Nonlinear control of a dc microgrid for the integration of photovoltaic panels," *IEEE Transactions on Automation Science and Engineering*, vol. 14, no. 2, pp. 524–535, 2017.

[11] R. H. Lasseter, "Smart distribution: Coupled microgrids," *Proceedings of the IEEE*, vol. 99, no. 6, pp. 1074–1082, 2011.

[12] S. M. Ashabani and Y. A. r. I. Mohamed, "New family of microgrid control and management strategies in smart distribution grids; analysis, comparison and testing," *IEEE Transactions on Power Systems*, vol. 29, no. 5, pp. 2257–2269, 2014.

[13] E. Rokrok, M. Shafie-Khah, and J. P. S. Catalão, "Comparison of two control strategies in an autonomous hybrid microgrid," in *2017 IEEE PES Innovative Smart Grid Technologies Conference Europe (ISGT-Europe)*, pp. 1–6, 2017.

[14] S. K. Kollimalla, M. K. Mishra, and N. L. Narasamma, "Design and analysis of novel control strategy for battery and supercapacitor storage system," *IEEE Transactions on Sustainable Energy*, vol. 5, no. 4, pp. 1137–1144, 2014.

[15] J. Dulout, B. Jammes, L. Seguier, and C. Alonso, "Control and design of a hybrid energy storage system," in *2015 17th European Conference on Power Electronics and Applications (EPE 15 ECCE-Europe)*, pp. 1–9, 2015.

[16] B. Liu, F. Zhuo, Y. Zhu, and H. Yi, "System operation and energy management of a renewable energy-based dc micro-grid for high penetration depth application," *IEEE Transactions on Smart Grid*, vol. 6, no. 3, pp. 1147–1155, 2015.

[17] H.Bevrani, B. Francois, and T.Ise, *Microgrid Dynamics and Control*. John Wiley and Sons Inc, 2017.

[18] R.Lasseter, A.Akhil, C.Marnay, J.Stephens, J.Dagle, R. Guttromson, A. S.Meliopoulous, R. Yinger, and J. Eto, "Consortium for electric reliability technology solutions white paper on integration of distributed energy resources the certs microgrid concept," tech. rep., Lawrence Berkeley National Laboratory, 2002.

[19] C. Marnay, S. Chatzivasileiadis, C. Abbey, R. Iravani, G. Joos, P. Lombardi, P. Mancarella, and J. von Appen, "Microgrid evolution roadmap," in *2015 International Symposium on Smart Electric Distribution Systems and Technologies (EDST)*, pp. 139–144, 2015.

[20] I. Patrao, E. Figueres, G. GarcerÃ¡, and R. GonzÃ¡lez-Medina, "Microgrid architectures for low voltage distributed generation," *Renewable and Sustainable Energy Reviews*, vol. 43, pp. 415 – 424, 2015.

[21] M. Soshinskaya, W. H. Crijns-Graus, J. M. Guerrero, and J. C. Vasquez, "Microgrids: Experiences, barriers and success factors," *Renewable and Sustainable Energy Reviews*, vol. 40, pp. 659 – 672, 2014.

[22] K. Prakash, A. Lallu, F. R. Islam, and K. A. Mamun, "Review of power system distribution network architecture," in *2016 3rd Asia-Pacific World Congress on Computer Science and Engineering (APWC on CSE)*, pp. 124–130, 2016.

[23] D. Kumar, F. Zare, and A. Ghosh, "Dc microgrid technology: System architectures, ac grid interfaces, grounding schemes, power quality, communication networks, applications, and standardizations aspects," *IEEE Access*, vol. 5, pp. 12230–12256, 2017.

[24] K. A. Prakash, A. Lallu, F. R. Islam, and K. A. Mamun, "Review of power system distribution network architectur," *2016 3rd Asia-Pacific World Congress on Computer Science and Engineering (APWC on CSE)*, pp. 124–130, 2016.

[25] T. M. Kishorbha and D. Mangroliya, "Recent trades in distribution system„" *International Journal of Advance Engineering and Research Development*, vol. 2, p. 211–217, 2015.

[26] S. Saranya and S. Amitrtharaj, "Protection of low voltage ring bus type dc distributed network system with probe power unit," *," International Journal of Engineering Development and Research*, vol. 3, p. 436–440, 2015.

[27] H. Willis, *Power distribution planning reference book*. New York: M. Dekker, 2004.

[28] M. Sochinskayaa, "Distributed networks: experiences, barriers and success factors," *Renewable and Sustainable Energy Reviews*, p. 5–30, 2014.

[29] N. Cristian, A. Ahmed, and B. Dakyo, "Impact analysis of distributed generation on mesh and radial distribution network. overview and state of the art," in *PLUMEE Conference - Romania*, 2013.

[30] F. Z. Peng, Y. W. Li, and L. M. Tolbert, "Control and protection of power electronics interfaced distributed generation systems in a customer-driven microgrid," in *Conference Paper: Calgary, AB, Canada*, 2009.

[31] A.Bidram, V. Nasirian, A. Davoudi, and F.L.Lewis, *Cooperative Synchronization in Distributed Microgrid Control*. Springer, 2017.

[32] S. Sen and V. Kumar, "Microgrid control: A comprehensive survey," *Annual Reviews in Control*, vol. 45, p. 118–151, 2018.

[33] D. E. Olivares, A. Mehrizi-Sani, A. H. Etemadi, C. A. Cañizares, R. Iravani, M. Kazerani, A. H. Hajimiragha, O. Gomis-Bellmunt, M. Saeedifard, R. Palma-Behnke, G. A. Jiménez-Estévez, and N. D. Hatziargyriou, "Trends in microgrid control," *IEEE Transactions on Smart Grid*, vol. 5, no. 4, pp. 1905–1919, 2014.

[34] Q. L. LAM, *Advanced control of microgrids for frequency and voltage stability:robust control co-design and real-time validation*. PhD thesis, Université Grenoble Alpes, 2016.

[35] E. Unamuno and J. A. Barrena, "Hybrid ac/dc microgrids part ii: Review and classification of control strategies," *Renewable and Sustainable Energy Reviews*, vol. 52, pp. 1123 – 1134, 2015.

[36] T. L. Vandoorn, J. C. Vasquez, J. D. Kooning, J. M. Guerrero, and L. Vandevelde, "Microgrids: Hierarchical control and an overview of the control and reserve management strategies," *IEEE Industrial Electronics Magazine*, vol. 7, no. 4, pp. 42–55, 2013.

[37] M. Mahmoud, M.N.Alyazidi, and M. Abouheaf, "Adaptive intelligent techniques for microgrid control systems: A survey," *International Journal of Electrical Power and Energy Systems*, vol. 90, pp. 292 – 305, 2017.

[38] M. A. Mahmud, M. J. Hossain, H. R. Pota, and N. K. Roy, "Nonlinear distributed controller design for maintaining power balance in islanded microgrids," in *2014 IEEE PES General Meeting | Conference Exposition*, pp. 1–5, 2014.

[39] J. M. Guerrero, J. C. Vasquez, J. Matas, L. G. de Vicuna, and M. Castilla, "Hierarchical control of droop-controlled ac and dc microgrids—a general approach toward standardization," *IEEE Transactions on Industrial Electronics*, vol. 58, no. 1, pp. 158–172, 2011.

[40] A. Bidram and A. Davoudi, "Hierarchical structure of microgrids control system," *IEEE Transactions on Smart Grid*, vol. 3, no. 4, pp. 1963–1976, 2012.

[41] A. M. Yahya, A. Mahmoud, and L.Youm, "Etude et modellisation d'un generateur photovoltaique," *Revue des Energies Renouvelables*, vol. 11, no. 3, pp. 473–483, 2008.

[42] B. E. A. Saleh and M. C. Teich, *Fundamentals of Photonics*. John Wiley and Sons Sons, Inc, 1991.

[43] S. Nasrand, M. Petit, M. Iordache, and O. Langlois, "Stability of dc micro-grid for urban railway systems," *International Journal of Smart Grid and Clean Energy*, vol. 4, no. 2, pp. 261–268, 2015.

[44] N. Onat, "Recent developments in maximum power point tracking technologies for photovoltaic systems," *Hindawi Publishing Corporation International Journal of Photoenergy*, vol. 2010, pp. 1–11, 2010.

[45] K. Visweswara, "An investigation of incremental conductance based maximum power point tracking for photovoltaic system," *Energy Procedia*, vol. 54, pp. 11 – 20, 2014. 4th International Conference on Advances in Energy Research (ICAER 2013).

[46] N. Drir, L. Barazane, and M. Loudini, "Comparative study of maximum power point tracking methods of photovoltaic systems," in *2014 International Conference on Electrical Sciences and Technologies in Maghreb (CISTEM)*, pp. 1–5, 2014.

[47] W. Xiao, *A modified adaptive hill climbing maximum power point tracking (MPPT) control method for photovoltaic power systems*. PhD thesis, Vancouver : University of British Columbia Library, 2003.

[48] K. K. Kumar, R. Bhaskar, and H. Koti, "Implementation of mppt algorithm for solar photovoltaic cell by comparing short-circuit method and incremental conductance method," *Procedia Technology*, vol. 12, pp. 705 – 715, 2014.

[49] C. Liu, B. Wu, and R. Cheung, "Advenced algorithm for mppt control of photovoltaic systems," in *Canadian Solar Buildings Conference Montreal,*, 2004.

[50] S. Frey, *Railway Electrification System and Engineering.* White Word Publications, 2012.

[51] R. R. Pecharroman, A. Lopez-Lopez, A. P. Cucala, and A. Fernandez-Cardador, "Riding the rails to dc power efficiency: Energy efficiency in dc-electrified metropolitan railways," *IEEE Electrification Magazine*, vol. 2, no. 3, pp. 32–38, 2014.

[52] A. Mohd, E. Ortjohann, A. Schmelter, N. Hamsic, and D. Morton, "Challenges in integrating distributed energy storage systems into future smart grid," in *2008 IEEE International Symposium on Industrial Electronics*, pp. 1627–1632, 2008.

[53] E. Korsaga, Z. Koalaga, D. Bonkougou, and F. Zougmore, "Comparaison et determination des dispositifs de stockage appropries pour un systeme photovoltaique autonome en zone sahelienne," *Journal International de Technologie, de l'Innovation, de la Physique, de l'Energie et de l'Environnement*, vol. 4, no. 3, pp. 1–24, 2018.

[54] N. RIZOUG, *Modélisation électrique et énergétique des supercondensateurs et méthodes de caractérisation : Application au cyclage d'un module de supercondensateurs basse tension en grande puissance.* PhD thesis, l'Ecole Centrale de Lille et l'Université des Sciences et Technologies de Lille., 2006.

[55] F. Díaz-González, A. Sumper, O. Gomis-Bellmunt, and R. Villafáfila-Robles, "A review of energy storage technologies for wind power applications," *Renewable and Sustainable Energy Reviews*, vol. 16, no. 4, pp. 2154 – 2171, 2012.

[56] S. Vazquez, S. M. Lukic, E. Galvan, L. G. Franquelo, and J. M. . Carrasco, "Energy storage systems for transport and grid applications," *IEEE Transactions on Industrial Electronics*, vol. 57, no. 12, pp. 3881–3895, 2010.

[57] J. Symanski, B. Mahato, and K. Bullock, "Defining a recombination efficiency for sealed, lead acid batteries a material balance approach," *Journal of The Electrochemical Society*, vol. 135, pp. 548–551, 1988.

[58] K. Divya and J. Ostergaard, "Battery energy storage technology for power systems an overview," *Electric Power Systems Research*, vol. 79, no. 4, pp. 511 – 520, 2009.

[59] D. C. Holzman, "The vanadium advantage: Flow batteries put wind energy in the bank," *Environmental Health Perspectives*, vol. 115, p. A358–A361, 2007.

[60] J. M. Carrasco, L. G. Franquelo, J. T. Bialasiewicz, E. Galvan, R. C. PortilloGuisado, M. A. M. Prats, J. I. Leon, and N. Moreno-Alfonso, "Power-electronic systems for the grid integration of renewable energy sources: A survey," *IEEE Transactions on Industrial Electronics*, vol. 53, no. 4, pp. 1002–1016, 2006.

[61] M. Lavabre, *conversion de l'Energie cours et exercices resolus.* Editions Casteilla, 2001.

[62] J-L.Dalmasso, *Cours d'Electrotechnique 2 : Traitement de l'Eergie Electrique (convertisseurs statiques.* Edition Belin, 1984.

[63] T.Wildi and G.Sybille, *Electrotechnique 4em Edition.* De boeck, 2005.

[64] G.-L. Francisco, "Model of photovoltaic module in matlab," *II CIBELEC*, pp. 1–5, 2005.

[65] H. Tian, F. M. David, K. Ellis, E. Muljadi, and P. Jenkins, "A cell-to-module-to-array detailed model for photovoltaic panels," *Solar Energy*, vol. 86, pp. 2695–2706, 2012.

[66] V. J. ChIn, Z. Salam, and K. Ishaque, "Cell modelling and model parameters estimation techniques for photovoltaic simulator application: A review," *Applied Energy*, vol. 154, pp. 500–519, 2015.

[67] H.-L. Tsai, C.-S. Tu, and Y.-J. Su, "Development of generalized photovoltaic model using matlab/simulink," in *Proceedings of the World Congress on Engineering and Computer Science San Francisco, USA*, 2008.

[68] J. Hernanz, J. Martin, I. Z. Belver, J. Lesaka, E. Guerrero, and E. P. Perez, "Modelling of photovoltaic module," in *International Conference on Renewable Energies and Power Quality (ICREPQ10) Granada (Spain)*, 2010.

[69] H. He, R. Xiong, and J. Fan, "Evaluation of lithium-ion battery equivalent circuit models for state of charge estimation by an experimental approach," *Energies 2011*, vol. 4, pp. 582–598, 2011.

[70] S.M.Mousavi and M. Nikdel, "Various battery models for various simulation studies and applications," *Renewable and Sustainable Energy Reviews*, vol. 32, pp. 477 – 485, 2014.

[71] O.Gergaud, G.Robin, B.Multon, and H. AHMED, "Energy modeling of a lead-acid battery within hybrid wind/photovoltaic systems," in *European Power Electronic Conference 2003*, (TOULOUSE, France), p. 8pp, 2003.

[72] P. Y. Julien and F. deneve., "upercapacitors and lead acid batteries integration in a vsc d-statcom for energy storage," Master's thesis, Poitier university and Power Quality Department:AREVA T&D, 2010.

[73] Y. Wang, "Modeling of ultracapacitor short-term and long-term dynamic behavior," Master's thesis, University of Akron, 2008.

[74] S. Kim, W. Choi, K. Lee, and S. Choi, "Advanced dynamic simulation of supercapacitors considering parameter variation and self-discharge," *IEEE Transactions on Power Electronics*, vol. 26, no. 11, pp. 3377–3385, 2011.

[75] S. R. Sanders, J. M. Noworolski, X. Z. Liu, and G. C. Verghese, "Generalized averaging method for power conversion circuits," *IEEE Transactions on Power Electronics*, vol. 6, no. 2, pp. 251–259, 1991.

[76] Merdassi.A, *La modellisation Automatique pour l'electronique de puissance.* Editions Universitaires Europeennes, 2010.

[77] B. Lehman and R. M. Bass, "Switching frequency dependent averaged models for pwm dc-dc converters," *IEEE Transactions on Power Electronics*, vol. 11, no. 1, pp. 89–98, 1996.

[78] A. Merdassi, L. Gerbaud, and B. Seddik, "General average modelling for power electronics systems: Automatic building approach," in *Conference: Conference: 9th International Conference on Modeling and Simulation of Electric Machines, Converters and Systems, At Quebec, Canada*, 06 2008.

[79] A. P. N. Tahim, D. J. Pagano, E. Lenz, and V. Stramosk, "Modeling and stability analysis of islanded dc microgrids under droop control," *IEEE Transactions on Power Electronics*, vol. 30, no. 8, pp. 4597–4607, 2015.

[80] B. Iovine.A, Benamane Siad.S and Damm.G, "Management of the interconnection of intermittent photovoltaic systems through a dc link and storage," *ERCIM, European Research Consortium for Informatics and Mathematics*, no. 97, 2014.

[81] M. J. Carrizosa, F. D. Navas, G. Damm, and F. Lamnabhi-Lagarrigue, "Optimal power flow in multi-terminal hvdc grids with offshore wind farms and storage devices," *International Journal of Electrical Power & Energy Systems*, vol. 65, pp. 291 – 298, 2015.

[82] J. M. Guerrero, P. C. Loh, T. Lee, and M. Chandorkar, "Advanced control architectures for intelligent microgrids—part ii: Power quality, energy storage, and ac/dc microgrids," *IEEE Transactions on Industrial Electronics*, vol. 60, no. 4, pp. 1263–1270, 2013.

[83] D. Sera, R. Teodorescu, J. Hantschel, and M. Knoll, "Optimized maximum power point tracker for fast changing environmental conditions," in *2008 IEEE International Symposium on Industrial Electronics*, pp. 2401–2407, 2008.

[84] J.Barton and D. Infield, "Energy storage and its use with intermittent renewable energy.," *EEE Transactions on Energy Conversion*, vol. 19, pp. 441–448, 2004.

[85] S. Adhikari and F. Li, "Coordinated v-f and p-q control of solar photovoltaic generators with mppt and battery storage in microgrids," *IEEE Transactions on Smart Grid*, vol. 5, no. 3, pp. 1270–1281, 2014.

[86] J. Lee, B. Han, and N. Choi, "Dc micro-grid operational analysis with detailed simulation model for distributed generation," in *2010 IEEE Energy Conversion Congress and Exposition*, pp. 3153–3160, 2010.

[87] H. Khalil, *Nonlinear Systems*. Pearson; Edition, 2002.

[88] H. Abbes, H. Abid, K. Loukil, A. Toumi, and M. Abid, "Etude comparative de cinq algorithmes de commande mppt pour un systeme photovoltaique," *Revue des Energies Renouvelables*, vol. 17, no. 3, pp. 435 – 445, 2014.

[89] M. E. Glavin, P. K. W. Chan, S. Armstrong, and W. G. Hurley, "A stand-alone photovoltaic supercapacitor battery hybrid energy storage system," in *2008 13th International Power Electronics and Motion Control Conference*, pp. 1688–1695, 2008.

[90] R. S. Bhatia, B. Singh, D. K. Jain, and S. P. Jain, "Battery energy storage system based power conditioner for improved performance of hybrid power generation," in *2008 Joint International Conference on Power System Technology and IEEE Power India Conference*, pp. 1–6, 2008.

[91] F. Ongaro, S. Saggini, and P. Mattavelli, "Li-ion battery-supercapacitor hybrid storage system for a long lifetime, photovoltaic-based wireless sensor network," *IEEE Transactions on Power Electronics*, vol. 27, no. 9, pp. 3944–3952, 2012.

[92] S.Bacha, I.Munteanu, and A.I.Bratcu, *Power Electronic Converters Modeling and Control: with Case Studies*. Advanced Textbooks in Control and Signal Processing, Springer London, 2013.

[93] S. R. Sanders, J. M. Noworolski, X. Z. Liu, and G. C. Verghese, "Generalized averaging method for power conversion circuits," *IEEE Transactions on Power Electronics*, vol. 6, no. 2, pp. 251–259, 1991.

[94] Y. Jin, J. Xu, G. Zhou, and C. Mi, "Small-signal modeling and analysis of improved digital peak current control of boost converter," in *2009 IEEE 6th International Power Electronics and Motion Control Conference*, pp. 326–330, 2009.

[95] W. Tang, F. C. Lee, and R. B. Ridley, "Small-signal modeling of average current-mode control," *IEEE Transactions on Power Electronics*, vol. 8, no. 2, pp. 112–119, 1993.

[96] J. Sun and R. M. Bass, "Modeling and practical design issues for average current control," in *APEC '99. Fourteenth Annual Applied Power Electronics Conference and Exposition. 1999 Conference Proceedings*, vol. 2, pp. 980–986, 1999.

[97] S. M. Cherati, N. A. Azli, S. M. Ayob, and A. Mortezaei, "Design of a current mode pi controller for a single-phase pwm inverter," in *2011 IEEE Applied Power Electronics Colloquium (IAPEC)*, pp. 180–184, 2011.

[98] *L. H. Dixon, Average Current Mode Control of Switching Power Supplies,Unitrode Power Supply Design Seminar Manual, 1990.*

[99] A. T. Elsayed, A. A. Mohamed, and O. A. Mohammed, "Dc microgrids and distribution systems: An overview," *Electric Power Systems Research*, vol. 119, pp. 407 – 417, 2015.

[100] H. Li, J. Peng, W. Liu, and Z. Huang, "Stationary charging station design for sustainable urban rail systems: A case study at zhuzhou electric locomotive co, china," *Sustainability*, vol. 7, pp. 465–481, 2015.

[101] E. Jimeenez, M. J. Carrizosa, A. Benchaib, G. Damm, and F. Lamnabhi-Lagarrigue, "A new generalized power flow method for multi connected dc grids," *International Journal of Electrical Power & Energy Systems*, vol. 74, pp. 329 – 337, 2016.

[102] F. A. Inthamoussou, J. Pegueroles-Queralt, and F. D. Bianchi, "Control of a supercapacitor energy storage system for microgrid applications," *IEEE Transactions on Energy Conversion*, vol. 28, no. 3, pp. 690–697, 2013.

[103] K. Ogata, *Modern Control Engineering, 5th Edition.* Pearson, 2010.

[104] H. Bourles., *Linear Systems.* ISTE Ltd and John Wiley and Sons, 2010.

université PARIS-SACLAY

ÉCOLE DOCTORALE
Sciences et technologies de l'information et de la communication (STIC)

Titre: Commande de MicroGrids DC pour l'intégration des énergies renouvelables

Mots clés: Énergie renouvelable, Contrôle non linéaire,Stockage d'énergie, Micro-Grids, Stabilité, Méthodes de Lyapunov.

Résumé: La forte proportion des sources d'énergie intermittentes présente de nouveaux défis pour la stabilité et la fiabilité des réseaux électriques. Dans ce travail nous considérons la connexion de ces sources avec un système de stockage hybride via un MicroGrid à courant continu (DC) afin de satisfaire les contraintes de connexion au réseau de distribution (les Grid-Codes).
L'objectif principal ici est de concevoir un système pouvant répondre à ces exigences et nous permettant d'obtenir un comportement Plug and Play; cette approche est basée sur la "philosophie System of Systems", utilisant des méthodologies de contrôle distribué.
Cette thèse constitue une contribution à la commande de MicroGrids DC et introduit une analyse rigoureuse de la dynamique du système. La stabilisation de ce système repose sur des dispositifs de stockage: les batteries pour l'équilibre énergétique et la réponse à long terme dues aux variations des flux d'énergie, tandis que les supercondensateurs traitent l'équilibre des puissances et des variations rapides du système.
Nous présenterons d'abord l'analyse du MicroGrid DC dont le contrôle est conçu à partir des modèles détaillés des sources d'énergie et des systèmes de stockage. Ce réseau peut présenter un comportement instable créé par l'intermittence des sources, les commutations des convertisseurs et leurs électronique de puissance et les courants oscillatoires produits par certains types de charges. Par conséquent, le système est sujet à des variations rapides et lentes. La stabilisation de tels systèmes reposera sur le fonctionnement de différentes technologies de stockage, telles que la batterie et les supercondensateurs, qui opèrent dans différentes échelles de temps.
Nous proposons un schéma de contrôle hiérarchique, basé sur la théorie du contrôle non linéaire, en particulier de Lyapunov, le backstraping et de linearization entrée/sortie. Le MicroGrid DC proposé et son contrôle sont vérifiés à la fois par simulations et par expérimentation. Les résultats montrent la bonne performance du système sous des variations de production et de consommation.

Université Paris-Saclay
Espace Technologique / Immeuble Discovery
Route de l'Orme aux Merisiers RD 128 / 91190 Saint-Aubin, France

université PARIS-SACLAY

ÉCOLE DOCTORALE
Sciences et technologies de l'information et de la communication (STIC)

Title: DC MicroGrids Control for renewable energy integration

Keywords: Renewable Energy, Nonlinear control, Energy storage, MicroGrids, Stability, Lyapunov methods.

Abstract: The large penetration of intermittent energy sources, presents new challenges to power systems' stability and reliability; we consider in this work their connection through a Direct Current (DC) MicroGrid and a hybrid storage system, in order to satisfy constraints of connection to the network (the so-called Grid-Codes). The main objective here is to design a system that can fulfil these requirements and allow us to attain a Plug and Play behaviour; this approach is based on the "System of Systems philosophy" using distributed control methodologies.

This thesis constitutes a contribution for DC MicroGrid control and introduces a rigorous dynamics' analysis. The stabilisation of the system is based on storage devices: batteries for energy balance and long term response of power flow, while supercapacitors deal with power balance and fast response.

First it will be presented the analysis of the DC MicroGrid which control is designed based on detailed models of energy sources and storage systems. This grid may present an unstable behaviour created by the source's intermittent output power, switching ripples from the power converters and their power electronic and oscillatory currents produced by some types of loads. Therefore the system is subject to both fast and slow variations. The stabilisation of such systems will be based on the operation of different technologies of storage, such as battery and supercapacitor, in different time scales.

We propose a hierarchical control scheme, based on nonlinear control theory, in particular Lyapunov, backstepping and input/output feedback linearization. The proposed DC MicroGrid and its control are then verified both by computer simulations and by experiments. The results show the good performance of the system under variations on production and on consumption.

Université Paris-Saclay
Espace Technologique / Immeuble Discovery
Route de l'Orme aux Merisiers RD 128 / 91190 Saint-Aubin, France